Biomimetic Scaffolds and Mechano-Hypoxia Conditioning for Meniscus Tissue Engineering

by

Alexander Roy Andras Szojka

A thesis submitted in partial fulfillment of the requirements for the degree of

Doctor of Philosophy

in

Experimental Surgery

Department of Surgery
University of Alberta

Abstract

The menisci are a pair of knee joint structures that are wedge-shaped in cross-section and semi-lunar in superior view. They play roles in force distribution that help maintain the health of the articular cartilage. In adults, the menisci can be divided into a fibrous, vascularized outer region and a fibrocartilaginous, avascular inner region. Being avascular, the inner regions cannot heal upon injury, which predisposes the knee to early osteoarthritis development. The principal biochemical constituents of meniscus fibrocartilage include type I collagen and hyaline cartilage-associated biochemicals type II collagen and aggrecan. Meniscus fibrocartilage is synthesized and maintained by cells known as meniscus fibrochondrocytes (MFCs), which exist natively in a hypoxic and mechanically-loaded environment. Meniscus tissue engineering (MTE) aims to generate cell-based meniscus replacements *in vitro* that slow or prevent osteoarthritis development after incidence of non-healing meniscus injuries. This is accomplished using a suitable combination of biomaterial scaffolds, cells, and growth signals. To this end, this thesis focuses on: i) development of biomimetic meniscus scaffolds; ii) investigating the MFC response to combined hypoxia and mechanical loading; and iii) identifying how this knowledge can be used to enhance fibrocartilage histogenesis *in vitro*.

Chapter 1 and Chapter 2 introduced the research topic with a review of meniscus development, comparative anatomy, and hypoxia and mechanical loading in MTE. This review suggested that the fibrocartilaginous phenotype of the adult human inner meniscus is likely an adaptation to its hypoxic and mechanically-loaded environment. The first project (Chapter 3) described design and production of 3D

printed biomimetic meniscus scaffolds. The second project (Chapter 4) presented an investigation of the simultaneous response of MFCs to combined hypoxia and supplementation of the growth factor TGF-β3 in high-density cell aggregates (pellets). These treatments had synergistic interactions that potently promoted fibrocartilage histogenesis. Chapter 5 extended this study to a larger-scale model with a porous type I collagen scaffold. Hypoxia had few effects in this scaffold, even when combined with mechanical loading (dynamic compression (DC)). Chapter 6 investigated the factorial effects of cell expansion, hypoxia, and culture time to identify more suitable static pre-culture conditions on the scaffold before treatment with hypoxia and mechanical loading. Cell expansion had few effects, but mechanical properties and the hypertrophic phenotype increased continually up to the latest measured time point (9 weeks). Hypoxia suppressed both the hypertrophic phenotype and mechanical property development. Based on these outcomes, Chapter 7 investigated an intermediate pre-culture period in normal oxygen levels prior to a short-term treatment with hypoxia and mechanical loading (DC) to identify their effects on transcriptome-wide gene expression. The immediate MFC response to the combined treatment supported fibrocartilage histogenesis in an additive rather than synergistic manner. Chapter 8 described a series of four follow-up studies that used a shortened pre-culture period of 3 weeks based on experiences in Chapter 7 prior to hypoxia and mechanical loading treatments. First, the treatments were extended to five days and to include additional types of daily mechanical loading: i) a novel DC regime combining displacement and load control, and ii) cyclic hydrostatic pressure. The original DC regime, used in Chapter 7, was most effective in gene regulation. RNA sequencing showed that the longer-term combined treatment also supported fibrocartilage histogenesis, especially in promoting the hyaline cartilage-like aspect of the inner meniscus phenotype. The second and third studies of Chapter 8 showed that the gene expression response to DC saturated after 5 minutes and increased in magnitude with higher applied strain. The last study considered a long-term treatment of mechano-hypoxia conditioning,

applying continuous hypoxia with four daily incidents of DC. The outcomes included increased equilibrium dynamic modulus to levels that rival the native meniscus, although further experimentation is required. Chapter 9 summarized the work and suggested future research directions.

This thesis has three main contributions: i) the design of biomimetic meniscus scaffolds that can be used for complete meniscus tissue engineering; ii) the knowledge that the gene expression response of MFCs to combined hypoxia and mechanical loading is, after up to five days, primarily additive; and iii) the early evidence that combined hypoxia and mechanical loading, "mechano-hypoxia conditioning," can be a useful strategy to promote fibrocartilage histogenesis *in vitro* for MTE.

Preface

This thesis is an original work by Alexander Szojka. I am happy to discuss its contents and can be reached at my permanent email address, arszojka at gmail.com. As of September 2021, Chapters 3-8 and Appendices A, C, and D have been published in peer-reviewed journals as listed below. The published version of Chapter 8 underwent major truncation and subsequent peer-review, whereas the version included in this thesis is the original full length manuscript. Articles marked with * were equal first-authorships. Appendix B is not currently expected to be published elsewhere.

Chapter 3: A. R. Szojka, K. Lalh, S. H. Andrews, N. M. Jomha, M. Osswald, and A. B. Adesida, "Biomimetic 3D printed scaffolds for meniscus tissue engineering," *Bioprinting*, vol. 8, pp. 1–7, 2017

Chapter 4*: A. R. Szojka, B. D. Lyons, C. N. Moore, Y. Liang, M. Kunze, E. Idrees, A. Mulet-Sierra, N. M. Jomha, and A. B. Adesida, "Hypoxia and TGF-β3 Synergistically Mediate Inner Meniscus-Like Matrix Formation by Fibrochondrocytes," *Tissue Engineering - Part A*, vol. 25, no. 5-6, pp. 446–456, 2019

Chapter 5: A. R. Szojka, C. N. Moore, Y. Liang, S. H. Andrews, M. Kunze, A. Mulet-Sierra, N. M. Jomha, and A. B. Adesida, "Engineered human meniscus matrix-forming phenotype is unaffected by low strain dynamic compression under hypoxic conditions," *PLoS ONE*, vol. 16, no. 3 March, F. Zhao, Ed., e0248292, 2021

Chapter 6: A. R. Szojka, Y. Liang, R. d. C. Marqueti, C. N. Moore, E. J. N. Erkut, M. Kunze, A. Mulet-Sierra, N. M. Jomha, and A. B. Adesida, "Time course of 3D fibrocartilage formation by expanded human meniscus fibrochondrocytes in hypoxia," *Journal of Orthopaedic Research*, jor.25046, 2021

Chapter 7: A. R. Szojka, R. d. C. Marqueti, D. X. Li, C. W. Molter, Y. Liang, M. Kunze, A. Mulet-Sierra, N. M. Jomha, and A. B. Adesida, "Human engineered meniscus transcriptome after short-term combined hypoxia and dynamic compression," *Journal of Tissue Engineering*, vol. 12, 2021

Chapter 8, Appendix C, Appendix D: A. R. A. Szojka, D. X. Li, M. E. J. Sopcak, Z. Ma, M. Kunze, A. Mulet-Sierra, S. M. Adeeb, L. Westover, N. M. Jomha, and A. B. Adesida, "Mechano-Hypoxia Conditioning of Engineered Human Meniscus," *Frontiers in Bioengineering and Biotechnology*, vol. 9, Article 739438, 2021

Appendix A*: H. A. Elkhenany, A. R. Szojka, A. Mulet-Sierra, Y. Liang, M. Kunze, X. Lan, M. Sommerfeldt, N. M. Jomha, and A. B. Adesida, "Bone Marrow Mesenchymal Stem Cell-Derived Tissues are Mechanically Superior to Meniscus Cells," *Tissue Engineering Part A*, ten.TEA.2020.0183, 2020

During completion of this work, Alexander Szojka contributed to full-length manuscripts published in peer-reviewed journals that are not contained in this thesis. These are references [8–13]. Alexander Szojka is a co-first author on [12] and second author on [10, 13].

Studies with human tissues were conducted in accordance with the approval from the University of Alberta's Health Research Ethics Board, Biomedical Panel, study ID: Pro00018778.

Acknowledgements

Completion of this work was only made possible through the combined efforts of many hands and minds.

Foremost, I recognize Adetola Adesida, the Principal Investigator of this project and my supervisor. I owe him my sincere gratitude for taking me on as a student and for guiding my formation as a scientist and engineer. I thank and look up to him for his incredible work ethic in building an environment in which I was given every opportunity to succeed.

I next recognize the Canadian public and charitable donors for their financial support of basic science research. Their funding is responsible for all the data generated herein towards making cell-based meniscus replacements a reality and for enabling me to train as a scientist. I humbly thank them for the opportunity and aspire to return dividends on this investment throughout my career in service to my country.

I thank Aillette Mulet-Sierra and Melanie Kunze, the technical staff in Dr Adesida's lab, for years of good conversation and for thousands of aliquots and PCR reactions. I also thank Leila Laouar of the closely-affiliated Dr Jomha lab for her tremendous organizational efforts.

I extend my thanks to those who served as advisors and examiners throughout completion of this project. Specifically, these are Nadr Jomha and Samer Adeeb on my research committee, whose ideas and feedback led to drastic improvement in the quality of this work and whose many reference letters made it possible for me to acquire research funding. I thank Jana Rieger for her supervisory contributions in the early part of my studies, Hasan Uludag and Larry Unsworth for their thoughtful

Table of Contents

7 Human Engineered Meniscus Transcriptome After Short-term Combined Hypoxia and Dynamic Compression **126**

List of Tables

List of Figures

Chapter 1

Structural Differences Between the Inner and Outer Regions of the Adult Human Meniscus

This chapter has not been previously published nor peer-reviewed.

1.1 Introduction

This chapter introduces relevant aspects of human meniscus physiology as a lead-in to the central research question and hypothesis to be investigated. The chapter ends with an overview of the thesis chapter structure

1.2 Basic meniscus anatomy

The menisci are a pair of load-bearing soft tissue structures in the knee joint located between the hyaline cartilage of the femoral condyles and tibial plateau (Figure 1.1). They are bathed in synovial fluid, which provides nutrition and lubrication for joint movement. The menisci are wedge-like in cross-section and semi-lunar in superior view.

The menisci are anchored to the tibial plateau at their anterior and posterior ends and also to the joint capsule at their inferior peripheral edge. However, they retain some freedom to translate and deform. The shape and mobile nature of the

menisci allow them to dynamically increase congruence between articulating surfaces throughout the range of knee motion and loading[14]. In doing so, they protect the non-healing hyaline cartilage from excessive stress.
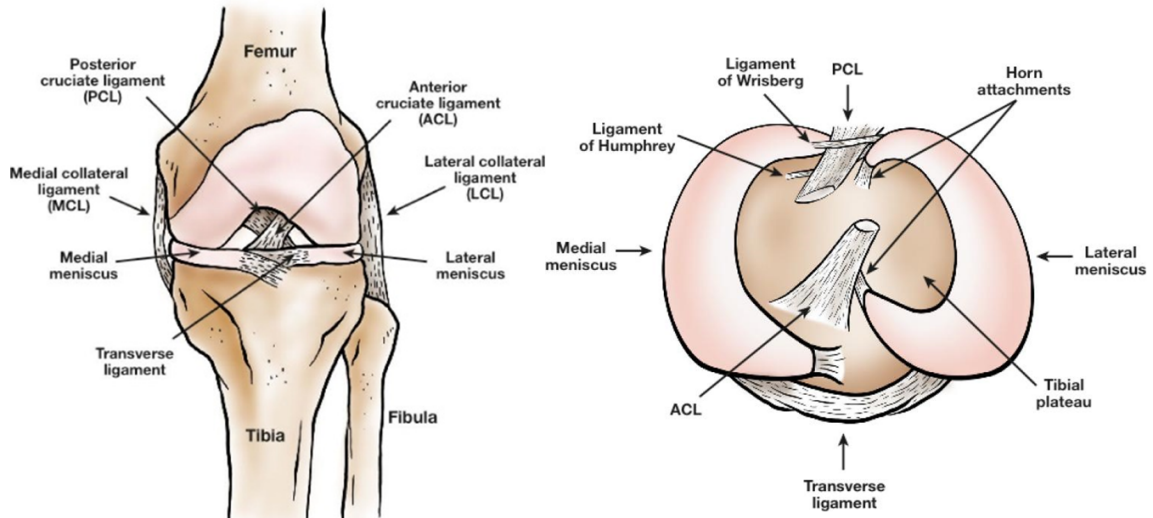
Figure 1.1: The knee menisci. Reproduced from [15].

Non-healing injuries to the menisci can disrupt their load-distributing function, which leads to damaging levels of stress on the articular cartilage. Over time, the cartilage becomes increasingly thin, which can be detected radiographically and is described as radiographic osteoarthritis (OA)[16]. Non-healing injuries to the menisci are thus a causal factor for early knee OA development[17]. Injuries to the menisci also occur incidentally during the normal progression of knee OA[18]. Although arthroscopic partial meniscectomy can help restore knee function following non-healing meniscus injury, it is also tied to early OA development[19, 20]. OA is a degenerative disease with no cure that afflicts millions of Canadians at great economic cost[21].

The menisci contain a heterogeneous population of cells known as meniscus fibrochondrocytes (MFCs) and a hydrated extracellular matrix (ECM)[22]. MFCs secrete, organize, and maintain the ECM, which provides the menisci with their functional mechanical properties. The main biochemical constituent of the menisci is type I

collagen. Type I collagen can be found throughout the entire meniscus structure. It is largely arranged in bundles oriented circumferentially and radially.

1.3 Inner and outer region differences

In adult humans, the menisci show differences between the outer and inner regions in: i) cell and ECM morphology; ii) blood supply and healing capacity; and iii) mechanical loading. These differences are summarized in Figure 1.2.

A) MFC and ECM morphology

Chondrocyte-like cells

Fibroblast-like cells

Large parallel bundles of type I collagen

B) Healing capacity and vascular supply

Vascular (healing)

Avascular (non-healing)

Vascular (healing)   Avascular (non-healing)

C) Loading environment

Circumferential stress state   Hydrostatic pressure
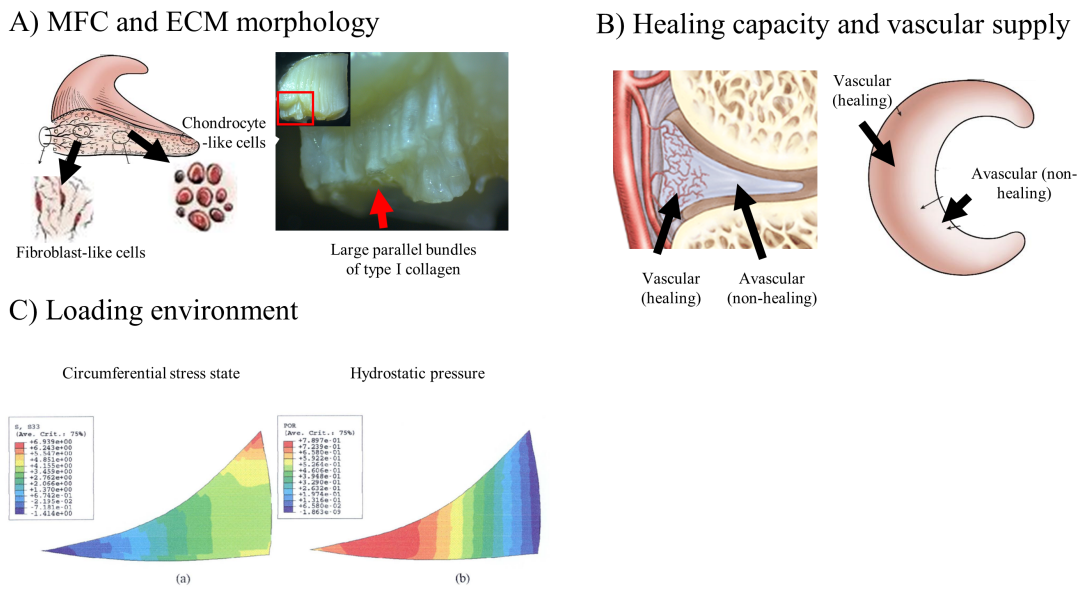
Figure 1.2: Inner vs. outer regional differences in the menisci. Images are adapted from [15, 24, 26]. Additional useful references include [23] and [25].

1.3.1 MFC and ECM morphology

MFCs from the outer regions are more elongated and fibroblast-like, whereas inner region MFCs are more ovoid and chondrocyte-like. Type II collagen and aggrecan, biochemicals usually associated with hyaline cartilage, appear only in the inner regions and are assumed to be synthesized by the more chondrocyte-like cells in the MFC population. The inner meniscus regions are classified as fibrocartilage because they contain type I collagen along with these hyaline cartilage-associated biochemicals.

1.3.2   Blood supply, oxygen, and healing capacity

Blood provides tissues with an oxygen supply mainly through hemoglobin, which increases the oxygen-carrying capacity of blood by about 50 times[27]. Blood also provides tissues with their healing capacity[27]. Only the outer meniscus regions have a blood supply and the ability to heal[28]. Hemoglobin is absent in the synovial fluid surrounding the menisci and what little oxygen is present, ranging from 0 to 7% saturation, is rapidly depleted during even light exercise[29]. Thus, the inner regions of the menisci have limited access to oxygen and resident cells thus exist in low oxygen conditions known as hypoxia (HYP).

1.3.3   Mechanical loading

Upon loading, the outer regions of the menisci transmit tensile forces between their bony attachment sites. The tension is resisted by the bundles of type I collagen[23]. The weight-bearing inner regions transmit compression forces across the joint. These forces are transmitted by water in the ECM, which is retained upon loading by the localized network of type II collagen and aggrecan[30, 31].

1.4   Research question and hypothesis

How do the spatial differences in MFC and ECM morphology, blood supply and healing capacity, and mechanical loading in the adult human menisci relate to one another? This is an interesting question from clinical and tissue engineering perspectives. Non-healing meniscus injuries pose a large disease burden through their contribution to knee OA development. Further, successful generation of engineered meniscus grafts will likely require that they have similar matrix morphology to healthy meniscus, and the answer to this research question could lead to a biomimetic strategy to promote this process. The hypothesis proposed and investigated in this thesis is that blood supply (specifically oxygen supply) and mechanical loading are jointly

responsible for regulating the ECM-forming behaviour of MFCs to produce the avascular phenotype of the adult inner meniscus regions.

1.5   Thesis overview

An outline of this thesis is provided in Table 1.1. Each of chapters 3-8 begins with a contextualizing preface followed by an abstract detailing the project or experiment as in typical stand-alone peer-reviewed articles.

The central hypothesis of this work is first tested in Chapter 2 by a literature review spanning developmental biology, comparative anatomy, and tissue engineering experiments. Chapter 3 diverged from the hypoxia and mechanical loading theme to focus on the scaffold aspect of meniscus tissue engineering using 3D printed polycaprolactone. The remaining chapters turned to actual tissue formation using human MFCs from partial meniscectomy specimens. Chapter 5, Chapter 7, and Chapter 8 directly test for interactions between hypoxia and mechanical loading at the molecular and protein levels, while Chapter 4 and Chapter 6 test the effects of hypoxia under various static conditions. Chapter 3 and the Appendices detail projects that are only indirectly related to the central hypothesis that were carried out incidentally as interesting paths for investigation. All of these projects fall under the more general theme of meniscus tissue engineering.

Table 1.1: Thesis chapter structure. Apart from Chapter 3 and Appendix A, all studies used human MFCs. Chapters 5-8 and all appendices used porous type I collagen scaffolds. HYP: hypoxia, DC: dynamic compression, CHP: cyclic hydrostatic pressure.

Chapter	Description
1	Thesis development
2	Review of HYP and mechanical loading
3	Design of biomimetic meniscus scaffolds
4	HYP & TGF-β3 supplementation in pellets
5	Long-term (2 week) HYP, low strain DC, and TGF-β3 supplementation
6	Cell expansion, HYP, and culture time
7	Short-term (24h) HYP and high strain DC
8	Mechano-hypoxia conditioning • Medium-term (5 days) HYP & high strain DC or CHP • DC loading saturation (5 vs 60 minutes) • DC loading aggression (pre-culture duration, strain) • Long-term (3 week) mechano-hypoxia conditioning
9	Summary and future directions
Appendices	
A	Functional comparison of MFCs and BMSCs
B	MFC yields from meniscus specimens
C	Seeding density pilot study
D	Orbital shaking pilot study

Chapter 2

Hypoxia and Mechanical Loading in Development of the Non-Healing Inner Meniscus Phenotype

This chapter has not been previously published nor peer-reviewed.

2.1 Introduction

This chapter reviews the literature concerning the fibrocartilaginous phenotype of the adult human inner meniscus regions to identify the likely contributions of hypoxia and mechanical loading. The topics reviewed are: i) human meniscus developmental biology; ii) comparative anatomy of meniscus, dense fibrous connective tissues, and hyaline cartilage; and iii) meniscus tissue engineering studies manipulating oxygen tension and mechanical loading. The chapter concludes with a brief synthesis and summary highlighting gaps in the literature.

2.2 Human meniscus developmental biology

Researchers have long speculated that mechanical loading—especially weight-bearing—during development and life is related to i) the progressive refinement of the organization and composition of meniscus ECM, and ii) the recession of blood vessels from the inner regions[28, 32–37]. At 14 weeks of development, meniscus cells are fibroblast-

like with little intervening ECM and appear disorganized (Figure 2.1). The earliest reported organization of meniscus ECM into circumferential and radial directions is at 17-weeks of development[34]. Interestingly, this nearly coincides with early detection of fetal leg movements at 15 weeks[38]. This suggests that the mechanical loading resulting from these movements could plausibly play a role in supporting the organization of meniscus cells and their ECM.

14 weeks   17 weeks   25 weeks
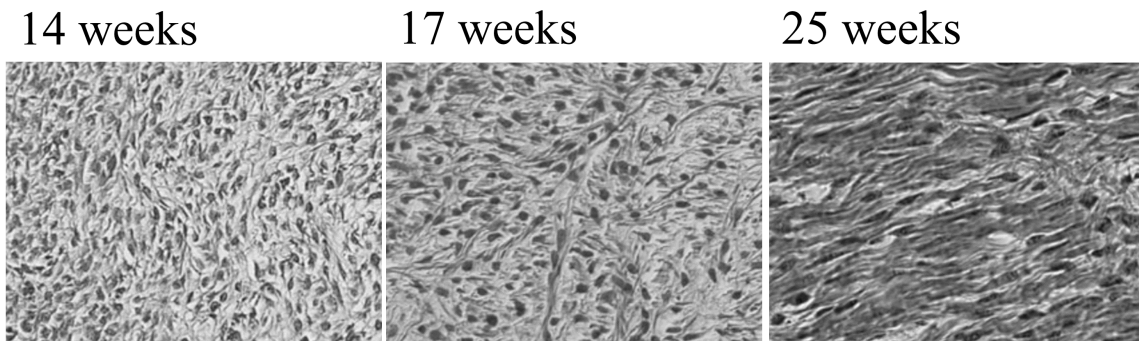
Figure 2.1: Human meniscus cell and ECM morphology in pre-natal development. Adapted from [34]. Useful images of post-natal development are available in [35]; unfortunately permission to reprint these here was not granted by the copyright holder.

Although chondrocyte-like cells have been observed in the menisci of newborns, type II collagen was not detected in fetal menisci[32]. In a large study in the early 1980s, fibrocartilage was reported as absent in meniscus specimens from fetuses and children up to age 11 but abundant in adults[33, 35]. However, fibrocartilage matrix was recently (2021) demonstrated in child cadaver menisci via Safranin-O staining but with no type II collagen detected[39]. The authors indicated by personal communication that positive Safranin-O staining in the inner regions of the menisci was consistently observed in meniscus specimens from donors as young as 0-2 years old[39]. It can be inferred that processing and staining or visualization techniques have wide ranging sensitivity differences for detecting the fibrocartilage phenotype. Overall, this indicates that the fibrocartilage phenotype may be a gradual development after birth.

While the menisci are fully vascularized at birth, blood vessels begin to recede from the inner regions by 3 months. By 11 years, only the occasional vessel penetrates into

the inner regions[33, 35, 36](Figure 2.2). At 18 years, only the outer 1/3 is vascularized and after 75 years, only the outermost margin[28, 36]. Notably, the non-weight-bearing meniscal insertions retain a greater blood supply than the weight-bearing inner meniscus regions[28]. This suggests that weight-bearing is likely a key factor in the meniscus de-vascularization process.
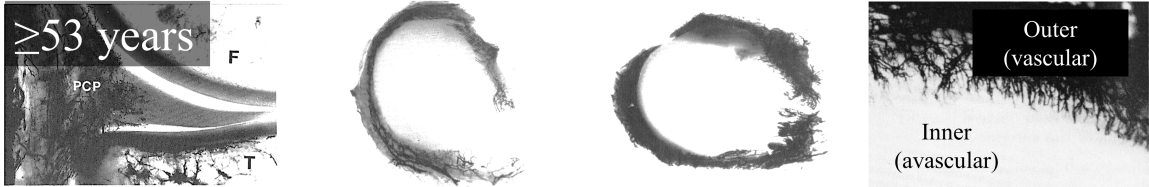
Figure 2.2: Human meniscus blood supply. Blood vessel detection in cadavers by India ink injection (all specimens ≥53 years). Adapted from [28]. Useful images for comparison are available in [36], but unfortunately permission to reprint these images was not granted by the copyright holder.

The morphological changes in the menisci during development and life have also been investigated at the molecular level.

Vascular endothelial growth factor (VEGF) is a pro-angiogenic factor that stimulates endothelial cell proliferation and migration. VEGF increases ECM permeability to facilitate blood vessel invasion with potential effects on mechanical properties. It can be induced by inflammatory cytokines, mechanical overload, and hypoxia through hypoxia inducible factor-1 (HIF-1). It can be suppressed by the fluid pressurization that occurs during normal loading of cartilaginous tissue[40]. *VEGF* is expressed in fetal menisci and in menisci from OA joints in the outer region and near injuries, but is down-regulated in healthy adult menisci[32, 41].

Endostatin, which is a fragment of type XVIII collagen, and chondromodulin-1 (encoded by *CNMD* gene) are anti-angiogenic factors that act in part by suppressing VEGF effects on endothelial cells. Along with aggrecan and type II collagen mRNA precursors, *CNMD* transcription is regulated through SOX9, which is in turn regulated through HIF-1 and mechanical stress. Endostatin was more expressed in the

inner regions of normal adult menisci and *CNMD* more in the inner regions in menisci from OA joints[32, 42]. One author speculated that high expression of anti-angiogenic factors in the fibrocartilaginous adult inner meniscus may suppress inward growth of blood vessels to maintain its avascular nature and mechanical integrity[43].

Not all studies show the same trends in expression of pro- and anti-angiogenic factors. A proteomic study of adult healthy menisci did not show detection of VEGF nor chondromodulin-1 in the menisci. However, type XVIII collagen, indicative of endostatin, was detected in the outer region along with high levels of other anti-angiogenic factors including thrombospondin-1 and -3 in all regions[44].

Taken together, these studies suggest that regulation of blood vessels in the menisci is not just a macroscopic physical process due to weight-bearing; rather, it likely incorporates some degree of molecular control at the cellular level as well.

In summary, the differences between the inner and outer meniscus regions become more distinct throughout development into adulthood. The organization of meniscus ECM seems to be influenced by joint movement and especially load-bearing. The progressive loss of vascularity and development of fibrocartilage occurs in a similar time frame to increases in load bearing. Anti-angiogenic factors may suppress blood vessels in the inner meniscus regions to maintain its fibrocartilaginous phenotype and their expression is related to both vascular supply and mechanical loading. These observations are all consistent with the hypothesis that vascular supply (specifically oxygen) and mechanical loading co-regulate MFC and ECM morphology in the human menisci. An overview of human meniscus development is presented in Figure 2.3.

2.3   Comparative anatomy of human meniscus

Fibrocartilage appears in many tissues including the inner meniscus, the annulus fibrosus of the intervertebral disc, the enthesis where tendons and ligaments connect to bone, and the temporomandibular joint. Fibrocartilage can be described as an intermediate phenotype between dense fibrous connective tissues, e.g., ligament and

Prenatal

First year

Year 1+

14-15 weeks
Cells: dense fibroblasts
ECM: absent, no alignment
Vasc.: ubiquitous
Mechanics: Limb movements detectable

17-18 weeks
Cells: Parallel alignment & spindle-shaped, express VEGF and endostatin
ECM: Collagen bundles

~23-25 weeks
ECM: Arranged in circumferential and radial directions

Newborn (40 weeks)
Cells: occasional chondrocytes in small isolated islands
ECM: no sudden change
Mechanics: Birth, more freedom of motion

3 months
Cells: Lower density
ECM: More collagenous
Vasc.: Most in outer 2/3 (early recession)

6-9 months
Cells: More chondrocytes identified
Vasc: Inner 1/3 has only occasional vessels
Mechanics: Crawling or walking

1.5-9 years
ECM: More organized and refined, Safranin-O staining in inner region
Vasc.: Progressive loss
Mechanics: Increasing load-bearing

10-11 years
ECM: Reported as non cartilaginous
Vasc.: Outer 1/3, occasionally penetrating inwards

Young adult
Cells: Meniscus fibrochondrocytes. No (limited?) VEGF detected. Endostatin higher in inner meniscus
ECM: Abundant fibrocartilage in inner 2/3
Vasc: Outer 1/3 only

Later life (age 50+)
Cells: VEGF may appear in outer or injured regions. *HIF-1α* (mRNA) and ChM-1 may be higher in inner region (possibly OA-related)
ECM: Wide individual differences. Increased Safranin-O staining and even calcification in degeneration and disease
Vasc.: Restricted to outer 10-30%

Figure 2.3: Summary of human meniscus developmental milestones concerning cell and ECM morphology, vasculature (vasc.), and mechanics.

tendon, and hyaline cartilage. These tissue types show differences in cell and ECM morphology, blood supply and healing capacity, and mechanical loading, which can be presented as a spectrum to contextualize the phenotypes of the adult human menisci (Figure 2.4)[45, 46].

Fibrocartilage also appears in ligaments and tendons that wrap around bones in the vicinity of the articular region and this is described as an adaptation to compressive loading (Figure 2.5A)[52, 53]. Remarkably, grafting a direct "pure-tension" tendon to a wrap-around "tension-compression" region results in fibrocartilage formation in the articular region (Figure 2.5B). Further, grafting a fibrocartilaginous wrap-

11
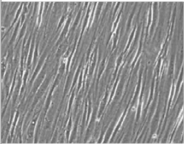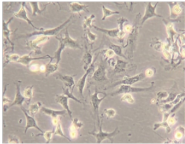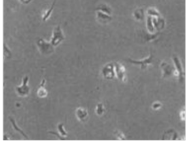
	Dense fibrous connective tissue	Fibrocartilage			Hyaline cartilage
	Tendon, ligament	**Outer meniscus**	**General fibrocartilage**	**Inner meniscus**	**Articular cartilage**
Main mechanical function and properties	Tension. Tensile elastic modulus: 800 MPa (adult Achilles tendon) (Waugh 2012)	Tension. Tensile elastic modulus 50-150 MPa circumferentially, 2-20 MPa radially (Tissakht 1995)	Tension and compression. Properties vary from tissue to tissue	Compression and tension. Compression equilibrium modulus: 0.1-0.2 MPa (Chia 2008)	Compression. Compressive equilibrium modulus: 0.8 MPa (Mow 1980)
Vascular supply, healing capacity	Good, some healing	Good initially but recedes over time, some healing	None	None	None
Cells	Fibroblasts	Fibroblast-like, usually grouped into MFC category	Fibrochondrocytes	MFCs (mixed fibroblast-like and chondrocyte-like cells in inner regions)	Chondrocytes
ECM morphology and composition	Dense parallel collagenous bundles. Contains type I and not II collagen, versican, decorin, biglycan, fibromodulin	Dense parallel collagenous bundles. Contains type I collagen, versican, decorin, biglycan, fibromodulin	Parallel bundles with islands of cartilaginous ECM. Contains variable amounts of types I and II collagens (e.g. 50:50 ratio in annulus fibrosus); versican and aggrecan, decorin, biglycan, fibromodulin	Amorphous. Contains mostly type I collagen with traces of type II, aggrecan.	Zones (superficial: collagen fibres aligned with surface; middle: fibres mixed orientation; deep: fibres perpendicular to surface). Contains collagen 50-73% (type II abundant, type I absent), aggrecan (GAGs 15-25% dry weight) (AufderHeide, 2004)
Phenotypic plasticity	Develops into fibrocartilage when grafted into a wrap-around region (compression)	See inner meniscus	Converts to dense fibrous connective tissue when joint is fixed and when grafted from wrap-around (compression) region to direct tension	Adipogenic, chondrogenic differentiation *in vitro*; capacity falls with prolonged expansion	Defects fill with fibrocartilage; cells become fibroblast-like with extended monolayer expansion

Figure 2.4: A spectrum for general comparison of adult dense fibrous connective tissues, fibrocartilage, and hyaline cartilage[47–51].

around tendon to a pure-tension region results in loss of fibrocartilage phenotype (Figure 2.5C). This evidence indicates that mechanical forces can directly cause the development or loss of the fibrocartilage phenotype.

In human tendon, *VEGF* was found expressed in fetal but not adult tendons, similar to its expression pattern in the menisci[40]. Interestingly, in a direct tendon *VEGF* was continually expressed throughout development but became down-regulated in the articular region of a wrap-around tendon after week 20 of pregnancy[40]. This was

consistent with increasing fetal movements around this time, suggestive of a mechanical role in *VEGF* regulation[40]. Cyclic hydrostatic pressure (CHP) down-regulated *VEGF* six-fold in monolayers of rat tendon cells[40]. These results indicate that the avascular nature of fibrocartilage tissue such as that found in the inner meniscus regions may be related to downregulation of pro-angiogenic factors by compressive loading.

Pauwels's theory of causal histogenesis proposes that the structure of connective tissues is the product of the mechanical stress environment that they experience[53]. The specific stimulus for cartilage histogenesis is proposed to be hydrostatic pressure at the cellular level, which can manifest at the tissue level as macroscopic tension or compression[53]. A rival theory proposed by Krompecher suggests that the specific stimulus for cartilage histogenesis is actually hypoxia, which occurs incidentally in pressurized soft tissues due to the occlusion of blood vessels[46, 54]. Extended to the menisci, this would suggest that the fibrocartilage phenotype of the inner regions may not entirely reflect developmental pre-programming, but rather the general adaptive response of connective tissues to mechanical loading mediated through hypoxia. This is consistent with how fibrocartilage in meniscus is confined to the inner weight-bearing regions and how its development appears to coincide with the initiation of weight-bearing.

In summary, fibrocartilage has many intermediate properties between the extremes of dense fibrous connective tissues and hyaline cartilage. The adult human menisci are more like dense fibrous connective tissues in their outer regions and fibrocartilage in their inner regions. The phenotypic plasticity demonstrated by tendons in the presence of compressive loads are reminiscent of the changes occurring in the menisci during the period of increasing load-bearing.
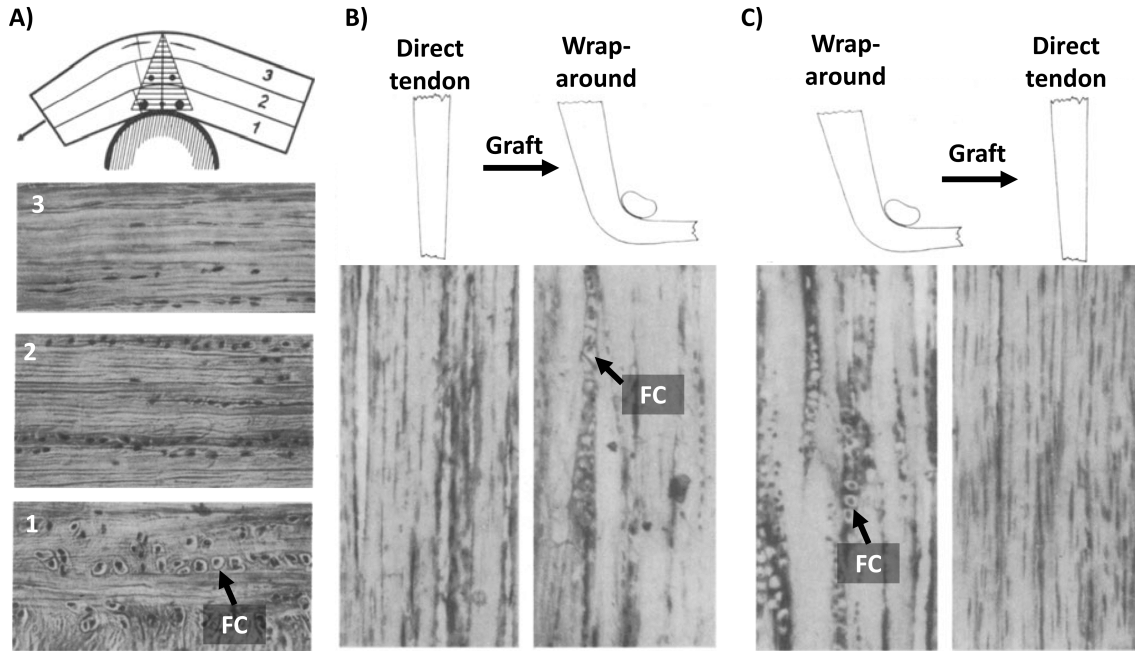
Figure 2.5: Fibrocartilage (FC) appearing in tendons in regions of compression. Adapted from Pauwels, 1980 (original sources Pauwels, 1940 and Ploetz, 1937)[53].

2.4 Review of hypoxia and mechanical loading in meniscus tissue engineering

Most studies of human native meniscus are observational in nature for practical and ethical reasons. Tissue engineering models make experimental study of human meniscus cells and tissue more feasible. Meniscus tissues are first obtained from sources such as cadavers, partial meniscectomies of the non-healing inner regions, and complete joint replacements. Cells are then isolated and often allowed to proliferate. The cells can then be stimulated by growth factors such as transforming growth factor β 1 or 3 (TGF-β1, TGF-β3) to form meniscus-like engineered tissues in 3-dimensional models. These models can be scaffold-free, such as in pellets and self-assembled constructs, or scaffold-based, using biomaterials such as type I collagen sponges and hydrogels. Regardless of the model, many replicates can be created that can then be divided into various conditions for comparison. Their responses can then be studied and related to what the native meniscus might experience in the body.

The degree to which results in such model systems can be related to the native meniscus is a question of external validity. Experiments in meniscus and cartilage tissue engineering take place in time frames of days up to a year under controlled conditions; in contrast, the human lifespan spans decades with wide inter-person variations in experience. Thus, the external validity in extrapolating results in engineered meniscus tissue models to the native meniscus is, generally speaking, low. However, these model systems are the best available strategy for experimental study of human tissues. Further, the mechanisms of gene regulation in response to stimuli such as low oxygen or mechanical loading may be similar *in vitro* and *in vivo*, even if, for example, dynamic compression (DC) doesn't accurately simulate a person exercising. Finally, these model systems provide information that can be directly applied towards improving engineered meniscus towards clinical applications.

The next sections review: i) hypoxia in meniscus tissue engineering with human MFCs; ii) mechanical loading in meniscus tissue engineering with human MFCs; and iii) combined hypoxia and mechanical loading in cartilaginous tissue engineering.

2.4.1 Hypoxia in meniscus tissue engineering with human MFCs

Almost all studies investigating human meniscus-derived cells under low oxygen (hypoxia relative to atmospheric levels of 20% O_2) come from Adesida-associated research groups starting in 2006. These articles are summarized in Table 2.1 (scaffold-free) and Table 2.2 (scaffold models). Other researchers have investigated oxygen effects on meniscus cells from animal sources, but those are not considered here.

Table 2.1: Hypoxia in meniscus tissue engineering with human MFCs in scaffold-free models

Author, year	Experiment setup	Manipulated variables	Outcomes	Conclusions
Adesida *et al.*, 2006[55]	OA joint menisci. Expand in 20% O_2, form pellets	FGF-2 during expansion, 5 or 20% O_2 during culture	HYP increased *SOX9*, *COL1A2* with FGF-2 only, increased proteoglycans but not collagen II	Hypoxia is useful following FGF-2 in expansion
Adesida *et al.*, 2007[56]	OA joint menisci. Divide into outer 1/3, inner 2/3. Measure tissue gene expression. Expand cells in 20% O_2. Form pellets.	Outer vs. inner tissues, outer vs. inner MFCs with 5 or 20% O_2.	Tissues: inner 2/3 more *HIF-1α* and mRNA of its targets. Pellets: HYP lowered *COL1A2* for outer MFCs and increased it for inner MFCs, and increased *COL2A1* for both but especially outer MFCs which had minimal expression in NRX.	HYP may regulate inner meniscus phenotype, but inner and outer MFCs have differing responses
Liang *et al.*, 2017[8]	Partial meniscectomy (younger donors, inner region). Expand (TGF-β1 and FGF2) (T1F2). Form pellets.	Model (monolayer vs pellets), expansion degree (8 to 4000-fold), 3 vs. 20% O_2	Expansion reduces chondrogenic phenotype. HYP increased chondrogenic gene & protein markers.	MFCs chondrogenic up to P2 (64-128 fold expansion with T1F2). Partial meniscectomy and OA menisci respond similar to HYP in pellets.

Table 2.2: Hypoxia in meniscus tissue engineering with human MFCs in scaffold-based models

Author, year	Experiment setup	Manipulated variables	Outcomes	Conclusions
Adesida *et al.*, 2012[57]	OA joint menisci. Expand (FGF-2). Seed type I collagen sponge-like scaffold (DuraGen).	3 or 20% O_2 for both expansion and tissue culture.	HYP decreased type II collagen, no change to proteoglycans.	HYP response in this scaffold differs from the pellet model.
Croutze *et al.*, 2012[58]	OA joint menisci. Divide into outer 1/3, inner 2/3. Expand FGF-2. Measure monolayer gene expression. Seed type I collagen sponge-like scaffold (DuraGen).	Expansion degree (P1 vs. P3), much lower fold increases than Liang *et al.* 2017. 3 and 20% incubator O_2 for both expansion and tissue culture.	In monolayers, both expansion and HYP decreased chondrogenic genes. HYP reduced chondrogenic gene and protein markers. Inner, outer MFCs were effectively equivalent.	Chondrogenic gene expression is lost with monolayer expansion. HYP response in this scaffold differs from pellets. Cell isolation region not important in this scaffold.
Tan *et al.*, 2011[59]	OA menisci. Expand inner middle region MFCs. Seed layered scaffold of PLGA, hyaluronic acid, chitosan, types I/II collagens, and chondroitin-6-sulfate.	Expansion degree (P1-4, no growth factors). 2 or 20% O_2 for P3 cells and scaffolds.	Expansion past P1 reduced chondrogenic phenotype. HYP increased proliferation and increased mRNA of col I and chondrogenic markers.	Chondrogenic gene expression is lost in monolayer expansion. HYP in these scaffolds was similar to that seen in pellets and dissimilar to the type I collagen sponge scaffold.

In pellets, hypoxia promoted formation of cartilaginous ECM components aggrecan and type II collagen through $SOX9$[8, 56, 60]. This finding is consistent with another that the inner meniscus has increased mRNA expression levels of $HIF\text{-}1\alpha$ and its target genes[56]. Hypoxia was observed to have similar cartilage-promoting effects in pellets of MFCs regardless of whether the meniscus tissues came from partial meniscectomy or joint reconstructions for severe OA, although these were not compared in a single study. A similar pro-cartilage effect was observed for hypoxia in a scaffold-based culture model using a multi-layered "biomimetic" biomaterial containing types I/II collagens and chondroitin-6-sulfate, a glycosaminoglycan found in aggrecan[59]. Interestingly, in a type I collagen sponge-like scaffold the hypoxia response of MFCs differed from the pellet model: culture in hypoxia actually hindered the chondrogenic response of MFCs compared to 20% O_2[57, 58]. It has been proposed that this is related to the MFC tissue source, although the outcomes in the pellet model suggest it is more likely related to the type I collagen scaffold affecting cell behaviour.

Summary

Taken together, these studies show that human MFCs can respond to hypoxic conditions by promoting expression of the hyaline cartilage-type matrix phenotype *in vitro*, but that the effect is sensitive to the culture model being used. This provides mechanistic support at the cellular level for how the fibrocartilage phenotype may develop in the inner regions of the menisci in response to mechanical loading and the resultant hypoxic environment.

2.4.2 Mechanical loading in meniscus tissue engineering with human MFCs

Mechanical loading of tissue engineered constructs is a promising strategy to enhance development of functional mechanical, biochemical, and histological properties. Types of mechanical loading include uniaxial DC and tension, shear, static and intermittent hydrostatic pressure, and combinations of these. DC involves alternating

linear compression and de-compression of a typically cylindrical-shaped tissue between two flat platens, although it can also be performed in a meniscus shape with a rounded indenter intended to mimic aspects of the femoral condyles in the knee. Dynamic tension involves stretching and de-stretching a band of tissue that is typically secured at either end by a clamp or by wrapping the tissue around posts. Shear is typically applied at a tissue surface using a loading device that rotates in alternating directions. Shear can also be fluid-based, for example via forced perfusion. Hydrostatic pressure mechanical loading involves pressurization of the medium surrounding a tissue, for example by pressurizing the air above the medium using a pump. The mechanical loading applied in an experiment is designed to mimic aspects of the native tissue environment. For example, dynamic tension may be most appropriate for tissue engineering tendon, whereas compression, shear, or hydrostatic pressure may be favoured for cartilage and meniscus. Most experiments are limited to a single type of loading for practical reasons.

Mechanical loading can provide cues that affect cell proliferation, metabolism, and differentiation as well as ECM organization, degradation, and synthesis[61]. Deformation-based mechanical loading, i.e., DC, tension, and shear can improve nutrient and waste transfer[61]. There is evidence that deformational loading can also provide a directional information to facilitate ECM organization; impressively, assembly of collagen fibres was improved under dynamic loading conditions even in the absence of cells[62]. An honest review of the tissue engineering literature, however, will show that the effects of mechanical loading are variable and sensitive to factors such as the applied loading regime, construct maturity, scaffold material, and many other factors[63]. Generally, hypoxia is more robust as a stimulus for promoting cartilage synthesis than is mechanical loading.

Mechanical loading of tissue engineered constructs has been best studied using articular chondrocytes and mesenchymal stem cells. A comprehensive review as of 2017 of DC studies in articular chondrocytes is provided in [63], and a review of meniscus

mechano-biology is provided in [64]. Mechanical loading studies in meniscus often use animal derived cells. As of 2020, there are only five published mechanical loading studies using human meniscus-derived cells, apart from those included in this thesis. These five studies are summarized in Table 2.3 and Table 2.4. No studies before this research project apply DC to engineered meniscus tissues made with human MFCs. For this reason, the review here is extended to include studies applying DC in meniscus tissue engineering using animal cells (Table 2.5). Studies of mechanical loading types besides DC with animal MFCs, studies using MSCs and not MFCs, and studies aiming to generate other tissues (even other types of fibrocartilage) were considered outside the scope of this short review. However, they are often referenced in later chapters in this thesis where appropriate.

Table 2.3: Hydrostatic pressure in meniscus tissue engineering with human MFCs

Authors, year	Experiment details	Manipulated variables	Outcomes	Conclusions
Suzuki *et al.*, 2006[65]	Partial meniscectomy. Isolate and pre-culture cells in alginate 3 days	One application of intermittent or static hydrostatic pressure for 4h	Cyclic and static hydrostatic pressure increased type I collagen mRNA but not aggrecan. Static reduced MMP-1, MMP-13; cyclic increased TIMP-1 and -2.	Hydrostatic pressure had early support for type I collagen synthesis and maintenance
Zellner *et al.*, 2015[66]	OA joint menisci. Divide outer 1/3, inner 2/3. Expand and form pellets.	Intermittent hydrostatic pressure for week 1 only. Weeks (1, 2, 3). Outer vs. inner.	Intermittent hydrostatic pressured delayed ECM accumulation especially for inner, but it later improved type II collagen in both regions and sGAG in inner.	Intermittent hydrostatic pressure had a delayed benefit of improved ECM formation. Outer cells had better chondrogenic potential.

Table 2.4: Dynamic tension in meniscus tissue engineering with human MFCs

Authors, year	Experiment setup	Manipulated variables	Outcomes	Conclusions
Baker *et al.*, 2010[67]	OA joint menisci. Expand outgrown cells. Load onto polycaprolactone strips and culture 7 weeks.	Add cyclic tensile loading for 2 weeks.	Loading had small increase in tensile stiffness for 2/3 donors, collagen for 1/3.	Very weak evidence for dynamic tensile loading's utility. Only an abstract was published.
Kanazawa *et al.*, 2012[68].	OA joint menisci. Divide inner/outer. Expand and seed collagen I-coated stretchers for 24h.	2, 4, 8h loading (0.5 Hz, 0-5%). Inner vs outer.	Loading increased *COL2A1* and *SOX9* in inner, and *COL1A1* in outer. In inner, stretch increased *SOX9* phosphorylation and *SOX9* enhancer activity in *COL2A1*.	Inner and outer tension responses differ. Tension in inner cells may regulate type II collagen.
Furumatsu *et al.*, 2012[69]	OA joint menisci. Divide inner/outer halves. Expand seed collagen I-coated stretchers for 24h.	0, 2, 4h of loading (0.5 Hz, 0-5%). Inner vs outer cells. CTGF supplementation.	More CTGF in outer region. Loading increased *COL1A1*, *CTGF*, and CTGF protein in inner. Loading increased Smad2/3 in inner. Loading induced Smad3 to CTGF promoter.	Inner and outer tension responses differ. Stretch induces CTGF with Smad3 in inner cells and may have a role in the inner meniscus phenotype.

Table 2.5: DC in meniscus tissue engineering with animal MFCs. GFs: growth factors. FBS: fetal bovine serum.

Authors, year	Experiment setup	Manipulated variables	Outcomes	Conclusions
Huey & Athanasiou *et al.*, 2011[70]	Bovine calf MFCs mixed 1:1 with articular chondrocytes. Fresh cells in "meniscus-like" molds pre-cultured 10 or 17 days. Load (1h/day cycling 1 min on/off, 1 Hz, 0-10%) in medium (without GFs).	Loading start day. Loading had a compression and tension component due to geometry.	Early loading showed functional property gains, reaching 280 kPa relaxation modulus.	Mechanical stimulation can enhance matrix and mechanical properties.
Ballyns & Bonassar *et al.*, 2012[71]	Bovine calf MFCs. Fresh cells (50 M/mL) in alginate meniscus shape. Medium 10% FBS, no GFs.	0/7/15% strain, 3x/wk 1h on/off/on, 1 Hz	DC superior outcomes at 2 but not 6 wks. Higher strain better.	Long-term DC performance needs more study.
Puetzer *et al.*, 2012[72]	Bovine calf MFCs. Fresh cells in 2% alginate meniscus shape. Medium 10% FBS, no GFs.	7/15% strain, 3x/wk, 1h on/off/on, 1 Hz. Part 1: Load 1/2/4 wks with rest up to 4 wk total. Part 2: Load 2 wks, rest 0/2/4 wks.	Loading had mixed outcomes. Better matrix under loading but generally less GAG.	The benefits of loading not very clear. Edit experiment parameters for future work.

Table 2.5: *Continued from previous page*

Puetzer & Bonassar, 2016[73]	Bovine calf MFCs. Fresh cells in type I collagen gel in meniscus shape, clamped at horns. Medium 10% FBS, no GFs.	3x/wk, 1h on/off/on, 1 Hz. 2/4/6 wks, 5/10% strain (at horns).	More leading improved eq. compression modulus. Biochem. not clear, possibly more GAG in compression.	Physiological loading and clamping are desirable for meniscus-like architecture formation.

Summary

While mechanical loading treatments can have pro-fibrocartilage effects, they are not always consistent across different types of related measurements (i.e., combinations of gene expression and mechanical, biochemical, and histological properties). This highlights the challenge of achieving efficacious mechanical loading in engineered tissues, which is noted in reviews on the subject[63, 74]. The evidence indicates that mechanical loading can influence MFC behaviour through means other than development of a hypoxic microenvironment as occurs physiologically. Notably, in tissue engineering model systems *in vitro* there are no blood vessels to occlude and thereby promote hypoxia. However, mechanical loading can still promote hypoxia by impeding nutrient transfer at the interface of a loading platen or a clamp.

2.4.3 Combined hypoxia and mechanical loading in cartilaginous tissue engineering

The combination of hypoxia and mechanical loading in cartilage development has been discussed since the 1960s[54, 75]; however, research in this domain remains limited. There is no published research on combined hypoxia and mechanical loading in meniscus tissue engineering, although the idea was proposed in a PhD thesis and related grant (2009-2012)[76]. The studies that directly investigate combined hypoxia and mechanical loading for cartilaginous tissue engineering are reviewed in Table 2.6. Two reviews on the subject (2011 and 2015) provide useful diagrams of how hypoxia and mechanical loading may affect cartilaginous tissue formation, which are reproduced in Figure 2.6 and Figure 2.7.
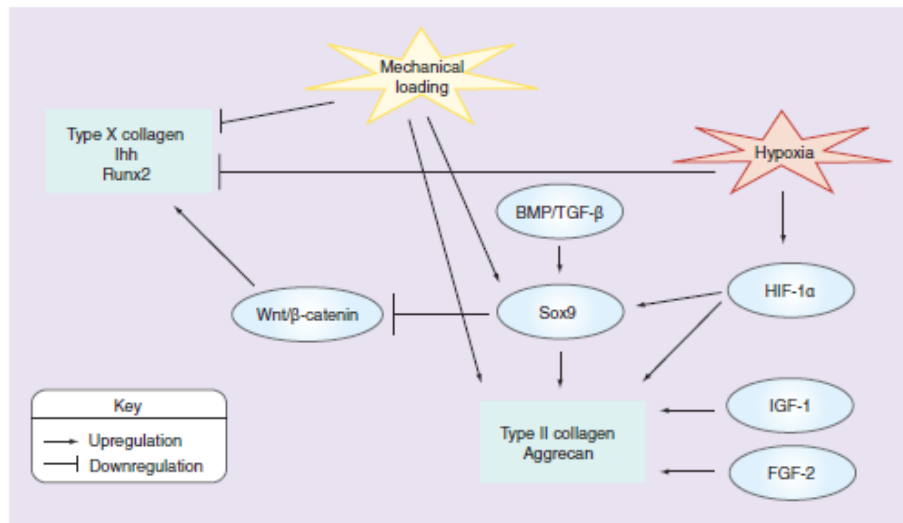
Figure 1. Signaling pathways modulating mRNA expression of chondrogenic genes. Both moderate hypoxia and mechanical loading inhibit pathways leading to hypertrophy and osteogenesis while stimulating the production of cartilage-building proteins.

Figure 2.6: Interactions of hypoxia and mechanical loading in chondrogenic gene regulation. Reproduced from [77].
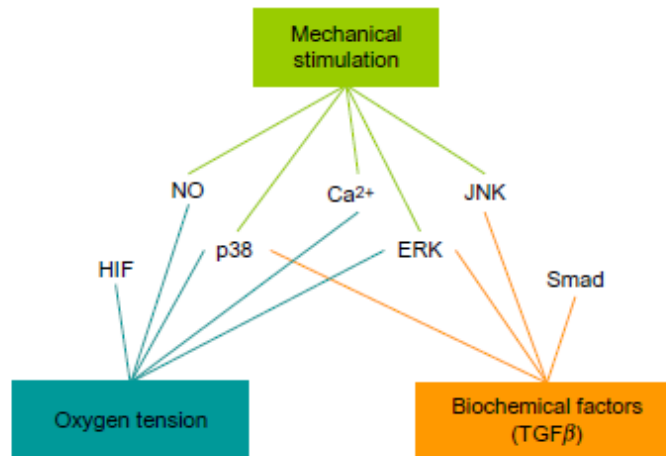
Figure 2.3 Reaction of cells to their environment. Cells react to their environment through activation of different intracellular signaling pathways. Whereas a specific environmental factor can act through several pathways, a specific pathway can be activated by different exogenous factors. Therefore, the cellular response to one specific stimulus is always dependent on other environmental factors as well. HIF, hypoxia inducible factor; NO, nitric oxide; ERK, extracellular signal-regulated kinase; JNK, c-Jun N-terminal kinase.

Figure 2.7: Interactions of hypoxia and mechanical loading in cell signalling. Reproduced from [78].

Table 2.6: Combined hypoxia & mechanical loading in cartilaginous tissue engineering

Authors, year	Experiment setup	Manipulated variables	Outcomes	Conclusions
Domm *et al.*, 2000[79]	De-differentiated bovine articular chondrocytes (ACs, assumed adults) in monolayer and alginate beads	Culture model (monolayer vs. alginate), oxygen (20/5%), CHP (8 h/day, 3 bar/30 min then 1 bar/2 min, applied only in HYP)	Type II collagen: none in monolayers. HYP/static had the most whereas HYP/CHP had less than HYP alone.	HYP promotes cartilage phenotype whereas CHP can negate HYP effects
Hansen *et al.*, 2001[80]	Adult bovine ACs in monolayers	Oxygen (20/5%), CHP (0.1-0.3 MPa, on/off cycles: 5 s/5 s, 30 min/2 min, 2 min/30min for 10 h/day.	HYP promoted proliferation and types II/IX collagen. It suppressed type I. CHP had mixed results but increased proliferation, collagen secretion, and stabilized chondrocyte phenotype. Effects of HYP and CHP were additive.	Combined HYP and CHP have additive effects and may be a powerful tool in cartilage tissue engineering

Table 2.6: *Continued from previous page*

Wernike *et al.*, 2007[81]	Bovine ACs (4-8 month calves) in fibrin gel within polyurethane scaffolds (8x4 mm) and placed within a ring of nasal cartilage with lysed cells to confine the loading for four weeks with 10% FBS	Oxygen (21/5%), DC 10-20% strain with shear 25oth at 0.5 Hz, 1h/day	HYP promoted cartilage phenotype. DC/shear reduced type I collagen mRNA and improved matrix synthesis.	The HYP effects were more convincing than those for mechanical stimulation. Combined HYP and mechanical stimulation can be an effective tool in cartilage tissue engineering although the authors note the work is preliminary.
Meyer *et al.*, 2010[82]	Porcine BMSCs (4 month) in 2% agarose in cylinders (5x3 mm) for 6 weeks with or without TGF-β3	Oxygen (21/5%), DC 0-10% at 1 Hz, 1 h/day, 5 days/week. DC was continuous or delayed (weeks 4-6 only). TGF-β3. Annulus/core regions.	Chondrogenesis required TGF-β3 supplementation, was better in HYP and in the cores, was either not affected or else reduced by DC regardless of continuous/delayed application.	HYP is more potent than DC in promoting chondrogenesis.

Table 2.6: *Continued from previous page*

| Parker *et al.* 2013[83] | Bovine ACs (18 month) in 3% agarose, 5/5 mm cylinders | Oxygen (21/5%), inflammatory modulators (fibronectin fragment (FN-f) or IL-1β (pro-inflammation), L-NIO (anti-inflammation), DC 10 min/rest 5 h50 min, 6 or 48 h total, 0-15% strain, 1 Hz | FN-f and IL-1β induced catabolic effects, co-incubation with L-NIO suppressed them to baseline. DC had strong pro-cartilage and anti-catabolic effects. HYP also promoted cartilage formation | DC and HYP each had beneficial effects for cartilage formation, though the study was only short term. |

2.4.4 Summary

The cartilaginous tissue engineering literature suggests that the combined treatment of hypoxia and mechanical loading will have additive and not synergistic effects when applied in meniscus tissue engineering, and that HIF-1, SOX9, TGF-β, and inflammation will be important mediators of its effects. It is clear that hypoxia and especially mechanical loading are not so robust as treatments that their effects are invariant in different experimental setups. Thus, for a combined treatment to be an effective tool for meniscus tissue engineering, it will be necessary to identify conditions wherein each treatment has positive effects.

2.5 Synthesis

The diagram in Figure 2.8 is proposed as an attempt to harmonize previous literature and summarize some ways of how normal compression loading and low oxygen may together act to produce the avascular fibrocartilage phenotype of the inner meniscus.
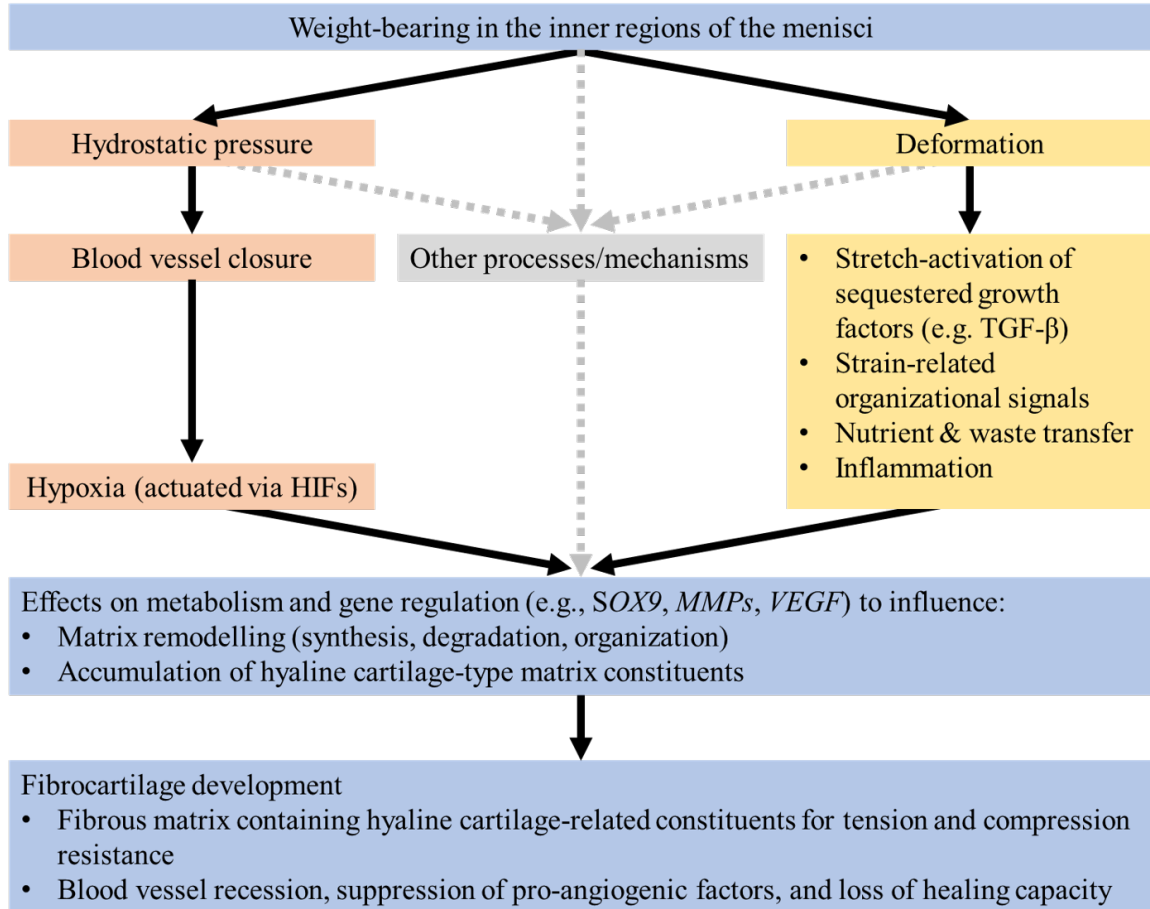
Figure 2.8: A summary of ideas in previous literature assembled to show how the fibrocartilage phenotype may develop in human menisci.

Normal compression loading of the meniscus during weight-bearing reduces oxygen supply by forcing blood vessels closed; this is the concept proposed by [54]. Through hypoxia-inducible factors and potentiated by activation of growth factors such as TGF-β, this low oxygen environment then promotes expression of genes such as *SOX9*, leading to cartilaginous ECM formation that provides the properties to better resist compressive strain. The matrix properties are maintained through suppression of catabolic enzymes such as MMPs along with suppression of VEGF activity to prevent re-vascularization[43]. The deformational aspect of mechanical loading types such as DC may have further effects such as stretch-activation of sequestered growth factors in the extracellular matrix. Thus, in the absence of growth factor supplementation it

is possible that DC could induce matrix formation through endogenous growth factor expression, sequestration, and stretch-activation. This could possibly be promoted by strategies that increase growth factor accumulation in the matrix, such as co-culture of MFCs with another cell type with higher endogenous growth factor expression. Deformational loading may have advantages over hydrostatic pressure and hypoxia as it can also provide organizational signals through an applied strain field and increase nutrient and waste transfer[62, 84].

Figure 2.8 has an interesting implication for *in vitro* study of the menisci. If weight-bearing contributes to fibrocartilage development in the native inner meniscus by forcing blood vessels closed and creating a hypoxic environment, then it stands to reason that the key treatment to enhance meniscus fibrocartilage histogenesis *in vitro*, where no blood vessels are present, is hypoxia. Thus, hypoxia *in vitro* could mimic meniscus mechanical loading *in vivo* to the extent that loading results in a hypoxic microenvironment. It will be possible to identify the individual effects of mechanical loading on MFC gene expression, independent of oxygen tension, using factorial experiments *in vitro*.

2.6 Chapter summary

This chapter's review identified these literature gaps pertaining to hypoxia and/or mechanical loading:

- No studies have combined hypoxia and mechanical loading in meniscus, and it is unknown how hypoxia and mechanical loading signals interact at the molecular level in general.

- No studies have used DC in engineered human meniscus.

- It is unclear why the hypoxia response of human engineered meniscus differs between pellets and scaffolds.

In conclusion, hypoxia and mechanical loading appear to be important factors for development of the inner meniscus phenotype. The use of hypoxia and mechanical loading *in vitro* is a physiologically-relevant combination that may have utility in promoting aspects of the fibrocartilage phenotype, specifically its hyaline cartilage-like components. Genome-wide RNA sequencing will allow an unbiased assessment of potential interactive regulation by hypoxia and mechanical loading using *in vitro* tissue engineering models.

Chapter 3

Biomimetic 3D Printed Scaffolds for Meniscus Tissue Engineering

Contributing authors:

Alexander R. A. Szojka, Karamveer Lalh, Stephen H. J. Andrews, Nadr M. Jomha, Martin Osswald, Adetola B. Adesida

This chapter has been previously published in part as:

A. R. Szojka, K. Lalh, S. H. Andrews, N. M. Jomha, M. Osswald, and A. B. Adesida, "Biomimetic 3D printed scaffolds for meniscus tissue engineering," *Bioprinting*, vol. 8, pp. 1–7, 2017

3.1 Preface

This work is not related to the hypoxia and mechanical loading theme introduced in Chapters 1 and 2. The bulk of this work was completed as my undergraduate summer research project in 2015. This work was part of a collaboration between the Dr Adesida lab at the University of Alberta and the Institute for Reconstructive Sciences in Medicine (iRSM) at the Misericordia Hospital, Edmonton, made possible by Jana Rieger and Martin Osswald. Much of the project's success is owing to Karamveer Lalh, my undergraduate student colleague at the time. Stephen Andrews made the

suggestion to incorporate circumferential fibres throughout the entire structure, and the key insight that made this possible using Boolean operations is owing to the guidance of Andrew Grosvenor and Heather Logan, staff at iRSM. Nadr Jomha, a surgeon scientist specialized in lower extremity joint reconstruction, suggested and guided development of the suture tabs. Completing the work and having it published as a peer-reviewed article was the first task of my graduate studies beginning May 2016 with Dr Adesida.

I presented the project at the following conferences: 1. 2015 Summer Students' Research Day, Faculty of Medicine and Dentistry, University of Alberta; 2. 2015 Students' Union Undergraduate Research Symposium, University of Calgary; 3. 2016 Sunnybrook Research Prize Competition, Sunnybrook Research Institute, Toronto (finalist); 4. 2016 Alberta Biomedical Engineering Conference, Banff (Best poster award); 5. 2017 Tom Williams Surgical Research Day, Department of Surgery, University of Alberta (1st Place Poster Award, Basic Science). I also described the work in an essay that was awarded a Mensa Canada Scholarship.

3.2 Abstract

The menisci distribute loads to protect the articular cartilage of the knee joint from excessive stress. Injuries to their avascular inner regions do not heal, disrupt function, and increase the risk for knee osteoarthritis. Meniscus tissue engineering aims to restore normal meniscus function by use of regenerated tissue on bioengineered scaffolds. The primary purpose of this study was to design and 3D print polycaprolactone scaffolds that recapitulate the shape and structural components of the meniscus extracellular matrix to provide a template and structural support for cell-based meniscus regeneration. A secondary aim was to characterize 3D printed polycaprolactone scaffold fibre architectures with varied fibre spacings, offsets between layers, and circumferential orientations in terms of their equilibrium compressive modulus. Meniscus scaffolds were produced layer-by-layer with a biomimetic fibre architecture

inspired by the circumferentially- and radially- oriented collagen fibre bundles found in the native tissue. Suture tabs were incorporated to facilitate fixation at the meniscal horns and the coronary attachments. These scaffolds were designed to have 100% pore interconnectivity and 61% porosity. The equilibrium compressive modulus at 10% strain of the meniscus scaffold architecture was 18.8 ± 3.1 MPa (mean $\pm$ standard deviation, n=3) and ultimate load in a suture pull-out test on the anterior horn suture tab was 32 N. The scaffolds produced in this study demonstrate a promising strategy for meniscus tissue engineering as they provide a biomimetic template for regeneration of functional components of the meniscus extracellular matrix.

3.3 Introduction

The menisci are two fibrocartilaginous structures in the knee that are semi-lunar in superior view and wedge-like in cross section. Their deformable shape and mobile nature serve to dynamically maintain congruency between the rounded femoral condyles and the relatively flat tibial plateau throughout various degrees of knee loading and flexion[14]. The menisci thereby more than double the contact area for load transmission in both the medial and lateral knee joint compartments, reducing stress on the articular cartilage[85].

Injuries to the inner meniscal regions impair normal function and poor vascularization limits their healing response[28]. Partial meniscectomy for non-healing injuries can provide relief of symptoms but is associated with greater prevalence of radiographic osteoarthritis (OA) in the long term[86]. A promising strategy to mitigate the development of OA is tissue engineering (TE) of meniscus replacements. TE meniscus replacements can be generated with the use of porous scaffolds infiltrated with cells expressing a meniscus extracellular matrix (ECM)-forming phenotype[87]. These scaffolds are designed to provide structural support and serve as a template for *de novo* tissue formation.

The meniscus ECM provides the mechanical properties necessary for the meniscus

to withstand dynamic compressive, tensile, and shear forces under normal loading conditions[30]. For this reason, recapitulation of the native meniscus ECM is essential for functional meniscus tissue engineering. Bundles of type I collagen fibres pass throughout the central meniscus body oriented predominantly in a circumferential direction[23]. These are largely continuous with the insertional ligaments which anchor the menisci to the tibial plateau[23]. The bundles are of the order of 0.1 mm in diameter and are responsible for the tissue's large circumferential stiffness in tension[23]. The menisci are further joined to the tibial plateau at the inferior edge of their periphery by structures termed the coronary attachments or coronary ligaments[88]. Type I collagen tie-fibre bundles and sheets also pass from the outer meniscal periphery towards its inner avascular region, contributing to radial stiffness and holding the circumferential fibres together[89–91]. Upon knee loading, the menisci displace peripherally due to their wedge-like shape. This loading strains the circumferentially-oriented type I collagen bundles and insertional ligaments/meniscal roots, causing large hoop stresses to develop. Meniscal tears that sever the circumferential fibres or the meniscal root attachments abrogate meniscus function and are associated with OA development, while tears parallel to the circumferential fibres are less disruptive to function but still increase the risk of OA development[92–94]. Thus, it is essential for a tissue engineered meniscus replacement to replicate the functionality of these extracellular matrix components.

Much work has already been done to develop biomimetic or anatomically-shaped meniscus scaffolds[71, 95–102]. 3D printing is an advantageous technique for this objective as it allows replication of the overall meniscus shape for generation of patient-specific scaffolds[97] and fine control of the internal fibre architecture. 3D printing has been used in combination with growth factor-containing microspheres to create scaffolds that direct zone-specific cell differentiation to regenerate tissues similar to the native meniscus[98]. These scaffolds also included superficial circumferentially-oriented fibres that mimic the predominant internal fibre orientation of the native

meniscus[98]. However, scaffolds with circumferentially-oriented fibres throughout their entire structure have not previously been demonstrated using 3D printing.

Our objectives in the present study were to design and produce biomimetic 3D printed meniscus scaffolds that reproduce the predominant circumferential and radial type I collagen orientations found in the native tissue and include an attachment strategy like the meniscal roots and the coronary attachment to the tibial plateau. We also aimed to investigate the effects of varying scaffold architectural parameters including fibre spacing, offsets between layers, and fibre orientation on equilibrium modulus in unconfined compression.

3.4 Materials and methods

3.4.1 Meniscus imaging and processing

A fresh meniscus sample (n=1) was acquired from a skeletally mature sheep after approval from a institutional ethics committee at the University of Alberta, Edmonton, Canada (Figure 3.1A). The sample was laser scanned (Shape Grabber, Canada) to acquire a 3D surface model in stereolithography (.stl) format (Figure 3.1B). The model was processed using computer-aided design (CAD) tools (Magics, Materialise, Belgium and Geomagic Freeform, 3D Systems, USA) to convert it to a solid model and improve its suitability for 3D printing. This involved removal of extraneous artifacts from the laser scan, smoothing of surfaces, and extension of the base to a horizontal plane to facilitate 3D printing on a flat platform without the need for sacrificial materials (Figure 3.1C). Suture tabs at the meniscal horns and coronary attachment were created by merging rectangular prisms with the meniscus model in consultation with an expert in lower extremity joint reconstructive surgery (Figure 3.1D).

The model was manually sliced into 37 layers which were customized to have either circumferential or radial fibre orientations. Even-numbered layers were given a circumferential orientation using Boolean operations with a template of concentric
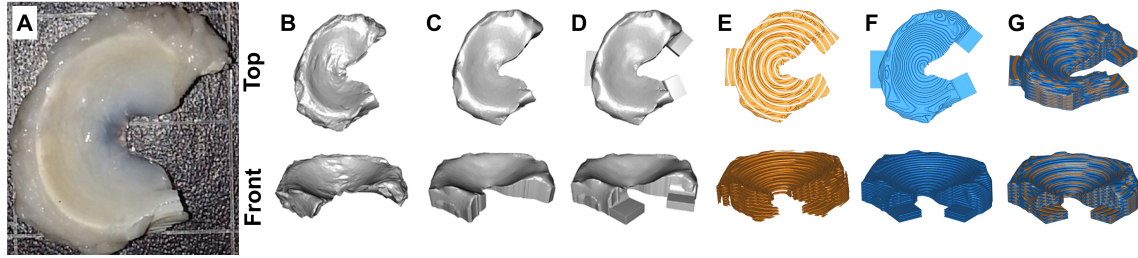
Figure 3.1: Sequential images documenting conversion of the meniscus sample into the completed model for 3D printing. A) Meniscus sample; B) Raw laser-scanned 3D meniscus model; C) Model after processing to remove artifacts, smoothen edges, and flatten base; D) Model with suture tabs added for attachment to the tibia; E) Even numbered layers demonstrating ring-shaped structures, which were printed along their contours. Layers are separated by 200 µm gaps, to be filled by the odd numbered layers; F) Odd numbered layers with sheets, which were converted by the printer software into fibres deposited in a 90° grid pattern with offsets between layers. Layers are separated by 200 µm of empty space; G) Completed solid biomimetic meniscus 3D model by combining the models such that the layers of E) fit into the empty spaces of F), resulting in alternating circumferential fibres (even-numbered layers) and sheets (odd-numbered layers).

rings. To create meniscus models with the circumferential orientations, concentric ring-shaped models were generated using CAD tools to be 0.20 mm in height to correspond with the layer thickness, and 0.90 mm in width and separation distance both to correspond with the fibre spacing. These were duplicated multiple times and stacked on top of each other along the common ring axis with 0.20 mm separation distance, thus leaving gaps for layers with radial fibres described below. The entire structure of concentric rings was then duplicated. The meniscus model was then placed within the ring structure and a Boolean subtraction operation was performed to leave a hole in the shape of the meniscus model inside the ring structure. A second Boolean subtraction was then performed to remove the ring structure with the hole in it from the duplicated, unaltered ring structure. The result was a layered structure in the shape of the meniscus model composed entirely of circumferential rings, with gaps in between layers to be later occupied by the radial fibre layers (Figure 3.1E). During 3D printing, this circumferential ring structure was deposited using the "print contours" option in the printer software (Visual Machines, EnvisionTec, Germany),

which directs the printer to deposit material along the edges of the input models for each layer. Due to the size and spacings of the concentric ring template, the final 3D printed scaffold had layer heights of 0.20 mm and 0.90 mm fibre spacings in these layers. We note that this protocol is easily adaptable for other layer heights, fibre spacings, and strand diameters by simply modifying the concentric ring template. For the layers corresponding to the gaps in the circumferential structure, a similar procedure was carried out but with solid discs in place of concentric rings. The result was a structure of stacked flat sheets in the shape of the meniscus model with 0.20 mm gaps separating them (Figure 3.1F). During 3D printing, the stacked flat sheets were deposited using the "print inner structure" option on the printer software, which automatically converted each disc into fibres rotating 90° between each odd-numbered layer with the fibre spacing and offsets between layers specified as 0.90 and 0.45 mm, respectively (Figure 3.1F). These fibres were oriented to ensure alignment in the posterior region of the scaffold, where the native meniscus is stiffest radially, as well as in the anterior region[90]. This grid was used in place of fibres radiating from the scaffold centre, i.e., a true radial orientation, because it resulted in more homogeneous pore sizes across the entire structure while still stabilizing the circumferentially-oriented fibres as the radial-tie fibres do in the native tissue[91]. To complete the model, the meniscus-shaped rings and discs structures were then superimposed such that they filled each others' gaps (Figure 3.1G). The final meniscus model mimicked the native tissue in terms of its overall shape, fibrillar collagen microarchitecture, and horn and coronary attachments.

3.4.2   3D printing

All scaffolds were 3D printed by fibre deposition of molten 43-50 kDa molecular weight polycaprolactone (PCL) pellets (Polysciences, USA, catalogue #19561). Early experimentation revealed these to be less viscous when melted than 80 kDa PCL pellets (Sigma-Aldrich, USA, catalogue #440744), allowing faster fibre extrusion and use of

a smaller needle for extrusion of lower diameter fibres. Scaffolds were produced using a 4th generation 3D-Bioplotter Manufacturer Series (EnvisionTec, Germany). Relevant 3D printing parameters are summarized in Table 3.1. These parameters were optimized by printing small porous PCL blocks $10 \times 10 \times 3$ mm^3 and assessing their quality in terms of fibre consistency, amount of stringing (residual material not detaching from the needle), and adhesion to previous layers. Continuous strands (fibres within layers are attached to their neighbours at their ends) rather than detached strands were used to reduce stringing. Layers were designed to overlap each other by 1/3 of the strand diameter to provide increased contact area at locations where fibres overlapped between layers. This was expected to impart scaffolds with increased mechanical integrity.

Table 3.1: Summary of 3D printing parameters suitable for 43-50 kDa polycaprolactone.

Property	Value
Material temperature set point	110°C
Platform temperature set point	20°C
Extrusion air pressure	6 bar
Printer fibre extrusion speed	1.4 mm/s
Needle gauge	24 Ga
Needle cannula length	3 mm

3.4.3 Development of 3D fibre architecture

To determine a suitable 3D fibre architecture for the meniscus scaffolds in terms of fibre spacing (FS) and offsets between layers, $40 \times 40 \times 3$ mm^3 porous PCL sheets were 3D printed. Fibre spacing was defined as the centre distance between parallel strands. The 3D printed sheets had fibres alternating 90° between layers with a single defined fibre spacing throughout (0.60, 0.70, 0.80, 0.90, 1.00 mm) with or without offsets between layers of 0.5×FS (Figure 3.2).
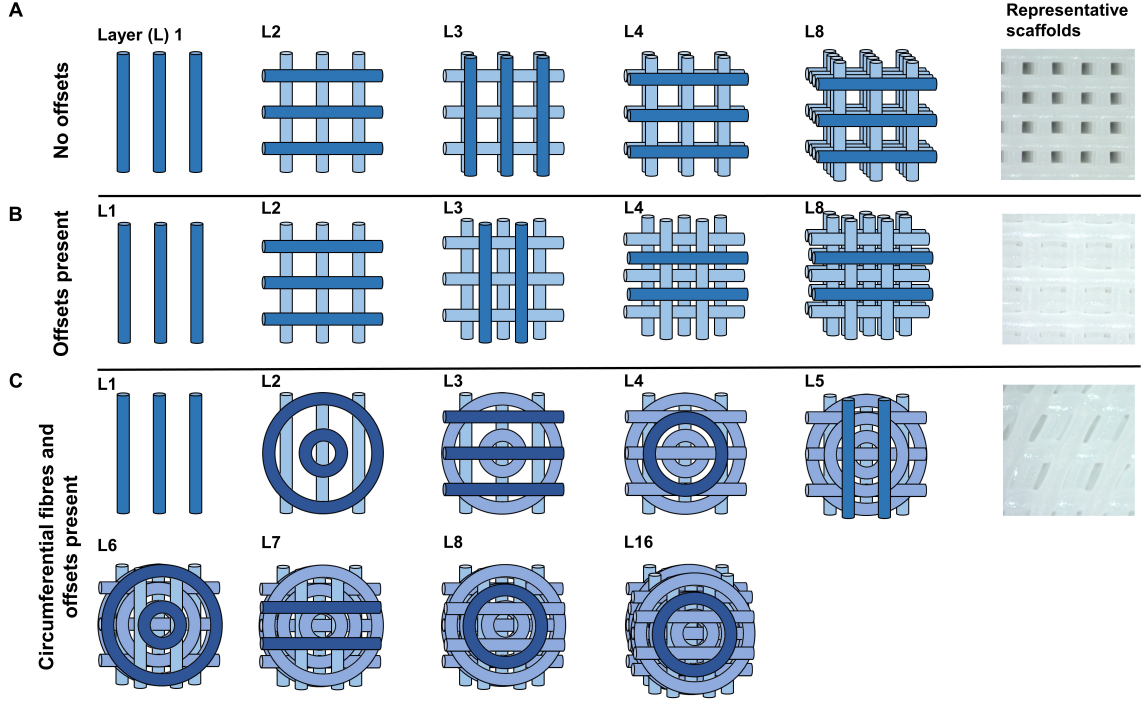
Figure 3.2: Illustration of scaffold construction layer by layer for different fibre archi-
tectures. The fibres of the uppermost layer are coloured more darkly at each step of
scaffold construction. A) No offsets between layers, with the fibre pattern repeating
every 2 layers; B) Offsets between layers, with the fibre pattern repeating every 2
layers; C) Offsets present along with circumferential fibres, with the fibre pattern re-
peating every 8 layers. This is the fibre architecture used for producing the meniscus
shaped scaffolds.

The use of offsets had clear effects on scaffold stiffness through the mechanism
illustrated in Figure 3.3. Based on this preliminary finding, a fibre spacing of 0.90
mm with offsets was used for producing the meniscus-shaped scaffolds. The porosity
of the fibre architecture was estimated using the following geometry-based equation
derived from the void space between fibres and their cross-sectional area (Figure 3.3).

$$Porosity = \frac{voidspace}{totalspace} = \frac{h \times FS - \pi \times \frac{d^2}{4}}{h \times FS} \tag{3.1}$$

where h=layer height, FS=fibre spacing, and d=strand diameter.
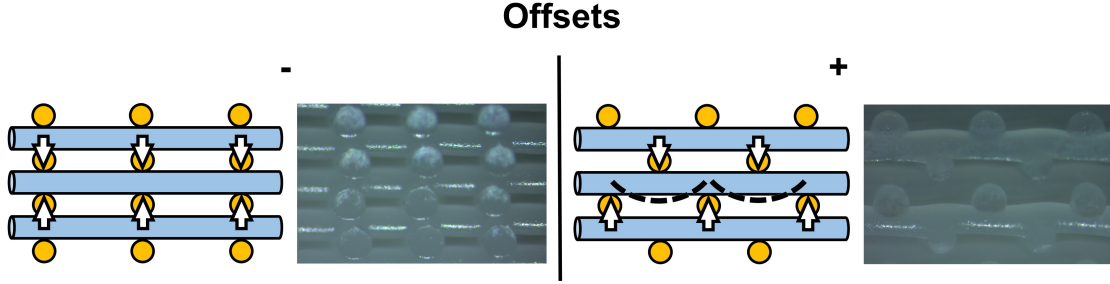
Offsets

Figure 3.3: Comparison of the response to vertical compressive loading between scaffolds without (-) and with (+) offsets between layers. Illustrations indicate internal force transmission through the scaffolds and the resultant bending response, while cross-sectional images of representative scaffolds reveal their structures.

3.4.4 Mechanical characterization

Compression

The 3D printed sheets and meniscus scaffolds were used to characterize the influence of fibre architecture on scaffold uniaxial compressive mechanical properties. A 6 mm biopsy punch was used to obtain cylindrical discs. The height and diameter of these discs were measured using digital Vernier calipers. Discs were preloaded to 5 N to ensure complete contact between the discs and the platens. Discs then serially underwent stress relaxation tests (5/10/15/20 % strain) with a ramp rate of 0.5 mm/s and dwells of 500 s, which were sufficient for equilibrium (Δforce<1 %/min) (Figure 3.4A). Tests were completed at room temperature in air using a 225 N load cell on a Biodynamic 5200 system (TA Instruments, USA) tuned in displacement control. Equilibrium modulus (Em) was calculated at the end of the relaxation periods as:

$$E_m = \frac{\sigma}{\epsilon} = \frac{\frac{F}{A_o}}{\frac{h-h_o}{h_o}} \tag{3.2}$$

where σ is the average stress, ϵ is the nominal strain, F is the load cell force reading zeroed just before the platen connected to the load cell contacted the scaffolds, A_o is the initial scaffold contact surface area calculated using the diameter value, h is the displacement normalized to the reading immediately prior to the first stress relaxation step, and h_o is the initial scaffold height.

43

Pull-out force

A suture pull-out test was conducted on the horns of the 3D printed meniscus scaffolds using a protocol adapted from a previous study[103]. An Ethicon 1 (4.0 metric) suture was passed back and forth once through the tab separated by 3.0 mm and tied with square knots with 8 throws to prevent any slipping. The ends of the thread were aligned parallel to each other and then secured using cyanoacrylate adhesive to a folded piece of sandpaper to prevent slipping, placed as near to the tab as possible. The scaffold and the sand paper were then mounted to opposing tensile grips connected to a 225 N load cell on the Biodynamic 5200 system tuned in load control (Figure 3.4). The tab was first preloaded to 20 N and then unloaded to 2 N to allow the knot to reach a stable configuration. It was then loaded from 5-20 N for 1000 cycles at 1 Hz followed by a pull to failure test at 1 N/s.
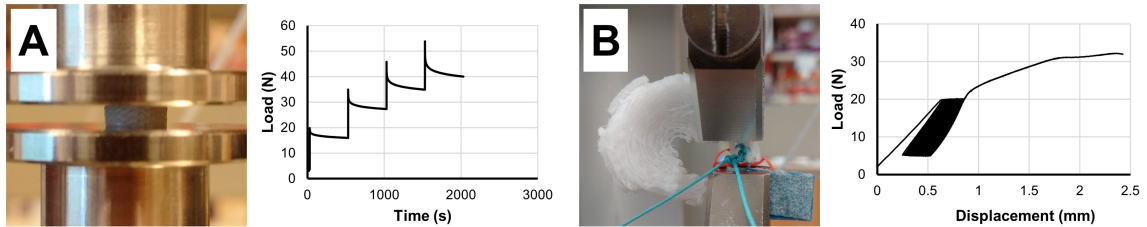
Figure 3.4: Mechanical test set-ups and typical curves generated. A) Unconfined compression of polycaprolactone discs and a characteristic load vs. time plot showing four steps of 5% strain each. Preconditioning step omitted for clarity. B) Suture pull-out test on the biomimetic meniscus scaffold anterior horn tab and the load vs. displacement plot showing initial loading, displacement creep over 1000 cycles, and the final load to failure test.

3.5 Results

The meniscus scaffolds and sheets were 3D printed per the input models, reproducing the meniscus 3D geometry with a controlled internal fibre architecture incorporating circumferential fibres (Figure 3.5). Circumferential fibres were present in all even-numbered scaffold layers while a 90° grid of fibres was present in odd-numbered layers

(Figure 3.5). Suture tabs were included at each horn and the coronary attachment. Residual stringing contributed to variation in the mass of the scaffolds (Figure 3.5, Table 3.2). The scaffold properties are summarized in Table 3.2.

Table 3.2: Summary of biomimetic meniscus scaffold properties.

Property	Value
Number of layers	37
Layer thickness	0.2 mm
Fibre diameter	0.3 mm
Fibre architecture	Circumferential and 90° grid
Fibre spacing	0.90 mm
Mass (mean± standard deviation, n=10)	0.978 ± 0.095 mm
Model porosity	61%
Model pore interconnectivity	100%
Image processing time	5.5h
Print time	2.5h
Material costs	Negligible (<$1 CAD/scaffold)
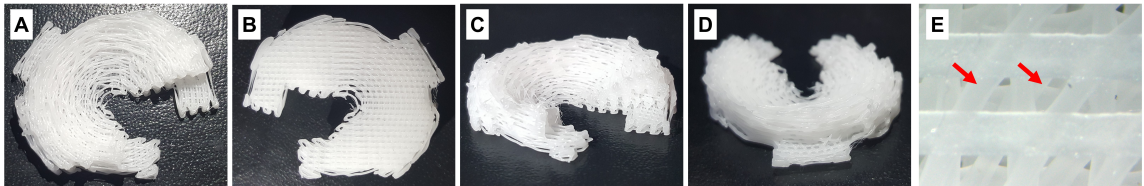
Figure 3.5: 3D printed meniscus scaffolds with a biomimetic fibre architecture. A) Top view; B) Bottom view; C) Front view; D) Back view; E) Close-up to reveal the internal fibre architecture. Arrows indicate offset circumferential fibres between layers.

Equilibrium modulus for scaffold discs decreased with increased strain for all fibre spacings (Figure 3.6A). Offsets between layers resulted in reduced equilibrium modulus compared to scaffolds printed without offsets (Figure 3.6B). Scaffolds with the circumferential fibre architecture had increased equilibrium modulus compared to

those with straight fibres (Figure 3.6C). Coefficients of variation (COV) for scaffolds with straight strands were on average 3.8±1.8% across all strain levels and fibre spacings. In contrast, COV for the circumferential fibre architecture used in the meniscus scaffolds was 14.1±2.4%.
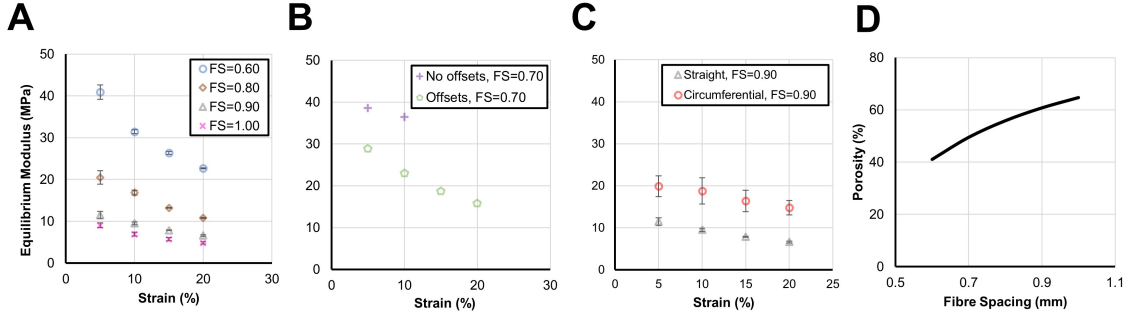
Figure 3.6: A) Relationship of fibre spacing (FS, in mm) to equilibrium modulus (EM) in compression for scaffolds with offsets between layers. B) The effects of offsets between layers on EM for FS=0.70 mm. Only two values are available for the "no offsets, FS=0.70" case due to limitations of the 225 N test instrument load cell. C) The effects of straight vs. biomimetic (superimposed circumferential and straight) fibre orientations for FS=0.90 mm and offsets. All points for A-C) represent mean±SD for n=3 scaffolds; in several cases, standard deviation bars are hidden behind markers. The exception is the "offsets, FS=0.70" case in B), for which values were obtained through parabolic interpolation of EM values from A) at each strain level (all R^2>0.99). D) Analytical relationship of porosity to FS for scaffold models with layer height=0.20 mm and fibre diameter=0.3 mm.

The suture pull-out test demonstrated displacement creep during 1000 loading cycles followed by yielding at 22 N and failure at an ultimate load of 32 N (Figure 3.4B). Failure occurred by the knot tearing through the internal region of the tab while leaving its periphery intact.

3.6 Discussion

In this study, we produced knee meniscus-shaped scaffolds via 3D printing using poly-caprolactone (PCL) with an internal fibre architecture that mimicked the predominant collagen fibre orientation in native menisci. In addition, the scaffolds included suture tabs as an implantation strategy placed at the native medial meniscus at-

tachment sites. We also demonstrated the capability of tuning scaffold equilibrium modulus by controlling fibre architecture with fibre spacing, offsets between layers, and fibre orientations (Figure 3.6).

Two essential considerations for scaffold-based tissue engineering include pore interconnectivity and porosity. 3D printing is advantageous over other production techniques as 100% pore interconnectivity can be designed directly into the scaffold model, as it was in this study. Likewise, 3D printing allows control over porosity through modification of architectural parameters such as fibre spacing, albeit with simultaneous changes to equilibrium modulus (Figure 3.6). Porosity may also be increased by decreasing needle inner diameter; however, it was found that attempts to produce thinner strands using a 27 Ga (ID = 0.2 mm) needle made printing times prohibitively slow, even at an extrusion pressure of 7 bar, which is near the maximum pressure permitted by the 3D Bioplotter printer. During the 3D printing process, there was a propensity for residual stringing at elevated layers. This was in part due to more frequent raising of the 3D printer's robot head, as elevated layers required less material. The scaffolds were produced with a flat base to avoid the need for sacrificial materials during 3D printing. This was deemed to be a reasonable approximation for the native menisci, which as soft tissues conform upon loading to the shape of the relatively flat tibial plateau. We expect that the scaffolds will behave in a similar way upon loading.

We used a laser-scanner to produce the 3D model of the ovine meniscus sample. This technique was practical for the purposes of this study but may not be translational for future clinical application of tissue engineered menisci. Recently, research groups have used MRI imaging to create 3D meniscus models non-invasively[97, 102]. Furthermore, another group has shown that 3D printed PCL fibres with fibre spacings of approximately 300-500 µm can direct collagen alignment for generation of a meniscus-like matrix orientation[104]. Taken together with the techniques developed in the present study, patient-specific meniscus scaffolds which mimic the native col-

lagen fibre architecture could be produced non-invasively using mirror images of the meniscus in the contralateral healthy knee, as the menisci demonstrate reasonable bilateral symmetry under normal conditions[104, 105]. Once produced, the personalized scaffold would need to be functionalized for cell adhesion, seeded with a cell population, and then cultured with the fibre architecture providing a template for meniscus regeneration. The efficacy of the relatively large fibre spacings and circumferential orientations used in the present study in guiding ECM alignment remains to be determined.

Polycaprolactone was selected for this study for several reasons. It has been used previously for 3D printing meniscus scaffolds[97, 98, 101, 102]. It has excellent biocompatibility, and has been approved for a variety of health-related applications by the Food and Drug Administration (FDA)[106]. In vivo studies using the rat model indicate that PCL undergoes slow degradation in molecular weight over time and that low MW fragments are completely excreted without accumulation in any body tissues[107]. From a practical perspective, PCL is advantageous due to its low cost and high manufacturability by 3D printing. PCL surfaces can also be easily linked to RGD peptide to promote cell attachment, survival, and proliferation [108]. Many cell types including culture expanded meniscus cells as well as bone marrow, adipose, and synovial fluid-derived mesenchymal stem cells can be seeded on the PCL-RGD scaffolds for synthesis of the fibrocartilaginous matrix known to be responsible for the biomechanical functionality of the meniscus within the knee joint[55, 57, 109–111].

A 3D printed PCL meniscus scaffold was previously developed and seeded with poly(lactic-co-glycolic acid) (PLGA) microspheres encapsulating different growth factors between the meniscus inner and outer regions in order to direct cell differentiation to be similar to the native tissue[98]. This technique could be used in combination with the biomimetic fibre architecture template demonstrated in the present study to produce type I collagen bundles in the outer meniscus region aligned circumferentially. Furthermore, by varying the fibre spacing parameter within layers, different pore sizes

and mechanical properties could be produced between the inner and outer scaffold regions to capture the regional variation in the native meniscus. Another group presented an idealized scaffold model in the generic meniscus shape incorporating a circumferential fibre architecture; however, their data revealed that these fibres were only present for superficial layers and not throughout the entire 3D printed structure as would be required for mechanical integrity and function[101, 102]. The Boolean operation modeling strategy described in section 2.1 of the present study could be used to convert their idealized models to have the precise shape of the meniscus tissue models they obtained using MRI.

The finding that offsets between layers reduce equilibrium modulus is explained by considering how fibre intersections are supported. When offsets are not used, the fibre intersections are supported from above and below by direct contact with neighbouring fibres; in contrast, with offsets in place the intersections are suspended, which allows fibre bending to occur upon compression (Figure 3.3). A similar mechanism may account for the greater equilibrium modulus found for the circumferential fibre architecture. This architecture was a combination of offset circumferential fibres and an offset 90° grid, which together resulted in regions of considerable fibre overlap and thus support in regions where the circumferential fibres ran roughly parallel to fibres in the 90° grid. This may also account for the greater coefficient of variation found for this architecture, as each scaffold tested would have a slightly different degree of overlap. The equilibrium moduli of 3D printed PCL scaffolds found in this study (5-41 MPa) were generally similar to the non-equilibrium compressive moduli found in a previous study (11-39 MPa for the same strand diameter), although it should be noted that differences in scaffold structure and mechanical tests exclude the possibility of direct comparisons[112].

It was demonstrated in this study that scaffold architectural properties such as fibre spacing, offsets between layers, and fibre orientation can be modified to control equilibrium compressive modulus. There are orders of magnitude between the equi-

librium moduli in unconfined compression of the meniscus scaffolds (e.g., 14.8±1.7 MPa at 20% strain) and those for discs cut from human meniscus explants (23-67 kPa)[113]. We note that it is unrealistic to expect that this property should be comparable between the scaffolds and a meniscus explant. The unconfined compression stress relaxation test, while convenient for gaining a sense of the compressive properties of 3D printed scaffolds, is not representative of the in situ dynamic mechanical environment experienced by the menisci. This involves dynamic conversion of axial loads into circumferential tensile loads, resulting in axial compression and lateral extrusion of the menisci[91]. The circumferential stiffness in tension of the menisci ranges from 100-300 MPa, and the associated average strain along the periphery of the medial meniscus under physiological loading is 2.4±1.6%, indicating an applied hoop stress on the order of 5 MPa[91, 114]. Similarly, the equilibrium moduli of the menisci are not at all representative of the compressive stiffness of intact menisci during physiological load. Andrews *et al.* demonstrated a dynamic modulus on the order of 3 MPa for meniscal samples in confined compression at physiological loading rates which was almost 20 times greater than the equilibrium modulus measured in those same samples[115]. Their findings also demonstrated significant influence of sample preparation on the resultant mechanics and speculated that in vivo stiffness of the menisci is even greater than their findings due to the low permeability of meniscus tissue. Therefore, the initial compressive properties of our scaffolds may appropriately mimic the compressive properties of the menisci for implantation.

The investigation of the scaffold properties was simplified and limited in that it considered only a narrow aspect of scaffold mechanics without regard to tensile, shear, and frictional properties, all of which are relevant for functional meniscus tissue engineering. As well, there remains uncertainty in how the scaffolds' properties will change in response to ECM formation by a seeded cell population, repeated loading, and material degradation. Considering that the superior aspects of the scaffolds were noticeably rough due to their layered nature, achieving low friction surfaces that

maintain articular cartilage health will likely be contingent upon stimulating robust meniscus-like tissue growth upon the scaffolds. Cell seeding and tissue culture experiments will thus be necessary to determine the suitability of the scaffolds for meniscus replacement.

The native meniscal horns can withstand ultimate loads on the order of 500 N while the anterior meniscal horn suture tab experienced ultimate failure at 32 N[116]. Although the operating range of the meniscal horns is less than their ultimate failure load, this value provides a benchmark with a built-in safety factor for scaffolds that can be used in future design iterations. The suture tabs will provide a means for fixation of a cell-seeded meniscus construct into an underlying bone tunnel using a suture anchor with local abrasion of cancellous bone to accelerate healing. The joint will be protected from load-bearing and flexion for an immobilization period for tissue regeneration and scaffold tab integration into newly formed tissue. A non-resorbable suture may be used to hold the meniscus construct in place as the PCL material is replaced by tissue. However, it will be necessary to ensure that the newly formed tissue integrating the scaffold into the bone is mechanically competent to prevent implant failure.

3.7   Conclusion

We demonstrated the production of biomimetic 3D printed meniscus scaffolds that emulate the predominant type I collagen fibre architecture in the native tissue. These scaffolds include circumferentially-oriented fibres passing through the internal scaffold structure in alternating layers, held together by a 90° grid of fibres as the radial tie fibre sheets do in the native tissue. The circumferential fibres were continuous with suture tabs as an attachment strategy of the scaffolds for implantation. We also demonstrated control over PCL scaffold compressive equilibrium modulus through variation of fibre architectures with different fibre spacings, offsets between layers, and fibre orientations. Future efforts will be dedicated to grow fibrocartilaginous

tissue upon the meniscus scaffolds under appropriate physical and biochemical stimulation to evaluate the efficacy of the PCL fibre architecture in directing aligned ECM formation, followed by knee joint studies to determine *in vivo* performance and further optimize scaffold properties. In closing, the meniscus scaffolds in their present form may provide a template for biomimetic tissue growth, which represents a promising strategy for meniscus tissue engineering.

3.8   Acknowledgements

3.9   Funding sources

3.10   Author contributions

Scaffold development: AS, KL, SA, NJ, AA; Mechanical tests: AS, SA; Ideation: SA, NJ, MO, AA; Manuscript: AS, SA, NJ, KL, AA; Research funding support: NJ, AA.

Chapter 4

Hypoxia and TGF-β3 Synergistically Mediate Inner Meniscus-like Matrix Formation by Meniscus Fibrochondrocytes

Contributing authors:

Alexander R. A. Szojka*, Brayden D. Lyons*, Colleen N. Moore, Yan Liang, Melanie Kunze, Enaam Idrees, Aillette Mulet-Sierra, Nadr M. Jomha, Adetola B. Adesida

*: Equal contributing authors

4.1 Preface

It was clear from the outset that the full-scale meniscus scaffolds detailed in Chapter 3 were not amenable to investigation of hypoxia and mechanical loading. Sheets with

a similar polycaprolactone (PCL) fibre architecture as the full-scale scaffolds were printed and then cored with 6-mm biopsy punches as a potential scaffold for experiments in tissue growth. However, the difficulty in using 3D printed PCL in cell culture was immediately apparent, as seeded cell concentrates would pass right through the pores and cells could hardly be detected on the surface of the fibres. Clearly, filling the scaffolds with, for example, a hydrogel or else modifying the PCL was necessary. Early attempts at these encountered obstacles such as the hydrogel contracting away from the PCL fibres. To simplify, my efforts moved on to using scaffold-free pellets and a commercial type I collagen scaffold for the remainder of this research project. Another graduate student eventually began investigating bioprinting meniscus using the models developed in Chapter 3.

The specific motivation for this project came from [117], a study accepted in June 2016. This work demonstrated spontaneous chondrogenesis of human bone marrow-derived mesenchymal stem cells (BMSCs) in pellets under hypoxia without growth factor supplementation, leading us to question whether human MFCs would demonstrate a similar response. I carried out this project jointly with Brayden Lyons, another MSc student at the time in the Adesida lab. In a similar study, I later investigated whether the spontaneous chondrogenesis effect could be replicated using adipose-derived MSCs with Samia Rahman, an undergraduate summer student. This work is currently accepted for publication[13].

The project presented in Chapter 4 was presented by Colleen Moore, an undergraduate summer student, at the 2017 Alberta Biomedical Engineering Conference.

One final note is that I attempted to visually detect intra-pellet hypoxia using "Hypoxyprobe" in this study. The early results seemed to indicate that in hypoxia-cultured groups, cells throughout the entire pellets experienced hypoxia, whereas in normoxia-cultured groups only cells in the core regions experienced hypoxia. However, I could not replicate these results and they had to be excluded. One challenge was that the matrix and cell densities varied widely between groups. I believe this

may have unevenly impaired the degree of penetration of the Hypoxyprobe reagent (pimonidazole) into the pellets and the effectiveness of preparation steps for incubation with the fluorescing anti-pimonidazole antibody.

4.2 Abstract

The objective of this work was to investigate hypoxia and TGF-β3 effects on inner meniscus-like extracellular matrix (ECM) formation and related gene expression by meniscus fibrochondrocytes (MFCs).

Aggregates of human MFCs were cultured for 3 weeks under hypoxia (3% O_2) or normoxia (atmospheric O_2) with or without TGF-β3 supplementation (10 ng/mL). Inner meniscus-like ECM formation was assessed by biochemistry, histology, and immunofluorescence. mRNA expression of ECM-related genes, *TGF-β* isoforms 1-3, and HIF-1 targets were assessed by qRT-PCR.

Hypoxia and TGF-β3 supplementation synergistically induced inner meniscus-like ECM formation at the protein level with similar effects on ECM-related gene expression. Hypoxia alone did not induce an inner meniscus-like ECM-forming response nor upregulate mRNA of TGF-β isoforms. Expression of HIF-1α and HIF-1 target genes suggested that HIF-1 was a likely contributor to the observed synergistic interactions of hypoxia and TGF-β3 supplementation.

In conclusion, hypoxia and TGF-β3 supplementation synergistically induced inner meniscus ECM formation by adult human MFCs. Hypoxia alone is insufficient to induce an inner meniscus ECM-forming response in this culture model.

4.3 Introduction

The knee menisci play important roles in load distribution, load transmission, and joint stability[30, 118, 119]. Injuries to their non-healing avascular inner regions increase the risk for knee osteoarthritis (OA) development[28, 120, 121]. Damaged inner

55

meniscus tissue may be removed through arthroscopic partial meniscectomy but this may put the knee at risk for OA development[122–124]. The aim of meniscus tissue engineering is to generate functional cell-based meniscus replacements to prevent OA development following non-healing meniscus injuries[125, 126].

The extracellular matrix (ECM) provides the meniscus with its functional properties[113]. The ECM of the inner meniscus is primarily composed of types I and II collagen and proteoglycans such as aggrecan[113, 127, 128]. It is thus of interest to study cell sources and culture conditions which favour synthesis of these ECM constituents[15]. One promising autologous cell source is the surgical discards obtained during partial meniscectomy consisting of small pieces of the inner meniscus[129, 130]. These tissues house a heterogeneous population of cells collectively known as meniscus fibrochondrocytes (MFCs)[129], which "synthesize and maintain the ECM" in vivo[131]. MFCs can be expanded to large numbers with combined TGF-β1 and FGF-2 (T1F2) supplementation while retaining their inner meniscus-like ECM-forming capacity[8].

High density 3-dimensional (3D) cell aggregates allow study of culture conditions favouring meniscus-like ECM formation in vitro[132]. Reduced oxygen tension (hypoxia, HYP) is a physiological condition for MFCs and their associated ECM in the inner meniscus regions, as they reside within the hypoxic knee environment of synovial fluid and have limited blood supply in adults[28, 29]. The use of hypoxic incubator conditions in vitro has been shown to enhance meniscus-like ECM formation by cells derived from a variety of human tissues including meniscus, articular cartilage, and bone marrow when combined with TGF-β3 supplementation[8, 55, 133–135].

The HYP response of MFCs has been shown to be mediated through hypoxia-inducible factor-1 mu (HIF-1α)[56]. At normal oxygen levels, HIF-1α protein is degraded, whereas in HYP it is stabilized and forms the active HIF-1 transcription factor complex, which increases expression of genes whose products support metabolic adaptation, vascularization (e.g., vascular endothelial growth factor (*VEGF*)), syn-

thesis of cartilaginous matrix (e.g., sex-determining region Y-box 9 (*SOX9*)), and collagen biosynthesis (e.g., collagen prolyl 4-hydroxylase (I)) and decreases expression and activity of osteogenic transcription factor Runt-related transcription factor (*Runx2*), a transcription factor for hypertrophic marker type X collagen[136–138]. Recent reports also suggest that TGF-β stabilizes SOX9 protein leading to increased transcription of its gene products such as *ACAN* and *COL2A1*[139, 140]. Hypoxic culture without growth factor supplementation led bone marrow-derived mesenchymal stem cells (BM-MSCs) to form inner meniscus-like ECM, which was purported to be through endogenous upregulation of another member of the TGF-β family, TGF-β1[117]. Furthermore, HIF-1 and TGF-β have been shown to promote *VEGF* mRNA transcription in a synergistic manner[136, 141]. These results suggest hypoxia and TGF-β may likewise enhance *SOX9*-mediated inner meniscus ECM formation by MFCs in a synergistic manner. However, to our knowledge no experiments have i) compared the individual effects of hypoxia alone and TGF-β3 supplementation alone to their combined treatment in MFCs to assess if the interactions are synergistic or additive in nature, and ii) determined if hypoxia alone can induce an inner meniscus-like ECM forming response by adult MFCs.

Therefore, in this study we investigated the individual and combined effects of hypoxic (HYP) tissue culture relative to normoxia (NRX) and TGF-β3 supplementation on human T1F2-expanded MFCs in an aggregate model.

4.4 Materials and methods

4.4.1 MFC release and expansion

Our methods were adapted closely from our previous work with human MFCs[8]. Human meniscus surgical discards (n=5) were collected from donors undergoing partial meniscectomy with approval from the University of Alberta Health Research Ethics Board – Biomedical Panel. MFCs were isolated from tissues and expanded with 1

ng/mL TGF-β1 and 5 ng/mL FGF-2 (T1F2)[8].

4.4.2 Cell aggregate formation and culture

At the end of passage 1 (P1) (1 week), MFCs were counted and population doublings (PD) were calculated (Table 4.1)[8, 142]. Aggregates of 5×10^5 MFCs were prepared by centrifugation as described previously for chondrogenic differentiation and were incubated under either NRX or HYP (3% O_2) in 0.5 mL of a chemically-defined serum-free medium changed twice weekly, with or without supplementation of 10 ng/mL of TGF-β3[8]. Media for HYP groups was normalized to HYP incubator conditions for 2 hours prior to being used. All HYP aggregates were cultured in an X3 XVivo system (Biospherix, USA). Aggregates were harvested after 3 weeks.

Table 4.1: Meniscus tissue donor details. M: male, F: female, #: years old, PD: population doublings.

Identifier	Meniscus	PD	PD/day
F46	Medial	3.15	0.45
F41	Medial	3.03	0.43
M19	Lateral	3.18	0.45
M26_lateral	Lateral	3.55	0.51
M26_medial	Medial	4.05	0.58

4.4.3 Quantitative biochemistry

Aggregates (1-2) from each condition per donor were weighed and stored -80°C[8]. Aggregates were later digested using proteinase K solution for glycosaminoglycan (GAG) and DNA quantification using 1,9-dimethylmethylene blue (DMMB) and CyQuant Cell Proliferation assays.

4.4.4 Qualitative histology and immunofluorescence

Aggregates (1-2) from each condition per donor were weighed and paraffin-embedded[8]. Two donors (M26_lateral and F41) were used for histological staining and immunofluorescence (Table 4.1). These donors were specifically chosen as they had the greatest wet weights among donors in TGF-β3 groups, providing the best chance of showing growth factor supplementation-independent inner meniscus-like ECM formation. Paraffin-embedded aggregates were sectioned at 5 μm onto glass slides[8] and stained sequentially with Mayer's Haematoxylin, Fast Green FCF, and Safranin-O to detect sulphated proteoglycans[8]. Types I and II collagen were detected by immunofluorescence with 1:200 dilutions of primary antibodies, rabbit anti-collagen I (CL50111AP-1, Cedarlane, US) and mouse anti-collagen II (II-II6B3, Developmental Studies Hybridoma Bank, US), and secondary antibodies, goat anti-rabbit (ab150080, Abcam, UK) and goat anti-mouse (ab150117, Abcam, UK), as described previously. Cell nuclei were detected by 4',6-diamidino-2-phenylindole (DAPI)[8].

4.4.5 mRNA gene expression analysis by quantitative real-time polymerase chain reaction (qRT-PCR)

Aggregates (1-2) from each condition and donor were placed into TRIzol reagent and immediately frozen at -80°C to prevent gene expressional changes[8]. RNA was later extracted, quantified, and 100 ng was reverse transcribed to complementary DNA (cDNA) which was stored at -20°C[8]. cDNA was later amplified with gene-specific primers by qRT-PCR[8, 56]. ΔCt (threshold cycle) values were calculated by subtracting Ct values of each gene of interest (GOI) from the average Ct value of reference genes *YWHAZ*, *β-actin*, and *β2-microglobulin*. ΔCt values were used in statistical analysis because they are on a linear scale to satisfy the normality assumption, while 2ΔCt values were presented in figures with a $\log_{10}$-Y axis to emphasize exponential amplification during qRT-PCR. Mean and standard deviations were calculated based on the ΔCt values to reflect the statistical analysis performed and were likewise then

converted to 2ΔCt format for presentation.

4.4.6 Data analysis and statistical notes

The five meniscus specimens were all cultured in parallel. Two specimens came from the same donor but were treated independently during analysis (Table 4.1). Since wet weight data was collected for aggregates designated for both biochemistry and histology, there were 2-4 readings for each condition per donor. There were 1-2 readings of all other metrics for each condition per donor, which were averaged to obtain more stable dependent variables prior to statistical analysis in SPSS 24 (IBM, USA)[143].

For each metric, two-way analysis of variance (ANOVA) with hypoxia (±) and TGF-β3 supplementation treated as within-subjects factors was carried out to assess for synergistic effects[143, 144] In cases with a significant ($p<0.05$) interaction term of HYP and TGF-β3 the biological interpretation was that the effects were synergistic, i.e., the combined effect was "manifest in a non-additive manner"[144]. In these cases, the four simple main effects (1. NRX vs. HYP for -TGF-β3; 2. NRX vs. HYP for +TGF-β3; 3. -TGF-β3 vs. +TGF-β3 for NRX; 4. -TGF-β3 vs. +TGF-β3 for HYP) were tested using paired t-tests. In cases with a non-significant interaction term, the individual main effects of HYP and TGF-β3 were reported instead. P-values from 0.05 to 0.10 were considered as weak evidence.

To summarize quantitative data, principal component analysis (PCA) was applied to all metrics pooled across conditions and donors using the correlation matrix, with gene expression values used in ΔCt format. Individual metrics were excluded if their Kaiser-Meyer-Olkin (KMO) measures for sampling adequacy fell below 0.5 (this applied only to *TGF-β2*).

4.5 Results

4.5.1 Quantitative wet weights and biochemistry (n=5)

During culture, the aggregates in HYP/+TGF-β3 were observed to be the largest-looking with the most media metabolism assessed visually by colour change, whereas those in NRX/-TGF-β3 were the smallest-looking. Wet weights were measured to indicate accumulation of ECM during the 3-week culture period (Figure 4.1A). The two-way interaction term of HYP and TGF-β3 was significant, giving statistical evidence for synergism in wet weight. Between the growth factor-free groups HYP/-TGF-β3 and NRX/-TGF-β3, there was a difference (95% CI) of 0.86 mg (0.46 to 1.26 mg, p=0.004).
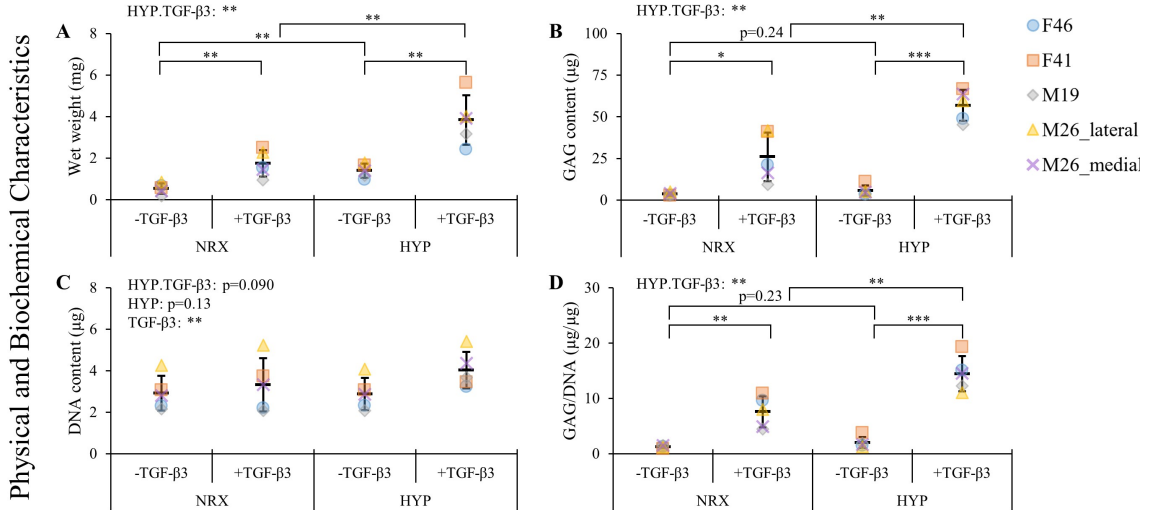
Figure 4.1: Quantitative physical and biochemical analysis for aggregates of adult human passage 1 T1F2-expanded meniscus cells after 3 weeks' culture. A) Wet weight, B) glycosaminoglycan (GAG) content, C) DNA content, and D) GAG/DNA. Each shape/colour represents samples from the same meniscus tissue and each data point represents the mean of 1-4 replicates. P-values are from two-way ANOVA within subjects. HYP.TGF-β3: interaction term between oxygen tension and TGF-β3 supplementation. HYP: Hypoxia (3% O_2), NRX: Normoxia (atmospheric O_2). Significant differences are labelled as: *p<0.05, **p<0.01, ***p<0.001.

Glycosaminoglycan (GAG) contents were measured to probe accumulation of inner meniscus ECM molecules (Figure 4.1B). The two-way interaction term of HYP and TGF-β3 indicated synergism (Figure 4.1B). There was minimal GAG in the -TGF-β3 groups and no difference between them (p=0.24). Thus, the increased wet

weight in HYP/-TGF-β3 relative to NRX/-TGF-β3 was not due to GAG accumulation. Among +TGF-β3 groups, there was no difference in %GAG/wet weight between HYP (range 1.2 to 2.0%) and NRX (1.0 to 1.8%) (data not shown) (p=0.56). Thus, HYP/+TGF-β3 had increased accumulation of inner meniscus ECM molecules relative to NRX/+TGF-β3 but no difference in composition in terms of %GAG/wet weight.

DNA content was measured as an indicator of cell content and proliferation (Figure 4.1C). The two-way interaction term of HYP and TGF-β3 approached significance (p=0.090), providing weak evidence for synergism. Moreover, the main effect of HYP was not significant (p=0.13) and the specific comparison between -TGF-β3 groups did not approach significance (p=0.54). However, the main effect of TGF-β3 showed an increase (95% CI) of 0.77 g (0.39 to 1.16 g, p=0.005) from -TGF-β3 to +TGF-β3 groups.

Finally, GAG content was normalized to DNA content for each aggregate to assess how much GAG accumulated relative to cell content (Figure 4.1D). The two-way interaction term of HYP and TGF-β3 indicated synergism in GAG/DNA contents. Thus, the increased GAG content in HYP/+TGF-β3 was not only the product of increased cell content but also superior GAG retention and/or synthesis per cell (Figure 4.1CD). Additionally, there was no difference between HYP/-TGF-β3 and NRX/-TGF-β3 (p=0.23). Thus, aggregates in -TGF-β3 groups showed minimal capacity to synthesize and/or accumulate GAG regardless of the oxygen tensions investigated.

4.5.2   Qualitative histology and immunofluorescence (n=2)

For both donors, aggregates in +TGF-β3 groups stained intensely for sulphated proteoglycans (Figure 4.1A & Figure S4.1. Aggregates in -TGF-β3 groups did not stain for Safranin-O, corroborating their low GAG contents (Figure 4.1 & Figure S4.1). Type II collagen was only detected in +TGF-β3 groups (Figure 4.3A & Figure S4.2A). Taken together with biochemical and histological results, this confirms that HYP

without TGF-β3 supplementation did not induce an inner meniscus-like ECM-forming response (Figures 4.1 to 4.3).
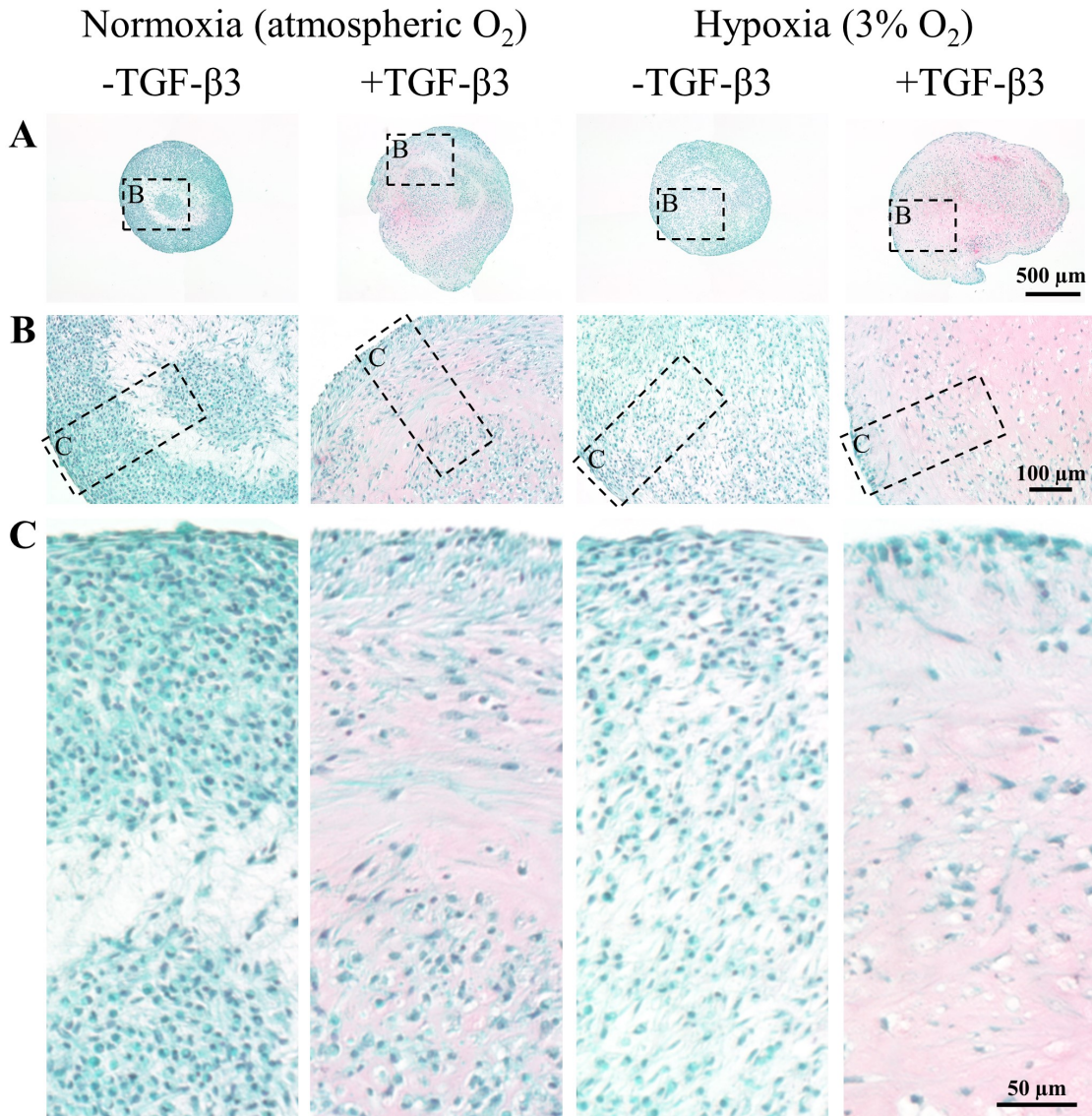
Figure 4.2: Qualitative histological investigation of ECM for one representative donor (M26_lateral, i.e., yellow triangles in Figures 4.1 and 4.4 to 4.6). 5 µm sections of paraffin-embedded aggregates of adult human T1F2-expanded meniscus cells cultured for 3 weeks were stained with Safranin-O for sulphated proteoglycans (pink), Fast Green FCF as protein counterstain, and Mayer's Haematoxylin for cell nuclei. Scale bars are shared within rows.

For the M26_lateral donor, type II collagen staining intensity was higher in HYP/+TGF-β3 than NRX/+TGF-β3 indicating increased concentration (Figure 4.3A), whereas
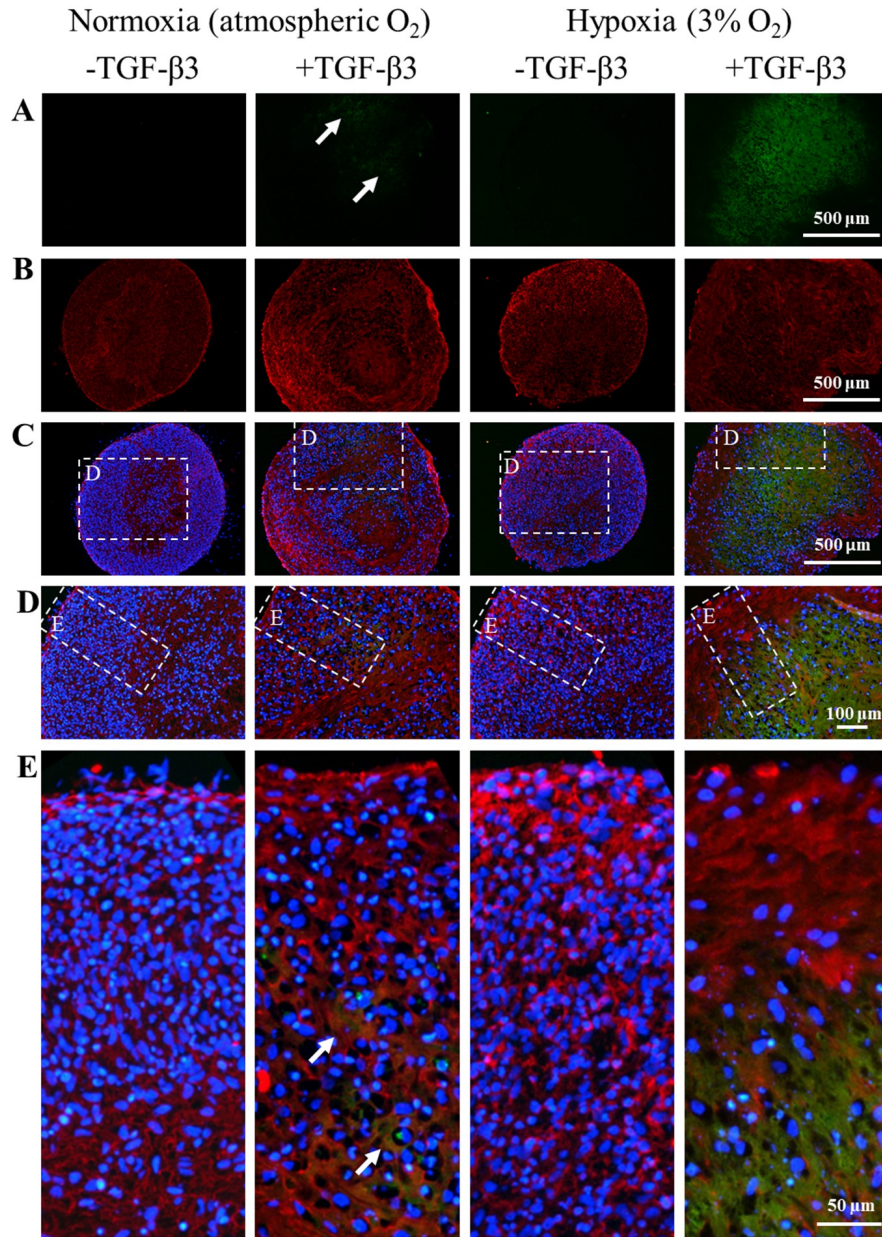
Figure 4.3: Qualitative immunofluorescence-based investigation of ECM for one representative donor (M26_lateral, i.e., yellow triangles in Figures 4.1 and 4.4 to 4.6). 5 μm sections of paraffin-embedded aggregates of adult human T1F2-expanded meniscus cells cultured for 3 weeks were immunofluorescently-labelled for types II (green) and I (red) collagens and cell nuclei (blue). A) Type I collagen; B) Type II collagen; CDE) Overlay of types I and II collagen and DAPI. Arrows in the Normoxia/+TGF-β3 group point out the faint immunofluorescence of type II collagen. Scale bars are shared within rows.

for the F41 donor, the staining intensity between these conditions were both comparable to the former donor's HYP/+TGF-β3 condition (Figure S4.2). Thus, in +TGF-β3 groups there were donor-specific responses in NRX/+TGF-β3 in synthesis and/or accumulation of type II collagen. Given the greater size of aggregates in HYP/+TGF-β3 relative to NRX/+TGF-β3, these findings suggest this group had more accumulation of sulphated proteoglycans and type II collagen. For both donors, type I collagen was detected in all conditions (Figure 4.3B & Figure S4.2).

For both donors, aggregates in +TGF-β3 groups had regional variations in cell morphologies, with some cells surrounded by non-staining lacunae-like pericellular matrices and others that appeared more fibrous and seamlessly-integrated into proteoglycan-rich ECM (Figure 4.2C & Figure S4.1C). For both donors, the -TGF-β3 groups had little ECM with densely-packed cells lacking lacunae-like pericellular matrices. The cells were most densely-packed in the NRX/-TGF-β3 group, which was consistent with the lower wet weight and comparable DNA content in NRX/-TGF-β3 relative to HYP/-TGF-β3 (Figures 4.1 and 4.2).

4.5.3 Quantitative mRNA gene expression analysis by qRT-PCR (n=5)

To gain mechanistic insight into the protein-level findings, we measured relative mRNA expression of inner meniscus ECM-related molecules, *TGF-β* isoforms *1-3*, and HIF-1 targets.

Inner meniscus ECM-related macromolecules

ACAN was measured as an indicator for synthesis of the predominant proteoglycan in the inner meniscus (Figure 4.4A). The two-way interaction term of HYP and TGF-β3 indicated synergism in *ACAN*, which corroborated protein-level findings and suggested that the proteoglycan-rich ECM observed in +TGF-β3 groups likely contained aggrecan (Figure 4.1 & Figure 4.2, Figure S4.1). In -TGF-β3 groups there was low relative *ACAN* expression and a downward trend from NRX to HYP (p=0.086),

whereas in +TGF-β3 groups there was a fold increase (95% CI) of 5.7 (3.3 to 9.8, p<0.001) from NRX to HYP.
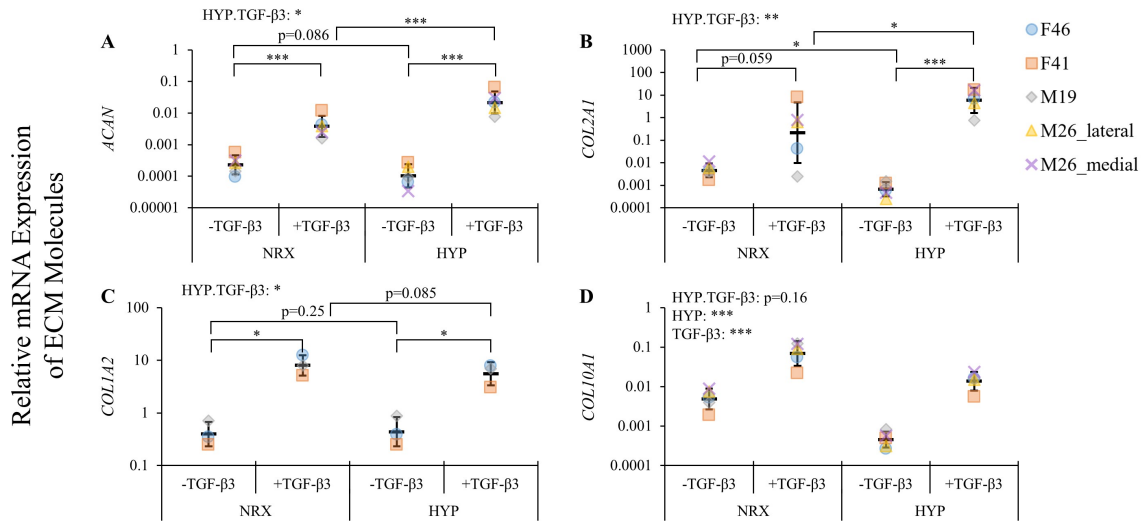
Figure 4.4: Relative mRNA expression of ECM molecules by qRT-PCR for aggregates of adult human T1F2-expanded meniscus cells after 3 weeks' culture. Each shape/colour represents samples from the same meniscus tissue and each data point represents the mean of 1-2 replicates. Amplification of *COL1A2* was poor for the matched medial/lateral M26 donor in all conditions and is omitted. P-values correspond to two-way within subjects ANOVA for ΔCt ($Ct_{\text{reference average}}$-$Ct_{\text{gene of interest}}$) values, while relative expression is presented as $2^{\Delta Ct}$. HYP.TGF-β3: interaction term between oxygen tension and TGF-β3 supplementation. HYP: Hypoxia (3% O_2), NRX: Normoxia (atmospheric O_2). Significant differences are labelled as: *p<0.05, **p<0.01, ***p<0.001.

COL2A1 was measured to provide quantitative mRNA-level validation for the qualitative type II collagen protein immunofluorescence results (Figure 4.4B). The two-way interaction term of HYP and TGF-β3 indicated synergism. In -TGF-β3 groups there was comparatively low *COL2A1* with a decline in HYP, whereas in +TGF-β3 groups there was fold-increase (95% CI) of 27.5 (2.1 to 36.6, p=0.024) in HYP relative to NRX. For the M26_lateral donor, from NRX/+TGF-β3 to HYP/+TGF-β3 there was a 7.0-fold increase in *COL2A1* but only a 1.8-fold increase in wet weight, which may explain the dramatic increase in type II collagen protein immunofluorescence intensity in the latter group (Figure 4.1A, Figure 4.3A, Figure 4.4B). For the F41 donor, from NRX/+TGF-β3 to HYP/+TGF-β3 there was only a 2.1-fold

increase in *COL2A1* and a 2.3-fold increase in wet weight, which may explain why staining intensity was similar between these conditions (Figure 4.1A, Figure 4.4B, Figure S4.2).

For *COL1A2*, the matched medial and lateral donor (M26) had poor amplification for all conditions and was thus not included (Table 4.1). For the remaining 3 donors, the two-way interaction term between HYP and TGF-β3 indicated synergism (Figure 4.4C). In -TGF-β3 groups, there was comparatively low *COL1A2* and no difference between NRX and HYP (p=0.25).

COL10A1 was measured as a representative hypertrophic marker (Figure 4.4D)[145]. The two-way interaction term between HYP and TGF-β3 was not significant (p=0.16). However, the main effect of HYP compared to NRX showed a fold-decrease (95% CI) of 7.3 (4.3 to 12.4, p¡0.001); HYP thus suppressed *COL10A1* even in the absence of TGF-β3 supplementation. Furthermore, the main effect of TGF-β3 showed a fold-increase of 20.8 (13.5 to 31.8, p<0.001) from -TGF-β3 to +TGF-β3 groups.

Endogenous *TGF-β1*, *TGF-β2*, and *TGF-β3* were measured for mechanistic insight into the lack of an ECM-forming response in the HYP/-TGF-β3 condition (Figure 4.5). For *TGF-β1*, the two-way interaction term of HYP and TGF-β3 supplementation approached significance (p=0.086), which provided weak evidence for synergism. The main effect of HYP showed a fold-increase (95% CI) of 2.2 (1.7 to 3.0, p=0.001) from NRX to HYP, although this was clearly driven by the HYP/+TGF-β3 condition as there was no trend towards a difference between HYP/-TGF-β3 and NRX/-TGF-β3 (p=0.38). Furthermore, the main effect of TGF-β3 on relative *TGF-β1* mRNA showed a fold-increase of 2.2 (1.8 to 2.8, p=0.001). The two-way interaction term of HYP and TGF-β3 indicated synergism in *TGF-β2*. In -TGF-β3 groups, there was a fold-decrease in HYP of 1.8 (1.0 to 3.3, p=0.043). For relative *TGF-β3*, the two-way interaction term of HYP and TGF-β3 supplementation approached significance (p=0.055), providing weak evidence for synergism. The main effect of HYP approached significance (p=0.068), providing weak evidence for a HYP effect. The

main effect of TGF-β3 showed a fold-increase of 2.8 (1.5 to 5.0, p=0.010).
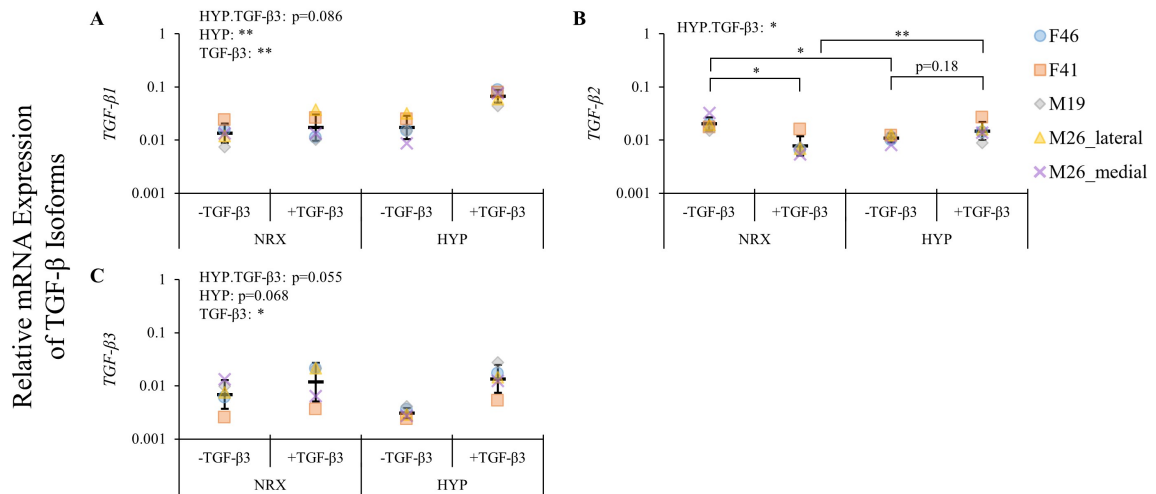
Figure 4.5: Relative mRNA expression of TGF-β isoforms by qRT-PCR for aggregates of adult human T1F2-expanded meniscus cells after 3 weeks' culture. Each shape/colour represents samples from the same meniscus tissue and each data point represents the mean of 1-2 replicates. P-values correspond to two-way within subjects ANOVA for ΔCt (Ct$_{\text{reference average}}$-Ct$_{\text{gene of interest}}$) values, while relative expression is presented as $2^{\Delta\text{Ct}}$. HYP.TGF-β3: interaction term between oxygen tension and TGF-β3 supplementation. HYP: Hypoxia (3% O_2) NRX: Normoxia (atmospheric O_2). Significant differences are labelled as: *p<0.05, **p<0.01, ***p<0.001.

HIF-1α and its target genes

Relative mRNA expression of *HIF-1α* and representative HIF-1 target genes were chosen as this transcription factor plays critical roles in oxygen homeostasis and may be an important transcription factor highly expressed in the inner human meniscus[56, 146]. For *HIF-1α*, the two-way interaction term of HYP and TGF-β3 was not significant (p=0.72) (Figure 4.6A). Moreover, the main effect of HYP was also not significant (p=0.29). However, the main effect of TGF-β3 showed a fold-increase (95% CI) of 2.5 (1.8 to 3.4, p=0.001). *SOX9* is a highly relevant HIF-1 target gene as it is a transcription factor itself for inner meniscus-related genes *ACAN* and *COL2A1* (Figure 4.6B). The two-way interaction term of HYP and TGF-β3 indicated synergism in *SOX9* expression. There was comparatively low *SOX9* in -TGF-β3 groups with no difference between NRX and HYP (p=0.17), whereas in +TGF-β3 groups there

was a fold-increase (95% CI) of 4.3 (2.2 to 8.2, p=0.003) from NRX to HYP. *SOX9* expression tended to mirror that of *ACAN* and *COL2A1*, implying that SOX9 protein was expressed and transcriptionally active (Figure 4.4AB & Figure 4.6B). *VEGF* was measured as it has roles in the hypoxia response and has been shown to be co-operatively promoted by HIF-1 and TGF-β (Figure 4.6C)[136, 141]. The two-way interaction term of HYP and TGF-β3 approached significance (p=0.070), providing weak evidence for synergism in *VEGF* expression. The main effect of HYP showed a fold-increase (95% CI) of 4.8 (3.0 to 7.6, p=0.001) from NRX to HYP. Furthermore, the main effect of TGF-β3 showed a fold-increase of 14.0 (7.6 to 25.9, p<0.001). Finally, mRNA expression of HIF-1 target genes *P4Hα(I)* and *PHD2* were measured to further examine the role of HIF-1 in each group (Figure 4.6DE). There was no evidence of synergism in *P4Hα(I)* (p=0.50). However, the main effect of HYP showed a fold-increase (95% CI) of 2.2 (2.0 to 2.5, p<0.001) while the main effect of TGF-β3 supplementation showed a fold-increase of 2.9-fold (2.5 to 3.4, p¡0.001). For *PHD2*, the two-way interaction term of HYP and TGF-β3 indicated synergism. There were no significant differences found between -TGF-β3 groups (p=0.17). While there was weak evidence for a marginal (1.1-fold) decline from NRX/-TGF-β3 to NRX/+TGF-β3 (p=0.055), there were small significant increases in expression in the combined treatment group HYP/+TGF-β3 relative to HYP/-TGF-β3 (1.4-fold, p=0.003) and NRX/+TGF-β3 (1.9-fold, p<0.001).

4.5.4 Principal component (PC) analysis

PC analysis was applied to summarize quantitative data (Figure S4.3A). *COL1A2* was excluded due to poor amplification for two donors. The KMO measure for *TGF-β2* fell below 0.5 and so this data was also excluded. Two components had eigenvalues greater than 1. PC1 and PC2 described 64.9% and 18.6% of the total variance (eigenvalues=8.4 and 2.4) in wet weight, GAG content, DNA content, and *ACAN*, *COL2A1*, *COL10A1*, *TGF-β1*, *TGF-β3*, *HIF-1α*, *SOX9*, *VEGF*, *P4Hα(I)*, and *PHD2*
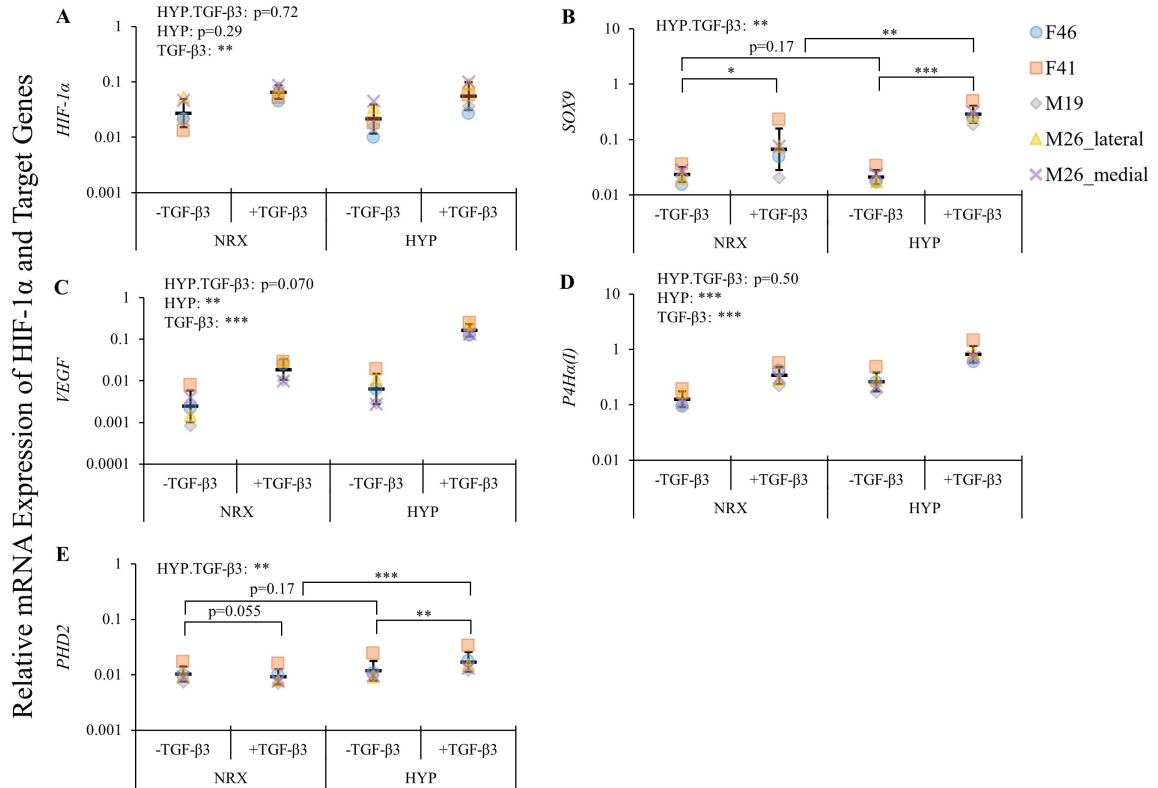
Figure 4.6: Relative mRNA expression of *HIF-1α* and downstream HIF-1 target genes *VEGF*, *SOX9*, *P4Hα(I)*, and *PHD2* by qRT-PCR for aggregates of adult human T1F2-expanded meniscus cells after 3 weeks' culture. Each shape/colour represents samples from the same meniscus tissue and each data point represents the mean of 1-2 replicates. P-values correspond to two-way within subjects ANOVA for ΔCt (Ct$_{\text{reference average}}$-Ct$_{\text{gene of interest}}$ values, while relative expression is presented as 2ΔCt. HYP.TGF-β3: interaction term between oxygen tension and TGF-β3 supplementation. HYP: Hypoxia (3% O_2), NRX: Normoxia (atmospheric O_2). Significant differences are labelled as: *p<0.05, **p<0.01, ***p<0.001.

(Figure S4.3A). PC1 correlated most strongly with wet weight, GAG content, *ACAN*, *COL2A1*, *TGF-β1*, *SOX9*, *VEGF*, and *P4Hα(I)* (Figure S4.3A). Larger PC1 scores were thus interpreted to reflect an inner meniscus-like ECM-forming phenotype. For its part, PC2 correlated best with *COL10A1* and *TGF-β3* (Figure S4.3A). Thus, larger PC2 scores were interpreted to indicate a more hypertrophic phenotype. The scatterplot of PC1 and PC2 scores showed general clustering of points into the four experimental conditions (Figure S4.3B).

4.6 Discussion

In this study, we found that HYP and TGF-β3 supplementation synergistically promoted quantitative protein and mRNA-level measures of inner meniscus-like ECM formation by adult human MFCs. This finding was complemented by histological observations of superior accumulation of sulphated proteoglycans and type II collagen in HYP/+TGF-β3 relative to all other groups. We further found that the concentrations of these ECM constituents within aggregates appeared to be as high, if not higher, in HYP/+TGF-β3 relative to NRX/+TGF-β3. These findings add to evidence demonstrating the effectiveness of HYP for tissue engineering the inner meniscus and similar tissues[8, 55, 147, 148]. To summarize the quantitative data, we used principal component (PC) analysis and found that aggregates in each condition generally clustered together on a plot PC1 and PC2, demonstrating they tended to share a common ECM-forming phenotype. Further limiting PC analysis to wet weight, GAG content, *ACAN*, *COL2A1*, *TGF-β1*, *SOX9*, *VEGF*, and *P4Hα(I)* showed that a single component explained 88.2% of variance and correlated strongly with wet weight (R=0.94) (data not shown). This demonstrates that in this culture model, information as simple to obtain as wet weight could potentially be used to easily assess the extent of inner meniscus-like ECM formation.

The beneficial effects of HYP for synthesis and accumulation of inner meniscus-like ECM were largely dependent upon TGF-β3 supplementation. In HYP/-TGF-β3 relative to NRX/-TGF-β3, expression of inner meniscus ECM molecule genes *ACAN* and *COL2A1* declined and there was no observed difference in *COL1A2* and *SOX9*. Further, there was a decline in mRNA expression of *TGF-β2* and *TGF-β3* and no difference in *TGF-β1*. Given that *SOX9* is a transcription factor for *ACAN* and *COL2A1* and that *SOX9* is stabilized by TGF-β, this suggests suppression of *SOX9*-mediated transcription in HYP/-TGF-β3 relative to NRX/-TGF-β3, perhaps due to reduced TGF-β-mediated *SOX9* stabilization[139, 140].

These findings for MFCs differ from the inner meniscus-like ECM-forming (chondrogenic) response to HYP without growth factor supplementation observed for human (aged 20-43) BM-MSCs, which was associated with increased endogenous *TGF-β1* expression[117]. This may be related to the differentiated nature of MFCs relative to BM-MSCs. Interestingly, in the present study there was elevated expression of *TGF-β1* and *TGF-β3* in HYP/+TGF-β3 relative to HYP/-TGF-β3, suggesting that TGF-β3 supplementation leads to positive feedback in endogenous *TGF-β* expression in this cell culture model. Future study will consider whether transient TGF-β3 supplementation can initiate positive feedback in endogenous *TGF-β* expression to induce a sustained ECM-forming response by adult human T1F2-expanded MFCs under HYP. This might help explain the sustained ECM-forming response following transient TGF-β3 supplementation shown by chondrocytes and BM-MSCs from bovine calves[149, 150].

Although the inner meniscus ECM-forming response to HYP was dependent upon TGF-β3 supplementation, several other HYP effects were independent of TGF-β3 supplementation. Firstly, *COL10A1* was suppressed regardless of TGF-β3 supplementation, indicating that hypoxia-mediated suppression of hypertrophic markers may be at least in part independent of TGF-β3 supplementation. Secondly, aggregates cultured in HYP/-TGF-β3 and HYP/+TGF-β3 were larger in wet weight than their NRX counterparts. In -TGF-β3 groups, this was despite having unchanged or reduced expression of all ECM genes measured in HYP relative to NRX. This may reflect post-transcriptional regulation of ECM synthesis, expression of different ECM components altogether, or enhanced stabilization and entrapment of newly-synthesized ECM by collagen cross-linking through lysyl oxidases (LOXs), whose expression is dependent on HYP-dependent HIF-1 activity[147, 151]. Finally, HIF-1 target gene *VEGF* was elevated by HYP regardless of TGF-β3 supplementation. Together, these results indicate that there was increased HIF-1 activity in HYP relative to NRX within +TGF-β3 and within -TGF-β3 groups.

The mechanisms underlying the observed synergy of HYP and TGF-β3 supplementation in modulating inner meniscus-like ECM protein expression and mRNA expression of related genes were suspected to involve HIF-1. *HIF-1α* mRNA was enhanced with TGF-β3 supplementation to comparable degrees in both NRX and HYP groups, suggesting that TGF-β3 supplementation primed these aggregates for an elevated HIF-1 response. This is consistent with previous findings that various cytokines and growth factors including TGF-β1 mediate HIF-1 activity[152]. Coupled with the known hypoxia-dependence of HIF-1 protein activity, the combined treatment of HYP/+TGF-β3 would be expected to elicit the maximal HIF-1 response. Indeed, mRNA expression of all HIF-1 target genes investigated here (*VEGF*, *SOX9*, *P4Hα(I)*, and *PHD2*) suggest this may have been the case although HIF-1 protein was not measured directly.

4.7   Conclusion

We found that hypoxia and TGF-β3 supplementation synergistically enhanced inner meniscus-like ECM formation by T1F2-expanded adult human MFCs in an aggregate model. The evidence in this study is consistent with a HIF-1α-mediated mechanism for the observed synergy. We further found that TGF-β3 supplementation increased HIF-1α mRNA expression, which would support HIF-1 activity based on the known hypoxia-dependence of HIF-1α stability. Finally, we demonstrated that inner meniscus-like ECM formation was dependent upon TGF-β3 supplementation in this culture model and that hypoxia alone does not upregulate mRNA expression of TGF-β isoforms.

4.8   Funding sources

4.9   Author contributions

4.10   Supporting information

Figure S4.1: Qualitative histological investigation of ECM for one representative donor (F41, i.e., orange squares in Figures 4.1 and 4.4 to 4.6). 5 µm sections of paraffin-embedded aggregates of adult human T1F2-expanded meniscus cells cultured for 3 weeks were stained with Safranin-O for sulphated proteoglycans (pink), Fast Green FCF as protein counterstain, and Mayer's Haematoxylin for cell nuclei. Scale bars are shared within rows.
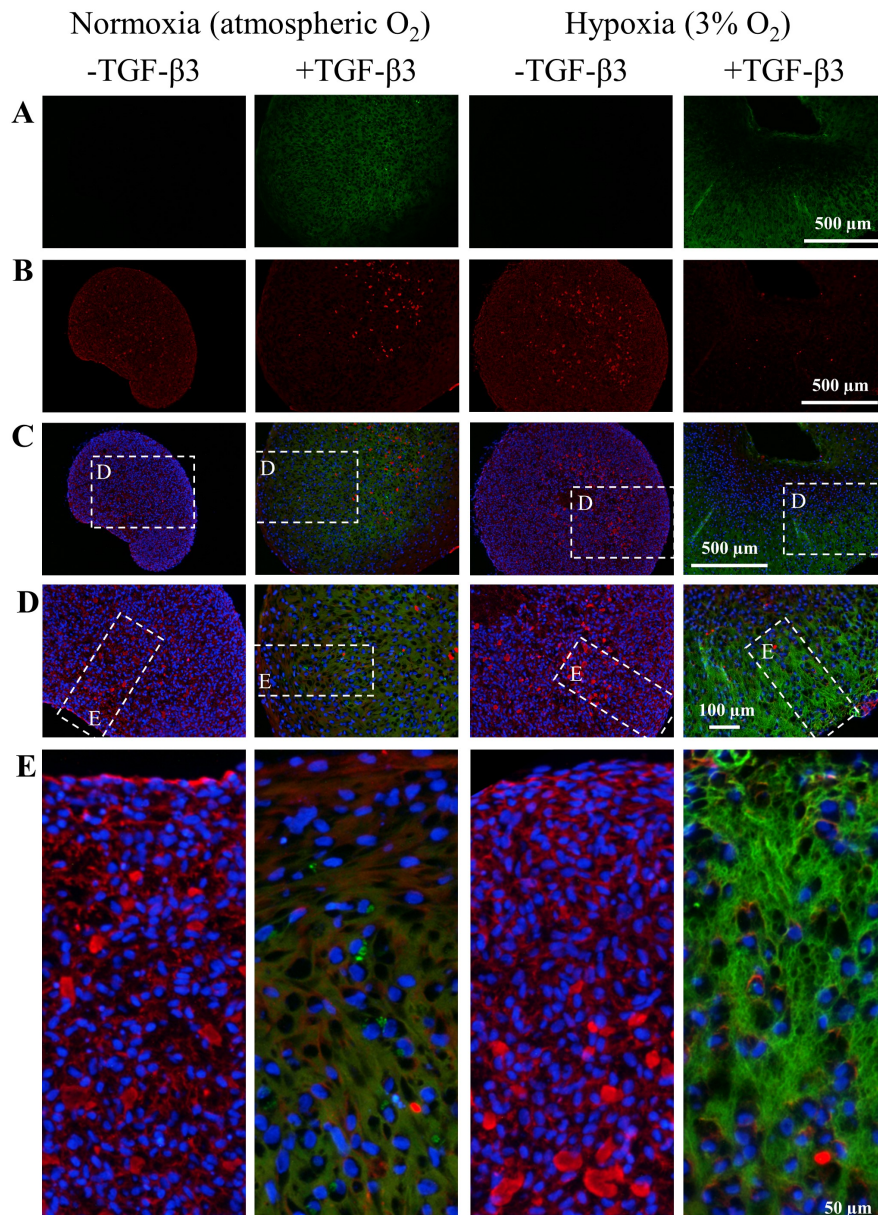
Figure S4.2: Qualitative immunofluorescence-based investigation of ECM for one representative donor (F41, i.e., orange squares in Figures 4.1 and 4.4 to 4.6) 5 µm sections of paraffin-embedded aggregates of adult human T1F2-expanded meniscus cells cultured for 3 weeks were immunofluorescently-labelled for types II (green) and I (red) collagens and cell nuclei (blue). A) Type I collagen; B) Type II collagen; CDE) Overlay of types I and II collagen and DAPI. Scale bars are shared within rows.

A

	Correlations	
	PC1	PC2
Wet weight	0.94	<0.30
GAG content	0.91	0.38
DNA content	0.57	<0.30
ACAN	0.82	0.52
COL2A1	0.79	0.53
COL10A1	<0.30	0.93
TGF-β1	0.92	<0.30
TGF-β3	<0.30	0.85
HIF-1α	0.30	0.78
SOX9	0.91	0.34
VEGF	0.92	<0.30
P4Hα(I)	0.94	<0.30
PHD2	0.80	-0.45

B

Principal Component 2 / Principal Component 1

T3 / HYP / Combined

Conditions

NRX/-TGF-β3
NRX/+TGF-β3
HYP/-TGF-β3
HYP/+TGF-β3

Donor identifiers

☐ F46
○ F41
◇ M19
△ M26_lateral
✕ M26_medial
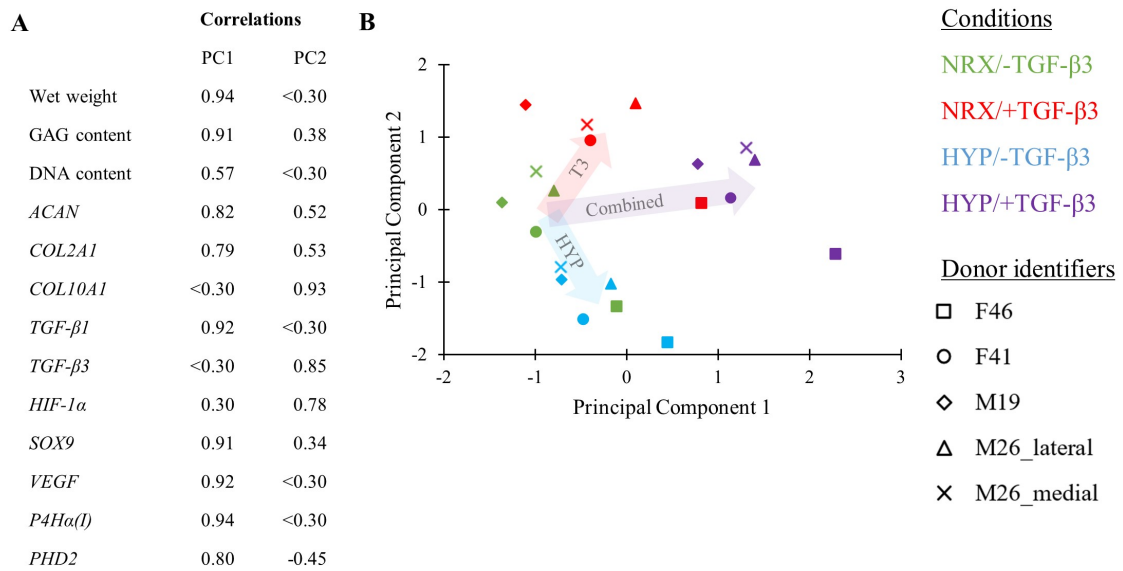
Figure S4.3: Principal component (PC) analysis of the correlation matrix of wet weight, GAG content, DNA content and relative mRNA gene expression of *ACAN*, *COL2A1*, *COL10A1*, *TGF-β1*, *TGF-β3*, *HIF-1α*, *SOX9*, *VEGF*, *P4Hα(I)*, and *PHD2*. PC1 and PC2 respectively accounted for 68.1% and 15.8% of variability in the correlation matrix. A) Correlations (loadings) of PC1 and PC2 with each variable. B) Scatterplot of component scores. Arrows show the net direction of the individual and combined effects of HYP and TGF-β3 supplementation relative to the NRX/-TGF-β3 condition.

Chapter 5

Engineered Human Meniscus' Matrix-Forming Phenotype is Unaffected by Low Strain Dynamic Compression Under Hypoxic Conditions

Contributing authors:

Alexander R. A. Szojka, Colleen N. Moore, Yan Liang, Stephen H. J. Andrews, Melanie Kunze, Aillette Mulet-Sierra, Nadr M. Jomha, Adetola B. Adesida

This chapter has been previously published as:

A. R. Szojka, C. N. Moore, Y. Liang, S. H. Andrews, M. Kunze, A. Mulet-Sierra, N. M. Jomha, and A. B. Adesida, "Engineered human meniscus matrix-forming phenotype is unaffected by low strain dynamic compression under hypoxic conditions," *PLoS ONE*, vol. 16, no. 3 March, F. Zhao, Ed., e0248292, 2021

5.1 Preface

In parallel to the unsuccessful attempts at growing tissue on PCL described in the preface to Chapter 4, my early cell culture work with Karamveer Lalh and Yan Liang

compared the effects of growth factors during monolayer expansion on mechanical property development in engineered meniscus tissues on type I collagen scaffolds. This work was, unfortunately, also largely unsuccessful. A major problem was that the different growth factors we investigated radically changed the contractility of the MFCs on type I collagen scaffolds, which led to issues in measuring mechanical properties which were our main outcome variables. I salvaged what data I could and provided it as supplementary material for this manuscript, which is briefly discussed at the beginning of the results section as preliminary work.

Much of the first experiment in this study that is fully described in this publication was carried out in parallel to the pellet study in Chapter 4 as a complement using type I collagen scaffolds. Three more donors were later added in the dynamic compression portion of the study.

This project was presented at the 2017 Summer Students' Research Day, Faculty of Medicine and Dentistry, University of Alberta by Colleen Moore, an outstanding undergraduate summer student whom I had the privilege to mentor in summer 2017.

5.2   Abstract

Low oxygen and mechanical loading may play roles in regulating the fibrocartilaginous phenotype of the human inner meniscus, but their combination in engineered meniscus tissue remains unstudied. Here, we investigated how continuous low oxygen ("hypoxia") combined with dynamic compression would affect the fibrocartilaginous "inner meniscus-like" matrix-forming phenotype of human meniscus fibrochondrocytes (MFCs) in a porous type I collagen scaffold. Freshly-seeded MFC scaffolds were cultured for 4 weeks in either 3 or 20% O_2 or pre-cultured for 2 weeks in 3% O_2 and then dynamically compressed for 2 weeks (10% strain, 1 Hz, 1 h/day, 5 days/week), all with or without TGF-β3 supplementation. TGF-β3 supplementation was found necessary to induce matrix formation by MFCs in the collagen scaffold regardless of oxygen tension and application of the dynamic compression loading regime. Nei-

ther hypoxia under static culture nor hypoxia combined with dynamic compression had significant effects on expression of specific protein and mRNA markers for the fibrocartilaginous matrix-forming phenotype. Mechanical properties significantly increased over the two-week loading period but were not different between static and dynamic-loaded tissues after the loading period. These findings indicate that 3% O_2 applied immediately after scaffold seeding and dynamic compression to 10% strain do not affect the fibrocartilaginous matrix-forming phenotype of human MFCs in this type I collagen scaffold. It is possible that a delayed hypoxia treatment and an optimized pre-culture period and loading regime combination would have led to different outcomes.

5.3   Introduction

The menisci play important mechanical roles in the knee [15, 30]. In humans, their weight-bearing inner region develops a fibrocartilaginous phenotype throughout life with morphological differences from the outer region (Table 5.1)[32, 33, 35–37, 44, 153]. In adults, the inner region is avascular and non-healing whereas the outer region has a peripheral blood supply that provides some healing capacity. Inner meniscus injuries disrupt knee function and may cause early osteoarthritis development[17, 18, 154].

The aim of meniscus tissue engineering is to generate meniscus tissue replacements that restore function and prevent osteoarthritis after non-healing injuries. Knowledge of how the human inner meniscus phenotype is regulated will facilitate development of these replacements. Human tissue engineering models allow study of how meniscus fibrochondrocytes (MFCs), the cells primarily responsible for synthesis and maintenance of the inner meniscus, regulate fibrocartilaginous matrix formation in response to biophysical factors present in the knee joint[155]. Two factors believed to play regulatory roles in the inner meniscus phenotype are oxygen tension and mechanical loading.

Table 5.1: Summary of relevant general inner-outer meniscus differences in adults.

Aspect	Inner (2/3 or more)	Outer (1/3 or less)
Tissue phenotype	Fibrocartilage	Dense fibrous connective tissue (ligament- and tendon-like)
Cell morphology	Fibrochondrocytes (MFCs): a mixed population of fibroblast and chondrocyte-like cells	Fibroblast-like
ECM composition	Type I collagen, trace amounts of type II collagen and aggrecan	Type I collagen
Blood supply and healing capacity	Avascular, non-healing	Vascularized, healing
Loading environment	Weight-bearing (compression), tension	Tension

Oxygen appears to mediate the inner meniscus phenotype. The inner regions of the adult menisci exist in a low oxygen environment, as they are avascular and surrounded by the hypoxic synovial fluid[28, 29, 156]. Low oxygen conditions, described as "hypoxic" or "physioxic" to reflect the native inner meniscus microenvironment, affect development of meniscus cell-based engineered tissues[2, 8, 10, 55–59, 148]. Hypoxic culture of human meniscus cell-based engineered tissues promotes formation of cartilaginous matrix components type II collagen and aggrecan[2, 8, 55, 56, 59], which provide compression resistance through their water-retaining properties[52, 91]. Hypoxia-mediated chondrogenesis is regulated through transcription factor hypoxia-inducible factor-1 (HIF-1), gene expression of transcription factor SRY-related high-mobility group (HMG) box-9 (*SOX9*), and growth factors such as transforming growth factor-β (TGF-β)[2, 56, 60]. Studies in our research group, however, show that cartilaginous matrix formation under hypoxia by human meniscus cells differs between scaffold-free pellets and a larger-scale type I collagen scaffold, which warrants further investigation[2, 57, 58]. One possible explanation for these differing results is the cell source.

The scaffold studies used meniscus from older (ages 54-79) donors undergoing knee replacements for severe osteoarthritis whereas the pellet study used meniscus tissues from younger (ages 19-46) donors without osteoarthritis. As well, the pellet study had continuous hypoxia treatment without re-oxygenation during medium changes using an XVivo incubator system (Biospherix, USA), whereas the scaffold studies used standard hypoxia incubators with tissues re-oxygenated briefly during medium changes.

Mechanical loading also appears to mediate the inner meniscus phenotype[33, 35–37]. Dynamic deformational loading (e.g., dynamic tension, dynamic compression) and cyclic hydrostatic pressure[157], which mimics the pressurization of fluid in cartilaginous matrix during weight-bearing, have been applied to study the biosynthetic response of meniscus explants and meniscus cell-based engineered tissues[64–73, 158–164]. Only five mechanical loading studies to date use human meniscus cells or tissues. These studies showed either improved cartilaginous matrix formation under loading or no effects[65–69]. Although dynamic compression has been applied to investigate the mechanical behaviour of human meniscus explants (see, for example[113]), its effects on biosynthesis in human meniscus explants and engineered tissues remain unstudied.

Hypoxia and mechanical loading have not previously been combined for engineering meniscus cell-based tissues in vitro. Confined dynamic compression under hypoxia of bovine chondrocytes in polyurethane scaffolds seemed to synergistically stabilize the chondrocyte phenotype in a preliminary study[81]. TGF-β3 supplementation and hypoxia but not unconfined dynamic compression had beneficial effects on chondrogenic differentiation in porcine bone marrow-derived mesenchymal stem cells (BM-MSCs) in agarose[82]. Dynamic compression of rabbit BM-MSCs in agarose under normal oxygen levels, however, induced chondrogenesis as effectively as TGF-β1 supplementation[165].

Here, we investigated how combined hypoxia and dynamic loading may regulate

the fibrocartilaginous inner meniscus phenotype, which could lead to a "biomimetic" strategy for meniscus tissue engineering[2, 57, 110]. We used human MFCs from the inner meniscus regions, isolated from young donors undergoing partial meniscectomy but without osteoarthritis, because they are a promising cell source for clinical translation. The MFCs were seeded on a porous biomaterial scaffold made of type I collagen, the main biochemical constituent of human inner meniscus. We first investigated hypoxia effects under static conditions and then dynamic compression effects under hypoxic conditions. The experiments were performed with or without TGF-β3 supplementation to determine if hypoxia under static conditions and hypoxia combined with dynamic compression could induce a fibrocartilaginous matrix-forming response without exogenous growth factors.

Our hypotheses were that the fibrocartilaginous, "inner meniscus-like" matrix-forming phenotype of MFCs would be: i) promoted by hypoxia but dependent upon TGF-β3 supplementation[2], and ii) promoted by dynamic compression under hypoxia regardless of TGF-β3 supplementation.

5.4   Materials and methods

Two related experiments – Part 1: hypoxia and TGF-β3 supplementation effects, and Part 2: dynamic compression and TGF-β3 supplementation effects under hypoxia – were carried out as outlined in Figure 5.1. Unless otherwise specified all methods have been previously described in detail[[8, 57].

5.4.1   Ethics and sample collection

Meniscus specimens were collected during arthroscopic partial meniscectomies at the Grey Nuns Community Hospital and the University of Alberta Hospital in Edmonton with patient consent waived in accordance with the University of Alberta human research ethics board's approval #Pro00018778 to use surgical cast-offs with non-identifying information for scientific research purposes.
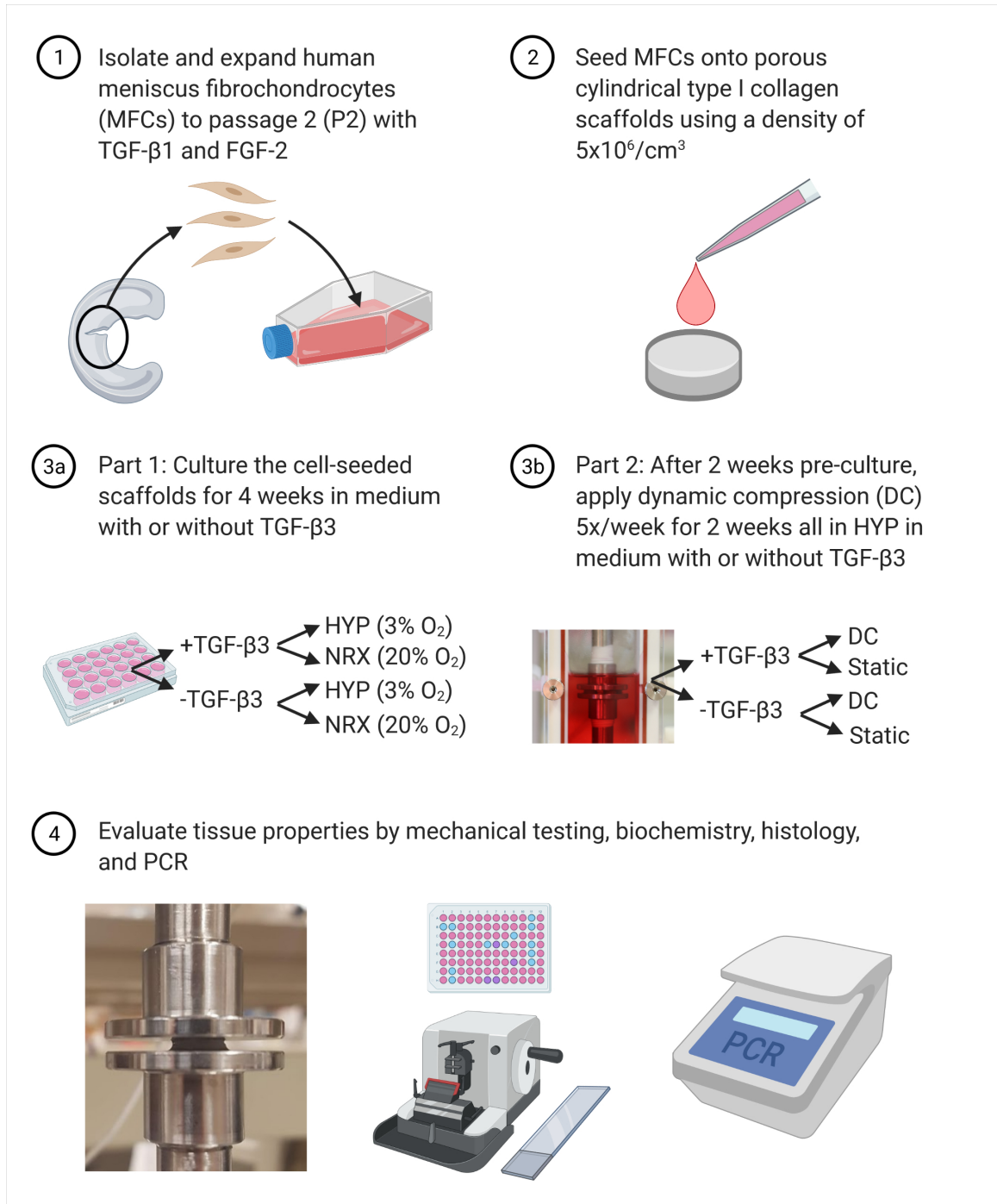
Figure 5.1: Study outline. HYP: hypoxia. NRX: normoxia.

5.4.2 Cell and tissue culture

Meniscus tissues from seven male donors ages 19-39 were digested overnight in type II collagenase (0.15% w/v; 300 units/mg). Cells from all donors were kept separate

from one another, i.e., cells from different donors were never pooled to preserve inter-donor variation (donor details and the exact breakdown of data generated from each donor are available in the dataset provided with the published manuscript online). Four donors were cultured for part 1 only, and three were cultured for both parts 1 and 2. As a recovery period, MFCs were placed in standard tissue culture flasks in monolayer with a standard basal expansion medium containing 10% v/v fetal bovine serum (FBS) for 48 hours. For cell expansion, MFCs were put into fresh flasks at a density of $10^4/cm^2$ in humidified incubators with 5% CO_2. The basal medium (BM) was supplemented with 1 ng/mL TGF-β1 and 5 ng/mL FGF-2 in the main experiments, a combination that was shown to increase proliferation rates while maintaining the cells' matrix-forming capacity compared to basal medium (BM) and BM+FGF-2 alone (Figure S5.1).

MFCs were expanded to passage 1 or 2 (population doublings 2.9-4.1), a degree of expansion shown previously to produce MFCs with good fibrocartilaginous matrix-forming capacity[8]. MFCs were collected and seeded onto 10-mm diameter type I collagen scaffolds (3.5-mm thick, pore size 115±20 μm) at a density of $5 \times 10^6/cm^3$. For tissue formation, cell-seeded scaffolds were cultured in a defined serum-free chondro-genic tissue culture medium, but with or without the standard addition of 10 ng/mL of TGF-β3 in incubators containing 3 or 20% O_2 and 5% CO_2 (X3 XVivo, Biospherix, USA) for up to 4 weeks[2, 8]. Medium changes for hypoxia groups occurred within a 3% O_2 environment, i.e., the hypoxia treatment was continuous.

5.4.3   Dynamic compression

After two weeks of pre-culture with or without TGF-β3 supplementation in hypoxia (3% O_2) engineered tissues were transferred onto custom platens fitted to chambers containing 110 mL of the tissue culture medium on a Biodynamic 5210 system (TA Instruments, USA). Tissues were pre-loaded to 0.01-N each and dynamically com-pressed at least five times per week for two more weeks to 10% strain at 1 Hz for 1

hour per day with static vehicle controls in replicate chambers. Apart from reduced dynamic loading time (2 weeks vs. 3 & 6 weeks), this regime is the same as was applied in the context of comparing individual and combined effects of hypoxia (5% O_2), dynamic compression, and TGF-β3 supplementation on chondrogenic differentiation with or without a 3 week pre-culture period, but in a different culture model (four month old porcine bone marrow-derived mesenchymal stem cells in 2% agarose hydrogels)[82].

5.4.4 Mechanical analysis

During loading, the compression modulus from the first and last cycles were determined by dividing the change in force by the applied strain and the cross-sectional area. After the culture period, tissues were individually tested using unconfined compression stress relaxation tests. Tissues were pre-loaded to 0.01 N and then compressed to 10% strain using a strain rate 50% strain/s[7, 166]. Tissues were allowed to relax to equilibrium. The peak change in force was used to calculate the instantaneous modulus and the equilibrium change for the equilibrium modulus.

5.4.5 Quantitative biochemical and qualitative histological and immunofluorescence analysis

For biochemistry, after mechanical testing tissues were solubilized in proteinase K. Glycosaminoglycan contents were measured using the dimethylmethylene blue (DMMB) assay and DNA contents with the CyQUANT cell proliferation assay.

For qualitative histology, tissues were processed for paraffin embedding, sectioned at 5 µm, and stained with all of Safranin-O, Fast Green FCF, and Meyer's haematoxylin. Immunofluorescence was performed for types I and II collagens and cell nuclei by 4',6-diamidino-2-phenylindole (DAPI). The anti human type I collagen antibody showed only minute traces of cross reactivity with the bovine type I collagen scaffold.

5.4.6 Gene expression analysis

RNA was isolated using TRIzol reagent and reverse transcribed into cDNA for quantitative real-time polymerase chain reaction (qRT-PCR) analysis using the gene specific primers listed in Table S5.1. Expression of genes of interest was normalized to the mean expression level of reference genes *YWHAZ*, *β-actin*, and *B2M* and presented using the $2^{\Delta Ct}$ method[167]. Statistics were computed using ΔCt values.

5.4.7 Statistical analysis

Mean replicate values for each donor were used for statistical analysis in SPSS 26 (IBM, USA). Two-way ANOVA was performed with TGF-β3 supplementation and oxygen tension or dynamic compression as fixed factors and donor as a random factor. All data was assumed to be normally distributed. When the interaction effect between fixed factors was significant, four pairwise comparisons were made (e.g., i) NRX/-TGF-β3 vs. HYP/-TGF-β3; ii) NRX/+TGF-β3 vs. HYP/+TGF-β3; iii) NRX/-TGF-β3 vs. NRX/+TGF-β3; iv) HYP/-TGF-β3 vs. HYP/+TGF-β3). When the fixed factor interaction effect was not significant, the significance of the main effects of each fixed factor were assessed. Linear correlations (Figure 5.5E-G) were computed after mean centering data from each donor to reduce the influence of variability between donors. This involved dividing values by the overall donor mean and multiplying by the grand mean.

5.5 Results

In preliminary work, FGF-2 supplementation increased proliferation rates compared to the basal medium (1.1-fold, p=0.030) (Figure S5.1A). FGF-2 combined with TGF-β1 (T1F2) caused a larger increase (1.6-fold, p<0.001) (Figure S5.1A). GAG/DNA and mechanical properties were comparable across conditions, indicating that the matrix-forming capacity of MFCs was maintained (Figure S5.1B-E). Given these re-

sults, the T1F2 expansion strategy was used throughout the rest of the study.

In Part 1 (static conditions), TGF-β3 supplementation significantly increased fibro-cartilaginous, "inner meniscus-like" matrix formation as assessed by GAG, GAG/DNA, and mechanical properties (Figure 5.2ACDE). DNA contents in TGF-β3 supplementation groups were also significantly higher (Figure 5.2B).
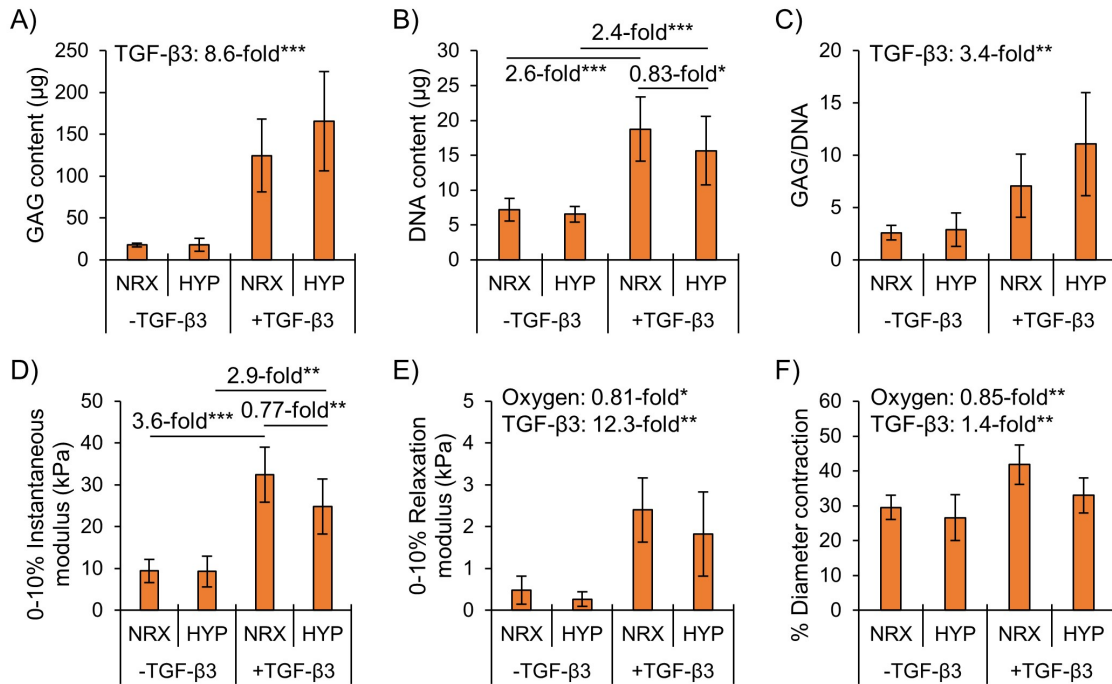
Figure 5.2: Biochemical accumulation was superior in TGF-β3 supplementation groups and mechanical properties were superior in normoxia. Differences were assessed by two-way ANOVA. *: $p < 0.05$, **: $p < 0.01$, ***: $p < 0.001$. NRX: normoxia, 20% O_2. HYP: hypoxia, 3% O_2.

Hypoxia did not affect GAG nor GAG/DNA in TGF-β3 supplementation groups (Figure 5.2AC). Constructs overall had 15% less contraction in hypoxia than normoxia (Figure 5.2F). During mechanical testing, the instantaneous force change across the strain step was not different between hypoxia and normoxia in TGF-β3 supplementation groups (p=0.85, S1 Dataset available in published manuscript). However, when the instantaneous modulus was computed by dividing the force change by the cross-sectional area it was 20% lower in hypoxia (p<0.05) (Figure 5.2D). Construct wet weights are available in Figure S5.2.

Histologically, groups without TGF-β3 supplementation had little synthesized matrix (Figure 5.3). While groups with TGF-β3 supplementation had regions of abundant synthesized matrix and stained more intensely with Fast Green than -TGF-β3 groups, much of the scaffold showed no cell activity (Figure 5.3). Matrix staining positively for Safranin-O, indicating a fibrocartilaginous phenotype, was detected only in the TGF-β3 supplementation groups (Figure 5.3). There were no large and consistent hypoxia effects assessed by histology alone; however, taken together with the quantitative results for DNA content and % diameter contraction, there was evidence for increased cell density in NRX/+TGF-β3 compared to HYP/+TGF-β3 (Figure 5.2BF & Figure 5.3). TGF-β3 supplementation groups had increased type I collagen intensity and were the only ones to show the presence of cartilaginous matrix component type II collagen, albeit only in traces (Figure S5.3A).
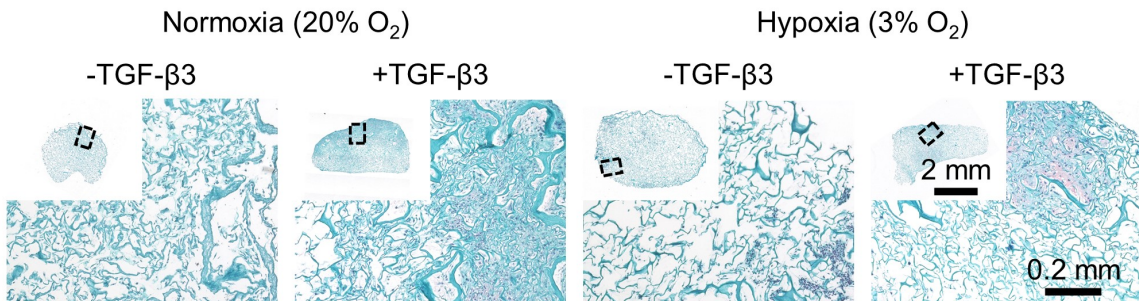
Figure 5.3: Safranin-O staining was superior in TGF-β3 supplementation groups and was not affected by hypoxia. Staining for a representative donor is presented. Staining was performed by combined Safranin-O (sulphated proteoglycans, pink), Fast Green (proteins, turquoise), and haematoxylin (cell nuclei, purple-dark green here).

TGF-β3 supplementation increased fibrocartilaginous matrix-related mRNA expression, whereas hypoxia had no detectable effects (Figure 5.4). Taken with protein-level observations, this indicates that normoxia-cultured constructs had superior mechanical properties due to different contractile characteristics rather than differences in functional matrix. Hypoxia thus did not induce a fibrocartilaginous matrix-forming response regardless of TGF-β3 supplementation.
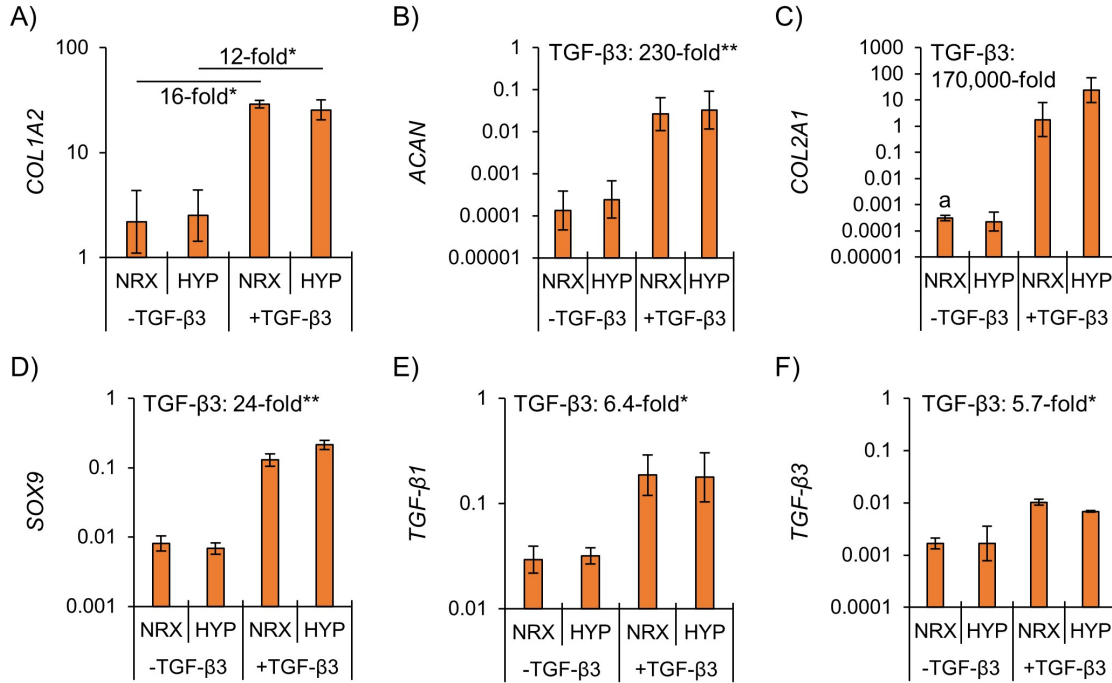
Figure 5.4: Inner meniscus gene expression was enhanced by TGF-β3 supplementation and was not affected by hypoxia. Differences were assessed by two-way ANOVA. *: $p<0.05$, **: $p<0.01$. NRX: normoxia, 20% O_2. HYP: hypoxia, 3% O_2. a: no amplification within 40 PCR cycles for at least one donor.

In Part 2, stress relaxation during the loading period could only be observed in +TGF-β3 groups (Figure 5.5A-C). The forces during loading were lower in groups without TGF-β3 supplementation, though they were higher than those due to friction alone in the bioreactor (Figure 5.5D). This confirmed that the tissues in -TGF-β3 groups were experiencing dynamic compression despite their poor mechanical properties. Regardless of TGF-β3 supplementation, platen liftoff occurred during the decompression phase near the end of the loading period, with forces dropping to 0 N below 5% strain (Figure 5.5D). However, during the compression phase (upper part of curves) the forces showed an immediate rise (Figure 5.5D). This indicated that contact was quickly re-established and that the elastic rebound of the tissues was only slightly too slow for the applied waveform (Figure 5.5D). The tissues cultured with TGF-β3 supplementation had similar heights from day to day (Figure 5.5E). The initial and final modulus during loading periods, calculated using the changes in

force across cycles at the start and end of the loading periods, showed clear increases over time in +TGF-β3 groups only (Figure 5.5FG). After the two-week dynamic compression period, there were no differences in mechanical properties between loaded and unloaded tissues (Figure 5.6DE). Thus, the rise in modulus during loading was attributed to increased culture time rather than to dynamic compression exerting matrix-strengthening effects.

Without TGF-β3 supplementation, biochemical and mechanical properties remained low despite the "biomimetic" combination of dynamic compression and hypoxia (Figure 5.6ACDE). TGF-β3 supplementation increased all measured properties, but there were no consistent effects of dynamic compression (Figure 5.6).

Safranin-O staining was detected only in TGF-β3 supplementation groups, with matrix being most concentrated at the outer edges (Figure 5.7). Dynamic compression had no discernible effects by histology (Figure 5.7). As in part 1, immunofluorescence confirmed the universal presence of type I collagen (Figure S5.3B). TGF-β3 supplementation groups had increased type I collagen intensity and were the only ones to show the presence of type II collagen (Figure S5.3B).

Dynamic compression had no consistent effect on expression of matrix-related genes (Figure 5.8). The only significant dynamic compression effect at the mRNA level was a decrease in *TGF-β1* (0.86-fold in DC vs. static, p<0.01) (Figure 5.8F).

Given that hypoxia under static conditions and dynamic compression under hypoxia did not affect the fibrocartilaginous matrix-forming phenotype, established hypoxia and loading-sensitive genes were measured to confirm that the cells were at least responsive to the treatments. Hypoxia-sensitive genes *LOX* and *VEGF* seemed higher in hypoxia but these were not statistically significant (Figure 5.9AB). *HIF-1α* and *HIF-2α*, genes whose products regulate expression of hypoxia-sensitive genes including *VEGF* and *LOX* but themselves are not necessarily regulated by hypoxia at the gene level[168, 169], were expressed in all groups but not differentially (Figure 5.9DE). Loading-sensitive genes *c-FOS* and *c-JUN*[170, 171] were not differentially expressed
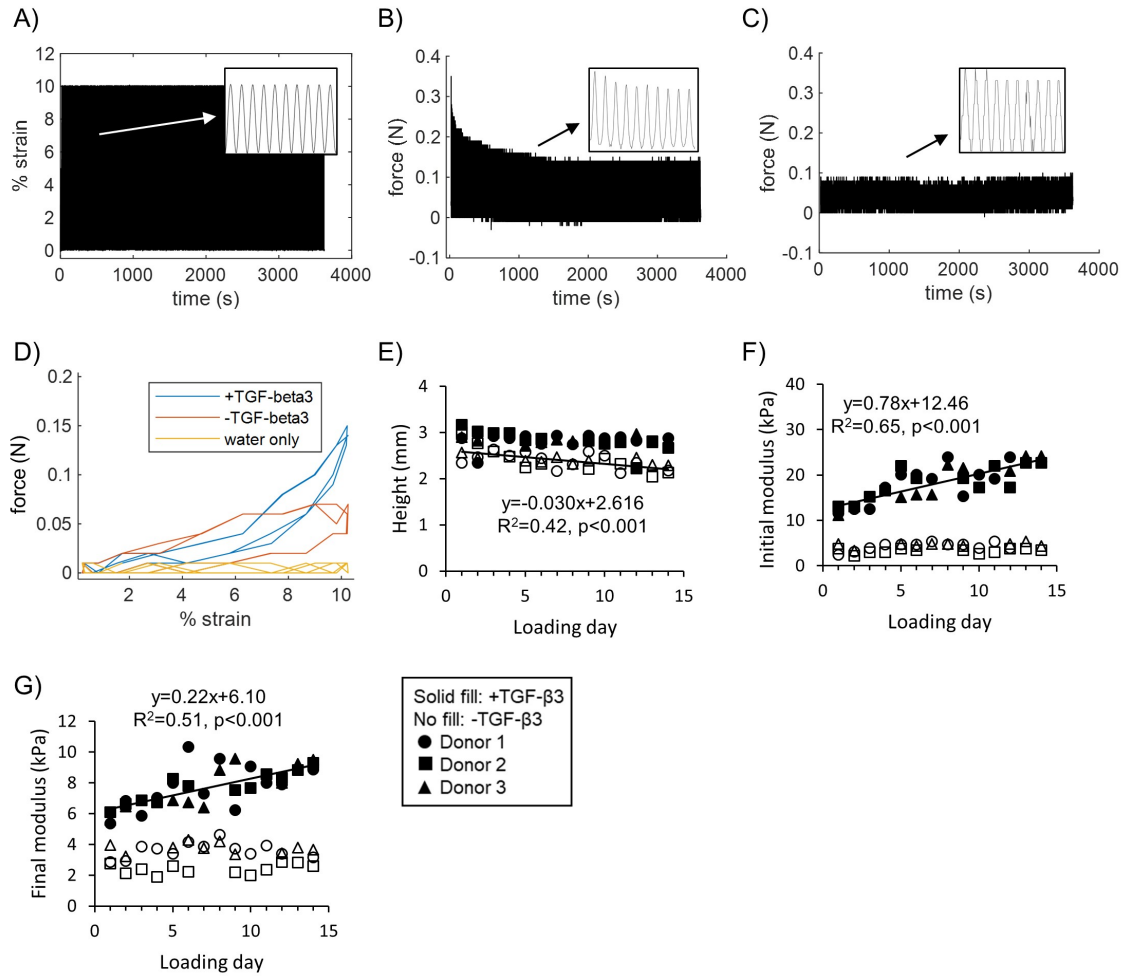
Figure 5.5: Dynamic compression loading summary. A) Tissues were compressed from 0-10% strain at 1 Hz for one hour (3600 cycles). B & C) Representative force vs. time plots for tissues (loading day 10) that had medium supplemented with or without TGF-β3, respectively. D) Representative force vs. strain plots for two cycles near the end of a loading period (loading day 10). The water only group was included to show the magnitude of any frictional forces using a comparable platen stroke. E) Sample heights were measured on each loading day and were used to calculate displacements for application of the 10% strain waveform. F & G) Peak and equilibrium moduli calculated using the force changes across the first and last cycles, respectively, of each loading period for each donor. Only significant (p<0.05) linear correlations were included.

between groups (Figure 5.9EF).
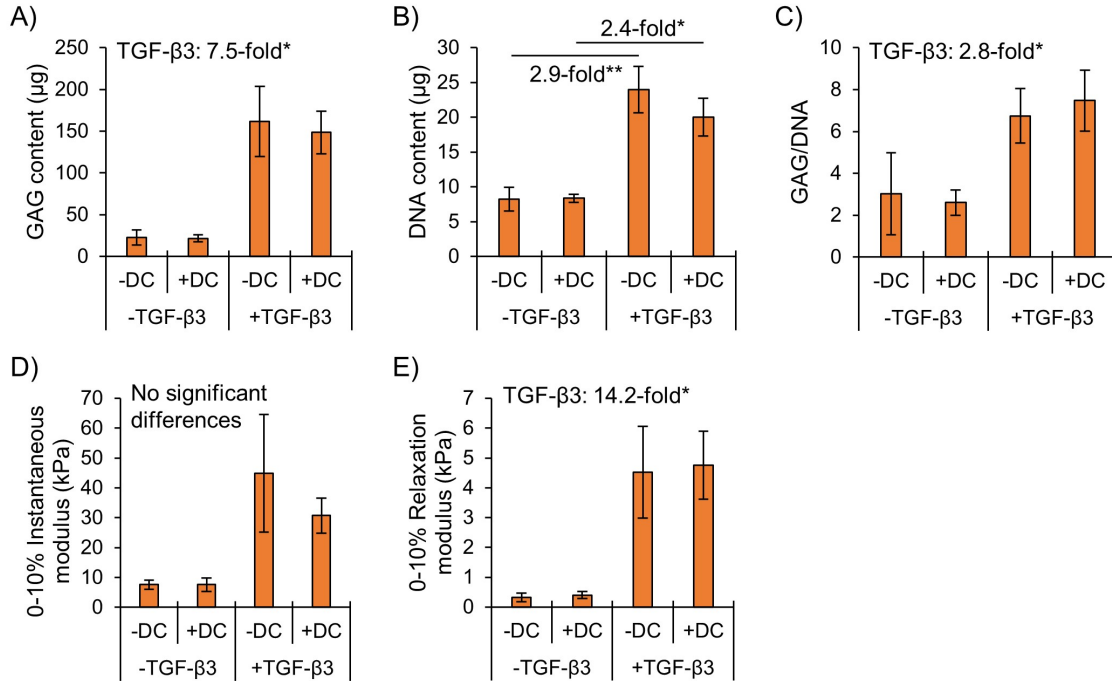
Figure 5.6: Biochemical and mechanical properties were not affected by dynamic compression under hypoxia, regardless of TGF-β3 supplementation. Tissues were pre-cultured statically for two weeks followed by two weeks of static or dynamic culture (10% strain, 1 Hz, 1h/day, 5×/week for two weeks). Differences were assessed by two-way ANOVA. *: $p < 0.05$, **: $p < 0.01$. DC: dynamic compression.
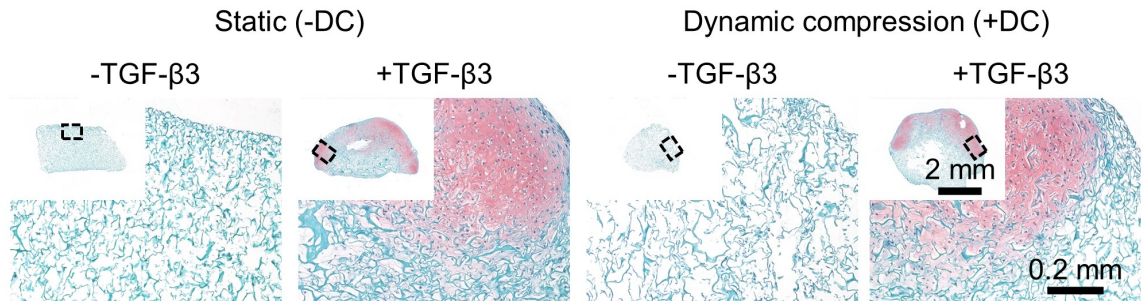
Figure 5.7: Safranin-O staining was not affected by dynamic compression under hypoxia, regardless of TGF-β3 supplementation. Staining was performed by combined Safranin-O (sulphated proteoglycans, pink), Fast Green (proteins, turquoise), and haematoxylin (cell nuclei, purple-dark green here).

5.6 Discussion

In preliminary work, we showed that MFCs expanded with the basal medium (BM)+T1F2 had faster proliferation rates and comparable subsequent matrix-forming capacity to
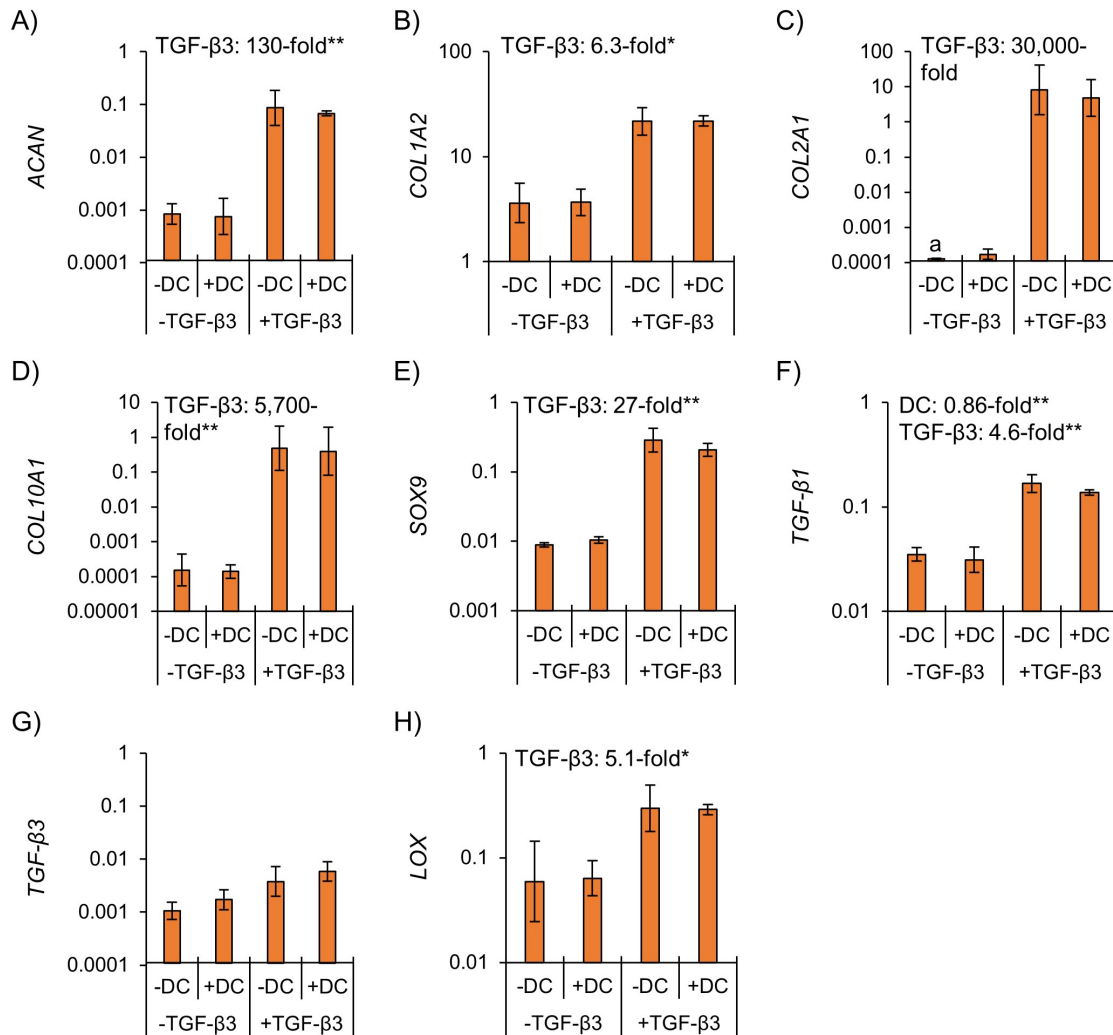
Figure 5.8: Inner meniscus gene expression was minimally affected by dynamic compression under hypoxia regardless of TGF-β3 supplementation. Tissues were pre-cultured statically for two weeks followed by two weeks of static or dynamic culture (10% strain, 1 Hz, 1h/day, 5×/week for two weeks). Differences were assessed by two-way ANOVA. *: $p < 0.05$, **: $p < 0.01$. DC: dynamic compression. a: no amplification within 40 PCR cycles for one donor.

those expanded in BM alone and BM+FGF-2. The FGF-2-mediated proliferation rate increase compared to basal medium was lower than previously reported (e.g., 1.1-fold here vs. 1.5 fold before), which may reflect differences in flask confluency, serum batches, and meniscus specimen source: relatively young and healthy joints undergoing arthroscopic partial meniscectomy here vs. older and osteoarthritic joints undergoing knee replacements before[8, 55].
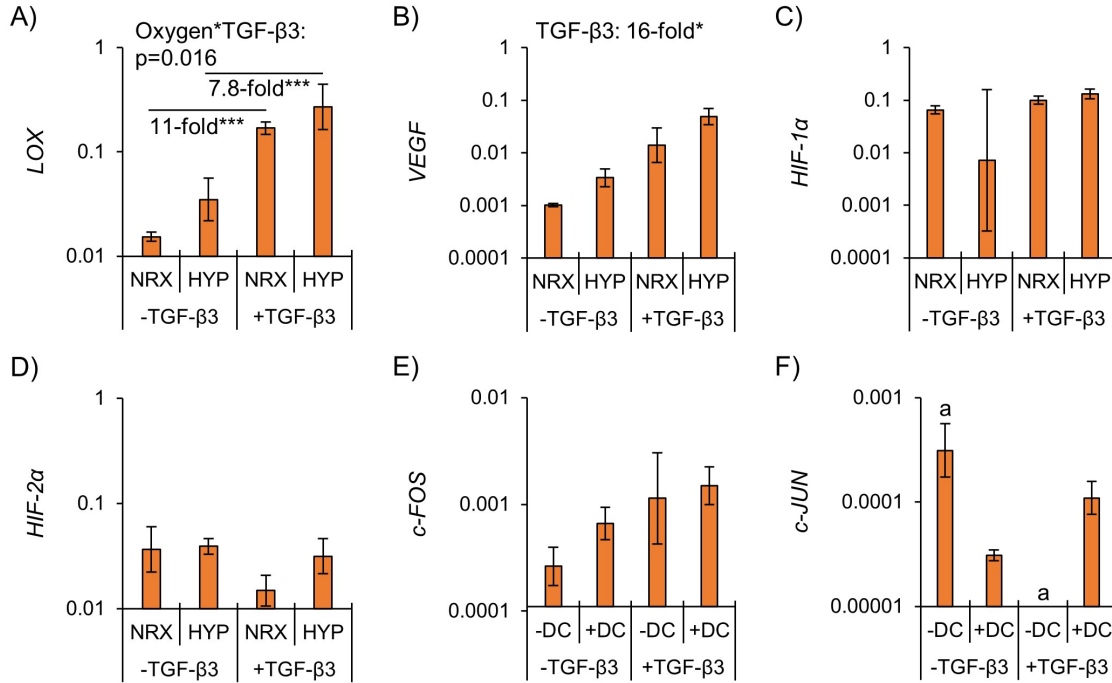
Figure 5.9: The treatments were ineffective at regulating hypoxia (A-D) and mechanical loading (E & F)-related genes. Differences were assessed by two-way ANOVA within donors (refer to the statistical analysis section). *: $p<0.05$, ***: $p<0.001$, a: no amplification within 40 PCR cycles for at least one donor. NRX: normoxia, 20% O_2. HYP: hypoxia, 3% O_2. DC: dynamic compression.

In part 1, we confirmed that continuous hypoxia alone was insufficient to induce a fibrocartilaginous matrix-forming phenotype in the type I collagen scaffold, complementing our result in the pellet model[2]. Unexpectedly, hypoxic compared to normoxic culture with TGF-β3 supplementation did not enhance the fibrocartilaginous matrix-forming phenotype. This contrasts with the synergistic increase in matrix formation by continuous hypoxia and TGF-β3 in the pellet model[2] and the hypoxia-mediated enhanced matrix formation in a polymeric scaffold layered with a biomimetic surface[59] by human meniscus-derived cells. However, this result is consistent with our previous work in this type I collagen scaffold using osteoarthritic joint meniscus cells, which had brief periods of re-oxygenation from hypoxia during medium changes[57, 58]. This indicates that the fibrocartilaginous matrix-forming response of meniscus-derived cells to TGF-β3 supplementation and hypoxia differs

between pellets and this scaffold model and is similar in MFCs from partial meniscectomy and total knee replacements, with re-oxygenation likely not playing a large role. We previously found differences in the MFC response to hypoxia in comparing models of a pellet and a meniscus decellularized matrix scaffold[10].

Possible underlying reasons for differences between studies may be oxygen diffusion dynamics, mediation of cell behaviour by the scaffold, cell density, and incubator oxygen tensions. Culture models such as pellets and self-assembling constructs may more accurately depict native tissues than traditional tissue engineering models incorporating an artificial scaffold[172]. It is possible that the differences in microenvironmental oxygen levels within the tissues were too small to observe a hypoxia-induced fibrocartilaginous matrix-forming phenotype. The increased contraction observed in normoxia would have reduced surface area for oxygen influx compared to the hypoxia group, reducing effective differences in oxygen levels. One strategy to mitigate confounding by differential contraction between oxygen tensions would be to pre-culture all tissues in a single oxygen condition to allow accumulation of contraction-resistant matrix before dividing tissues into different oxygen tensions. A pre-culture period in normoxia followed by exposure to hypoxic and mechanical loading conditions could mimic an aspect of human meniscus development: the menisci are initially fully vascularized but the inner regions become progressively devascularized in the first two decades of life with reducing oxygen supply and increasing mechanical loading[29, 35]. The hyaline cartilage aspect of the fibrocartilage phenotype develops in the inner regions during this time frame, suggesting this strategy could be used to possibly promote a more meniscus-like engineered tissue phenotype[35].

Given that mechanical loading seems to regulate the inner meniscus phenotype, we expected that dynamic compression would regulate MFC behaviour in the engineered tissues. Instead, dynamic compression under hypoxia did not induce a fibrocartilaginous matrix-forming phenotype without TGF-β3 supplementation nor enhance it in the presence of TGF-β3 supplementation. To confirm that cells within the tissues

were responding to the loading treatment, we measured expression of loading-sensitive genes *c-FOS* and *c-JUN* and found no differences regardless of TGF-β3 supplementation[170, 171]. Data collected during loading showed that force changes across compression cycles always remained larger than friction even at the end of the 1 h loading period for both TGF-β3 groups. Although tissue level loading was applied, there was thus no detectable mechanotransduction response.

A plausible explanation is that the applied loading regime with small strains was too mild to consistently modulate cell behaviour and that the matrix distribution in the scaffolds was too inhomogeneous. A different result could plausibly have been obtained by applying a more aggressive loading regime and using a pre-culture strategy that promotes accumulation of more homogeneously-distributed matrix. The less stiff, matrix-scarce regions in the scaffolds would have borne more of the applied deformation than the stiff, matrix-rich regions. This would have shielded cells from the applied loading and diminished its effects. Two underlying reasons for the inhomogeneous cell distribution are the static seeding method, which is simple but may result in less uniform cell distributions than dynamic seeding strategies, and insufficient time for the scaffold to fill up with newly-synthesized matrix[173]. Increasing the scaffold seeding density and culture time are reliable means to improve matrix accumulation[174]. Our preliminary data showed that doubling the seeding density and increasing pre-culture time from 3 to 9 weeks caused a 36-fold increase in compression modulus, indicating the promise of these strategies for future investigations(Figure S5.4).

The findings that TGF-β3 is necessary for matrix synthesis and that dynamic compression had few effects supports the results of work with porcine MSCs in agarose with a similar load regime[82]. However, unlike us, these authors observed hypoxia to exert chondrogenic effects and concluded that hypoxia is a more potent stimulator of chondrogenic differentiation than dynamic compression[82]. The shared dynamic compression result may reflect the load regime being suboptimal for both models,

while the differing oxygen effect may reflect the specific behaviour of MFCs on the type I collagen scaffold as discussed above[82]. Consistent with our loading results, a considerable proportion of studies applying dynamic compression in chondrocyte-based engineered tissues show no change in standard outcome measures of chondrogenesis[63]. In our opinion, this highlights the need for nuanced loading analysis and trial-and-error based optimization of loading regimes for each tissue culture model. A useful strategy based on our experiences here would be to reduce intra-donor variability, for example by using mean or pooled values from several replicates within donors and conditions. This would provide more stable values to aid in statistical detection of small mechanical loading effects with the same number of tissue donors. This could be useful because the added work from more tissue replicates is an order of magnitude smaller than that required for more donors in dynamic compression studies. A limitation of the commercial bioreactor used in the present study was its ability to only hold four replicates at once, which in this study needed to be divided amongst several assays (biochemistry, histology, gene expression). The inability to culture many replicates in this study could have precluded the detection of small dynamic compression effects with the limited number of cultured donors. Our future work will incorporate the use of a more optimal custom bioreactor.

Matrix staining for Safranin-O seemed more intense in Part 2 (dynamic compression and TGF-β3 supplementation effects) than in Part 1 (hypoxia and TGF-β3 supplementation effects) in +TGF-β3 supplementation groups. This was likely related to the different culture environments: part 1 used 24 well plates whereas part 2 used the commercial bioreactor, which had medium supplied in an extreme excess due to its large volume (27.5 mL/tissue construct/week compared to 3.7 mL/tissue construct/week in the 24 well plate).

Exogenous growth factors can overwhelm and mask the effects of stimuli such as dynamic compression[77]. In groups without TGF-β3 supplementation, cells bound to the scaffold with virtually no evidence of matrix formation after four weeks. However,

this should not necessarily have prevented transduction of tissue-level deformations to cells[175]. Cells can directly interact with collagen scaffolds to allow transduction of tissue-level loads without substantial cell-synthesized matrix[175]. Yet, no loading effects were observed. It is possible that a more optimized loading regime may have led to a different outcome, such as one incorporating both shear and dynamic compression[176]. An alternative approach would be to withdraw growth factor supplementation after a pre-culture period. This would allow for accumulation of de novo synthesized matrix before applying dynamic compression. Withdrawal of TGF-β supplementation after a pre-culture period had remarkable chondrogenic effects in bovine chondrocytes and carpal bone marrow mesenchymal stem cells[149, 150].

5.7   Conclusion

Our previous work demonstrated that: i) in pellets of human MFCs from partial meniscectomy, continuous hypoxia (3% incubator O_2) with TGF-β3 supplementation supports a more cartilage-like matrix-forming phenotype but hypoxia alone without growth factor supplementation (TGF-β3) is insufficient to induce matrix formation[2], and ii) in a type I collagen scaffold seeded with MFCs from total knee replacement (osteoarthritic joints), hypoxia with brief re-oxygenation during medium changes with TGF-β3 supplementation did not support a more cartilage-like matrix forming phenotype[57, 58]. The present study demonstrates that, in a type I collagen scaffold seeded with MFCs from partial meniscectomy, neither continuous hypoxia under static conditions nor hypoxia combined with dynamic compression to 10% strain induced a fibrocartilaginous inner meniscus-like matrix-forming phenotype in the absence of TGF-β3 supplementation. They also did not promote the inner meniscus-like matrix-forming phenotype when it was induced by TGF-β3 supplementation. Different outcomes may have been obtained with a different timing of hypoxia application and if the pre-culture and dynamic loading regime parameters had been further optimized to incorporate, for example, larger strains. This study provides the first investigation

of combined hypoxia and mechanical loading in meniscus cell-based engineered tissues and provides a baseline for future work. Eventually, this combinatorial strategy could be useful to better understand the behaviour of fibrochondrocytes in the native meniscus and to recapitulate differences between the inner and outer regions in tissue engineered meniscus replacements.

5.8   Acknowledgements

5.9   Funding sources

Program (ACF-MIBRP 27128 Adesida); AMS: Canadian Institutes of Health Research (CIHR MOP 125921 Adesida); NMJ and ABA: University of Alberta. The funders had no role in study design, data collection and analysis, decision to publish, or preparation of the manuscript.

5.10   Author contributions

ARAS: Conceptualization, data curation, formal analysis, funding acquisition, investigation, methodology, project administration, writing - original draft, writing - review & editing. CNM: Data curation. YL: Data curation. SHJA: Formal analysis, methodology, writing - review & editing. MK: Data curation, methodology AMS: Data curation NMJ: Funding acquisition, writing - review & editing ABA: Conceptualization, formal analysis, funding acquisition, investigation, methodology, supervision, writing - review & editing

5.11   Supporting information

Table S5.1: Primer sequences used in qRT-PCR. *: The *COL1A2* primer described in 10.1089/ten.tea.2019.0306 is preferred for future work.

Gene	Forward	Reverse	GenBank
ACAN	AGGGCGAGTG GAATGATGTT	GGTGGCTGTG CCCTTTTTAC	NM_001135.3
β-actin	AAGCCACCCC ACTTCTCTCT AA	AATGCTATCA CCTCCCCTGT GT	NM_001101.4
B2M	TGCTGTCTCC ATGTTTGATG TATCT	TCTCTGCTCC CCACCTCTAA GT	NM_004048.3
c-FOS	CGTCTCCAGT GCCAACTTCA	GGTCCGGACT GGTCGAGAT	NM_005252.4
c-JUN	CGGAGAGGAA GCGCATGA	TTCCTTTTTC GGCACTTGGA	NM_002228.4

Continued on next page

Gene	Forward	Reverse	GenBank
COL1A2	TTGCCCAAAG TTGTCCTCTT CT	AGCTTCTGTG GAACCATGGA A	AH002625.2
COL2A1	CTGCAAAATA AAATCTCGGT GTTCT	GGGCATTTGA CTCACACCAG T	NM_001844.5
COL10A1	GAAGTTATAA TTTACACTGA GGGTTTCAAA	GAGGCACAGC TTAAAAGTTT TAAACA	NM_000493.3
HIF-1α	GTAGTTGTGG AAGTTTATGC TAATATTGTG T	TCTTGTTTAC AGTCTGCTCA AAATATCTT	NM_001530.4
HIF-2α	GGTGGCAGAA CTTGAAGGGT TA	GGGCAACACA CACAGGAAAT C	NM_001430.5
LOX	AGGCCACAAA GCAAGTTTCTG	AAATCGCCTG TGGTAGCCAT A	NM_002317.7
SOX9	CTTTGGTTTG TGTTCGTGTT TTG	AGAGAAAGAA AAAGGGAAAG GTAAGTTT	NM_000346.3
TGF-β1	GGGAAATTGA GGGCTTTCG	AGTGTGTTAT CCCTGCTGTC ACA	NM_003239.4
TGF-β3	CTGGCCCTGC TGAACTTTG	AAGGTGGTGC AAGTGGACAG A	NM_003239.4
VEGF	GCACGGTCCC TCTTGGAA	CGGTGATTTA GCAGCAAGAA AA	NM_-001025366.3
YWHAZ	TCTGTCTTGT CACCAACCAT TCTT	TCATGCGGCC TTTTTCCA	NM_003406.3

Table S5.1 – *Continued from previous page*

Gene	Forward	Reverse	GenBank
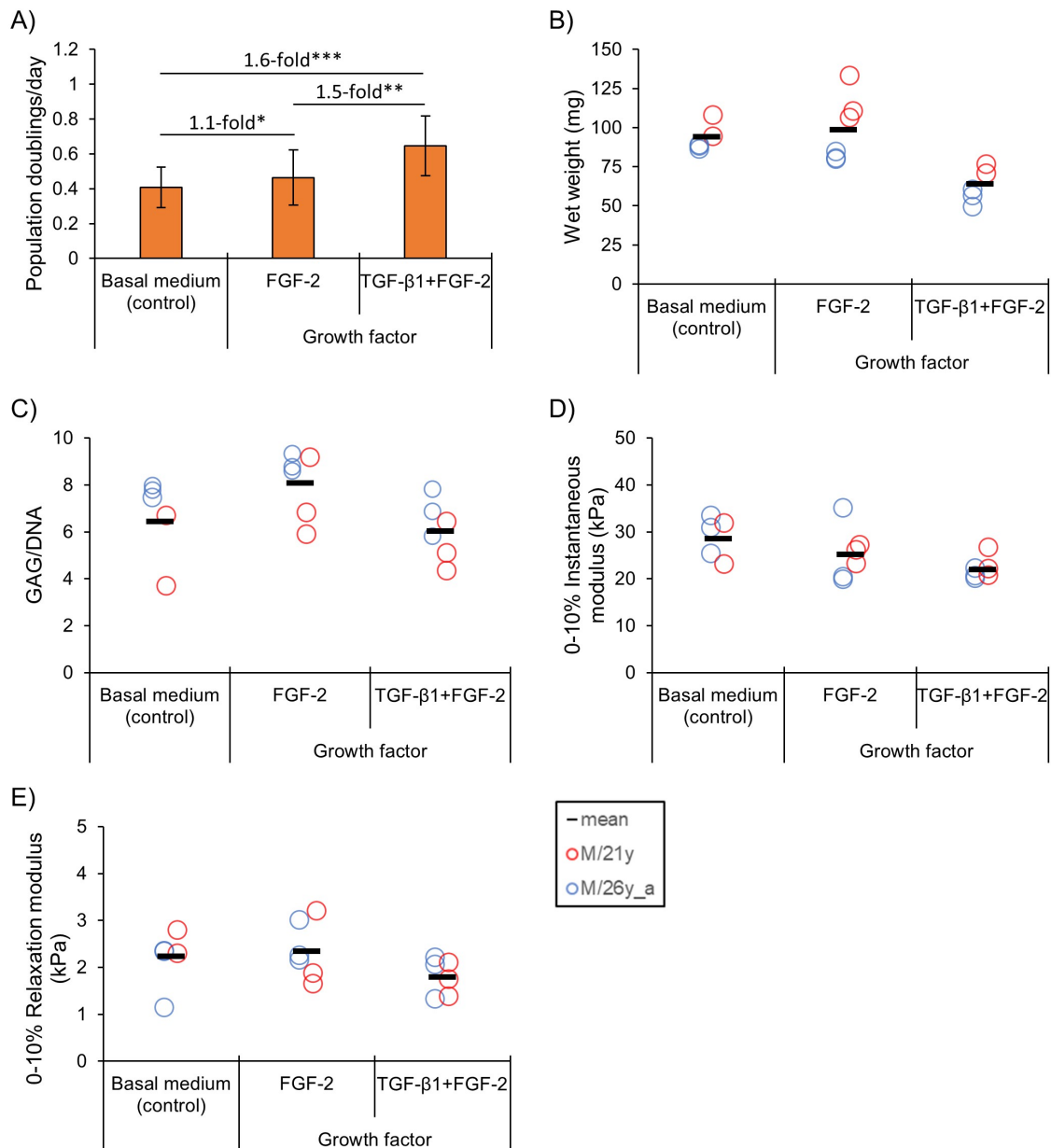
Figure S5.1: TGF-β1 and FGF-2 increased proliferation rates and maintained MFCs' matrix-forming capacity in preliminary work. A) All expansion medium contained 10% fetal bovine serum. B-D) Matrix formation was assessed after 3 weeks culture in this preliminary work. [TGF-β1]: 1 ng/mL, [FGF-2]: 5 ng/mL. Differences were assessed by one-way ANOVA. *: p<0.05, **: p<0.01, ***: p<0.001.
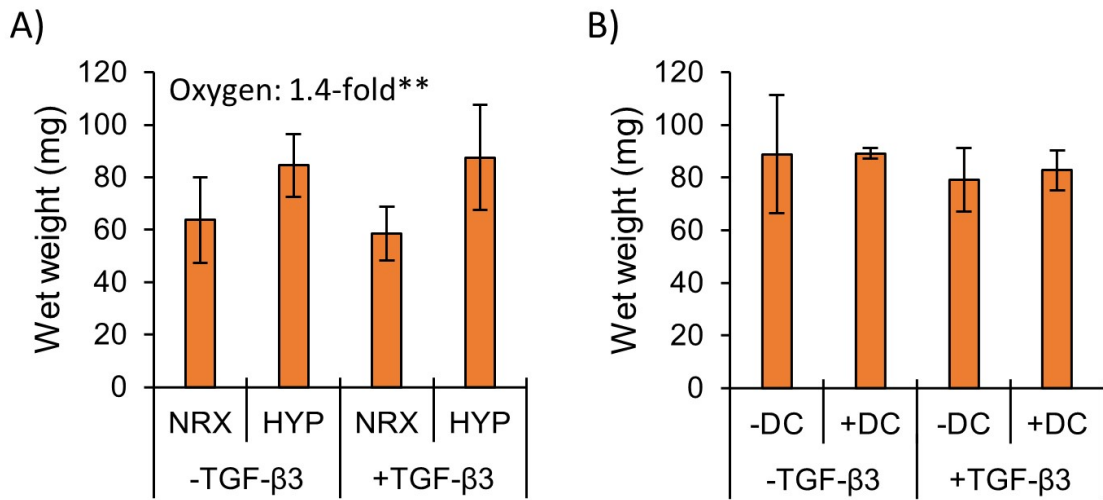
Figure S5.2: Tissue wet weights were larger in HYP and were not affected by DC.
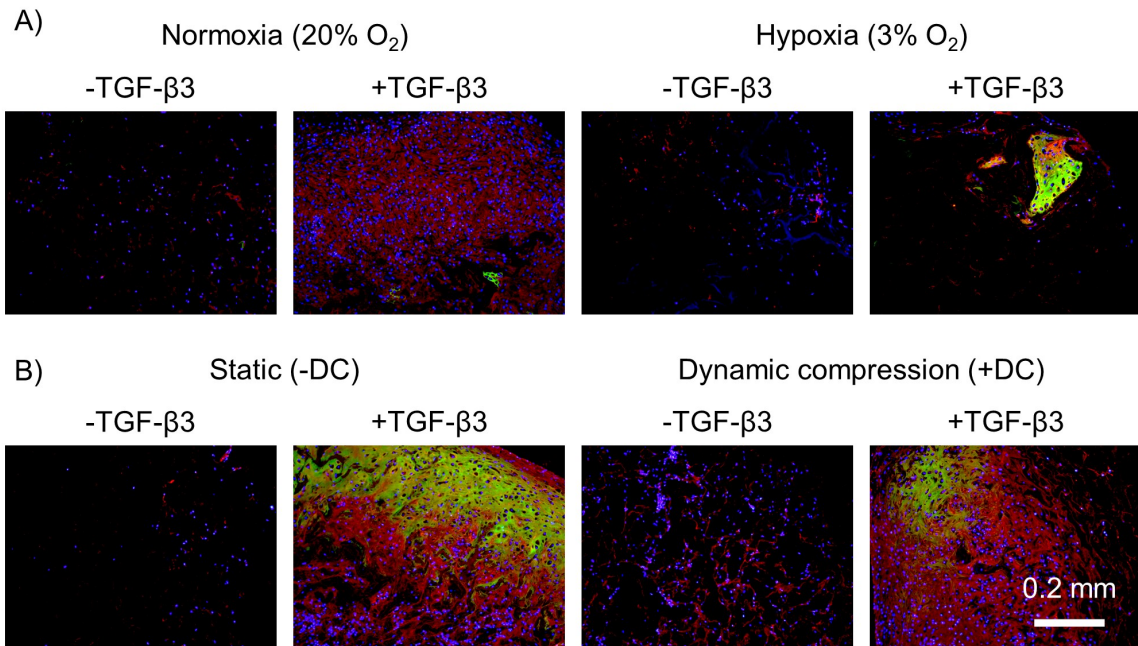
Figure S5.3: Expression of types I/II collagens was increased by TGF-β3 supplementation and was not detectably affected by hypoxia nor DC. Red: type I collagen, green: type II collagen, blue: cell nuclei by DAPI. All images share a common scale bar.
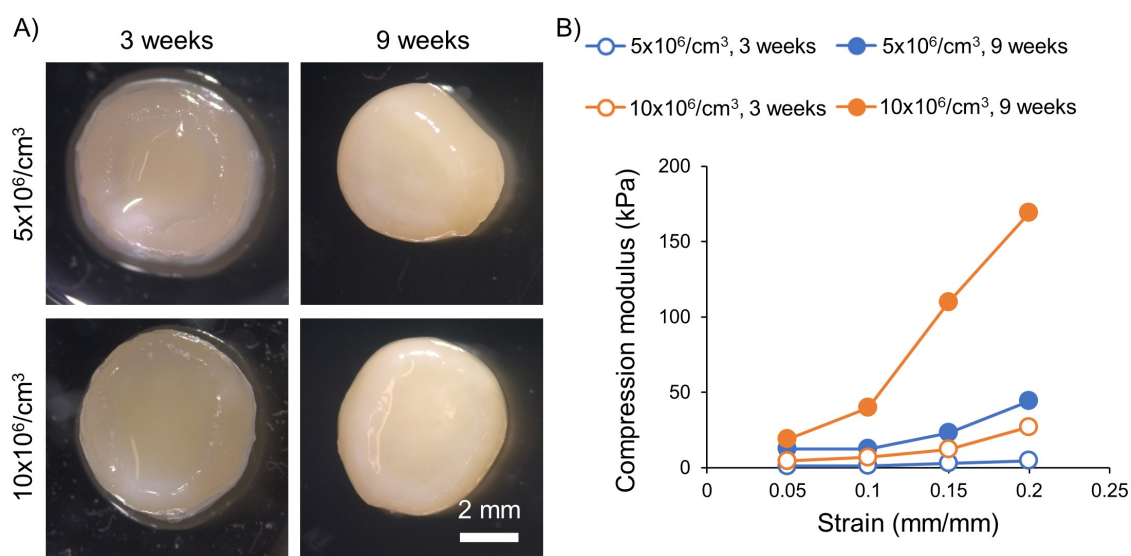
Figure S5.4: Higher seeding density and longer culture times improved matrix formation and mechanical properties. A) Tissue gross morphology at two seeding densities after 3- and 9-weeks' culture. B) Compression modulus in a ramp test up to 20% strain at 2% strain/minute. This mechanical test was modified from that used in the main study to better show the strain-stiffening behaviour of the tissue constructs.

Chapter 6

Time Course of 3D Fibrocartilage Formation by Expanded Human Meniscus Fibrochondrocytes in Hypoxia

Contributing authors:

Alexander R.A. Szojka, Yan Liang, Rita de Cássia Marqueti, Colleen N. Moore, Esra J. N. Erkut, Melanie Kunze, Aillette Mulet-Sierra, Nadr M. Jomha, Adetola B. Adesida

6.1 Preface

This study was motivated by the failures of the experiments in Chapters 4 and 5 to show the hypothesized outcomes. It was clear that the tissues formed in Chapter 5 on

the type I collagen scaffolds were not homogeneous and that mechanical properties were poor until the tissues were pre-compressed by strain offsets that, at the time, seemed likely to be damaging to cell viability. This study used three strategies to achieve a greater degree of matrix accumulation for mechano-transduction: increased culture time, lower degree of cell expansion, and increased seeding density compared to Chapter 5 (10 vs. 5×10^6 cells/cm^3). The study also included hypoxic culture in hopes to gain a better understanding of the general hypoxia non-response observed in Chapter 5.

I presented this work at the following conferences: i) 2018 Extreme Cryo and Alberta Regenerative Medicine Conference; ii) 2018 Tom Williams Surgical Research Day, Department of Surgery, University of Alberta (3rd Place Oral Presentation, Basic Science); iii) 2018 Gordon Research Seminar and Conference in Musculoskeletal Biology, Andover, New Hampshire.

6.2 Abstract

Adult human meniscus fibrocartilage is avascular and non-healing after injury. Meniscus tissue engineering aims to replace injured meniscus with lab grown fibrocartilage. Dynamic culture systems may be necessary to generate fibrocartilage of sufficient mechanical properties for implantation; however, the optimal static pre-culture conditions prior to initiation of dynamic culture are unknown. This study thus investigated the time course of fibrocartilage formation by human meniscus fibrochondrocytes on a 3D biomaterial scaffold under various static conditions. Human meniscus fibrochondrocytes from partial meniscectomy were expanded to P1 or P2 (3.0 ± 0.4 or 6.5 ± 0.6 population doublings), seeded onto type I collagen scaffolds, and grown in hypoxia (HYP, 3% O_2) or normoxia (NRX, 20% O_2) for 3, 6, or 9 weeks. Mechanical properties were not different between P1 and P2 cell-based constructs. Mechanical properties were lower in HYP, increased continually in NRX only, and were positively correlated with glycosaminoglycan content and accumulation of hyaline cartilage-

like matrix components. The most mechanically competent tissues (NRX/9 weeks) reached 1/5 of the native meniscus instantaneous compression modulus but had an increasingly hypertrophic matrix-forming phenotype. HYP consistently suppressed the hypertrophic phenotype. The results provide baselines of engineered meniscus fibrocartilage properties under static conditions, which can be used to select a pre-culture strategy for dynamic culture depending on the desired combination of mechanical properties, hyaline cartilage-like matrix abundance, and hypertrophic phenotype.

6.3 Introduction

The menisci are specialized tissues that play mechanical roles in the knee joint that include reducing stress on the articular cartilage[15, 30]. In adults, their weight-bearing inner regions are avascular and non-healing[25, 28]. Injuries to these regions disrupt function and contribute to osteoarthritis development[17]. The aim of meniscus tissue engineering is to generate mechanically competent engineered tissue constructs that can be implanted to restore meniscus function.

The functional mechanical properties of the menisci are provided by their organized extracellular matrix (ECM). Meniscus ECM contains large bundles of collagen fibres oriented circumferentially and radially to resist tensile strain during transmission of compressive forces across the joint[23, 177]. The main meniscus ECM biochemical is type I collagen[131]. In adults, the inner meniscus regions are classified as fibrocartilage as they additionally contain hyaline cartilage matrix components type II collagen and aggrecan[15]. Meniscus fibrocartilage is synthesized and maintained by a heterogeneous population of cells collectively referred to as meniscus fibrochondrocytes (MFCs)[22]. Two factors implicated in the development of the fibrocartilaginous phenotype in the inner human meniscus are low oxygen tension (hypoxia (HYP) here, also referred to as physioxia) and mechanical loading[28, 29, 35]. HYP incubator conditions and dynamic compression are each promising for meniscus and hyaline cartilage tissue engineering as they can promote formation of the matrix molecules

present in the native tissues[2, 60, 70–72]. They are also relevant for tissue engineering other fibrocartilages such as the annulus fibrosus, as fibrocartilage in general is avascular and appears in the body within fibrous tissues that experience dynamic compression[46, 52, 178]. In the context of meniscus, HYP and dynamic culture also more appropriately mimic the knee joint environment compared to static conditions for studying MFC physiology in tissue engineering model systems[29].

A recent study investigated combined HYP and dynamic compression on a type I collagen scaffold with human meniscus fibrochondrocytes (MFCs) [3]. Although the chondrogenic effects of HYP on MFCs in the pellet culture model have been replicated several times, they were not replicated on the type I collagen scaffold[2, 56–58, 109]. Rather, normoxia (NRX), as in typical atmospheric oxygen levels vs. HYP resulted in the highest mechanical properties, perhaps due to increased scaffold contraction. Further, the mechanical loading regime, which involved dynamic compression from 0-10% strain at 1 Hz for 1 h applied at least $5\times$/week for two weeks after a two week pre-culture period, had no effects on fibrocartilage tissue formation nor any detectable mechanotransduction response at the mRNA level. The explanatory hypothesis was that the newly formed ECM was too scarce and heterogeneous after the short pre-culture period for effective mechanotransduction under the applied dynamic compression regime, and thus a more optimal pre-culture strategy is required.

The objectives of this study were to investigate the time course of engineered fibrocartilage formation under various static conditions before initiation of a dynamic culture stimulus such as dynamic compression. Cell expansion (passage (P)1 vs. P2), oxygen tension (3 vs. 20% O_2), and culture time (3, 6, 9 weeks) were explored in a factorial manner. The main hypotheses were that mechanical properties would be superior for P1 vs. P2-based cells, in NRX vs. HYP, and at later time points[8, 179, 180].

6.4 Materials and Methods

Most methods used have been described in detail previously[8].

6.4.1 Generation of engineered human fibrocartilage

Meniscus specimens from n=6 donors were collected from partial meniscectomy surgeries with informed consent waived in accordance with the University of Alberta Health Research Ethics Board-Biomedical Panel (Study ID Pro00018778). As previously described, adherent MFCs were isolated by collagenase digestion and expanded to passage 1 (P1) or 2 (P2) in monolayer with an initial seeding density of $10^4/cm^2$ in a high-glucose DMEM supplemented with 10% fetal bovine serum, 1 ng/mL TGF-β1, and 5 ng/mL FGF-2. To form meniscus fibrocartilage constructs, MFCs were seeded at a density of 10^7 cells/cm^3 onto cylindrical type I collagen scaffold sponge scaffolds (diameter=10 mm, height=3.5 mm, weight=3.8 mg, DuraGen, Integra Lifesciences, USA). Meniscus constructs were cultured in normal atmospheric ("normoxia" (NRX), 20% O_2) or low oxygen ("hypoxia" (HYP), 3% O_2) in humidified incubators with 5% CO_2 using a standard serum-free chondrogenic medium containing 10 ng/mL TGF-β3 for 3, 6, or 9 weeks. Table S6.1 provides basic donor details and outlines the number of cell-seeded scaffolds from each donor set up for each assay.

6.4.2 Contraction analysis

After culture, constructs (n=4 donors) were weighed and imaged to capture their cylinder face surface areas. To assess radial and axial contraction, the changes in construct diameters and heights were divided by the original values.

6.4.3 Qualitative assessment of fibrocartilage formation

Constructs from a representative donor were fixed in formalin, paraffin-embedded, and sectioned radially at a thickness of 5 μm. Sections were then stained with Haematoxylin, Fast Green FCF, and Safranin-O or immunofluorescent labels for types I, II,

and X collagen.

6.4.4 Quantitative assessment of fibrocartilage formation

Constructs (n=4 donors) were placed between stainless steel platens attached to a 22 N load cell on a Biodynamic 5210 test instrument (TA Instruments, USA) and underwent two 10% strain steps at a strain rate of 50% strain/s each with 20 minutes of relaxation in unconfined compression[166, 181]. Similar tests were performed on cylindrical cores of native meniscus tissue cut in an axial direction from the inner regions of three additional partial meniscectomy specimens.

Instantaneous modulus (IM) was calculated as the peak force change across each strain step divided by cross-sectional area and change in strain (0.1). Relaxation modulus (RM) was calculated similarly but using the relaxation change in force.

Constructs (n=4 donors) were solubilized using proteinase K. Glycosaminoglycan (GAG) and DNA contents respectively were measured by the DMMB and CyQUANT Cell Proliferation assays.

6.4.5 Quantitative assessment of fibrocartilage matrix-forming phenotypes (P2 cells only)

Constructs (n=6 donors) were stored in TRIzol at -80°C until later RNA extraction, cDNA synthesis, and amplification with gene-specific primers by quantitative real-time polymerase chain reaction (qRT-PCR)(Table S6.2). Genes of interest were normalized to the mean expression of three reference genes (*YWHAZ*, *β-actin*, *B2M*) and presented using the $2^{\Delta Ct}$ method[167].

6.4.6 Statistical analysis

All quantitative data is available in a supplementary spreadsheet. Mean values of any replicates within conditions and donors were first computed. Analysis of variance was performed in SPSS 27 (IBM, USA) with passage, oxygen tension, and culture time treated as fixed factors and donor treated as a random factor. P values below 0.05 were

considered significant. Approximate normality was assessed using the Shapiro-Wilks test. At the mRNA level, statistics were computed using ΔCt values. There were no detected three-way interactions in any outcome variable. In cases of significant two-way interactions between fixed factors, the simple main effects in each level of the individual factors were compared by one-way ANOVA. When there were no significant two-way interactions, the main effects of each factor were assessed. All significant differences in main effects or simple main effects, as well as differences in the levels of the culture time variable, are presented in figures. No P value corrections were applied. The relationships between mechanical properties and %GAG/Wet weight were assessed by Pearson's correlation.

6.5 Results

6.5.1 Contraction analysis

Contraction was modulated by all of cell expansion, culture time, and oxygen tension (Figure 6.1A-C). Based on wet weight changes, the effects of culture time and oxygen tension were twice as large as cell expansion (Figure 6.1A). The scaffolds contracted most during the first three weeks before reaching a plateau (Figure 6.1A-C).
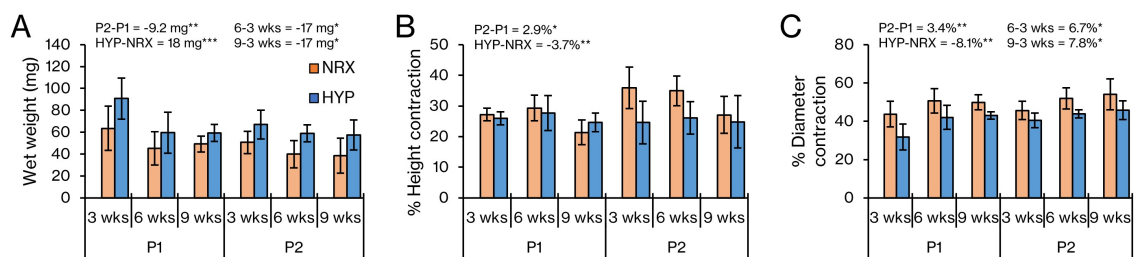
Figure 6.1: Contraction of engineered meniscus fibrocartilage was modulated by cell expansion, oxygen tension, and culture time. P: passage. HYP: hypoxia (3% O_2). NRX: normoxia (20% O_2). The bars represent mean ± standard deviation for n=4 donors. The mean difference between levels of significant factors in the ANOVA model are presented above the bars. *: p<0.05, **: p<0.01, ***: p<0.001.

6.5.2   Qualitative assessment of fibrocartilage formation

The unseeded bovine collagen scaffold stained for Fast Green but not Safranin-O nor the anti-human type I collagen antibody (data not shown). Fibrocartilaginous matrix, based on positive staining for sulphated proteoglycans and types I and II collagens, was present in all groups and qualitatively was not consistently affected by passage or by oxygen tension (Figure 6.2). Sulphated proteoglycans and type II collagen were faint and sparse at 3 weeks but progressively more intense and spread out at 6 and 9 weeks (Figure 6.2). Types I and X collagens didn't change consistently with culture time (Figure 6.2).

6.5.3   Quantitative assessment of fibrocartilage formation

The unseeded collagen scaffolds had a compression modulus of less than 2 kPa, and no measurable GAG, and DNA contents; thus, measured values in engineered tissues were the contribution of the seeded MFCs. The instantaneous moduli were nearly two orders of magnitude larger than the relaxation moduli (Figure 6.3A-D). All tissues were strain stiffening: mechanical properties approximately doubled from the first (0-10%) to the second (10-20%) strain step (Figure 6.3A-D). The engineered tissues in NRX/9 weeks reached 60% of the native meniscus values in the 0-10% instantaneous modulus but fell well short in the 10-20% instantaneous modulus due to more strain stiffening in the native tissues (Figure 6.3AB).

Longer culture times increased instantaneous and relaxation mechanical properties (Figure 6.3A-D). Mechanical properties were not significantly different between P1 and P2 nor between HYP and NRX (Figure 6.3A-D). As expected, longer culture times increased GAG content, GAG/DNA, and %GAG/WW (Figure 6.3EGH). The increases in these parameters seemed more consistent after 6 weeks in normoxia, with evidence of a plateau in hypoxia (Figure 6.3EGH). Longer culture times increased DNA contents initially in both oxygen tensions (Figure 6.3F). %GAG/WW correlated with both instantaneous and relaxation mechanical properties (Figure 6.3I).
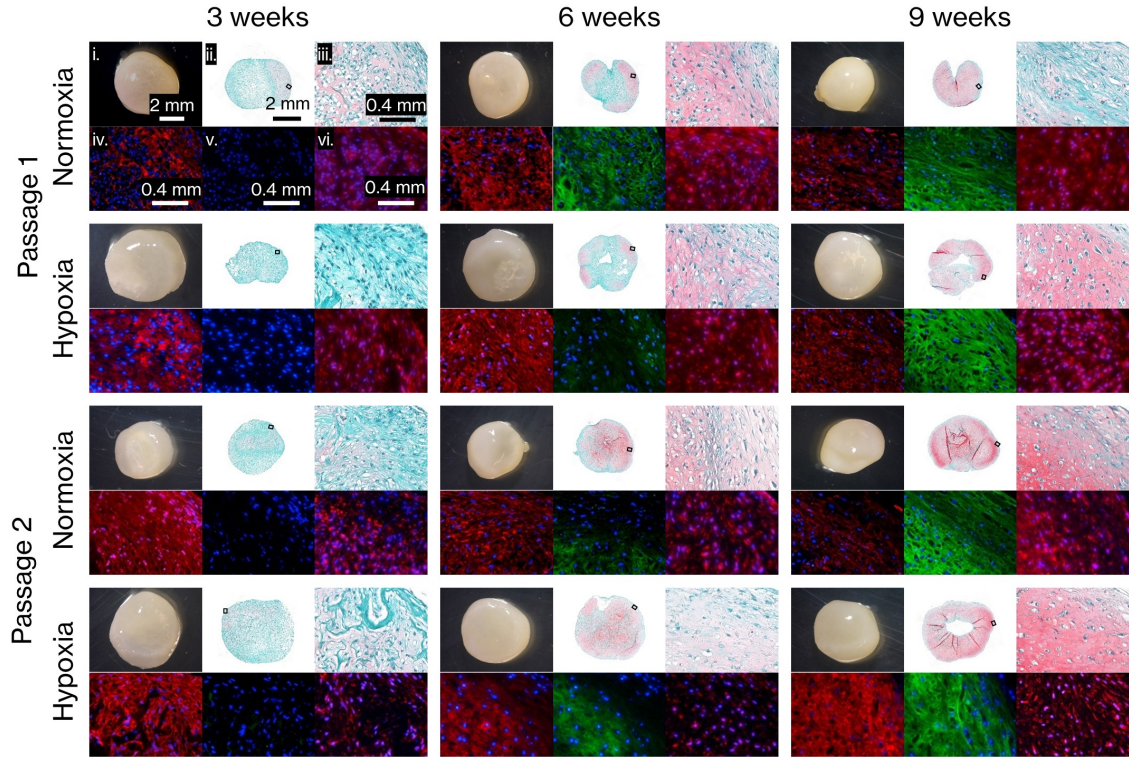
Figure 6.2: Staining for hyaline cartilage matrix markers became increasingly intense with culture time while oxygen tension and cell expansion had no detectable consistent effects. All images are radial sections of tissues from the M/29y donor. All images within subpanels are from the same engineered tissue. Sulphated proteoglycans are stained with Safranin-O with Fast Green as a counterstain for proteins and Haematoxylin as a counterstain for cell nuclei (subpanels ii and iii). Cells are labelled with DAPI in immunofluorescence images (subpanels iv, v, and vi) and antibodies against types I, II, and X collagens. Images in each panel follow the same order as in P1/NRX/3 weeks. Images of the same type share a common scale bar.

At 9 weeks, the mean mechanical and functional biochemical properties were always higher in NRX than HYP (Figure 6.3ABCDEGH). This indicates that NRX very likely did support higher mechanical and biochemical properties, but there was insufficient detection power for individual measurements (Figure 6.3).

6.5.4 Quantitative assessment of fibrocartilage matrix-forming phenotypes (P2 cells only)

At 3 weeks, the fibrocartilage matrix-forming phenotype at the mRNA level favoured expression of fibrous markers (*COL1A2* and *VCAN*) compared to cartilaginous (*COL2A1*
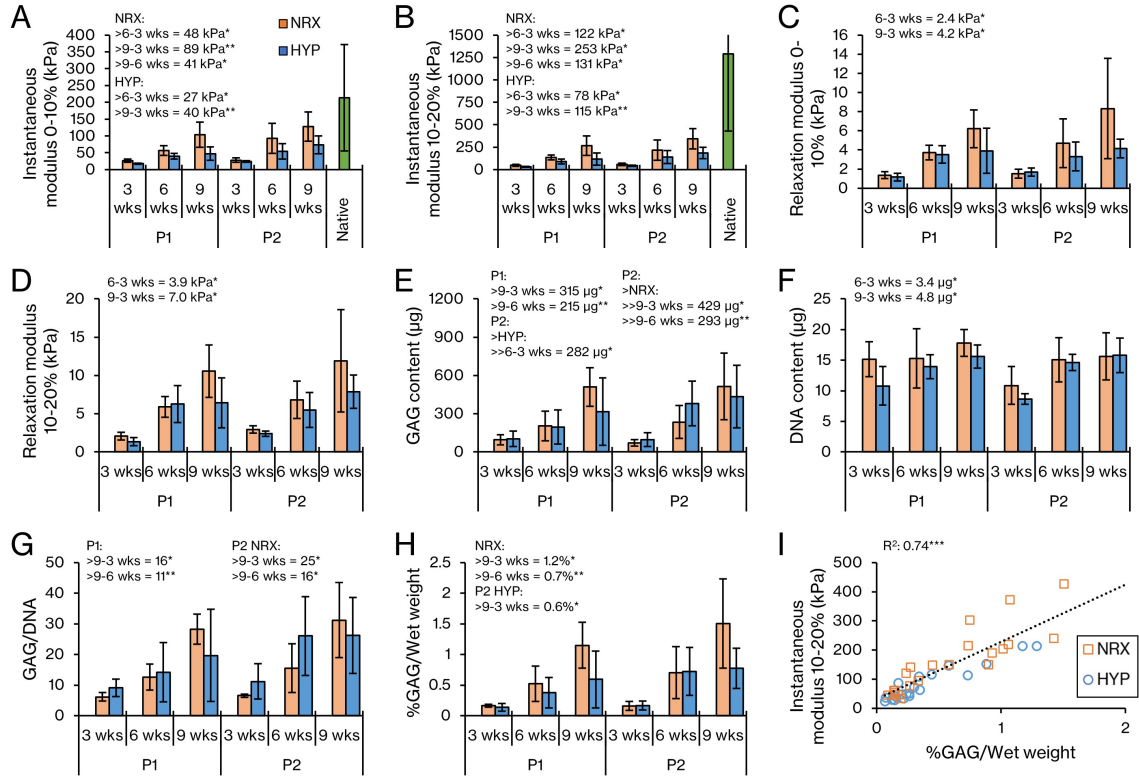
Figure 6.3: Mechanical and biochemical properties were most potently affected by culture time. P: passage. HYP: hypoxia (3% O_2). NRX: normoxia (20% O_2). GAG: glycosaminoglycans. The bars represent mean ± standard deviation from n=4 donors, except the native meniscus which is n=3 donors. The mean difference between levels of significant factors in the ANOVA model are presented above the bars. *: $p<0.05$, **: $p<0.01$, ***: $p<0.001$.

and *ACAN*) and hypertrophic (*COL10A1*) ones based on expression levels relative to the reference genes (Figure 6.4).

In both oxygen tensions, *COL1A2* expression was stable from 3 to 6 weeks but fell by 9 weeks (Figure 6.4C). This was accompanied by a decrease in *VCAN* in HYP/9-wks compared to NRX/9-wks (Figure 6.4B). There was a large increase in expression of hyaline cartilage matrix precursors *ACAN* and *COL2A1* from 3 to 6 weeks in both oxygen tensions, which was consistent with increases in Safranin-O and type II collagen staining (Figure 6.4AD). Hypertrophic marker *COL10A1* also increased dramatically from 3 to 6 weeks and continued to rise by 9 weeks but in normoxia only (Figure 6.4E). Hypoxia significantly reduced *COL10A1* expression compared to

116
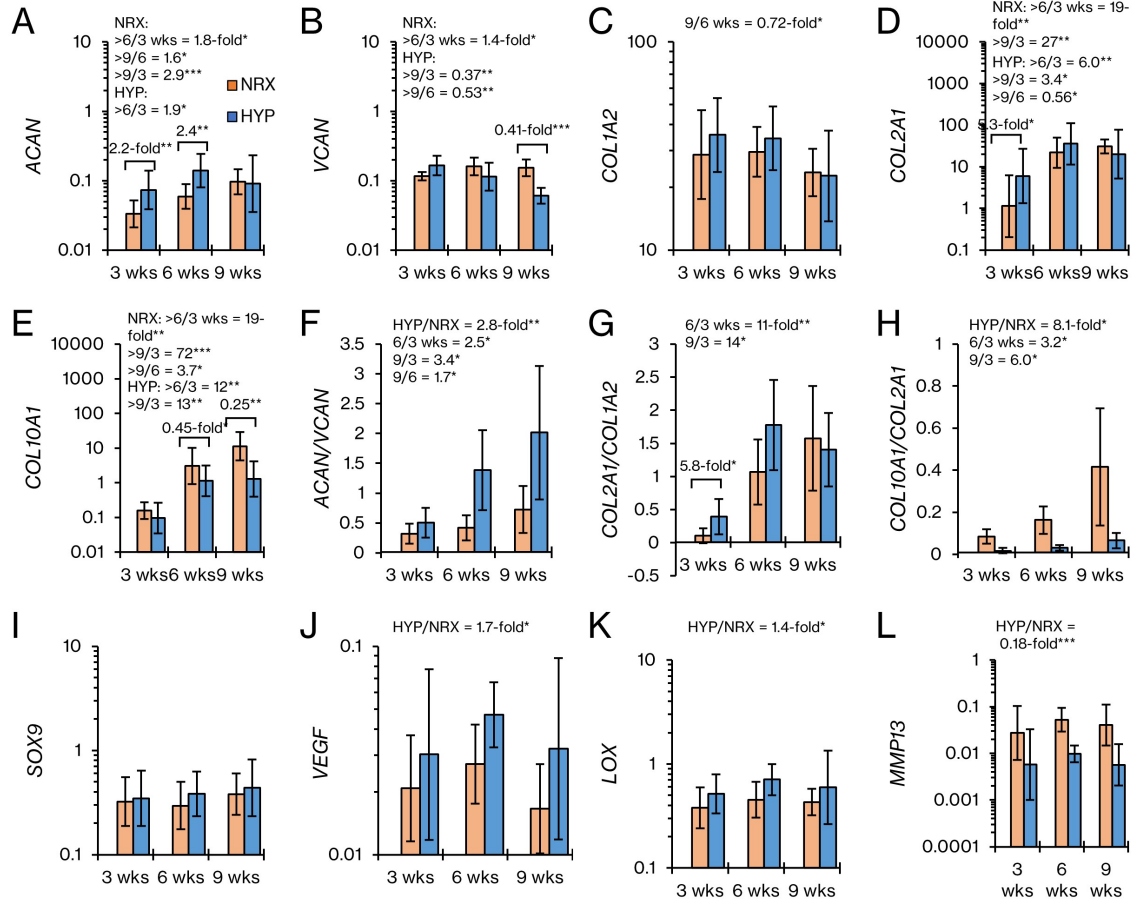
Figure 6.4: Gene expression profiles became increasingly chondrogenic with culture time and even hypertrophic in NRX only. HYP: hypoxia (3% O_2). NRX: normoxia (20% O_2). Expression of each gene is presented relative to the mean expression of three reference genes: *YWHAZ*, *β-actin*, and *B2M*. The bars represent mean ± standard deviation from n=6 donors. The expression ratios between the indicated levels of significant factors in the ANOVA model are presented above the bars. *: p<0.05, **: p<0.01, ***: p<0.001.

normoxia at 6 and 9 weeks (Figure 6.4E).

The *ACAN/VCAN* ratio increased with time without a plateau and was increased in HYP vs. NRX (Figure 6.4F). The *COL2A1/COL1A2* ratio was initially low, especially in NRX, but increased dramatically from 3-6 weeks and underwent no more significant changes (Figure 6.4G). The *COL10A1/COL2A1* ratio, indicating a more hypertrophic than cartilaginous phenotype, increased with time and was always higher in NRX vs. HYP (Figure 6.4H). Thus, the matrix-forming phenotype progressed from

predominantly fibrous at 3 weeks to cartilaginous at 6 and 9 weeks, and in NRX it became increasingly hypertrophic with time.

There were no differences between conditions in mRNA expression of cartilage matrix transcription factor *SOX9* (Figure 6.4I). Hypoxia increased expression of *VEGF* and *LOX* and suppressed expression of hypertrophic marker *MMP13* (Figure 6.4J-L).

An additional panel of 12 genes associated with hypoxia (*HIF-1α*, *HIF-2α*, *LOXL2*), hypertrophy (*RUNX2*, *IHH*, *PTHLH*), suppression of hypertrophy (*PTHLH*, *GREM1*, *FRZB*), and contraction (*TAGLN*, *ACTA2*, and *VCL*) are presented in Figure S6.1. The only significant culture time effects were increased *HIF-2α* at 6 weeks compared to 3 weeks. The only significant hypoxia differences in these genes were hypoxia increasing expression of *HIF-2α*, *LOXL2* and *GREM1* and decreasing IHH and *TAGLN* (this last gene at 3 weeks only) (Figure S6.1).

6.6   Discussion

Contrary to the hypothesis for cell expansion, there were no main effect differences in mechanical and biochemical properties between P1 and P2 cells (3.0 vs. 6.5 population doublings (PD)). The extent of cell expansion may have been small enough at P2 for the cells to not lose their capacity to form fibrocartilage matrix, which is a useful finding for the field of meniscus tissue engineering. These cells were however different in terms of scaffold contraction. Immediately after seeding, the cells in this model were suspended in the mechanically weak scaffold that contained large fluid-filled pores and little intervening matrix. The contraction analysis suggests that scaffold contraction was related to accumulation of cell-made matrix, which may impede further contraction by its superior mechanical properties compared to the scaffold material. Scaffold contraction has also been previously linked to the extent of cross-linking and expression of smooth muscle actin[182, 183]. If scaffold contraction is a major concern for an application, then it can be reduced by use of P1 rather than P2 cells. Alternatively, if there is a scarcity of the initial cell population, then

118

expansion to P2 cells may be more appropriate as P1 and P2 cells had comparable matrix-forming capacity.

Had all the cells from each donor in this study been expanded to P2, the range of obtainable cells would be from 150 million to 3.3 billion. An average human meniscus weighs less than 5 grams and contains between 13 and 27 million cells/g depending on the region[97, 184]. The T1F2 strategy to P2 could have yielded sufficient cells to engineer a total meniscus with at least the seeding density of the native tissue for all six donors. Thus, cell expansion is not a limiting factor for meniscus tissue engineering if this strategy is employed with similarly sized donor meniscal fragments as obtained in this study.

As hypothesized, culture time increased compressive mechanical properties through accumulation of functional matrix macromolecules. This supports the use of longer pre-culture times before initiation of dynamic culture to allow sufficient matrix to accumulate for mechanotransduction. Similar increases in mechanical properties attributable to accumulation of matrix are well documented, as is the beneficial effect of delaying initiation of dynamic culture, in other cartilaginous tissue engineering models[179, 185].

The evolution of instantaneous compressive mechanical properties was different between oxygen tensions, and there was a transition in the matrix-forming phenotype over time that was influenced by oxygen tension. These results indicate that pre-culture time and oxygen tension need to be considered simultaneously in selection of a pre-culture period. Extended pre-culture periods in HYP beyond 6 weeks may confer only marginal gains in mechanical and biochemical properties with reduced expression of important matrix gene. Taken with the increase in proteoglycan and type II collagen staining from 6 to 9 weeks, this indicates that absolute levels of related matrix proteins continue to accumulate beyond 6 and possibly 9 weeks but at diminishing rates. In contrast, extended pre-culture in NRX beyond 6 weeks may support larger gains in matrix properties but with an increasingly hypertrophic phenotype,

which may not be suitable for an application in meniscus tissue engineering. The increased contraction in NRX would have concentrated matrix biochemicals, which would logically increase mechanical properties[113]. As well, higher mRNA expression of matrix precursors *VCAN* and *COL10A1* in NRX could also have played some role. Increased collagen cross-linking in HYP, mediated through lysyl oxidase (*LOX*) and lysyl oxidase-like 2 (*LOXL2*), has previously been linked to improved mechanical properties in engineered cartilaginous tissues[169]. Given that mRNA expression of these genes was higher in HYP, this would have worked to reduce the differences in mechanical properties between HYP and NRX (Figure 6.4K & Figure S6.1C).

The most mechanically competent engineered tissues attained in this study were in the NRX/9-week groups, but they fell short of native meniscus properties. The measured human native meniscus values were comparable to reported values[49]. Accurate measurement of meniscus material properties in compression requires pre-compression to account for swelling, and thus the 10-20% strain step is most representative of the true meniscus properties[115]. The gap between engineered and native meniscus mechanical properties supports the notion that dynamic culture is necessary to prepare engineered tissues with sufficient mechanical properties to be appropriate for clinical use. In the engineered tissues from 6 to 9 weeks of culture, the intensity of sulphated proteoglycans appeared more in line with the inner regions of aged or degenerating meniscus than with healthy meniscus[128, 186–188]. However, the range in %GAG/WW (0.2-2.1%) was similar to the range (0.3-1.7%) from the middle regions of macroscopically-intact native menisci from 16-44-year old total knee joint donors but beyond the range (0.2-0.8%) from a spectrum of healthy and degenerated menisci from 12-50-year old meniscectomy donors[113, 127].

An interesting strategy is to pre-culture tissues in NRX to form initial matrix and then to transfer them into HYP[7]. This mimics how the native human meniscus loses much of its initial oxygen supply through vascular recession in the first two decades of life[28, 32, 34–36]. This could also be an improved way of assessing oxygen ten-

sion effects in collagenous scaffolds compared to the method of immediately dividing cell-seeded scaffolds into NRX and HYP as was done here. Differential contraction between NRX and HYP can obscure oxygen tension differences in matrix-forming phenotype because of differential scaffold contraction. A pre-culture period in NRX for 3 or 6 weeks to allow scaffold contraction to plateau (Figure 6.1) would eliminate this confounding variable.

This study had several limitations. First, the mRNA level analysis was limited to P2 cells, precluding assessment of cell expansion differences in the matrix-forming phenotype part. Second, there was no dividing of tissues into annulus and core regions. There could have been related spatial differences in properties due to diffusional limitations, which would be of high relevance for the oxygen tension analysis[82]. Cells in the core regions of the constructs, especially those cultured for 9 weeks, could have suffered from poor nutrient access. Strategies to improve nutrient diffusion into the interior regions of constructs, such as medium mixing on an orbital shaker, forced perfusion, and dynamic compression all could have affected the oxygen tension comparison in the present work[189–191]. Third, apart from the contraction analysis the assays were performed using singlicate engineered tissues. Using mean values of replicate cell-seeded scaffolds within conditions for each donor can increase statistical power by eliminating nuisance variability unrelated to the comparisons of interest. Fourth, with only three time points, there was limited resolution for establishing relationships between gene expression and protein and mechanical outcomes. Weekly time points from 0-9 weeks, combined with multiple replicates per condition per donor, could have provided more powerful trend analyses. Fifth, the complete population of adherent MFCs from donor tissues were used for practical reasons. However, the menisci contain subpopulations of cells that could differ in their responses to expansion and oxygen tension compared to the whole population[192]. Finally, mechanical testing was limited to a stress relaxation compression test. This was adequate for the objective of comparing pre-culture conditions and for a general comparison of

engineered and native meniscus. However, this test only captures a narrow aspect of meniscus mechanical behaviour[30].

6.7 Conclusion

This study investigated the time course of fibrocartilage formation by human MFCs on a type I collagen scaffold under various static conditions to identify a suitable static pre-culture strategy before initiation of dynamic culture. Cell expansion with combined TGF-β1 and FGF-2 to P1 and P2 (3.0 vs. 6.5 population doublings) are both appropriate, as there were no differences in mechanical and biochemical properties of the newly formed fibrocartilage. If the objective is to obtain engineered tissues that are more fibrous than hyaline cartilage-like, then shorter pre-culture times in NRX seem most appropriate, provided that sufficient matrix has accumulated and the loading regime is sufficiently aggressive for mechanotransduction. Alternatively, if more hyaline cartilage-like matrix is preferred, then pre-culture periods of 6 or 9 weeks in HYP or 6 weeks in NRX may all be appropriate. If the only concern is to attain the highest mechanical and biochemical properties, then culture in NRX for 9 weeks or even longer may be appropriate though these may raise concerns about development of a hypertrophic phenotype.

6.8 Acknowledgements

6.9 Funding Sources

6.10   Author Contributions

Alexander R. A. Szojka and Adetola B. Adesida designed the study. Alexander R. A. Szojka performed the experiments with assistance from Yan Liang, Colleen N. Moore, Rita de Cássia Marqueti, Esra J. N. Erkut, Melanie Kunze, Aillette Mulet-Sierra, and Adetola B. Adesida. Alexander R. A. Szojka wrote the manuscript with input from all co-authors. Nadr M. Jomha assisted with procuring clinical specimens and in reviewing and editing the manuscript. Adetola B. Adesida supervised and was responsible for acquiring financial support for the study.

6.11 Supporting Information

Table S6.1: Distribution of donors and tissue constructs among assays. Wet weights and scaffold dimensions for contraction analysis in Figure 1 were acquired using constructs for mechanical testing and biochemistry as well as for histology and IF. PD, population doublings; IF, immunofluorescence; M, male; F, female; Y, year.

		Analyses		
Donor	Passage (PD)	Mechanical testing and biochemistry	Gene expression	Histology and IF
M/16y	1 (2.7)	6		
	2 (6.6)	6	6	
M/26y	1 (2.8)	6		
	2 (6.5)	6	6	
M/29y	1 (3.2)	6		6
	2 (7.0)	6	6	6
F/32y	1 (3.5)			
	2 (6.0)	6	6	
M/33y	1 (3.5)	8		
	2 (5.7)	8	6	
M/34y	1 (3.8)			
	2 (5.9)	6	6	

Table S6.2: Gene-specific primer sequences used for quantitative real-time polymerase chain reaction.

Gene	Forward	Reverse	GenBank
ACAN	AGGGCGAGTG GAATGATGTT	GGTGGCTGTG CCCTTTTTAC	NM_001135.3
ACTA2	TGCCTGATGG GCAAGTGA	CTGGGCAGCG GAAACG	NM_001141945.2
β-actin	AAGCCACCCC ACTTCTCTCT AA	AATGCTATCA CCTCCCCTGT GT	NM_001101.4
B2M	TGCTGTCTCC ATGTTTGATG TATCT	TCTCTGCTCC CCACCTCTAA GT	NM_004048.3
COL1A2	GCTACCCAAC TTGCCTTCAT G	GCAGTGGTAG GTGATGTTCT GAGA	NM_000089.3
COL2A1	CTGCAAAATA AAATCTCGGT GTTCT	GGGCATTTGA CTCACACCAG T	NM_001844.5
COL10A1	GAAGTTATAA TTTACACTGA GGGTTTCAAA	GAGGCACAGC TTAAAAGTTT TAAACA	NM_000493.3
FRZB	GCATCCCCCT GTGCAAGT	GCAGGTGGTT GGGCATCTTA	NM_001463.4
GREM1	CATGTGACGG AGCGCAAATA	GCTTAAGCGG CTGGGTTTT	NM_013372.7
HIF-1α	GTAGTTGTGG AAGTTTATGC TAATATTGTG T	TCTTGTTTAC AGTCTGCTCA AAATATCTT	NM_001530.4
HIF-2α	GGTGGCAGAA CTTGAAGGGT TA	GGGCAACACA CACAGGAAAT C	NM_001430.5
IHH	CCTTGTCAGC CGTGAGGCCG	GCTGCCGGCT CCGTGTGATT	NM_002181.4

Continued on next page

Table S6.2: *Continued from previous page*

Gene	Forward	Reverse	GenBank
LOX	AGGCCACAAA GCAAGTTTCTG	AAATCGCCTG TGGTAGCCAT A	NM_002317.7
LOXL2	ACGGCCACCG CATCTG	TCCGTCTCTT CGCTGAAGGA	NM_002318.2
MMP13	CATCCAAAAA CGCCAGACAA	CGGAGACTGG TAATGGCATC A	NM_002427.4
PTHLH	CCGCCTCAAA AGAGCTGTGT	GGATGGACTT CCCCTTGTCA	NM_002820.2
RUNX2	GGAGTGGACG AGGCAAGAGT TT	AGCTTCTGTC TGTGCCTTCT GG	NM_001024630.4
SOX9	CTTTGGTTTG TGTTCGTGTT TTG	AGAGAAAGAA AAAGGGAAAG GTAAGTTT	NM_000346.3
TAGLN	GGCATGAGCC GCGAAGT	TCCTCCAGCT CCTCGTCATA CT	NM_001001522.2
VCAN	TGCTAAAGGC TGCGAATGG	AAAAAGGAAT GCAGCAAAGA AGA	NM_004385.5
VCL	GCGAATCCCA ACCATAAGCA	AGCATGGTGG CCTTCACTGT	NM_014000.2
VEGF	GCACGGTCCC TCTTGGAA	CGGTGATTTA GCAGCAAGAA AA	NM_001025366.3
YWHAZ	TCTGTCTTGT CACCAACCAT TCTT	TCATGCGGCC TTTTTCCA	NM_003406.3
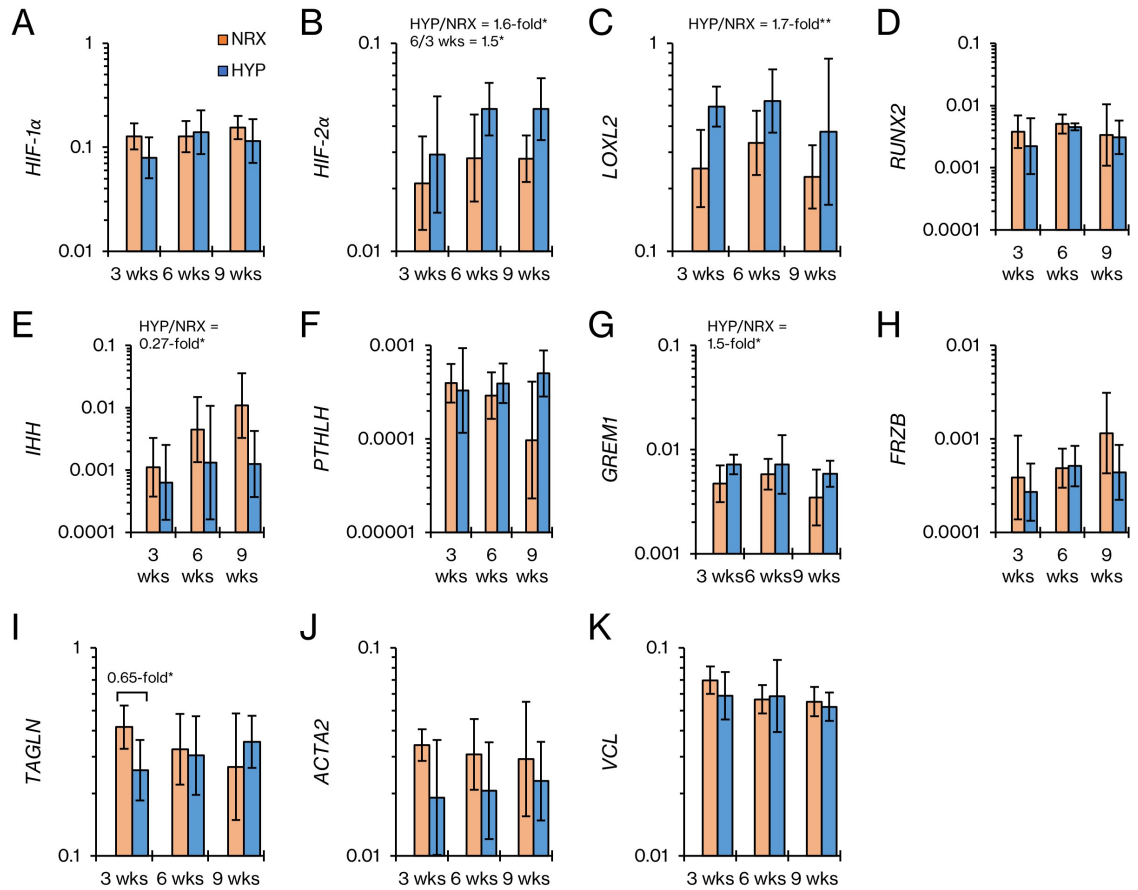
Figure S6.1: Expression levels of a panel of genes related to the low oxygen response (A, B), collagen cross-linking (C), hypertrophy (D-F), suppression of hypertrophy (G, H), and contraction (I-K). HYP: hypoxia (3% O_2). NRX: normoxia (20% O_2). Expression of each gene is presented relative to the mean expression of three reference genes: *YWHAZ*, *β-actin*, and *B2M*. The bars represent mean ± standard deviation from n=6 donors. The expression ratios between the indicated levels of significant factors in the ANOVA model are presented above the bars. *: $p<0.05$, **: $p<0.01$, ***: $p<0.001$.

Chapter 7

Human Engineered Meniscus Transcriptome After Short-term Combined Hypoxia and Dynamic Compression

Contributing authors:

Alexander R.A. Szojka, Rita de Cássia Marqueti, David (Xinzheyang) Li, Clayton W. Molter, Yan Liang, Melanie Kunze, Aillette Mulet-Sierra, Nadr M. Jomha, Adetola B. Adesida

7.1 Preface

In preparation for this study, I made several preliminary investigations with dynamic compression in which I manipulated the applied strain (15±7.5% and 30±15%), fre-

quency (1 vs. 2 Hz), initial scaffold diameter (6 vs. 8 vs 10 mm) and harvest time after completion of loading (0, 10, 20, 30 minutes, 1h, 24h). Rita de Cássia Marqueti, Clayton Molter, and Melanie Kunze each contributed to these efforts. Unfortunately, the results were stubbornly inconsistent. At the time of writing (June 2021) with the clarity of hindsight, I now know the main problem was that I was measuring genes that undergo small changes in response to loading. As a result, the signal I was looking was generally lost in noise from sources of variability; it would have been much more effective to use a highly loading-sensitive gene such as *c-FOS*. These preliminary investigations led me to useful conclusions, however, though they weren't related to the specific manipulated variables: I needed to use many tissue replicates for each MFC donor to narrow in on the signal in gene expression measurement; I needed my loading regime to be aggressive; and I needed to measure genes that had large effect sizes in response to loading. I am grateful to Dr Fred Berry of the Department of Surgery for giving me confidence that the RNA pooling strategy applied here could work, and to David Li for performing most of the RNA seq analysis as part of his undergraduate summer research project.

I presented this study at the following conferences: 1. 2019 Tom Williams Surgical Research Day, Department of Surgery, University of Alberta (2$^{\text{nd}}$ Place Poster Presentation, Basic Science) and 2. 2019 Alberta Biomedical Engineering Conference.

7.2 Abstract

This study investigates the transcriptome response of meniscus fibrochondrocytes (MFCs) to the low oxygen and mechanical loading signals experienced in the knee joint using a model system. We hypothesized that short term exposure to the combined treatment would promote a matrix-forming phenotype supportive of inner meniscus tissue formation. Human MFCs on a collagen scaffold were stimulated to form fibrocartilage over 6 weeks under normoxic (NRX, 20% O_2) conditions with supplemented TGF -β3. Tissues experienced a delayed 24h hypoxia treatment (HYP, 3% O_2) and

then 5 minutes of dynamic compression (DC) between 30 and 40% strain. Delayed HYP induced an anabolic and anti-catabolic expression profile for hyaline cartilage matrix markers (e.g., *SOX9*, 1.6-fold), while DC induced an inflammatory matrix remodeling response along with upregulation of both *SOX9* and *COL1A1*. There were 41 genes regulated by both HYP and DC. Overall, the combined treatment supported a unique gene expression profile favouring the hyaline cartilage aspect of inner meniscus matrix and matrix remodelling.

7.3   Introduction

The menisci are specialized tissues that perform important mechanical roles in the knee joint including weight bearing[15, 30]. Their inner regions are avascular and non-healing in adults[28]. Injuries to the inner regions disrupt function and predispose the knee to early osteoarthritis development[17]. Arthroscopic partial meniscectomy is a common treatment for non-healing inner meniscus tears, but it is also associated with early osteoarthritis development[193]. Meniscus tissue engineering aims to generate functional meniscus tissue constructs that can replace damaged and non-healing native meniscus tissue to restore function and delay osteoarthritis development.

The inner meniscus regions are fibrocartilaginous in adults[35]. The extracellular matrix is composed primarily of type I collagen organized into bundles that confer tensile properties[15, 131] It also contains hyaline matrix components such as type II collagen and aggrecan that confer compressive properties[15, 131] Meniscus matrix is synthesized and maintained by a heterogeneous population of cells referred to as meniscus fibrochondrocytes (MFCs)[22]. MFCs exist natively in a low oxygen and dynamically-loaded environment in adults, experiencing a complex combination of tension, compression, hydrostatic pressure, and shear forces[15, 28–30, 35]. Low oxygen conditions (known as hypoxia (HYP) or physioxia to reflect the inner meniscus native environment) and mechanical loading such as dynamic compression (DC) can each enhance expression of fibrocartilage matrix components by MFCs *in vitro*[2, 55,

59, 71, 148, 194]. However, little is known about how MFCs respond to these signals simultaneously, and how HYP and mechanical loading can be used in combination towards tissue engineering meniscus.

The objective of this study was to gain a better understanding of how MFCs respond to combined HYP and short-term DC at the global mRNA level using a model system of human meniscus. It was hypothesized that the combined treatment would promote a matrix-forming phenotype supportive of inner meniscus tissue formation.

7.4 Materials and methods

7.4.1 Ethics and sample collection

Non-osteoarthritic human meniscus samples from arthroscopic partial meniscectomies as a consequence of trauma at the Grey Nuns Community Hospital and the University of Alberta Hospital in Edmonton were collected with patient consent waived in accordance with the University of Alberta human research ethics board's approval #Pro00018778 to use surgical discards with non-identifying information for scientific research purposes.

7.4.2 Design of a dynamic compression (DC) bioreactor

A custom bioreactor was created out of stainless steel to fit a Biodynamic 5210 test instrument (TA Instruments, USA) positioned inside of a Biospherix X3 incubation chamber system (Figure S7.1). Aspects of the bioreactor design, such as the use of standard Petri dishes to hold samples, were inspired by Mauck *et al.* 2000[195].

7.4.3 Cell expansion and formation of engineered inner meniscus fibrocartilage

An overview of the experimental methods is provided in Figure 1. Inner meniscus specimens from n=3 independent donors were collected during partial meniscectomy (Figure 7.2A). Meniscus fibrochondrocytes (MFCs) were isolated by collagenase di-

gestion and were expanded to passage 2 in a high-glucose DMEM containing 1 ng/mL TGF-β1 and 5 ng/mL FGF-2[8].
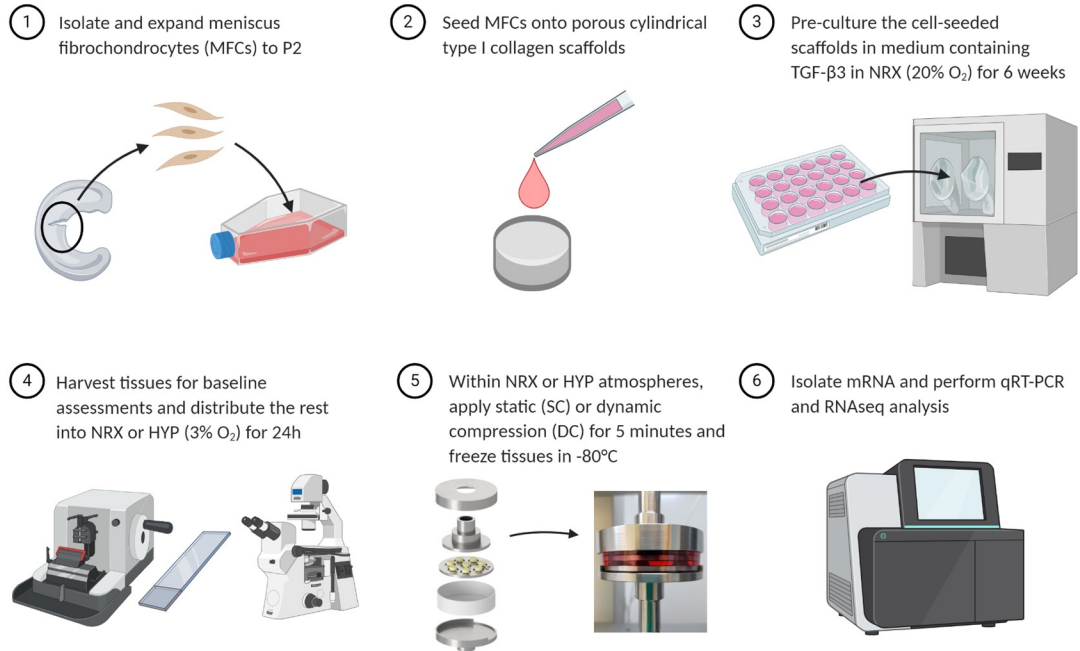
Figure 7.1: Experiment overview. Experiment steps 1-5 were repeated three times, each time using cells from a new human meniscus donor. P: passage. NRX: normoxia. HYP: hypoxia. Adapted from "Autologous Haematopoietic Stem Cell Transplant", by BioRender.com (2020).

MFCs were collected and seeded onto cylindrical type I collagen scaffolds (diameter = 10 mm, height = 3.5 mm, pore size = 115±20 µm, Integra Lifesciences, USA) at a density of $5 \times 10^6/cm^3$. The cell-seeded scaffolds were then pre-cultured for six weeks in a defined serum-free standard chondrogenic medium containing 10 ng/mL TGF-β3 for fibrocartilaginous matrix formation[8]. The duration was selected based on our unpublished data showing that tissues at this time point contain the primary matrix constituents of the inner meniscus (type I collagen, type II collagen, sulphated proteoglycans) and have substantial mechanical properties compared to shorter culture periods. A study using a similar type I collagen scaffold applied a single dynamic compression event after a comparable preculture period (7 weeks) and found it to

have anabolic effects in articular chondrocytes[171].

At the end of the pre-culture period, baseline tissues were harvested to confirm the presence of fibrocartilaginous matrix using histological staining and immunofluorescence. Briefly, tissues were fixed in formalin and paraffin-embedded, sectioned, and stained with Safranin-O for sulphated proteoglycans and antibodies for types I and II collagens by immunofluorescence[8].

7.4.4 Experimental conditions (n=3 donors, 3-4 replicates per condition per donor)

The remaining tissues were randomly assigned into six groups: hypoxia or normoxia with a loading group of either 1. vehicle control (VCtrl), 2. static compression (SC), or 3. dynamic compression (DC). For the oxygen division, tissues were placed into incubation chambers with 3% O_2 (hypoxia, HYP) or 20% O_2 (normoxia, NRX) and 5% CO_2 within an X3 Xvivo system (Biospherix, USA) for a 24h oxygen tension treatment. This duration was chosen to give time for the medium and tissues to equilibrate to the new environment but not undergo dramatic matrix-level protein changes.

With the atmosphere set to 5% CO_2 with 3% O_2 or 20% O_2, replicate tissues within each group were transferred into Petri dishes containing fresh culture medium and put into the bioreactor. Tissues in a VCtrl group were compressed until reaching a 0.01 N per tissue (Figure 7.1). The corresponding pre-load position was then re-used for all the five groups so that the strain calculations would be identical. The pre-load position was re-measured for each donor.

VCtrl consisted of samples reaching the pre-load position and then maintained in contact with the platens for five minutes. SC consisted of 30% compression with a five-minute hold. DC consisted of a 30% SC superimposed with 10% cyclic sinusoidal strain at 1 Hz for five minutes. These loading regime strain parameters were selected based upon preliminary work showing that although the tissues underwent rapid

stress relaxation during the first minutes of DC loading, the stress response magnitude remained adequate for at least five minutes with these parameters. A study using a similar type I collagen scaffold applied similarly large strains (10% static offset with 25% dynamic amplitude) in articular chondrocytes after a 7 week preculture period and identified the regime to have anabolic effects[171]. The specific strain levels and loading duration used here were selected after preliminary work showing that tissues underwent rapid stress relaxation but maintain a strong stress response to applied compression for the duration of the loading period with a sufficiently aggressive static strain offset.

After loading, the samples were removed from contact with the platens and given 30 minutes to rest for gene expression changes to occur. The samples were then transferred into TRIzol reagent and snap-frozen in liquid nitrogen for storage until the experiment was complete for all three donors.

7.4.5   RNA extraction

Total RNA was extracted with standard chloroform phase separation and isopropanol precipitation[8]. To confirm that the short-term treatments were effective in inducing gene expression changes, RNA was reverse transcribed into cDNA for quantitative real-time polymerase chain reaction (qRT-PCR) with gene-specific primers for loading-sensitive (*c-FOS* and *c-JUN*) and hypoxia-sensitive (lysyl oxidase, *LOX*) genes[170, 171] was also measured. Gene expression was compared to the average expression levels of three reference genes (Figure S7.2A).

SPSS 27 (IBM, USA) was used to compare mRNA expression measured by PCR across the different groups by analysis of variance (ANOVA) with oxygen tension and mechanical loading as fixed effects and donor as a random effect. Mean replicate values within each donor and condition were first calculated. The Shapiro-Wilk test was used to assess normality. The presence of any interactions was first assessed by the significance of the Oxygen tension*Mechanical loading term ($p<0.05$). In cases

of no significant interactions, the significance of the main effects were assessed. In cases where mechanical loading had a significant main effect, pairwise comparisons were made between the levels with no p value corrections applied. Fold changes were later compared between qRT-PCR and RNA-seq using Pearson's correlation (Figure S7.2C).

7.4.6 RNA sequencing and bioinformatics

Total RNA samples were purified using RNeasy Mini Kits (Qiagen, Germany) with a DNase digestion step according to the manufacturer's protocol. Equal masses of total RNA from 3 or 4 replicate samples within each condition and within each donor were pooled together to reduce inter-replicate variability (Figure S7.1B). To maintain inter-donor biological variation, pooled samples only consisted of replicates from the same donor, i.e., samples from different donors were not pooled together. With two oxygen tensions (HYP and NRX), three loading groups (VCtrl, SC, and DC), and three donors, there were thus a total of 18 RNA pools that underwent RNA sequencing.

Next-generation sequencing was performed by the University of British Columbia Biomedical Research Centre. Sequencing was performed on the Illumina NextSeq 500 with 20 million paired end 42bp $\times$ 42bp reads. 12946 expressed genes were studied.

RNA sequencing data analysis was performed using Partek® Flow® software, version 9.0.20.0622, Copyright © 2020, Partek Inc., St. Louis, MO, USA. Reads were aligned to the human genome hg38 using STAR-2.7.3a and quantified to a transcript model (hg38-RefSeq Transcript 94; 2020-05-01) using the Partek Expectation/Maximization (E/M) algorithm. Normalization was then conducted on samples with Add: 1.0, TMM and Log 2.0 methods and analysis of variance (ANOVA) was used for differential expression analysis for the oxygen tension, mechanical loading, and donor (random) effects. Differences in gene expression were considered significant if p values adjusted for the false discovery rate (q values) were less than 0.05. For certain comparisons, an absolute fold-change threshold of at least 2 was also applied. Cor-

relation analysis, principal component analysis (PCA), visualization of DEGs, and Venn diagrams were all conducted in Partek Flow software and further exploratory functional analysis was conducted using Gene Ontology (GO) enrichment.

7.5 Results

7.5.1 Baseline data

At the baseline, the donors had formed a spectrum of fibrocartilage tissues with expression comparable for type I collagen (Figure 7.2D) but variable for hyaline cartilage matrix markers (Figure 7.2CE). Average expression levels across experimental conditions between donors of a panel of meniscus-related genes supported these protein-level observations (Figure 7.2F). The more hyaline cartilage-like donors M/24y and M/30y had 29 and 66-fold higher expression of chondromodulin (*CNMD*) compared to the more fibrous M/33y donor. The most highly regulated gene between donors was *CYTL1*, which was 5.5 and 1091-fold upregulated in M/24y and M/30y respectively compared to M/33y. *BSP1* and *RANKL*, two bone-related genes, showed similar inter-donor trends (*BSP1*: 1, 13.8, and 234-fold; *RANKL*: 1, 4.2, and 86.4-fold).

During loading, the stress vs. time plots showed that tissues from the M/30y donor were much stiffer than from the other two donors in both SC and DC groups (Figure 7.3B-D). This was consistent with the protein-level histology and IF assessment (Figure 7.2C-E).

7.5.2 mRNA level analysis

qRT-PCR analysis

To confirm that the short-term treatments were effective, expression changes in genes sensitive to hypoxia (*LOX* and *SOX9*) and mechanical loading (*c-FOS* and *c-JUN*) were first measured by qRT-PCR. All four genes were significantly upregulated by either HYP or DC, which justified proceeding to more resource intensive RNA sequencing (Figure S7.1A).
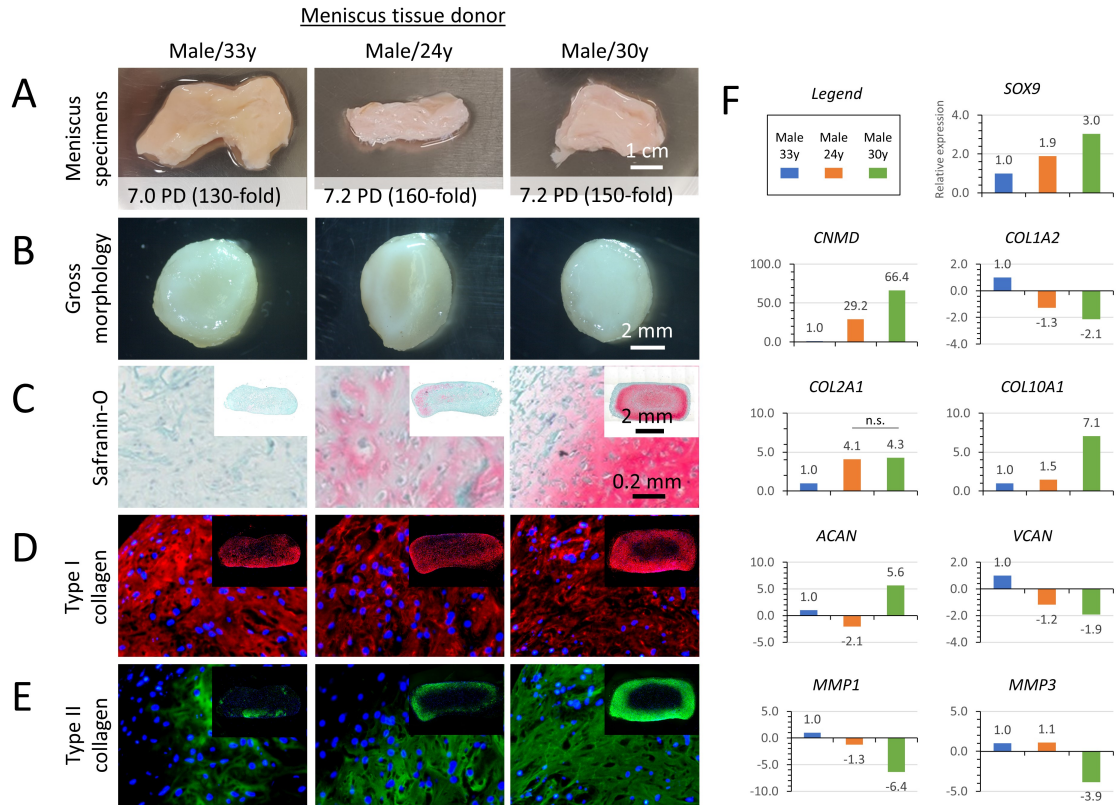
Figure 7.2: The donors formed a spectrum of engineered meniscus fibrocartilage at the six-week baseline before division into experimental conditions. A) Gross morphology of the donated meniscus specimens. PD: population doublings reached before scaffold seeding. B-E) Engineered fibrocartilage gross morphology and staining analysis. Panels in Safranin-O and types I/II collagen rows share common scale bars. Cell nuclei in immunofluorescence images are stained with DAPI (blue). F) Average expression levels for each donor, pooled across the experimental conditions, for a biased panel of meniscus-related genes. All pairwise comparisons not marked by "n.s." (not significant) were statistically different with p≤0.05.

Principal component (PC) and hierarchical clustering analysis

PCs 1-3 explained 73% of the variance in the RNAseq dataset (Figure 7.4A). There was clustering by oxygen tension and donor factors but not mechanical loading, suggesting that these factors had the largest effects. There were 8475 and 64 genes significantly regulated by oxygen tension and mechanical loading, respectively, indicating that oxygen tension was the more potent treatment than mechanical loading[82]. It should be appreciated that the treatment durations, though both relatively short
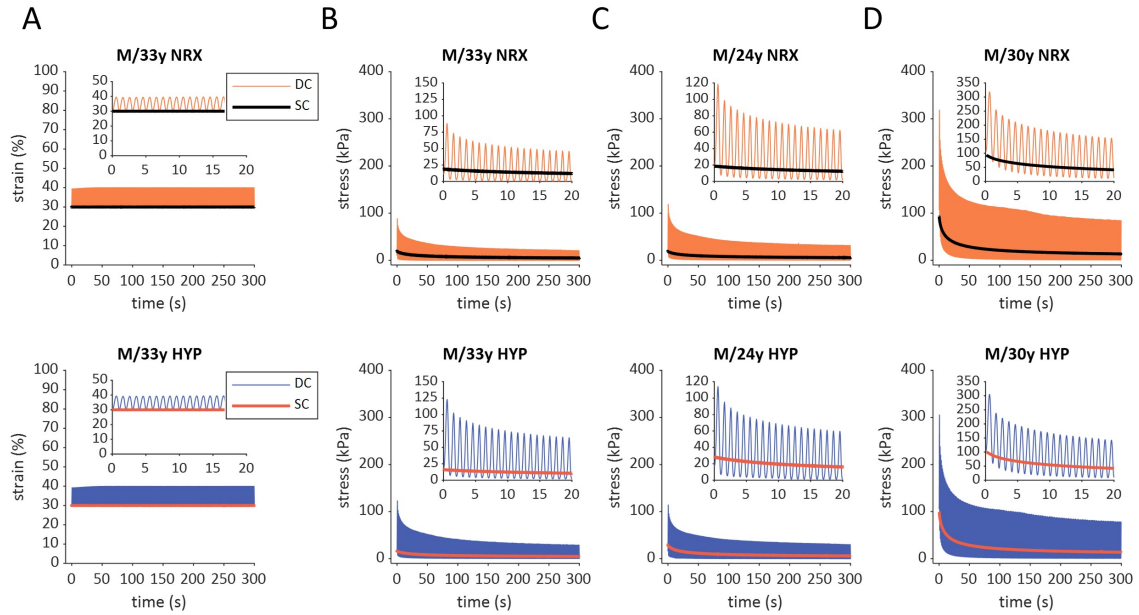
Figure 7.3: Mechanical loading summary of engineered meniscus fibrocartilage by donor. A) Strain vs. time for a representative donor. B-D) Average stress vs. time, computed as the forces reached during loading divided by the total cross-sectional area of engineered tissues in the bioreactor. The vehicle control groups (no compression) are excluded because the force data is noise. M: male. y: years. NRX: normoxia, 20% O_2. HYP: hypoxia, 3% O_2. DC: dynamic compression. SC: static compression. The figure legends in A) are shared by row.

compared to tissue engineering literature, were quite different from one another: 24h for hypoxia and 5 minutes DC+30 minutes rest for mechanical loading (Figure 7.4B). Hierarchical clustering for oxygen tension separated NRX and HYP samples at the highest level, indicating a robust oxygen tension response across the three donors (Figure 7.4C). Hierarchical clustering analysis for the DC vs. VCtrl samples showed a complete separation between VCtrl and loading groups and a partial separation between SC and DC (Figure 7.4D).

Combined effects of oxygen tension and mechanical loading

There were no genes with statistically significant (q<0.05) two-way interactions between oxygen tension and loading-related treatments, meaning that the effects of loading were not significantly different between oxygen tensions. Of the 8475 and
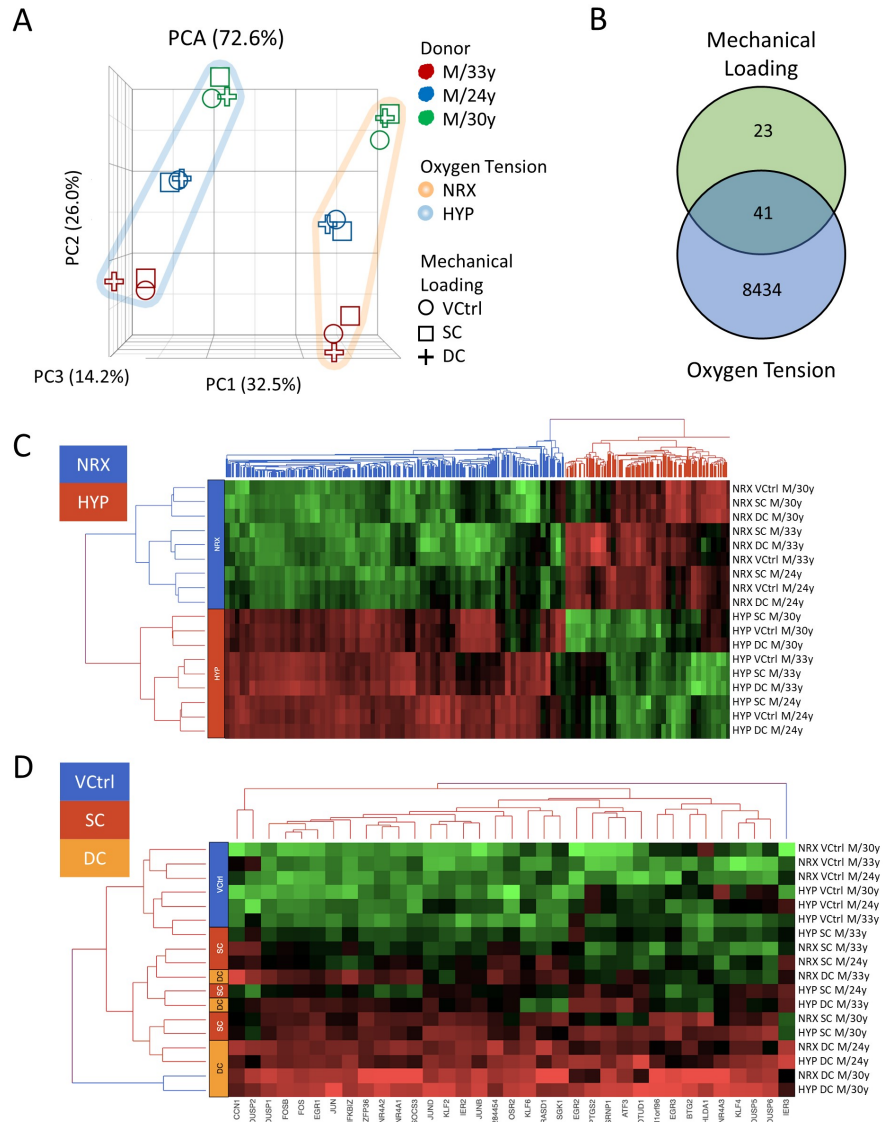
Figure 7.4: Oxygen tension had a more profound effect than mechanical loading. A) Principal component analysis. B) Venn diagram showing genes significantly (q ≤ 0.05) with significant main effects for mechanical loading, oxygen tension, or both. No genes were found with statistically significant two-way interactions between mechanical loading and oxygen tension. C) Differential expression heatmap and hierarchical clustering analysis of genes regulated at least 2-fold between oxygen tensions, narrowing the list of 8475 genes significantly regulated by hypoxia down to 806. The Z-score spectrum ranged from -3.12 (green, low expression) to +2.5 (red, high expression). Genes are not labelled for clarity. D) Similar information as C) but for mechanical loading. The Z-score spectrum ranged from -2.47 to +2.54.

64 genes respectively regulated by oxygen tension and mechanical loading, 41 were co-regulated by the treatments meaning that they had significant main effects for

each (Figure 7.4B). These genes are listed in Table 7.1. Generally, several of the co-regulated genes are involved in the response to endogenous stimuli and stress such as *ATF3*, *NR4A3*, *EGR2*, *DUSP2/5/6*, *JUND*, and *KLF4*. *RGS16* and *SOCS3* play inhibitory roles in signal transduction, while *IER3/5* and *PPP1R15A* play roles in stress resistance and recovery. *ADAMTS1*, *CCN1* and *PTGS2* are related to matrix remodeling and inflammatory responses, while *CSRNP1/2*, *MCL1*, and *PHLDA1* are related to apoptosis.

Table 7.1: Genes significantly (q ≤ 0.05, indicated by *) co-regulated by oxygen tension and mechanical loading. The HYP vs. NRX comparison included 9 samples from 3 donors in each oxygen tension, because the loading groups were combined for this comparison. The SC vs. VCtrl and DC vs. VCtrl comparisons each contained 6 samples from 3 donors because the oxygen groups were combined. Finally, the HYP*DC vs. NRX*VCtrl had only 3 samples from 3 donors because these were specific groups with no combining possible.

Symbol	Gene name	HYP vs. NRX	SC vs. VCtrl	DC vs. VCtrl	HYP*DC vs. NRX* VCtrl
ADAMTS1	ADAM Metallopeptidase With Thrombospondin Type 1 Motif 1	-2.12*	1.27	1.93*	-1.13
ATF3	Activating Transcription Factor 3	1.87*	2.18*	5.79*	13.38*
CCN1	Cellular Communication Network Factor 1	-1.35*	1.49	2.07*	1.51*
CCNG2	Cyclin G2	2.55*	-1.1	1.04	2.49*
CHD1	Chromodomain Helicase DNA Binding Protein 1	1.12*	1.08	1.28*	1.44*
CHMP1B	Charged Multivesicular Body Protein 1B	-1.31*	1.15	1.50*	1.16*
CLK1	CDC Like Kinase 1	1.88*	-1.1	1.44*	2.62*
CSRNP1	Cysteine And Serine Rich Nuclear Protein 1	1.38*	1.56	2.67*	4.08*
CSRNP2	Cysteine And Serine Rich Nuclear Protein 2	1.13*	1.16	1.34*	1.52*

Continued on next page

Table 7.1: *Continued from previous page*

Symbol	Gene name	HYP vs. NRX	SC vs. VCtrl	DC vs. VCtrl	HYP*DC vs. NRX*VCtrl
DUSP2	Dual Specificity Phosphatase 2	-1.61*	1.71	2.90*	1.88*
DUSP5	Dual Specificity Phosphatase 5	1.52*	1.74*	2.81*	5.15*
DUSP6	Dual Specificity Phosphatase 6	1.75*	1.92	3.02*	5.94*
EGR2	Early Growth Response 2	1.56*	1.77*	2.29*	3.99*
GEM	GTP Binding Protein Overexpressed in Skeletal Muscle	-2.72*	1.08	1.59*	-1.72*
HBEGF	Heparin Binding EGF Like Growth Factor	1.45*	1.39	1.71*	2.30*
IER3	Immediate Early Response 3	1.26*	1.49	2.56*	3.70*
IER5	Immediate Early Response 5	1.23*	1.37	1.85*	2.23*
JUND	JunD Proto-Oncogene, AP-1 Transcription Factor Subunit	1.35*	1.78*	2.71*	3.85*
KDM7A	Lysine Demethylase 7A	2.06*	-1.06	1.15	2.29*
KLF4	Kruppel Like Factor 4	1.41*	1.82*	3.20*	4.80*
LOC 284454	Uncharacterized LOC284454	-1.28*	2.22*	3.76*	3.21*

Continued on next page

Symbol	Gene name	HYP vs. NRX	SC vs. VCtrl	DC vs. VCtrl	HYP*DC vs. NRX*VCtrl
MCL1	MCL1 Apoptosis Regulator, BCL2 Family Member	1.12*	1.23	1.64*	1.86*
MIDN	Midnolin	-1.43*	1.35	1.44*	1.01
NR4A3	Nuclear Receptor Subfamily 4 Group A Member 3	1.30*	1.06	2.96*	5.08*
OTUD1	OTU Deubiquitinase 1	1.53*	1.42	2.23*	3.24*
PHLDA1	Pleckstrin Homology Like Domain Family A Member 1	-1.57*	1.52	2.59*	1.65*
PPP1R 15A	Protein Phosphatase 1 Regulatory Subunit 15A	2.15*	1.23	1.84*	4.44*
PPP1R 3B	Protein Phosphatase 1 Regulatory Subunit 3B	2.23*	-1.31*	-1.19	1.69*
PTGS2	Prostaglandin-Endoperoxide Synthase 2	3.59*	1.86	3.73*	17.11*
RASD1	Ras Related Dexamethasone Induced 1	-2.56*	3.33	9.47*	4.40*
RCAN1	Regulator of Calcineurin 1	2.19*	-1.12	1.21	2.93*
RGS16	Regulator Of G Protein Signaling 16	1.85*	1.45	1.90*	3.86*

Symbol	Gene name	HYP vs. NRX	SC vs. VCtrl	DC vs. VCtrl	HYP*DC vs. NRX*VCtrl
RND3	Rho Family GTPase 3	-1.15*	1.14	1.57*	1.36*
RSBN1	Round Spermatid Basic Protein 1	1.43*	-1.21*	-1.04	1.31*
SGK1	Serum/Gluco-corticoid Regulated Kinase 1	-1.39*	1.54	2.28*	1.67*
SLC25A 25	Solute Carrier Family 25 Member 25	-1.41*	1.37	1.51*	1.11
SLC2A3	Solute Carrier Family 2 Member 3	3.29*	-1.17	1.12	3.29*
SOCS3	Suppressor Of Cytokine Signaling 3	-1.65*	2.19	5.78*	3.79*
TRIB1	Tribbles Pseudokinase 1	1.69*	1.28	1.78*	3.02*
ZFP36L2	ZFP36 Ring Finger Protein Like 2	-1.59*	1.45	1.62*	1.01
ZNF507	Zinc Finger Protein 507	-1.16*	1.14	1.21*	1.05

Biological interpretation was performed using Gene Ontology (GO) enrichment analysis using the list of co-regulated genes. Selected pathways are presented in Table 7.2, with the complete pathway listing in the supplementary materials of the published manuscript[5]. The significantly enriched pathways included several relating to basic cellular functions such as catalytic activity and metabolic processes, as well as cellular signalling such as MAP kinase.

Table 7.2: Selected enriched pathways from Gene Ontology (GO) analysis of genes co-regulated by oxygen tension and mechanical loading, as well as the individual effects of each treatment. The full lists are available in the published manuscript online as supplemental materials[5].

Description	P-value	Genes in list
GO Pathway: 41 oxygen and mechanical loading regulated genes (FDR ≤ 0.05)		
Regulation of smooth muscle cell proliferation	5.88E-07	6
Regulation of phosphate metabolic process	8.79E-07	16
MAP kinase tyrosine/serine/threonine phosphatase activity	3.82E-06	3
Regulation of catalytic activity	6.30E-06	17
Regulation of cellular metabolic process	1.01E-05	28
GO Pathway: 806 hypoxia vs. normoxia genes (FDR ≤ 0.05, |FC| ≤ 2))		
Endoplasmic reticulum unfolded protein response	4.98E-15	29
Signal transduction	9.55E-15	262
Response to endoplasmic reticulum stress	2.89E-14	44
Extracellular space	8.81E-14	105
Response to hypoxia	2.16E-12	41
Angiogenesis	1.27E-10	39
Extracellular matrix	2.17E-10	54
Ion homeostasis	2.44E-10	66
Collagen-containing extracellular matrix	5.77E-08	41
GO Pathway: 35 DC vs VCtrl genes (FDR ≤ 0.05, |FC| ≤ 2)		
response to endogenous stimulus	3.30E-14	18
positive regulation of RNA metabolic process	1.02E-13	21

Continued on next page

Table 7.2: *Continued from previous page*

Description	P-value	Genes in list
DNA-binding transcription factor activity	2.53E-13	18
Positive regulation of cellular metabolic processes	3.98E-12	25
Response to hormone	5.43E-12	14
Positive regulation of cellular biosynthetic process	1.95E-11	20
Transcription factor AP-1 complex	1.96E-11	4
Cell differentiation	2.70E-11	19

Characterization of individual main effects for oxygen tension and mechanical loading

Of the 8475 genes regulated by oxygen tension, 806 had absolute value fold-changes, |FC| ≥ 2. The ten genes with the highest oxygen tension fold changes are shown in Table 7.3, with the complete list available in the published manuscript's supplementary materials[5]. The 24h hypoxia treatment had pro-fibrocartilage effects including upregulation of anabolic genes including *SOX9* (1.58-fold), *FGF-1* (3.29-fold), *MATN4* (2.39-fold), and *ACAN* (1.49-fold), and downregulation of catabolic genes *ADAMTS1* (2.12-fold) and *MMPs 1, 3* and *13* (4.50, 2.98, and 1.59-fold respectively). Selected enriched pathways from GO analysis are presented in Table 7.2, with the complete listing available in the published manuscript.

Table 7.3: Top ten genes that had the largest |FC| between HYP and NRX groups. *: q<0.05.

Symbol	Gene name	HYP vs. NRX	SC vs. VCtrl	DC vs. VCtrl
BHLHA15	Basic Helix-Loop-Helix Family Member A15	30.94*	1.08	1.02
KISS1R	KISS1 Receptor	30.52*	-1.12	-1.00
KTI12	KTI12 Chromatin Associated Homolog	-26.75*	1.07	-1.52
CDH15	Cadherin 15	18.43*	-1.26	1.03
ARFGEF3	ARFGEF Family Member 3	18.23*	1.11	-1.03
P2RY11	Purinergic Receptor P2Y11	16.59*	2.72	4.21
MT3	Metallothionein 3	14.88*	1.01	1.10
DERL3	Derlin 3	14.78*	1.18	1.33
STC1	Stanniocalcin 1	14.69*	1.12	-1.11
CKMT2	Creatine Kinase, Mitochondrial 2	13.55*	1.23	1.09

Of the 64 genes regulated by mechanical loading, 35 genes had |FC| ≤ 2. All of these fell within the DC vs. VCtrl comparison (Figure 7.5). These genes all showed a "step-up" in fold change and increased statistical significance in comparing first VCtrl to SC and then SC to DC (Figure 7.5). This indicates that SC did not upregulate a unique set of genes compared to DC; rather, it induced an intermediate gene expression phenotype between VCtrl and DC. The DC treatment was clearly more effective than the SC treatment in inducing a gene expression response. This is likely due to the dynamic loading aspect but also the added compression applied in DC (up to 40% total strain) compared to SC (up to 30%).

The ten genes with the highest fold-changes in DC vs VCtrl are shown in Table 7.4, with the complete list provided in the supplementary materials of the published manuscript[5]. Several genes related to the AP-1 transcription factor complex,

including *FOS*, *FOSB*, *JUN*, and *JUNB* were upregulated with roles in early signal transduction of mechanical stimulus. Further, many genes involved in inflammatory-related pathways such as *MAPK*, *IL-17*, and *TNF* signalling were also upregulated. Selected enriched pathways from GO analysis of the 35 genes significantly regulated by mechanical loading with $|FC| \geq 2$ are presented in Table 7.2, with the complete listing available in the published manuscript[5].

DC vs. VCtrl

24

5   2

4

0   0   0

SC vs. VCtrl   DC vs. SC

Gene	VCtrl	SC	DC
(DC vs. VCtrl) only			
RASD1	1	3.3	9.5*
SOCS3	1	2.2	5.8*
ERG3	1	2.8	4.4*
C11orf96	1	1.9	4.1*
KLF2	1	2.4	4.0*
JUN	1	1.7	3.3*
OSR2	1	2.0*	3.2*
KLF4	1	1.8*	3.2*
JUNB	1	1.9	3.0*
DUSP6	1	1.9	3.0*
NR4A3	1	1.1	3.0*
DUSP2	1	1.7	2.9*
DUSP5	1	1.7*	2.8*
JUND	1	1.8*	2.7*
CSRNP1	1	1.6	2.7*
NFKBIZ	1	1.7*	2.6*
PHLDA1	1	1.5	2.6*
IER3	1	1.5	2.6*
BTG2	1	1.4	2.4*
ERG2	1	1.8*	2.3*
SGK1	1	1.5	2.3*
OTUD1	1	1.4	2.2*
CCN1	1	1.5	2.1*
KLF6	1	1.5	2.1*

Gene	VCtrl	SC	DC
(DC vs. VCtrl) AND (DC vs. SC)			
NR4A2	1	4.4	19.8*†
PTGS2	1	1.9	3.7*†
(SC vs. VCtrl) AND (DC vs. VCtrl)			
FOSB	1	7.3*	22.9*
EGR1	1	4.6*	9.2*
ZFP36	1	2.3*	4.5*†
LOC284454	1	2.2*	3.8*
IER2	1	2.4*	3.6*
(SC vs. VCtrl) AND (DC vs. VCtrl) AND (DC vs. SC)			
FOS	1	7.3*	20.8*†
NR4A1	1	3.0*	8.4*†
ATF3	1	2.2*	5.8*†
DUSP1	1	2.3*	5.2*†

Figure 7.5: Dynamic compression was more effective in inducing a gene expression response than static compression. The data is pooled from both oxygen tensions. All listed genes were significantly regulated in at least one of the comparison groups with q ≤ 0.05 and |FC| ≥ 2. * significance relative to VCtrl; + significance relative to SC.

Table 7.4: Top ten mechanical loading genes that had the largest |FC| between DC and VCtrl groups. *: q<0.05.

Symbol	Gene name	HYP vs. NRX	SC vs. VCtrl	DC vs. VCtrl
FOSB	FosB Proto-Oncogene, AP-1 Transcription Factor Subunit	-1.03	7.26*	22.85*
FOS	Fos Proto-Oncogene, AP-1 Transcription Factor Subunit	1.15	7.30*	20.81*
NR4A2	Nuclear Receptor Subfamily 4 Group A Member 2	-1.37	4.35	19.80*
EGR1	Early Growth Response 1	1.15	4.56*	9.17*
NR4A1	Nuclear Receptor Subfamily 4 Group A Member 1	-1.54	2.95*	8.41*
DUSP1	Dual Specificity Phosphatase 1	-1.18	2.34*	5.21*
ZFP36	ZFP36 Ring Finger Protein	-1.16	2.33*	4.50*
EGR3	Early Growth Response 3	1.05	2.77	4.43*
C11orf96	Chromosome 11 Open Reading Frame 96	1.04	1.19	4.11*
KLF2	Kruppel Like Factor 2	1.24	2.35	3.95*

A biased panel of known meniscus fibrocartilage matrix-related genes were then considered to assess whether the combined treatment had beneficial effects for tissue formation at this early stage using unadjusted p values (Table 7.5). HYP clearly favoured matrix protection through consistent suppression of catabolic enzymes such as *ADAMTS1* (-2.12-fold) and *MMPs*. It also favoured development of the hyaline cartilage aspects of the inner meniscus through upregulation of *ACAN* (1.49-fold) and *SOX9* (1.58-fold) and suppressed the fibrous aspect through reduced expression of *VCAN* (-2.04-fold), *DCN* (-1.21-fold) (Table 7.5). DC had mixed effects, increasing both hyaline cartilage-like tissue marker *SOX9* (1.37-fold) and fibrous tissue marker *COL1A1* (1.33-fold), as well as the aggrecanases such as *ADAMTS1* (1.93-fold) (Ta-

ble 7.5).

Table 7.5: Expression comparisons between HYP/NRX, DC/VCtrl, and the double vs. no treatment groups HYP*DC/NRX*VCtrl for a biased selection of meniscus-related genes. The HYP vs. NRX comparison included 9 samples from 3 donors in each oxygen tension, because the loading groups were combined for this comparison. The DC vs. VCtrl comparisons each contained 6 samples from 3 donors because the oxygen groups were combined. The HYP*DC vs. NRX*VCtrl had only 3 samples from 3 donors because these were specific groups with no combining possible. *: p<0.05, ***: p<0.001.

Symbol	Gene name	HYP vs. NRX	DC vs. VCtrl	HYP*DC vs. NRX*VCtrl
ACAN	Aggrecan	1.49*	1.08	1.56*
ADAMTS1	ADAM Metallopeptidase With Thrombospondin Type I Motif 1	-2.12***	1.93***	-1.13
COL1A1	Collagen Type I mu 1 Chain	-1.19	1.33*	1.16
COL2A1	Collagen Type II mu 1 Chain	1.2	1.16	1.31
COL10A1	Collagen Type X mu 1 Chain	1.23	1.04	1.16
DCN	Decorin	-1.21***	1	-1.23***
MMP1	Matrix Metallopeptidase 1	-4.50***	1.07	-4.68***
MMP3	Matrix Metallopeptidase 3	-2.98***	1.03	-2.80***
MMP13	Matrix Metallopeptidase 13	-1.59***	1.08	-1.5*
SOX9	SRY-Box Transcription Factor 9	1.58***	1.37*	2.09***
VCAN	Versican	-2.04***	1.03	-1.96***

7.6   Discussion

This study investigated the global gene expression response of human MFCs to a short mechanical loading event under different oxygen tensions. Engineered tissues from the three donors were remarkably different in the degree of hyaline cartilage matrix formation at the baseline. Inter-donor variability was also a considerable factor after application of the experimental conditions based upon PCA. The donors appeared evenly spaced from one another on the PCA plot and covered a range of fibrous to cartilaginous matrix phenotype, which may improve the external validity of this study's findings with respect to the oxygen tension and mechanical loading treatments because the listed genes were identified as being significantly regulated across the three donors with differing matrix phenotypes. The RNA pooling strategy from multiple replicates within conditions and donors would have reduced the contributions of variability in culture and analysis, making it easier to detect these differences between donors. Pooled across the experimental conditions, several genes were identified with wide differences in expression levels between donors that correlated to the matrix phenotype, which may prove useful as candidate biomarkers for hyaline cartilage type matrix formation in this model. Previous work has also reported human MFCs to show considerable inter-donor variability[130]. This result highlights the importance of biological replication using multiple meniscus tissue donors[63].

During the early phases of monolayer expansion, MFCs lose their native expression of chondrogenic markers but these can be restored through 3D culture with TGF-β3[8, 60]. However, clearly there were wide inter-donor variations in the degree that MFCs re-express chondrogenic markers. For donors with more chondrogenic MFCs, shorter exposure to pro-chondrogenic conditions may be more appropriate to attain matrix compositions more representative of healthy adult meniscus[186]. The observed inter-donor differences cannot be attributed with certainty to a specific cause. The donors were of the same sex, of similar age, and their cells underwent similar

degrees of *in vitro* expansion[8, 55]. Two potential contributors were the proportion of inner vs. outer meniscus tissue in the donor samples and the injury details: the M/33y tissue specimen was more than twice as large as the others implying inclusion of parts of the outer fibrous regions and the M/30y donor had an associated ACL injury. Different injuries could affect the progenitor cell proportion within the harvested meniscus specimen with downstream effects on the matrix-forming capacity of isolated cells[196–200]. Although MFCs may be the most attractive cell type for meniscus tissue engineering applications[126], it is a challenge that their matrix-forming outcomes may depend upon uncontrollable factors such as the nature of the injury and the recruitment of local stem cell progenitors[7, 60, 201, 202]. Candidate gene biomarkers of the human inner avascular meniscus have been characterized relative to expanded and re-differentiated MFCs[203]. Chondroadherin (*CHAD*), which encodes a cartilage matrix adhesion-related protein, showed wide expression differences within that study and in the present work between the fibrous and hyaline-like donors (11-fold upregulation) with M/24y as the intermediate, suggesting its expression in tissue may provide early knowledge of a donor's downstream matrix forming capacity. Similar methods to predict the matrix-forming capacity of a donor's cells at an early stage may facilitate eventual clinical translation of meniscus tissue engineering-related technology.

The finding of no significant interactions between hypoxia and mechanical loading indicates that gene regulation by a single loading event did not seem to depend on whether the tissues were in a hypoxic or normoxic state at the measured time point. It should be appreciated that the study had limited power to detect statistical interactions. It was, however, interesting to find a list of genes regulated by both oxygen tension and mechanical loading. This indicates that the treatments can amplify or antagonize each other's effects through regulation of the same genes. The rightmost column of Table 7.1 shows how large combined fold changes could be produced in the double treatment group (HYP/DC) compared to the double control (NRX/VCtrl), as

the main effects are multiplied through cooperative co-regulation. For example, *ATF3* (1.9-fold HYP/NRX, 5.8-fold DC/VCtrl) and *PTGS2* (3.6-fold HYP/NRX, 3.7-fold DC/VCtrl) were respectively upregulated 13.4 and 17.1-fold in the double treatment compared to the control. Other genes had antagonistic co-regulation, with the HYP and DC effects neutralizing each other. For example, *ADAMTS1* was suppressed 2.1-fold by hypoxia and induced 1.9-fold by DC. Apart from cooperative or antagonistic co-regulation of specific genes between the oxygen and mechanical loading treatments, the unique genes regulated by the individual treatments are all regulated together in the combined treatment. Simultaneous treatments of oxygen tension and mechanical loading thus induce a unique combined gene expression profile. These genes were identified despite the wide differences in the degree of hyaline cartilage-like matrix between the three donors, suggesting that their expression may be robust to variations in this variable.

Table 7.5 shows the individual and combined effects of HYP and DC on a list of inner meniscus matrix-related genes. The clearest result was that the combined treatment supported development of a more hyaline cartilage-like matrix profile. The results were otherwise mixed: HYP strongly suppressed catabolic enzymes which was only partly balanced by increases in these enzymes by DC. The HYP and DC treatments also had opposing effects on fibrous tissue markers. This makes sense in the context of the native meniscus because the adult tissue contains both hyaline cartilage and fibrous tissue characteristics. The results thus offer early support for our hypothesis that combined hypoxia and mechanical loading would induce a matrix-forming phenotype favourable to inner meniscus tissue formation. Beyond the inner meniscus, this could be an important result for the field of hyaline cartilage tissue engineering. However, it remains to be determined how longer treatment durations would affect this profile and to what extent it would translate into protein and mechanical effects.

Previous work in combined hypoxia and mechanical loading in the context of other tissue engineering applications besides meniscus showed similar hypoxia-induced up-

regulation of hyaline cartilage matrix components as was observed here[80–82]. Hypoxia regulation of HIF-1 is well known to have pro-chondrogenic effects, and was recently shown to mediate anti-catabolic effects through suppression of MMPs as was observed here and by suppression of NF-κB signalling[204]. Previously, HYP increased *SOX9* in MFC cell pellets[56] but did not affect *SOX9* in MFC-seeded type I collagen scaffolds when applied immediately after cell seeding[57]. The results indicate that a delayed hypoxia treatment occurring after a NRX pre-culture period may allow HYP to exert chondrogenic effects in the type I collagen scaffold. This is further supported by yet unpublished data in this same culture model, which showed nearly 5-fold upregulation of *SOX9* for n=3 donors after 5 days of culture in HYP compared to NRX following a 3-week NRX pre-culture period.

Static compression (SC) was used as a control group for dynamic compression (DC). Under normoxic conditions, SC under normoxic conditions has been shown to inhibit matrix synthesis and promote matrix breakdown in meniscus and cartilage tissue such as through decreased synthesis of collagen and sulphated proteoglycans, reduced mRNA expression of precursors to type I collagen and proteoglycans such as aggrecan and decorin, and increased mRNA expression of *MMP-1*[51, 159, 162]. In contrast, under normoxic conditions in engineered meniscus and cartilage, DC can have anabolic or catabolic effects depending on the conditions measured through changes in outcomes such as GAG and collagen contents, mechanical properties, matrix organization, and mRNA expression of related genes[64, 70, 71, 73, 171, 205]. Here, the SC treatment had a fundamentally similar response to the DC treatment but with smaller effect sizes and less differential gene regulation. The reason that gene expression in SC was fundamentally like that of DC, i.e., pro-fibrocartilage, here may be due to the short treatment duration. Also, since the total level of strain in DC was up to 40% and only 30% in SC, the differences between these groups can't be solely attributed to the dynamic aspect of DC as it could have been due to the added compression. However, the large increase in *c-FOS* in DC (35.8-fold) compared to

SC (10.1-fold) relative to the unloaded VCtrl group suggests that the dynamic aspect accounts for much of the difference (Figure 7.2A).

Dynamic mechanical loading regimes of cartilaginous tissues such as meniscus may be described on a "loading aggression spectrum" from insufficient (no effects) to excessive (detrimental effects), with an intermediate optimum (beneficial effects)[63, 64, 206]. Placement of a DC regime on the spectrum depends on loading parameters (e.g., applied strains) and the matrix maturity prior to initiation of loading[63, 185]. Although the same loading regime applied to native meniscus tissue or in brittle hydrogels would likely be destructive, in our experiences engineered tissues on the porous type I collagen scaffolds can undergo large strains–well beyond 40%–without a dramatic loss of cell viability. The scaffolds themselves are readily compressible, and so the only relevant limits to the strains that can be applied are what the cell-made matrix can withstand. Despite the inter-donor variability in matrix maturity, a common set of genes was rapidly regulated by the short-term mechanical loading indicating a donor independent mechanotransduction response. Many of the genes upregulated by mechanical loading were stress and inflammation related. This suggests that for the maturity of engineered meniscus fibrocartilage used here, the applied loading regime may have been excessive. However, the panel of specific fibrocartilage related genes assessed by unadjusted p-values showed mixed anabolic and catabolic characteristics, with upregulation of a type I collagen precursor and chondrogenic regulator *SOX9*, but also precursors for aggrecanases. This indicates that the load regime induced matrix remodelling activities, which is remarkable given its short duration. The DC-induced increase in *SOX9* observed here is consistent with previous work in chondrocytes in a similar type I collagen scaffold with a single loading event[171]. The few published mechanical loading studies that investigated meniscus engineered with human MFCs all used normoxia and show mixed results, but generally induced anabolic effects such as increased expression of types I and II collagens, *ACAN*, and *SOX9*[65–67, 69, 207]. The initial gene expression profile under DC observed here has

promising early effects consistent with previous work and seems especially promising when combined with the matrix protecting and hyaline cartilage promoting effects of HYP.

Peak stress can be used as an indicator for the aggressiveness of a DC regime that cycles between two strain levels. In a similar culture model to the present study but on the last day of two weeks of loading after an initial two-week pre-culture duration, the peak stress during DC from 0-10% strain ranged from 1.9-2.4 kPa[3]. In contrast, the present study's DC groups reached peak stresses from 30-40% strain of 88-305 kPa. The pre-culture duration and loading regime in the current study were designed to provide much more aggressive DC loading than the previous work because no mechanotransduction effect had been observed. The beneficial effects of increased static pre-culture time on instantaneous compression modulus from 0-10% strain were clear between studies: four weeks previously led to a range between donors of 26-40 kPa, whereas six weeks here had a range of 57-163 kPa (data not shown). Based on stress values and the inflammatory gene profile induced here, the two matrix maturity and loading regime combinations are on opposite ends of the loading aggression spectrum. Our ongoing work investigates an intermediate combination of pre-culture duration and loading regime applied over a longer period under HYP and NRX conditions.

Early in life, the human menisci are vascularized and fibrous6. By adulthood, the inner meniscus regions transition to an avascular fibrocartilage phenotype with an organized functional matrix of type I collagen and hyaline matrix components[28, 35, 36]. Development of the adult inner meniscus phenotype is speculated to be related to increased mechanical loading during the first two decades of life, with the strain fields induced by deformational loading potentially guiding organization of the type I collagen[28, 32–37]. Being avascular and existing within the hypoxic synovial fluid, MFCs within the inner meniscus regions experience a low oxygen tension environment that may assist in development of hyaline cartilage matrix components[28,

29, 56]. The present study mimicked the low oxygen environment using HYP incubators, and mechanical loading by DC. The results suggest that HYP regardless of loading supports accumulation of hyaline cartilage aspect of fibrocartilage by promoting anabolism and suppressing catabolism. On the other hand, DC regardless of oxygen tension induces a mixed profile suggestive of matrix remodelling. This could be important to protect the integrity of the avascular matrix from loading-induced inflammation[208, 209]. The anabolic effects of hypoxia combined with the matrix remodelling effects of an optimized DC regime could help generate engineered meniscus with more physiological characteristics.

This study had two main limitations. The gene expression profiles were considered only at a single time point after loading. Previously, *FOSB* and *SOX9* expression immediately increased after an anabolic loading period and returned to baseline levels within hours in chondrocytes. Although the single time point of 30 minutes may have appropriately captured the early gene expression response to loading, it missed out on delayed and downstream mRNA changes[171]. The study also only considered a single and short-term loading event, and thus the mRNA and protein effects of longer loading durations under HYP compared to NRX remain unknown. Obviously, recurring loading events are more representative of meniscus physiology, and it is likely that longer term treatments would have favoured discovery of interactions between the treatments in individual genes. No protein analysis was performed to validate differences in mRNA content between groups because the harvest time point was so early after the loading period and it was expected that related protein changes would be limited compared to those at the mRNA level. It can thus only be assumed that changes in mRNA expression led to differential protein transcription. The RNAseq data pooled across groups was well supported by baseline protein and mechanical observations, however, making this a plausible assumption (Figure 7.2 and Figure 7.3). The stress vs. strain curves during loading showed an initial stress relaxation period followed by a plateau (Figure 7.3). Our future work will also investigate the effects

of DC regimes that extend well into the plateau region, as are typical in related literature[63].

7.7   Conclusion

A short-delayed hypoxia (HYP) treatment after six weeks of normoxic pre-culture was enough to induce an inner meniscus matrix-forming phenotype in engineered human meniscus tissue constructs. Early molecular level changes occur in response to static compression that are amplified by dynamic compression (DC). Delayed HYP regardless of loading supports accumulation of hyaline cartilage-type matrix by promoting anabolism and suppressing catabolism. On the other hand, DC regardless of oxygen tensions induces a mixed profile suggestive of matrix remodelling. Several genes were identified that are co-regulated by oxygen tension and compression loading. Altogether, these results indicate that simultaneous HYP and DC are promising as a combined treatment for inner meniscus tissue engineering.

7.8   Acknowledgements

7.9   Funding sources

7.10   Author contributions

All listed authors meet the Journal of Tissue Engineering criteria for authorship. AS and AA designed the study. AS and CW designed the bioreactor. AS and RM performed tissue culture. DL, AS, RM, and MK performed qPCR expression analysis. DL was responsible for RNA-Seq data analysis with Partek Flow software. AS and DL performed statistical analysis and prepared tables and figures. AS and DL wrote the manuscript with input from all co-authors. NMJ assisted with procuring clinical specimens and in reviewing and editing the manuscript. AA supervised and was responsible for acquiring financial support for the study.

7.11 Supporting information
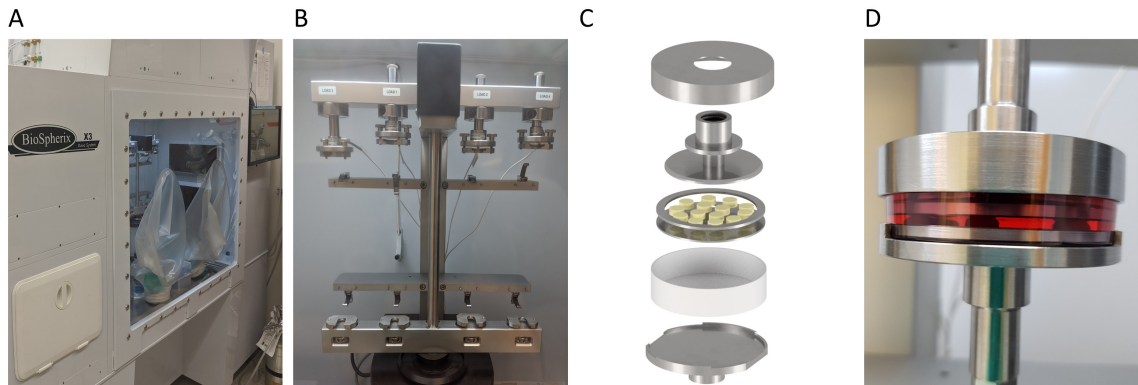
Figure S7.1: Equipment set up and bioreactor design. A) X3 Incubator System (Biospherix, USA). B) Biodynamic 5210 Test Instrument (TA Instruments, USA), positioned inside the X3 process chamber. C) Exploded view of the custom bioreactor. D) Assembled bioreactor containing medium and engineered meniscus fibrocartilage. The ring and Petri dish insert were intended to help keep the samples in place while bringing them into contact with the platen but their effectiveness was limited. These were removed in subsequent work because a more effective strategy was identified. Samples are now brought into contact with the platen first (0.01 N/sample) and then culture medium is added.
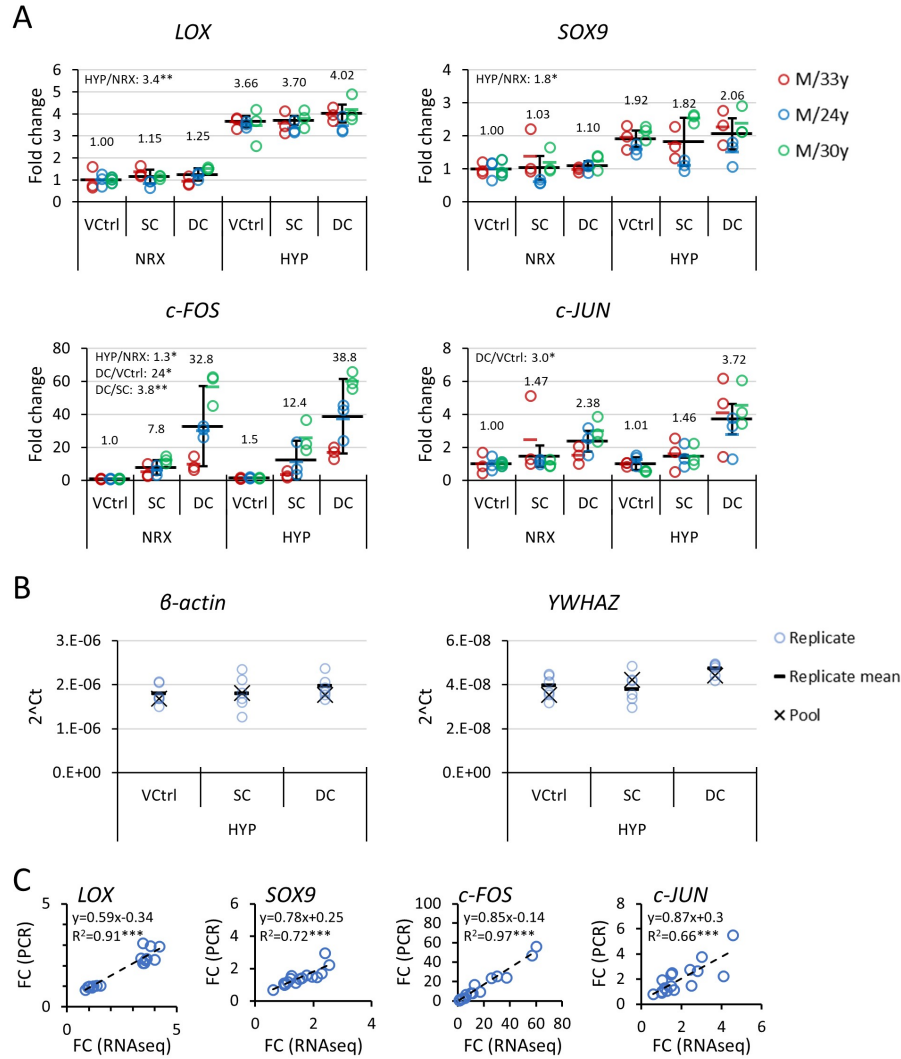
Figure S7.2: mRNA measurement by qRT-PCR, mRNA pool validation, and qRT-PCR vs. RNAseq correlations. A) Expression normalized in each donor to NRX/VCtrl. Tissue replicates are indicated by same colour circles. Differences are assessed by ANOVA with oxygen tension and loading as fixed factors and donor as random factor with replicate means. B) Pool validations. Equal RNA masses from replicates was pooled and then reverse transcribed alongside the individual replicates for analysis from one donor (M/30y). C) Correlations of fold changes from RNAseq and qRT-PCR. RNAseq data was generated using pooled RNA from 3-4 replicate tissues. This RNA underwent a purification procedure using RNeasy Minikits with DNA digestion (Qiagen). Associated qRT-PCR data points are from replicate means, always of 3 replicates as in A). qRT-PCR data was generated using RNA that had not yet undergone purification. M: male. y: years. NRX: normoxia, 20% O_2. HYP: hypoxia, 3% O_2. VCtrl: vehicle control. SC: static compression. DC: dynamic compression. FC: fold change. *: p<0.05, **: p<0.01, ***: p<0.001.

163

Chapter 8

Mechano-Hypoxia Conditioning of Engineered Human Meniscus

Contributing authors:

Alexander R.A. Szojka, David (Xinzheyang) Li, Malou E.J. Sopcak, Hilda (Zhiyao) Ma, Melanie Kunze, Aillette Mulet-Sierra, Samer M. Adeeb, Lindsey Westover, Nadr M. Jomha, Adetola B. Adesida

8.1   Preface

This study extends the results of Chapter 7 to longer time periods and different types of mechanical loading. It also provides more concrete evidence for experimental parameters used in Chapter 7 which were previously based on literature in other culture models or limited data: the duration of loading (5 minutes), pre-culture

period (6 weeks), and static strain offset (30%).

This work is much to the credit of David Li, an undergraduate summer student whose enthusiasm was the specific impetus for investigating many variables in its constituent experiments. In between Chapter 7 and this work, I carried out a large investigation using the hybrid force and displacement control dynamic compression regime described in this chapter. This investigation manipulated the strain (2, 5, 10%), the number of cycles (100, 200, 600), and the number of loading days per week (1, 2, and 5). The results of this work were not particularly promising and I shelved the work to complete at a later date. The hybrid dynamic compression regime was the direct suggestion of Dr Samer Adeeb, who upon hearing me debate the pros and cons of displacement and load control on their own, remarked, "can you not just use both displacement and load control?" To my knowledge, this idea of controlling the de-compression phase until a minimum force is reached is a unique solution to the problem of platen liftoff during dynamic compression in the tissue engineering field.

David Li presented the project at the following conferences: i) 2020 Summer Students' Research Day, Faculty of Medicine and Dentistry, University of Alberta; ii) Eureka Undergraduate Research Symposium, University of Alberta. David Li was awarded second place in the 2020 Eureka Cover Photo Contest at the University of Alberta using tissues generated in this study. I also presented this project at the following conferences: i) 2021 Annual Meeting of the Canadian Biomaterials Society, University of Waterloo, virtual (Abstract Merit Award), and ii) 2021 Tom Williams Surgical Research Day, Department of Surgery, University of Alberta, virtual (2nd Place Oral Presentation, Basic Science).

8.2 Abstract

This article evaluates simultaneous mechanical loading and hypoxia (mechano-hypoxia conditioning) as a strategy for human meniscus tissue engineering. Meniscus fibro-chondrocytes were pre-cultured on type I collagen scaffolds 3 or 6 weeks with TGF-β3

supplementation before treatment with dynamic compression (DC) or cyclic hydrostatic pressure (CHP) under hypoxia (3% O_2). DC was more effective in modulating gene expression than CHP after 5 days. Mechano-hypoxia conditioning (5 days) promoted hyaline cartilage-related mRNA precursors (e.g., 9.8-fold *COL2A1*, 3.8-fold *SOX9*) in an additive manner. There were diminishing returns for DC loading periods longer than 5 minutes. Higher DC strains increased the mRNA response but results for increased pre-culture time were inconclusive. Long-term mechano-hypoxia conditioning (21 days, DC) supported 3 to 4-fold gains in the dynamic compression modulus compared to baseline with a 10-fold suppression in hypertrophic marker *COL10A1* vs. controls. Mechano-hypoxia conditioning is promising for tissue engineering inner meniscus and likely also hyaline cartilage; however, optimization during longer courses of loading is essential.

8.3   Introduction

The menisci are a pair of knee joint structures that increase surface area for load transmission to protect the articular cartilage from excessive stress. They possess a functional extracellular matrix (ECM) composed primarily of type I collagen that is organized into a complex architecture conferring tensile stiffness[23]. In the second decade of life, the weight-bearing inner meniscus regions develop a fibrocartilage phenotype[32, 33, 35]. In addition to type I collagen, fibrocartilage contains hyaline cartilage-type matrix components type II collagen and aggrecan that provide compression stiffness[15, 131]. Meniscus ECM is synthesized and maintained by a heterogeneous population of cells known collectively as meniscus fibrochondrocytes (MFCs)[22]. During development and early childhood, the menisci are vascularized[28, 33, 34, 36]. However, as the fibrocartilage phenotype develops, the inner meniscus regions lose their vascular supply and become susceptible to non-healing injuries[28, 33–35]. These injuries disrupt normal function and cause painful symptoms that can be treated through partial meniscectomy. Non-healing meniscus injuries,

treated or untreated by partial meniscectomy, are associated with an increased risk of osteoarthritis development[17]. This article presents four experiments aimed at providing a better understanding of how MFCs regulate their matrix-forming phenotype and how this can be used towards developing better treatments for inner meniscus injuries (Table 8.1).

Table 8.1: Experiment summary. Experiments I & II were performed in parallel followed by experiments III & IV.

Experiment #	Description
I	Gene expression transcriptome after 5 days of hypoxia and mechanical loading. Part I: Mechanical loading type comparison and selection for RNAseq. Part II: 5-day hypoxia and mechanical loading transcriptome.
II	Dynamic compression in the viscous, fast relaxation vs. elastic, slow relaxation zones.
III	Dynamic compression regime aggression: strain and pre-culture effects.
IV	Long-term mechano-hypoxia conditioning for meniscus tissue engineering.

Connective tissues in general demonstrate the property of antifragility, meaning that they tend to gain from a certain range of stress and disorder[210]. Specifically, under physiological mechanical loading, they undergo growth and structural adaptations to maintain the organism's overall fitness in a changing environment[157, 210–212]. Ligament and tendon, which have some morphological similarity to the outer meniscus, express the fibrocartilage phenotype in wrap-around regions with bones as an adaptation to better withstand compressive load and shear[52, 157, 163]. A direct, "pure-tension" tendon grafted into a wrap-around region develops fibrocartilage at the bony articulation, whereas a fibrocartilaginous wrap-around tendon grafted to a pure-tension region loses the fibrocartilage phenotype[157]. These examples suggest that the fibrocartilage phenotype that develops in human meniscus could reflect an antifragile response of the tissue and its resident MFCs.

167

In vitro tissue engineering model systems provide the means to directly test experimentally how human cells regulate matrix synthesis in response to signals such as mechanical loading and hypoxia within a native tissue-like environment. They consist of a cell source seeded on a biomaterial with appropriate growth signals. Hypoxic *in vitro* culture can promote expression of the hyaline cartilage type phenotype in a wide variety of tissue engineering model systems using mesenchymal cell sources, including MFCs[55, 134, 178]. We recently showed that mechanical loading can also directly induce expression of *SOX9*, the main regulator of hyaline cartilage-type matrix, independently of oxygen tension in an *in vitro* model of the human meniscus[5]. This could account for the gradual development of a fibrocartilage phenotype in the weight-bearing inner meniscus regions. However, this was only after a 1-day treatment with a single mechanical loading regime (24h of hypoxia and 5 minutes of dynamic compression (DC) from 30-40% strain, 1 Hz), and the effect size for loading was much smaller than for hypoxia. In experiment I here, we thus had the objective to evaluate the transcriptome-wide effects of hypoxia combined with a repeated, longer term mechanical loading treatment. Before progressing to the transcriptome-wide response, we tested two types of DC regimes and cyclic hydrostatic pressure (CHP), which can mimic the fluid pressurization that occurs in the native meniscus during weight-bearing[65, 66].

Meniscus tissue engineering can also be used towards generation of replacement tissue constructs, making use of knowledge gained in model system experiments. Theoretically, the constructs can be designed and conditioned in vitro until they appropriately mimic native healthy meniscus properties so that, upon implantation, they slow osteoarthritis development compared to untreated damaged meniscus[213].

Mechanical loading-based conditioning strategies for engineered tissues aim to exploit their antifragile property. There exists a set of mechanical loading conditions that induce a beneficial adaptive response, stimulating functional gains in matrix properties over time such that the tissues are better prepared for a future loading

168

incident[63, 64, 74, 195]. This occurs at the physical level in part through arrangement of newly synthesized matrix molecules facilitated by dynamic strain, and at the cellular level, for example through changes in molecular mRNA expression of genes triggered through various means of mechanotransduction[214–216].

It is difficult to predict whether a loading regime will induce an antifragile growth response, have no effects, or be detrimental to tissue properties[63]. Several parameters need to be pre-determined for an engineered tissue model, including the static strain or stress offset, the dynamic strain or stress amplitude, the loading duration, and the loading frequency[74]. Further, the degree of matrix formation or maturity prior to application of DC can affect the response to the loading regime[185]. To achieve continued growth, it may even be necessary to adjust these parameters values as the tissue adapts to the repeated stimuli[217]. Optimizing these parameters is time-consuming because loading periods often extend for hours per day, limiting how many groups can be feasibly investigated[63]. Thus, in experiments II and III here we sought to gain a better understanding of how loading parameters affected the magnitude of the gene expression response in our engineered meniscus tissue model.

Engineered meniscus and cartilaginous tissues in general undergo stress relaxation during strain-controlled DC (Figure S8.1). The loading period can be divided into a viscous, fast-relaxation loading zone and an elastic, slow-relaxation loading zone. The viscous relaxation phenomenon is attributed to exudation of free fluid from the tissues' extracellular matrix, whereas the elastic response is due to repeated pressurization of fluid entrapped by proteoglycans such as aggrecan and tensile loading of matrix(40). We became interested in the relative contributions of the viscous, fast-relaxation and the elastic, slow-relaxation zones to the mRNA level response of MFCs exposed to DC. This knowledge could facilitate generation of mechanically conditioned tissues using DC by reducing the necessary loading time.

From our previous experiences, we knew that the viscous, fast relaxation zone was restricted to approximately the first 5 minutes of loading in our engineered human

169

meniscus model (Figure S8.1). This observation has also been noted by other research groups in meniscus tissue engineering[71]. Thus, in experiment II we compared gene expression after 5 and 60 minutes of DC with a control group loaded for 5 minutes and rested for 55 minutes. We hypothesized that any differences in gene expression between 5- and 60-minute groups would be attributable to the 55 minute difference in measurement time rather than beneficial effects of continued dynamic cycling. We also investigated serial short (5 minute) loading and rest periods for a total duration of 60 minutes to explore potential effects of repeated viscous, fast-relaxation zone loading. Based on these results, in experiment III we investigated how the aggressiveness of a DC loading regime affected the magnitude of the gene expression response. Specifically, we compared gene expression after DC from 10-20 vs 30-40% strain for pre-culture periods of 3 and 6 weeks. We hypothesized that more aggressive loading, i.e., loading using higher strain levels and longer pre-culture periods, would have larger fold increase in mechano-sensitive gene expression compared to static controls.

The primary outcomes of experiments I-III were gene expression. In experiment IV, we brought together the results of the first experiments to investigate protein and mechanical outcomes under long-term mechano-hypoxia conditioning. We used a large commercial bioreactor to load tissues automatically four times a day for three weeks, which was practical in comparison to the small custom bioreactor in experiments I-III which needed to be set up manually for each loading event. We hypothesized that this "mechano-hypoxia" conditioning would induce an antifragile growth response, leading to increased mechanical properties and matrix outcomes compared to static oxygen tension controls.

8.4 Materials and methods

Most methods were performed as previously described[5, 8]. The outlines of the four experiments are presented in Figure 8.1. Raw data for each experiment is provided in

Supporting Datasets 1-4 which will eventually be available with the published online version of this manuscript.
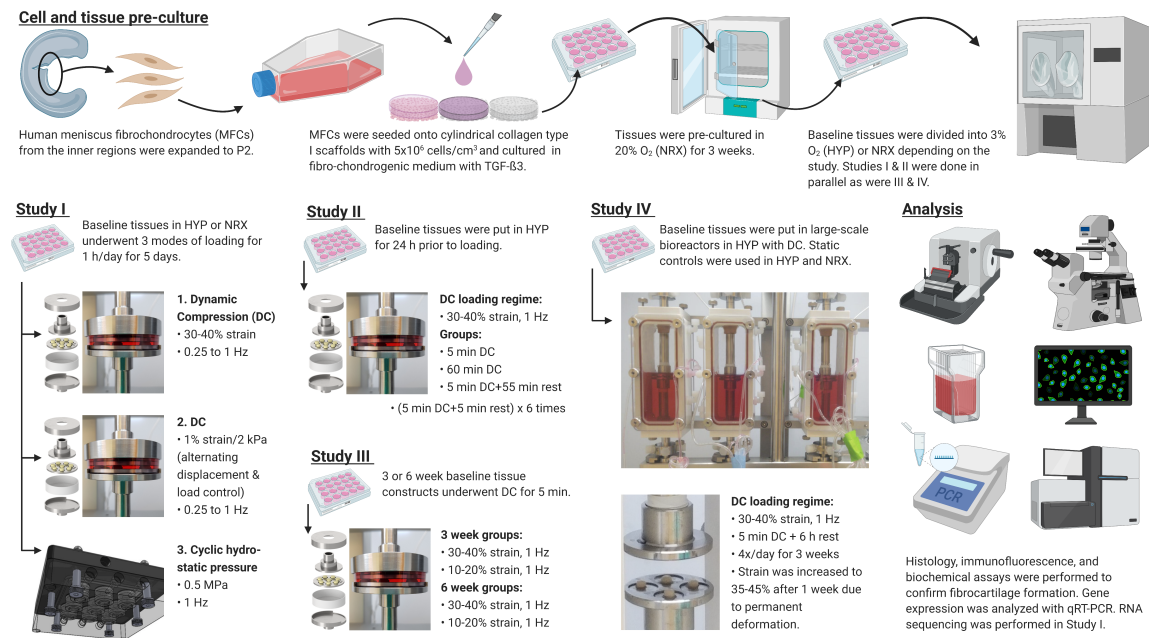
Figure 8.1: Experiment outlines. Created with Biorender.com (2021).

8.4.1 Ethics statement and sample collection

Human inner meniscus tissues from six donors were collected during arthroscopic partial meniscectomies in accordance with the University of Alberta Research Ethics Board's approval #Pro00018778. Donor details and how they were allocated to the different experiments are summarized in Table S8.1.

8.4.2 Cell and tissue pre-culture

Meniscus fibrochondrocytes (MFCs) were isolated by mincing, type II collagenase digestion, and recovery for 48h in monolayer as previously described[8]. Cells were expanded with combined 1 ng/mL TGF-β1 and 5 ng/mL FGF-2 until confluence in passage 1 (3.3±0.4 population doublings (mean ± standard deviation)) and stored in liquid nitrogen until needed. Cells were resuscitated and further expanded until confluence in passage 2 (6.5±0.9 total population doublings). Experiments I & II

were done in parallel using cells from 3 donors, while experiments III and IV were done in parallel with another 3 donors.

The cells were seeded onto type I collagen scaffolds (diameter=6 mm, height=3.5 mm, pore size=115±20 µm, Integra LifeSciences, NJ, USA). A pilot comparison of densities 5 and 30×10^6 cells/cm^3 found the former was more appropriate and was used for the remainder of the experiments (Supporting Document 1). Cell-seeded scaffolds were cultured in 24 well plates in a standard serum-free chondrogenic medium containing 10 ng/mL TGF-β3 in normoxia (NRX) incubators (95% air, 5% CO_2) for three weeks for initial matrix formation. Tissues at this point were considered baselines, i.e., raw material for experimentation, as they had not yet been divided into the experimental conditions. Tissues in the 24 well plates were placed on an orbital shaker in experiment I for the pre-culture period, but not in subsequent experiments because shaking tended to promote scaffold contraction without clear benefits related to the experiment objectives (Supporting Document 2).

8.4.3 Application of manipulated variables

All experiments had 3-week pre-culture periods in NRX for 3 weeks. Experiment III used both 3 & 6-week groups. Tissue replicates were randomly assigned into conditions in all experiments. Experiments I-III used a custom bioreactor[5], whereas experiment IV used a large-scale commercial bioreactor from the Biodynamic 5210 system (TA Instruments, USA). Apart from the pre-culture periods which took place in standard CO_2 incubators, all culture and loading took place within an X3 incubator system (Biospherix, USA). Strain values were computed using initial tissue heights based on a pre-load of 0.01 N/tissue. Stress values were computed using the tissue cross-sectional areas measured at the end of culture using ImageJ (NIH, v. 1.53e, USA). Initial/final dynamic moduli were computed as the peak to peak changes in stress in a single cycle at the start/end of the loading period divided by the change in strain (10%).

In experiment I, tissues experienced five days of continuous hypoxia (HYP, 3% O_2) or NRX and were subdivided for a 1h daily loading treatment: i) DC VCtrl, ii) DC 30-40%, iii) DC 1%/2 kPa, iv) CHP VCtrl, 5) CHP 0-0.5 MPa. For DC VCtrl, tissues were brought in near contact with the platens but without any compression. For DC 30-40%, tissues were compressed to 30% strain at 1% strain/s and then dynamically compressed up to 40% total strain, which previously induced a pro-fibrocartilage and matrix remodeling gene expression profile[5]. However, the loading frequency was modified to alternate cycle-to-cycle from 0.25 to 1 Hz to hedge against potential frequency dependence. DC 1%/2 kPa used a novel regime in which tissues were compressed by 1% strain (displacement control) and decompressed to a fixed stress of 2 kPa (load control) in each cycle. Preliminary work used 2% strain per cycle, but this led to excessive tissue compaction by the end of the loading period, and the de-compression target stress, 2 kPa, was the smallest that could be used without unstable noisy actuator motion. This loading regime ensured that the tissues were in contact with the platens for the entire loading period and that the tissues experienced a known deformation with each cycle, regardless of whether they fully bounced back during the decompression phase. For CHP groups, tissues were placed into a MechanoCulture TR system (CellScale, Canada) under the appropriate NRX or HYP atmosphere and sealed. CHP VCtrl had no pressurization, whereas CHP 0-0.5 MPa was cycled between 0 and 0.5 MPa at a fixed frequency of 1 Hz. The pressure was selected to max out the device capabilities with a fixed frequency of 1 Hz because the system did not allow programming to alternate frequencies as in DC groups. In all groups, tissues were harvested for gene expression and histological analyses 30 minutes after the final loading incident as before(27). There were 4 replicates for gene expression (RNAseq and qRT-PCR, 150 tissues total) and 1 for histological analysis (Safranin-O staining and types I/II collagen immunofluorescence) in all conditions for all donors. The gene expression response of tissues loaded for 1 vs. 5 days was assessed for 3 donors in NRX DC 1%/2 kPa (Figure S8.2).

In experiment II, all tissues were transferred into HYP for 24h on the day before applying the single loading event to measure the loading response under hypoxic conditions, though recent work showed the loading response did not vary significantly between oxygen tensions under similar conditions[5]. Based on experiences in experiment I, a fixed loading frequency of 1 Hz was used in experiments II-IV. The DC VCtrl group was treated as in experiment I. The dynamic compression (DC) groups were compressed to 30% strain at 1% strain/s and then dynamically compressed up to 40% strain at 1 Hz. In the "5c" (c=compression) and "60c" groups, samples respectively underwent 5 and 60 minutes of DC. In the "5c+55r" group (r=rest), samples underwent 5 minutes of DC and 55 minutes of rest held at 30% strain as a control for the time lag before harvest in 60c vs. 5c. In the "(5c+5r)x6" group, samples underwent 5 minutes of DC and 5 minutes of rest, repeated six times in a row (described previously as "cyclic rest")[218]. The groups 60c, 5c+55r, and (5c+5r)x6 were all "60 min" groups as they experienced some type of loading over the course of 60 minutes. All tissues were harvested for gene expression analysis 30 minutes after the end of the loading incident in each group. There were 4 replicates for gene expression in all conditions for all donors (60 tissues total).

In experiment III, tissues were assigned into 3- or 6-week pre-culture periods and 3 loading groups: static vehicle control, 10-20% strain, or 30-40% strain. Loading was applied for 5 minutes at 1 Hz in NRX. There were 2-3 replicates for gene expression in all groups (42 total) and 1 for histology. Donor 3 was not tested at the 6-week time point due to a shortage of cells.

In experiment IV, tissues were randomly assigned into 3 groups: NRX/static, HYP/static, and HYP/DC. Three donors were cultured and loaded simultaneously. Four tissue replicates in HYP/DC were placed between custom platens in large-scale bioreactors with 125 mL medium, while tissues in static culture were in 120 mL tubes with equivalent volumes of medium per tissue (2 tissues per tube, 2 tubes per condition per donor)[3]. Medium was circulated from the bioreactors into a hypoxic

incubator chamber for gas exchange. DC loading was applied four times a day from 30-40% strain at 1 Hz for 5 minutes per loading incident for three weeks. After 1 week, the strain levels were increased to 35-45% of the original sample heights for the rest of the loading period because the tissues had seemed to have undergone some permanent compaction. Tissues were harvested for gene expression, histology, or GAG/DNA analysis approximately 6 hours after the final loading period. This post-loading harvest time was increased in experiment IV compared to experiments I-III because dismantling the bioreactors took about 10 minutes each, and with three donors loaded simultaneously it would not have been possible to maintain 30 minutes with reasonable accuracy. The four tissue replicates in each condition were cut in half and then allocated to gene expression (3 halves/condition/donor), GAG/DNA (3 halves/condition/donor), or histology (2 halves/condition/donor). The half tissues in each analysis always came from a different replicate. Gene expression halves were placed into TRIzol and frozen at -80°C as fast as possible to minimize any gene expression changes unrelated to the treatments.

8.4.4 RNA extraction and qRT-PCR

RNA was isolated from each sample using standard techniques of chloroform phase separation and isopropanol precipitation (experiments I & II) or using PureSPIN MINI Spin Columns (Luna Nanotech, Canada) with a DNase I digestion step (experiments III & IV). For experiment I, a fixed mass of RNA based on concentration values (Nanodrop One, Thermo Scientific, USA) from each replicate was combined into a single pool to reduce nuisance inter-replicate variability for resource intensive RNA sequencing while preserving inter-condition and inter-donor variability[5]. The RNA pools were then purified using PuroSPIN MINI Spin Columns (Luna Nanotech, Canada) and sent for RNA sequencing at the University of British Columbia Biomedical Research Centre (UBC-BRC). RNA pools (experiment I) or RNA from individual samples (experiments II-IV) was reverse transcribed into cDNA and amplified by

quantitative real-time polymerase chain reaction (qRT-PCR) using the gene specific primers listed in Table S8.2.

Data was presented using the $2^{\Delta\Delta Ct}$t method(43). Statistical analysis was performed in SPSS 27 (IBM, USA) using ΔCt values. Analysis of variance (ANOVA) was performed with treatment groups as fixed factors and donor as a random factor followed by Tukey's post hoc test in experiments II-IV. No P value corrections were applied. The Shapiro-Wilk test was used to assess approximate normality. Wherever possible without loss of clarity, data were plotted donor-by-donor with colour and shape codes as indicated in Table S8.2. A supplementary data file will eventually be available with the published version of this manuscript.

8.4.5 Library preparation and next-generation sequencing

Based on the qRT-PCR results, only the DC 30-40% groups and their static controls in both oxygen tensions proceeded to more resource intensive RNA sequencing.

8.4.6 Bioinformatics

Next-generation sequencing was performed on the Illumina NextSeq 500 with 20 million paired end 42 bp x 42 bp reads and RNA sequencing data analysis was performed using Partek Flow software (Version 10.0.21.0302, Copyright 2021, Partek Inc., St. Louis, MO, USA). Alignment to the human genome hg38 was performed using STAR-2.7.3a and genes were quantified using the Partek E/M algorithm to an annotation model (hg38–RefSeq Transcripts 94; 2020-05-11). A noise reduction filter was applied, and gene counts were normalized using the Add: 1.0, TMM, and Log 2.0 methods. Differential expression analysis was conducted using analysis of variance (ANOVA) for oxygen tension and mechanical loading. Donor was included as a random factor. Significant differences in gene expression were assessed using a combination of minimum total gene counts, unadjusted p-values, adjusted p-values for false discovery rate (q-values), and minimum absolute fold-changes. Principal component analysis

(PCA), heatmaps, and visualization of differentially expressed genes (DEGs) were all conducted in Partek Flow software. MCL (Markov Cluster Algorithm) was used to cluster genes in the graph convolution network (GCN) by the structure of the node-edge graph.

8.4.7 Histology, immunofluorescence, and biochemistry

Tissues were fixed in formalin overnight at 4°C and then embedded in paraffin using standard methods. They were sectioned at 5 μm and put onto slides which were then stained for Safranin O, Fast Green, and Haematoxylin or else labelled with antibodies against human types I and II collagens as previously reported[8]. All histology/immunofluorescence images presented in results are from a single representative donor. Semi-quantitative analysis was performed in ImageJ.

For biochemistry, tissues were digested overnight in proteinase K as previously reported. GAG content was assessed using the dimethylmethylene blue (DMMB) assay with a chondroitin sulphate standard, and DNA by the CyQUANT Cell Proliferation Assay.

8.5 Results

8.5.1 Experiment I Part I: Mechanical loading type comparison and selection for RNAseq

At the end of the 3-week preculture period prior to treatments, the tissue phenotypes were fibrous with minimal staining for hyaline cartilage-type matrix components in all donors (Figure 8.2A).

The familiar strain and strain vs. time curves for DC 30-40% and CHP are presented in Figure 8.2B to highlight the features of the novel hybrid loading regime of DC 1%/2 kPa. There was creep up to about 40-45% in DC 1%/2 kPa in each 60-minute loading period due to maintenance of a minimum applied stress (Figure 8.2B). The peak stress in each cycle, reached during the 1% amplitude compression phases
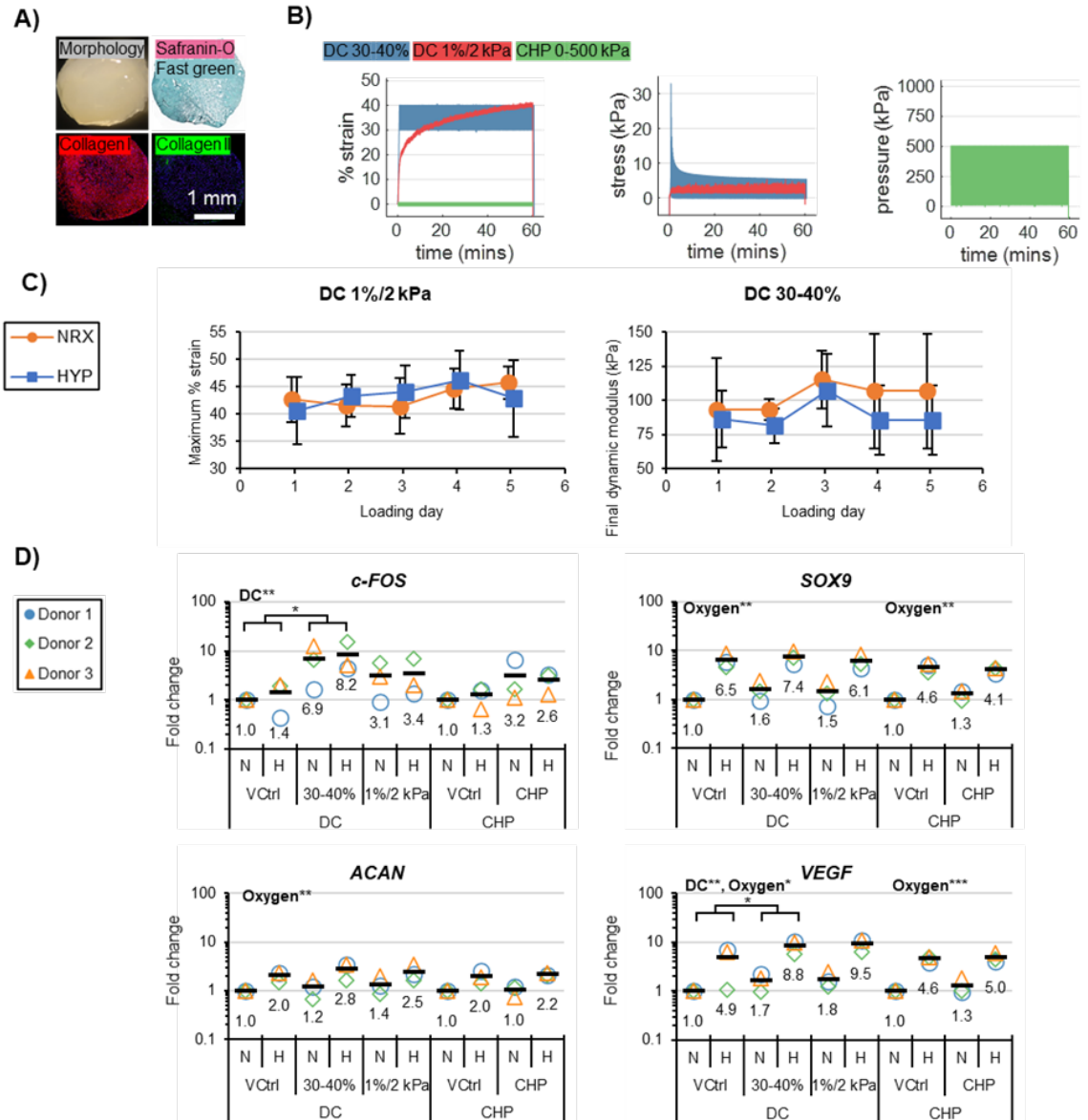
Figure 8.2: Experiment I: Comparison of mechanical and gene expression outcomes after 5 days of daily mechanical loading under HYP (H) or NRX (N). A) Representative tissue matrix phenotypes at the 3-week baseline. B) Representative stress and strain vs time curves in each loading group. C) Daily mechanical outcomes in each oxygen tension. D) Gene expression by qRT-PCR after the 5-day treatment. Values in DC and CHP are normalized to the N/VCtrl in each group. Two-way ANOVA was performed twice, once for DC and once for CHP groups. Significant factors are indicated at the top of each plot. *: $p < 0.05$, **: $p < 0.01$. NRX/N: normoxia. HYP/H: hypoxia. VCtrl: static vehicle control. DC: dynamic compression. CHP: Cyclic hydrostatic pressure.

of each cycle, also gradually increased due to strain stiffening. However, values remained smaller than the equilibrium peak stress values in DC 30-40%, indicating the 1%/2 kPa loading regime was less aggressive (Figure 8.2B).

Since the total strain was not fixed in DC 1%/2 kPa and the tissues are strain stiffening, the max % strain each day was used as the indicator for changes in mechanical competence in this group rather than the final dynamic modulus (Figure 8.2C). Across the 5 days, there were no changes in mechanical competency in DC 1%/2 kPa nor in DC 30-40% regardless of oxygen tension (Figure 8.2C).

There were no significant oxygen tension*mechanical loading interactions in gene expression by qRT-PCR. Significant loading effects were observed in DC 30-40% for *c-FOS* and *VEGF* (Figure 8.2D). The trends in gene regulation for DC 1%/2 kPa and CHP were not consistent between donors. *VEGF*, *SOX9*, and *ACAN* were respectively about 4.9-, 4.8-, and 2.1-fold upregulated in HYP compared to NRX. This indicated that the delayed 5-day hypoxia treatment promoted hyaline cartilage-type matrix expression in this culture model and to a greater extent than the 1-day delayed hypoxia treatment previously[5]. DC 30-40% proceeded to the more resource intensive RNA sequencing because of its superior performance relative to DC 1%/2 kPa and CHP.

8.5.2 Experiment I Part II: 5-day mechanical loading and hypoxia transcriptome

The first three principal components (PC) explained 63.5% of variability (Figure 8.3A). PCs 1 (26.0%), 2 (21.1%), and 3 (16.5%) showed clustering respectively for oxygen tension, DC, and donor, indicating consistency in the effect of each variable (Figure 8.3A).

The DC and hypoxia treatments each significantly regulated several thousand genes, even after filtering for q values < 0.05 and total counts to remove genes with low expression levels (Figure 8.3B). There were 692 genes with significant interac-

Figure 8.3: Experiment I: RNAseq outcomes from the 5-day DC 30-40% treatment in HYP and NRX. A) Left: The factors of oxygen tension, loading, and donor clustered on the first three principal components. Right: Heat maps (blue/red: down/up-regulation). B) Number of significant genes for each factor after sequential filters out of 12,491 total measured genes. Coregulated genes had both DC and hypoxia as significant factors. Interactions refer to the DC*HYP term.

tions between DC and hypoxia based on p values and counts > 250 but only 4 by the q values (Figure 8.3B). The interaction term p value distribution was right skewed rather than uniformly distributed, indicating that there were true interactions but insufficient detection power after adjustment for the false discovery rate (Figure 8.5A, left). We reasoned that a biologically relevant mechanical loading*oxygen tension interaction would affect groups of related genes and lead to similar regulation profiles. To test this, cluster analysis was performed on the 328 genes having with interaction term p values <0.01 for comparison to negative control lists of equal sizes constructed with the genes having the highest interaction p values (i.e., descending from p=1.00). Two clusters were identified from the p<0.01 gene list containing a significantly higher

percentage of genes than the top cluster in the negative control lists (Figure 8.4A, centre). Within the first cluster, genes tended to be downregulated by DC and the effect was more prominent in hypoxia, whereas in the second cluster genes tended to be upregulated by DC and the effect was more prominent in hypoxia (Figure 8.4A, right). The full cluster gene lists are provided in the S1 Dataset and the gene ontology for these clusters in Figure 8.4B. Of the four genes significant interaction q values, three appeared in cluster 1 (Figure S8.3).

DC had several GO terms related to negative- or down-regulation of biological processes (Figure 8.4C). The terms for the HYP gene list were more clearly linked to extracellular matrix synthesis than the gene lists for co-regulation and DC (Figure 8.4C). The fractions of genes related to each GO term also tended to be largest for HYP (Figure 8.4C). The top genes regulated by hypoxia, DC, and both (co-regulation) are presented in Figure 8.5A. Interestingly, the co-regulated gene list included upregulation of *SOX5* and *SOX6*, genes associated with chondrogenesis (Figure 8.5A, right).

To directly assess the effects of the hypoxia and DC treatments on expression of extracellular matrix genes, expression levels were compared for a panel of extracellular matrix genes based on GO terms. Hypoxia generally had larger effects on these genes than did DC (Figure 8.5B). DC combined with hypoxia led to a 10-fold increase in expression of type II collagen precursor gene *COL2A1* (Figure 8.5B). However, this did not correspond with differences in type II collagen protein between groups, and type I remained the more dominant collagen (Figure 8.5C). This indicates that the HYP/DC 30-40% treatment accelerated differentiation to a pro-hyaline cartilage-type matrix-forming phenotype, but insufficient time had passed for substantial related matrix accumulation.
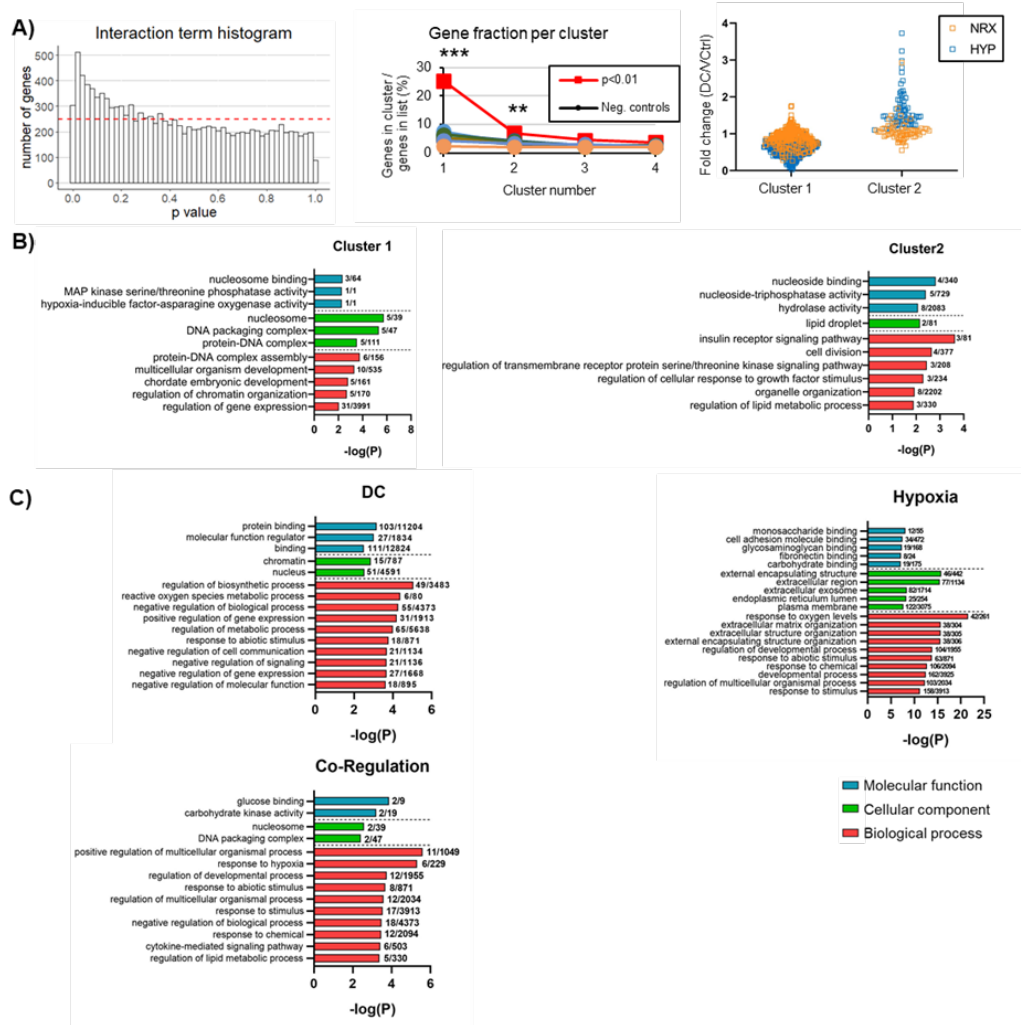
Figure 8.4: Experiment I: A) Oxygen tension and mechanical loading interaction analysis. Left: Interaction p value distribution amongst all 12,497 measured genes. The horizontal red line indicates the expected height of the bins had they been uniformly distributed. Centre: Cluster analysis performed on the 328 genes with interaction p<0.01 and on ten equally sized negative control lists with elevated p values (0.66<p<1.00). The gene percentages in clusters 1 & 2 in the p<0.01 group were compared to the negative control mean in cluster 1 by a two-tailed one sample t test. Right: Fold changes of DC/VCtrl by oxygen tension for the clusters constructed from the list with interaction p<0.01. B) Gene ontology for the top two interaction clusters (p<0.01). The fractions are the number of genes matching the GO term in the list divided by the total number of genes described by the GO term. C) Gene ontology for the individual treatments and co-regulation (q<0.05 and total count

>

250).
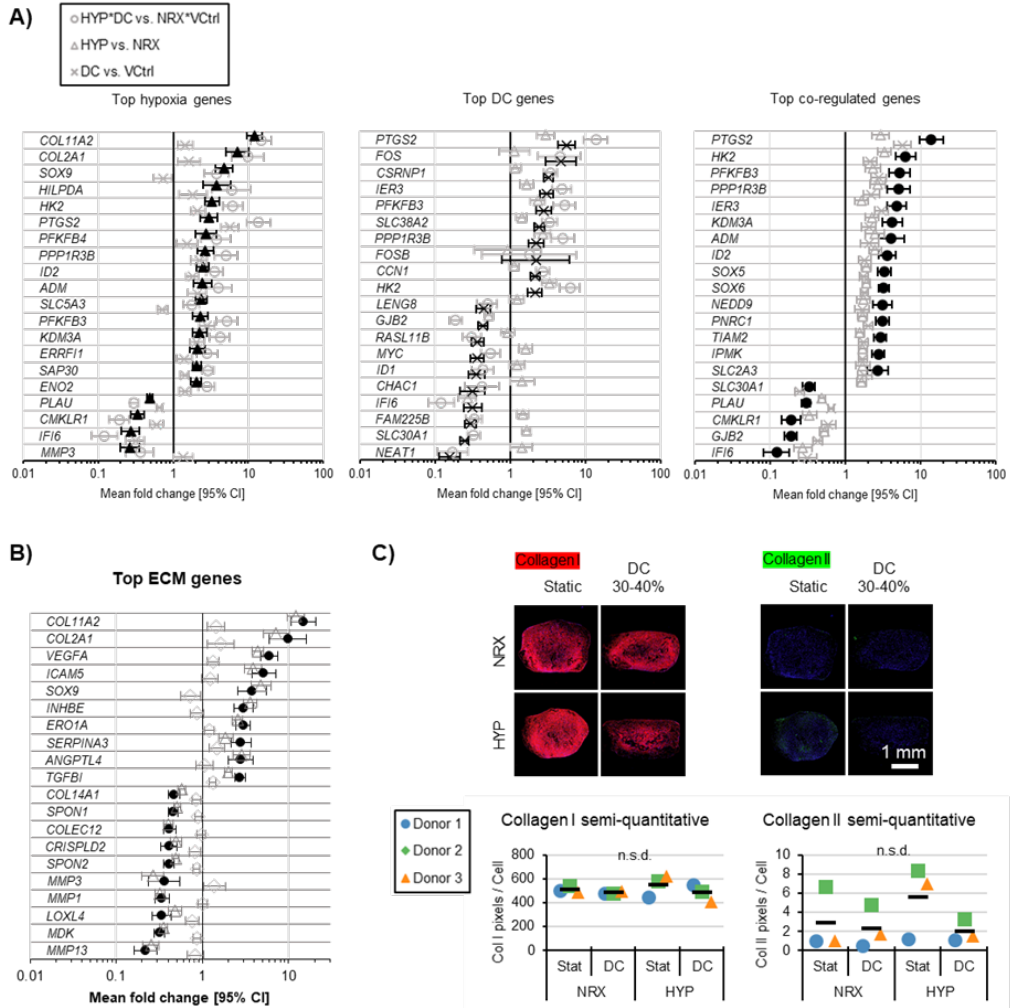
Figure 8.5: Experiment I: A) Significantly regulated (qleq0.05, total counts geq 250) genes with the largest absolute fold change by hypoxia, DC, or co-regulation (HYP/DC vs. NRX/VCtrl). The black shapes indicate the group used to generate the gene list. B) Top ECM-related genes by |FC| in HYP/DC vs. NRX/VCtrl (q<0.05, total counts > 250). C) Immunofluorescence of type I and II collagen protein after the loading treatment for a representative donor. Hardly any type II collagen was detected at this point for the donor shown. Semi-quantitative assessments show the mean ± standard deviation for 3 donors. N.s.d.: no significant differences.

8.5.3 Experiment II: dynamic compression in the viscous, fast relaxation vs. elastic, slow relaxation zones

Experiment II investigated gene expression outcomes after dynamic compression in the viscous, fast relaxation vs. the elastic, slow relaxation zones. The matrix phenotype of tissues at the time of loading were similar to experiment I (Figure 8.2A).

183

Representative strain and stress vs. time curves are presented in Figure S8.4. Based on the difference in peak stress between the first and last cycles in the DC 60-min group, relaxation reached 50, 90, and 95% completion after 14±4, 336±109, and 814±161 cycles. The viscous, fast-relaxation zone was thus approximately completed in about five minutes of loading.

Compared to the vehicle control, all loading groups had increased expression of *c-FOS* and inflammation gene *PTGS2* (Figure 8.6A). *c-FOS* was maximally expressed in 5c (17-fold upregulation), with no differences among the three 60-minute groups (Figure 8.6A). Expression of *c-FOS* thus rapidly increases upon initiation of loading and wanes shortly thereafter, regardless of whether loading continues or not. *PTGS2* showed a different time course of expression, continuing to increase beyond the 5c level (3.0-fold compared to the static vehicle control) to a similar level of about 4.5-fold in 60c and 5c+55r (Figure 8.6A). *NR4A1*, a nuclear transcription factor also related to inflammation, was upregulated only in the 60-minute groups and to a similar extent amongst them (Figure 8.6A). These results for *PTGS2* and *NR4A1* indicate that it is the initial loading period that induces the inflammatory response, with continued loading being less important given the similar expression levels in 60c and 5c+55r (Figure 8.6A). The repeat loading group, (5c+5r)x6, seemed similar to the other 60-minute groups in expression of these loading-sensitive and inflammatory genes (Figure 8.6A). Interestingly, the matricellular gene *CCN1*, which interacts with integrins and proteoglycans to perform a wide range of cellular functions, was most highly upregulated in 60c (Figure 8.6A). The master regulator of cartilage matrix formation, *SOX9*, was upregulated significantly in 5c, with weaker evidence for upregulation in 60c ($p<0.10$) (Figure 8.6A). *CNMD*, encoding the precursor to chondromodulin which is another regulator of cartilage matrix, was expressed at a low level and not differentially between groups. *VEGF*, encoding an important vascularization factor, had a small significant increase by DC in 5c only compared to the static vehicle control, and was significantly higher in 5c compared to 60c or 5c+55r (Figure 8.6A). There

were no significant differences in *MMP1* expression, while *ADAMTS1* was robustly induced by loading in the three 60 minute groups but not 5c, indicating delayed induction by DC regardless of loading duration (Figure 8.6A). There were no significant differences in expression of *ACAN* nor *COL1A1* (Figure S8.5). Taken together, these results indicate that it is DC loading in the viscous, fast-relaxation zone that is most important for inducing the gene expression response in this culture model.

To better understand why the early loading period was most important for inducing the mRNA response, the loading data in the 60c group was examined more closely. The slope of the stress-strain curve during the compression phase of a single cycle, i.e., the compression modulus, was halved after just 10 cycles and approached the equilibrium level within 300 cycles for all donors (Figure 8.6B). The stress began to fall to 0 kPa within the decompression phase of a single cycle after just 50 cycles for all donors (Figure 8.6B). This indicated that the tissues were coming out of contact with the platens because they were not rebounding fast enough for the 1 Hz sinusoidal DC frequency (Figure 8.6B). The strain level corresponding to re-establishment of contact during the compression phase of a single cycle steadily rose with continued cycling to a maximum of 35% for the three donors at the end of the 60-minute loading period (Figure 8.6B). This indicated that the effective strain amplitude, i.e., the actual strain amplitude experienced by the tissues while in contact with the platen based on the initial sample height, fell to about 5% by the end of the loading period (Figure 8.6B). Taken together with the decreased stress response over time, this helps explain why continued cycling beyond 5 minutes had limited marginal effects at the gene expression level.

8.5.4 Experiment III: Dynamic compression regime aggression

We next aimed to assess the effects of loading aggression on the short-term mRNA response. We had two hypotheses: i) More aggressive loading would be achieved
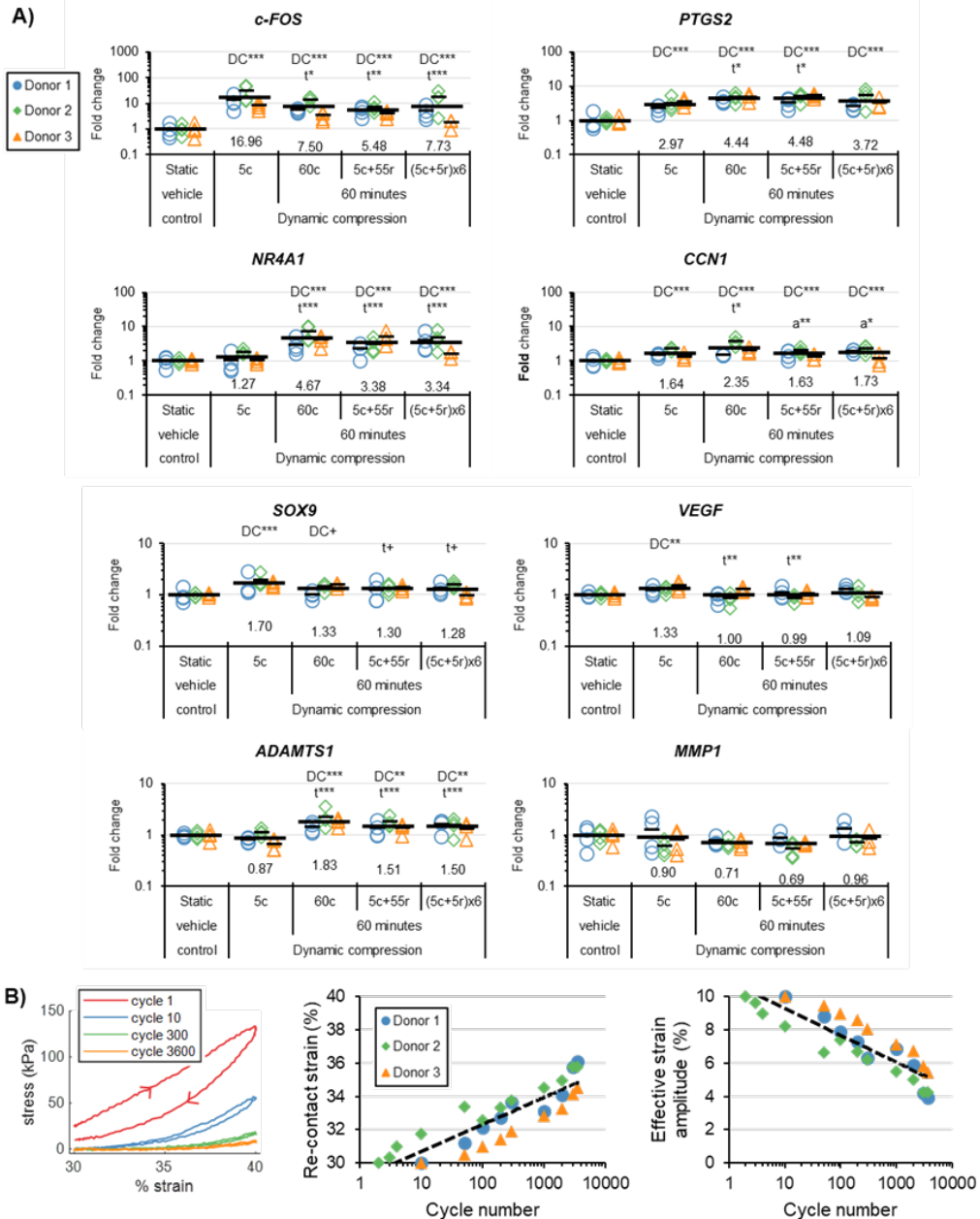
Figure 8.6: Experiment II: A) Gene expression measured 30 minutes after the end of treatment. "DC" indicates that a group is significantly different than the static vehicle control. "t" indicates that a DC group is significantly different than 5c. "a" indicates that a 60-minute group is significantly different than 60c. ***: $p<0.001$, **: $p<0.01$, *: $p<0.05$, +: $p<0.10$. B) Loading cycle analysis for the "60c" group (30-40% strain at 1 Hz for 60 minutes). The arrowheads show the direction of onloading and offloading. The re-contact strains were defined as the points within the compression phase when the force rose above 0 N, indicating contact. The effective strain amplitudes are calculated as 40% minus the strain at the re-contact points.

by using higher strain offsets and longer pre-culture periods due to more matrix compaction and more total matrix accumulation, respectively; ii) the higher strain offsets and longer pre-culture periods would induce larger fold increases in mechano-sensitive genes compared to the static vehicle control (VCtrl) for each preculture duration.

Initial and final dynamic moduli were consistently higher for increased strain levels, confirming that increased strain indeed led to more aggressive loading (Figure 8.7AB). The expected trend of increased dynamic moduli with increased pre-culture time was not always observed: donor 3 showed the reverse trend for initial dynamic modulus in DC 30-40% but the expected trends were observed in final dynamic modulus (Figure 8.7B). This inconsistency in initial dynamic modulus may have reflected settling of constructs during the initial loading period or inter-replicate variations in construct height. There was much more matrix staining positively for sulphated proteoglycans in 6-week groups for all 3 donors (Figure 8.7C).

Higher strains increased *c-FOS*, *SOX9*, and *PTGS2* expression regardless of pre-culture duration (Figure 8.7D). There was inter-donor variability in the gene expression response to DC 10-20% but expression levels generally fell between VCtrl and DC 30-40%, indicating a dose response to increased strain (Figure 8.7D). The effects of longer pre-culture durations were not consistent for the two available donors: donor 1 had larger fold increases in gene expression in 3 weeks compared to 6 weeks, whereas donor 3 showed the opposite trend (Figure 8.7D).

8.5.5 Experiment IV: Long-term mechano-hypoxia conditioning for meniscus tissue engineering

The initial and final dynamic moduli increased in a generally sigmoidal shape over the 3-week mechano-hypoxia conditioning period (Figure 8.8A). There was a jump in initial and final dynamic moduli after the strain offset was increased from 30 to 35% after 1 week due to strain stiffening, but the general trend continued (Figure 8.8A).
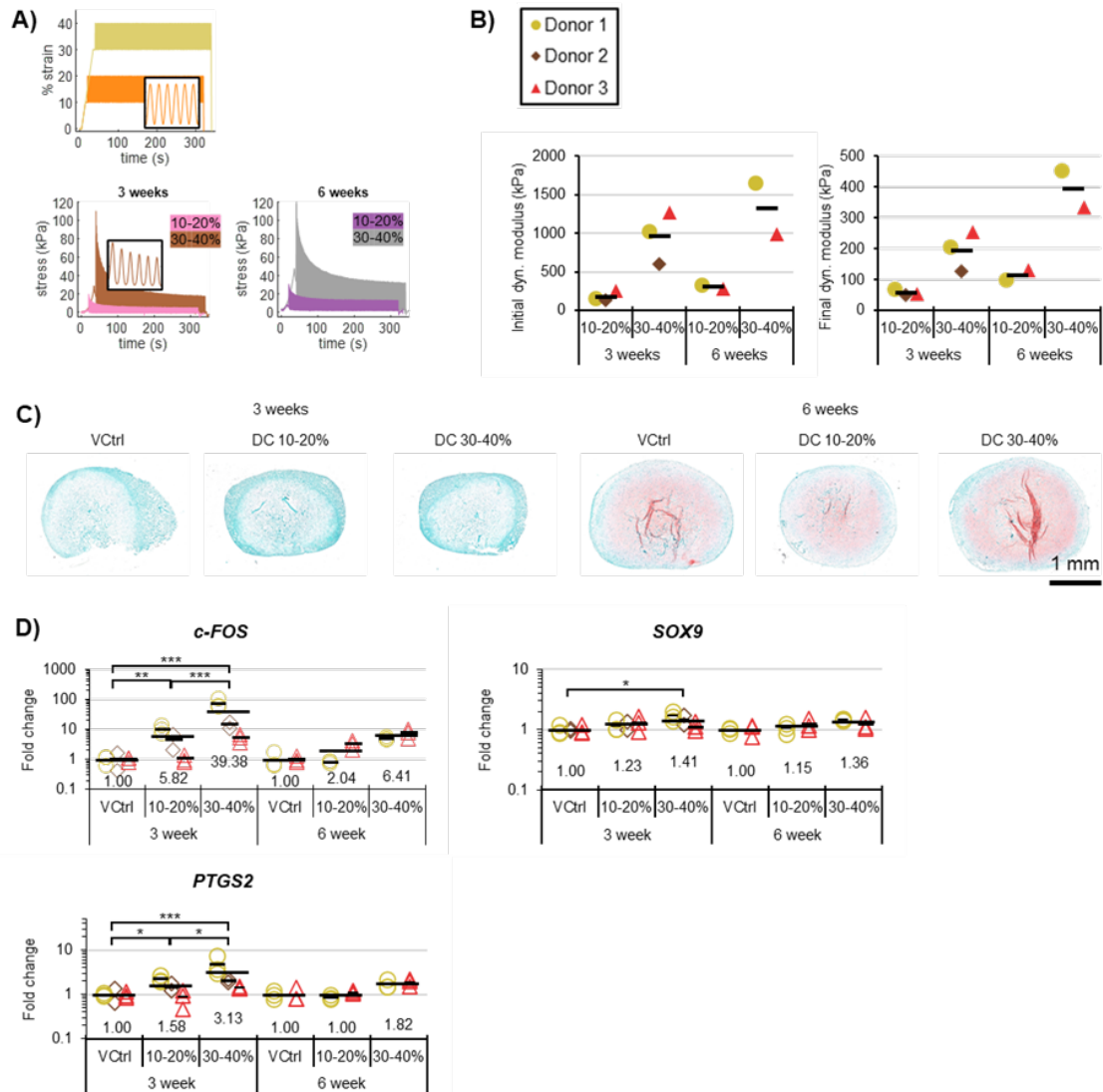
Figure 8.7: Experiment III: Loading aggression analysis. A) Representative strain and stress vs. time curves. B) Mechanical analysis. C) Representative safranin-O staining after loading at each time point. D) Gene expression post-loading by qRT-PCR. Values are normalized to the VCtrl group within each time point. Analysis of variance was restricted to 3-week groups because only two donors were available at 6 weeks. *: p<0.05, **: p<0.01, ***: p<0.001.

To compute the fold increase in each modulus without the contribution of increased strain, we took the product of the fold increases before (days 1-7) and after (day 8 onwards) the change in applied strain. Computed this way, the fold increase in initial and final dynamic moduli during loading ranged from 1.7 to 3.1-fold and 1.8 to 5.1-fold, respectively. Interestingly, the donor with the lowest dynamic mechanical

properties at the beginning of the culture period had the highest properties by the end and had a steep growth trajectory at the time of harvest. This suggests that mechano-hypoxia conditioning had consistently beneficial mechanical outcomes, but that the magnitude of the response varied widely between donors.
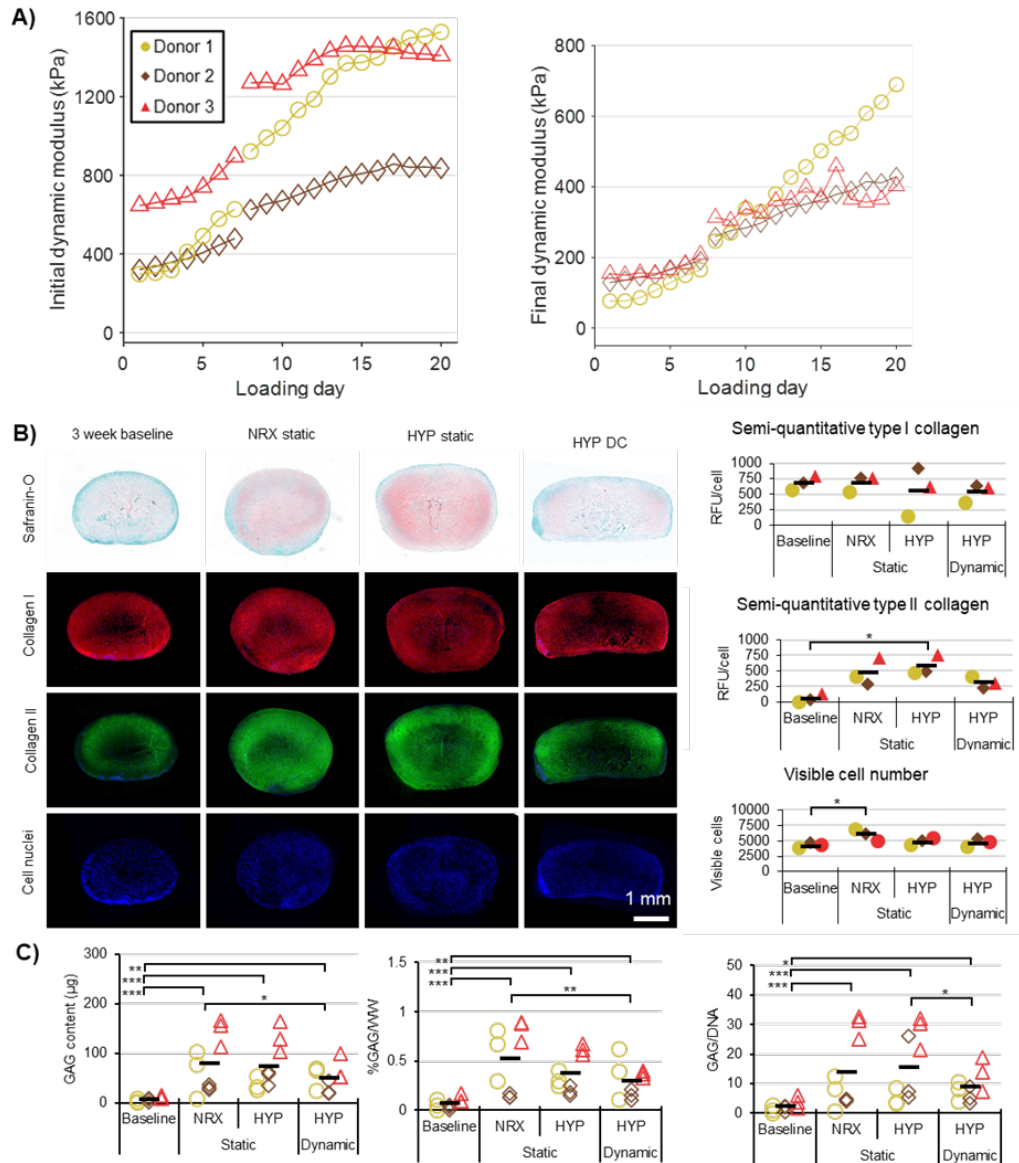
Figure 8.8: Experiment IV: Outcomes from long-term mechano-hypoxia conditioning. A) Mechanical performance over time for each donor. The strain offset was increased from 30-35% before loading on day 8, resulting in a jump in properties. For clarity, only 1 of 4 loading events is presented per day. B) Representative tissue matrix phenotypes. C) Biochemistry. GAG: glycosaminoglycans. WW: wet weight. *: $p<0.05$, **: $p<0.01$, ***: $p<0.001$.

Tissues in HYP/DC showed deformation histologically due to contact with the loading platens (Figure 8.8B). There was the most type II collagen fluorescence in HYP/stat and the least in HYP/DC apart from the 3-week baseline, with a similar trend for Safranin-O staining (Figure 8.8B). A core region with reduced staining had already developed by the 3-week baseline for all donors and it persisted for the entire 6-week culture period regardless of condition (Figure 8.8B). All groups had increased GAG outcomes compared to the baselines after the additional 3 weeks of culture (Figure 8.8C). These were generally superior for the static groups relative to HYP/dynamic (Figure 8.8C). This indicates that the mechanical loading treatment was affecting accumulation of matrix markers compared to static culture, perhaps through loss to the culture medium or changes in gene expression.

c-FOS did not have a significant increase in DC group, likely due to the 6h delay in harvest after the final loading event (Figure 8.9). *SOX9* was increased by both HYP and DC, but the magnitude of the increase in HYP (1.4-fold) was lower than it had been in the 5-day experiment (4.8-fold) (Figure 8.9). *VEGF* was increased in both HYP groups compared to NRX without a significant DC effect (Figure 8.9). *COL2A1*, *COL1A2*, and *ACAN* all showed a similar trend between groups with the most expression in HYP/stat and the least in HYP/DC, although it was not always significant (Figure 8.9). Both HYP and DC reduced *COL10A1* expression, combining for a 9-fold decrease in HYP/DC compared to NRX/static (Figure 8.9). HYP/stat had elevated *MMP3* but not *MMP13* compared to NRX/stat, which was surprising because they were both suppressed by HYP in the 5-day experiment (Figure 8.9 & Figure 8.5). HYP/DC had reduced expression of both, which may have helped to protect the matrix from degradation (Figure 8.9). This indicates that although mechano-hypoxia conditioning led to increased *SOX9* expression, expression of specific matrix markers was disrupted compared to static controls and especially hypertrophic matrix marker *COL10A1*.
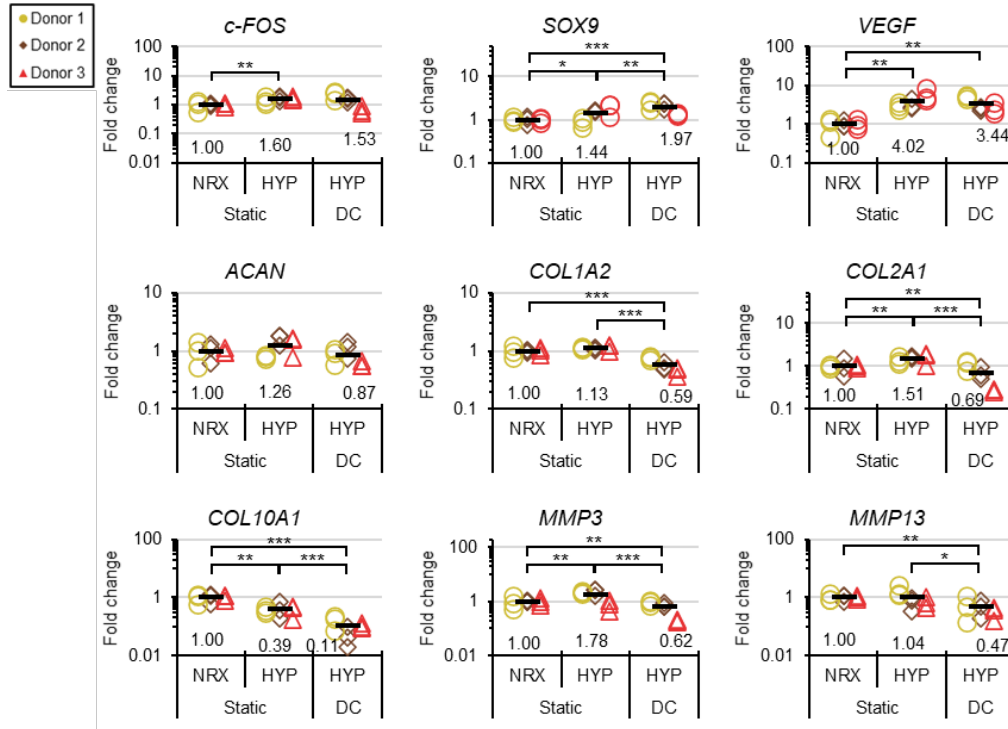
Figure 8.9: Experiment IV: Gene expression by qRT-PCR after the 3-week mechano-hypoxia treatment. *: p<0.05, **: p<0.01, ***: p<0.001.

8.6 Discussion

This article details four experiments aimed at understanding how meniscus cells respond to simultaneous mechanical loading and hypoxia and developing the use of "mechano-hypoxia conditioning" as a strategy for tissue engineering the inner meniscus. In all experiments, tissues were pre-cultured in NRX at least 3 weeks prior to any treatment in HYP.

In experiment I, we first found that the DC 30-40% regime induced a larger mechano-transduction response compared to DC 1%/2 kPa and 0-0.5 CHP. The hybrid alternating displacement-load control DC regime was a novel invention to take advantage of aspects of both displacement and load controlled platen movement. In pure displacement control, the platens are at risk of coming out of contact with tissues during the decompression phase, as was demonstrated in experiment II. In pure load control, the tissues may not undergo adequate deformation during compression

191

phases due to strain stiffening in the later stages of loading. The hybrid loading regime allowed us to be sure that the tissues remained in contact during decompression phases, and that they underwent the same deformation every compression phase. The combination of 1% strain and 2 kPa load turned out to be much less aggressive than the DC 30-40% regime based on stresses and the gene expression response even though the total accumulated strain by the end of the loading periods were similar. A different outcome may have been obtained had the strain amplitude been larger, for example 1.25 or 1.50%, though the challenge is ensuring the total accumulated strain does not become excessive and detrimental due to creep. This could be controlled in a future experiment by cutting off the loading period upon crossing a maximum strain threshold. Although this would cause the loading duration to be variable rather than fixed, the outcomes of experiments II & III indicate that the loading duration may be a less important parameter than strain after several minutes due to diminishing returns from the perspective of induction of a gene expression response. The previously published results of CHP up to 4 or 5 MPa in human meniscus cells in alginate beads and cell aggregates demonstrated that it can promote hyaline cartilage-type matrix expression with matrix-protective effects[65, 66]. These were not consistently replicated here, indicating that higher pressures than those produced by the configuration of our device are likely necessary to observe robust beneficial effects[219].

There were many more regulated genes detected by RNA seq in the five-day hypoxia-DC 30-40% 1 h/daily treatment than observed in our previous work that had a similar but shorter 1-day HYP and 5 min DC treatment[5]. Most genes were regulated independently, i.e., by only one of the treatments. HYP most clearly up-regulated fibrocartilage matrix-related genes, whereas DC regulated genes tended to be nucleus and inflammation related. A smaller set of genes was co-regulated by treatments, i.e., with significant effects for both hypoxia and DC. This led to large, combined fold changes when the effects were in the same direction. This was the case for hyaline cartilage-type matrix markers *COL2A1* (HYP: 7.2-fold, DC: 1.6-fold, com-

bined: 9.8-fold) and *ACAN* (HYP: combined: HYP: 1.9-fold, DC: 1.4-fold, combined: 2.7-fold), although the treatment duration was too short to observe increased type II collagen at the protein level. Indeed, the tissues were fibrous at this point with low expression of hyaline cartilage-type matrix markers and in this respect more closely resembled immature inner meniscus. There were far fewer genes with interactions, i.e., genes whose regulation by one variable depended on the level of the other variable. Apart from the identified interaction clusters, this indicates that the response of MFCs to simultaneous hypoxia and mechanical loading was largely additive rather than synergistic in nature at the molecular level[144]. In a longer-term treatment, the unique gene profiles induced in each group could lead to divergence of tissue properties that affect the reception and response to hypoxia and loading signals; thus, more interactions would surely be identified with a long treatment duration spanning weeks. Overall, the gene expression results indicated that the combined HYP/DC regime accelerated differentiation of the MFCs towards hyaline cartilage-type matrix expression, which was primarily driven by the HYP treatment. This is consistent with the theory expounded in the introduction that the fibrocartilage phenotype in the human inner meniscus is an antifragile response to weight-bearing, especially if weight-bearing promotes vascular recession and development of a more hypoxic microenvironment.

In experiment II, our main finding was that DC loading in the viscous, fast-relaxation zone was most important for inducing the gene expression response, supporting our hypothesis. Previous researchers identified that DC systems reached a mechanical steady state within five minutes of loading, which is consistent with this outcome[73]. Although there were often differences in gene expression levels between 5c and 60c groups, these were usually the result of the 55-minute difference in time rather than 55-minute difference in loading as supported by the 5c+55r group. Genes following this trend were *c-FOS*, *PTGS2*, *NR4A1*, *VEGF*, *ADAMTS1* all significantly, with *SOX9*, *ACAN*, and *COL1A1* having similar but non-significant trends.

DC loading as applied here thus upregulates genes associated with the early response to stimuli, inflammation, vascularization, and likely also hyaline cartilage-type matrix expression, which is largely consistent with previous work[171, 220].

The one measured gene to break the trend was *CCN1*, with twice the fold induction in 60c as in 5c+55r compared to the static vehicle control. *CCN1* encodes an extracellular matrix regulatory protein that detects mechanical signals such as membrane perturbations[221, 222]. This occurred even though the stress response declined dramatically during continued loading, and the effective strain amplitude became smaller and smaller. Thus, continued cycling beyond 5 minutes did induce a marginal effect at the mRNA level but only in one measured gene, *CCN1*.

The (5c+5r)x6 "cyclic rest" group was included to investigate to what extent tissues would recover in 5 minute periods between loading incidents, and whether a larger response to 60c could be induced by repeated intermittent "viscous" zone loading. Although there was partial recovery of the viscous, fast relaxation loading zone, the peaks were not nearly as large as those generated in the initial period of loading. Further, the gene expression trends in this group did not differ sufficiently from the other 60-minute groups to identify any advantages to this strategy. Longer rest periods in between loading cycles, such as 30 minutes up to several hours (such as 6 hours as in experiment IV), may be more promising. Short bouts of loading separated by a recovery period have been shown to effect larger responses than continuous loading in a variety of connective tissues such as bone. Our results seem to complement what has been described as a fundamental rule in bone tissue: the adaptive loading response saturates quickly, causing diminishing returns in extended loading durations[223].

The gene expression pattern and the mechanical loading analysis suggest some likely mechanisms for the results observed in experiment II. Activation of integrin-mediated mechano-sensing are known to lead to upregulation of immediate early genes *CCN1*, *NR4A1*, and *AP-1* related transcription factors such as *c-FOS*, as well as the inflammatory response with induction of *PTGS2* (*COX2*) similar to our observations

in the human engineered meniscus culture model[171, 224]. The early upregulation of *SOX9* and *VEGF*, two hypoxia-inducible genes, suggests that DC possibly induced hypoxia inducible factor (HIF)-1 transcription factor complex activity, as has previously been observed in the case of mechanical loading and overload[32, 225]. Matrix strain can trigger release and activation of growth factors such as TGF-β sequestered in the matrix in latent form, allowing them to bind to cellular receptors[84]. This mechanism could also explain the observed DC-induced increase in *SOX9* expression). More generally, it explains aspects of the antifragile growth behaviour of connective tissues in response to loading, as stretched cells undertake matrix synthesis to increase local stiffness in anticipation of future loading events of equal or greater size[210].

The primary result of experiment II has an important implication for DC-enhanced tissue engineering. As described in the introduction, there are many parameters that need to be appropriately selected[74]. Mechanical loading experiments become labour intensive as a single loading event can last an hour or more[74, 195]. In an excellent literature review of DC loading in chondrocytes, the authors expressed dismay at the lack of standardization between studies and were less optimistic about the prospects of using DC as a tool for tissue engineering cartilage upon reviewing the literature[63]. If five minutes of DC is all that is needed to induce the bulk of gene expressional changes, then it is much more feasible to investigate and optimize the necessary parameters.

Experiment II had several limitations. First is that the results could have some scaffold-dependence. The porous type I collagen scaffold has trivial mechanical properties compared to cell-made matrix, serving only to provide a 3-dimensional environment for attachment and matrix deposition. This is different than hydrogels that contribute to the tissues' elastic mechanical properties, potentially leading to larger marginal benefits of continued dynamic compression[226]. In the collagen scaffold-based engineered tissues, the early viscous force response may be due to fluid being pushed out from the matrix and scaffold pores, leading to matrix compaction. Once the fluid has been forcefully exuded, the tissue resistance to DC is greatly diminished

within the same loading event. The fluid does not return fast enough in the time scale of a 1 Hz loading cycle, leading to plastic height reductions and a reduced effective strain amplitude. A larger dynamic strain amplitude such as 20% may have induced more marginal gene expression changes in the "elastic loading zone", perhaps through better recruitment of collagen fibres into a stretched configuration[226, 227]. However, given the height decreases implied by Figure 8.6B, this may require an even larger static strain offset. A second limitation is that we used a biased panel of genes. It is likely that genes besides *CCN1* were regulated differentially between the 60c and 5c+55r groups but were not measured. However, the rapid decay in the stress response and effective strain amplitude with continued cycling that we observed provides confidence that our main conclusion is nevertheless correct. A third limitation is that we did not assess kinetic changes between conditions in the time course of gene expression[171]. Finally, although we demonstrated that mRNA level changes in response to DC predominantly occur in response to the first few minutes of loading, this does not indicate that continued cycling has no effect at the physical level in, for example, orienting matrix by the applied strain field[226]. However, because of the small stresses and effective strain amplitudes in the late stages of the DC loading period, we expect there would have been similar diminishing returns of continued cycling at the physical level to those we observed at the mRNA level[223].

As expected in experiment III, more aggressive loading was achieved by higher strains. This in turn led to a larger mechanotransduction response assessed through *c-FOS*, *SOX9*, and *PTGS2* expression. We had also hypothesized the longer pre-culture duration to increase loading aggressiveness due to increased matrix accumulation with accompanying larger fold changes in gene expression. However, the results were inconsistent between the two donors. It is possible that inter-replicate variations in matrix distribution and a limited number of replicates and donors contributed to this outcome. An interesting possibility is that the more mature, proteoglycan-rich matrix in the 6 vs. 3-week preculture group could have helped to shield cells from the applied

deformation, which may have had a tendency to reduce the gene expression response despite a generally larger mechanical stress response to the same applied strain[228].

With the knowledge that HYP and DC promote hyaline cartilage-type matrix gene expression and that the viscous, fast-relaxation region is most important for inducing the gene expression response, we then investigated long-term mechano-hypoxia conditioning as a strategy for meniscus tissue engineering. We wanted to set up a system that required virtually no user input for the duration of the culture period. The tissues showed promising increases in mechanical properties during the loading period. Part of these reflected normal growth with culture time; however, it is unlikely that culture time alone would have led to the sigmoid-shaped growth curves. The increase in final dynamic modulus in experiment III, conducted in parallel from 3 to 6 weeks in purely static culture for the available donors compared to the mechano-hypoxia treatment (after adjustment for higher strain levels in the second two weeks) were 2.2 vs. 5.1-fold (donor 2) and 1.3 vs. 1.8-fold (donor 3). This suggests that there was indeed accelerated development of mechanical properties in experiment IV. However, within experiment IV the mechano-hypoxia conditioned tissues had inferior matrix staining compared to static controls. Part of the reason for inferior staining is that DC likely promoted GAG loss to the medium, although this does not clearly account for differences in staining for specific collagens. Further, although there was increased *SOX9* in HYP/DC compared to static HYP and NRX, there was decreased expression of matrix precursors *COL1A2*, *ACAN*, *COL2A1*, and especially *COL10A1*. Given that 6h had passed since the previous loading event when samples were harvested and expression of these genes after a loading event has been shown to return to baseline in 3-8h, these expression differences from controls were unlikely to be transient[171, 227]. DC groups were held in contact with the platens during rest periods to prevent them from floating away. The static controls thus had larger exposed surface areas than DC groups, which likely supported better matrix outcomes through increased nutrient transfer. In the other direction, suppression of *MMP3* and *13* in HYP/DC

would have helped protect the collagen matrix from degradation.

The mechanical property growth curves had a sigmoid shape, which could have been the product of several factors. DC loading clearly induced a pro-inflammatory gene expression profile in experiments I-III. This could have contributed to an adaptation period early on with the shallower rate of increase reflecting normal growth with culture time before the beneficial effects of loading could have translated into proteins with mechanically appreciable outcomes. In the late stages of culture, it is possible that agents such as TGF-β3 could have degraded resulting in a decreased rate of growth since the medium was not refreshed. This could partially explain why $SOX9$ was expressed highest in HYP/DC but downstream matrix genes such as $COL2A1$ were decreased[139]. It is noted, however, that the supplied initial medium volume in the bioreactors was 5x what is necessary to maintain constructs for the same duration in standard tissue culture plates. Further, the initial dynamic modulus measurement in bioreactors was increasingly underestimated in the late stages of culture. This is because as the tissues grew stiffer, the actuator control became poorly tuned and it at worst only attained 8.5% dynamic strain in the first loading cycles on the last loading day; a full 10% dynamic strain amplitude was eventually achieved after a few dozen cycles and onwards due to progression of the viscous, fast-relaxation period. As a result, the initial (peak) dynamic moduli in the late stages of culture were underestimated by at least 15% but likely closer to 50% due to strain stiffening and pressurization under dynamic load. Finally, it is possible that in the late stages of culture the tissues were becoming accustomed to loading in the operating strain range, thus slowing the antifragile growth response.

Donor 1, whose engineered tissues initially had the worst mechanical properties and matrix staining, underwent the steepest rate of increase in mechanical properties and maintained a better growth profile near the end of the loading period. The growth observed in donor 1 is also indicative that loading while the matrix is in a less mature state, i.e., after a shorter preculture period, may be beneficial. This also suggests

that a loading regime tailored to a donor's specific degree of matrix accumulation and growth behaviour would be an interesting avenue to explore. One method would be to control the actuator to a minimum stress as was done in the 1%/2 kPa regime from experiment I but only intermittently, e.g., every 100 cycles, rather than within every cycle to limit the total accumulated strain.

Although aspects of experiment IV were promising, specifically the development of mechanical properties and the suppression of hypertrophic matrix markers compared to static controls, experiment IV had additional limitations that were not discussed above. First, the static control groups were not vehicle controls; rather, they were free swelling in tubes with equivalent volumes of medium on a per tissue basis. It would have been ideal to have 0, 30, and 40% static compression controls within replicate bioreactors to account for the reduced exposed surface area in HYP/DC, but unfortunately the number of available bioreactors was limiting. This was less of an issue in experiments I-III as they used the small Petri-dish compatible DC bioreactor with 0% DC vehicle control groups. For the same reason, experiment IV had no NRX/DC group for comparison. Third, there was no assessment of DC effects on matrix organization. This could be a mechanism through which mechano-hypoxia conditioning led to increased mechanical properties beyond affecting ECM composition. An advantage of deformational loading such as DC is the possibility for physical rearrangement of matrix, which could plausibly lead to mechanical property development.

A future experiment would need to address these limitations. As well, a priority would be to address the matrix-poor core regions in the tissues, which had already appeared by the 3-week baseline. Possibilities include using a gentle DC regime to promote media supply to the inner regions or forced perfusion during the pre-culture phase[229, 230]. The tissues could likely also profit from longer loading events during the late stages of culture as tissue growth causes the duration of the viscous, fast-relaxation region to increase. Variation in the duration of rest periods between

loading events could also be an interesting parameter, such as 6h (as used here) up to 3 days. Finally, the suppression of hypertrophic markers in combined HYP/DC suggests mechano-hypoxia conditioning as applied here may have utility in suppressing the hypertrophic phenotype in engineered articular cartilage with mesenchymal stem cells.

The rise in mechanical properties in experiment IV suggests mechano-hypoxia conditioning could be employed towards building a functional meniscus. The timing of the treatment—especially its hypoxia aspect—could be delayed until an organized and appropriately mature matrix of collagen fibres was formed within a biomimetic meniscus shape, potentially using boundary conditions and cell contraction or polymer fibres with a compression or tension-loading component to guide fibre formation[1, 231, 232]. Then, mechano-hypoxia conditioning could be initiated to promote mechanical property development and fibrocartilage maturation in the inner regions, mimicking an aspect of human meniscus development.

8.7   Conclusion

The main conclusions of the four experiments are as follows. As applied here, an hour of daily dynamic compression (DC) from 30-40% at 0.25-1 Hz under hypoxia (HYP, 3% O_2) for five days induces large-scale gene regulation, promoting inflammation but also expression of hyaline cartilage type matrix markers in engineered human meniscus. DC in the viscous, fast-stress relaxation zone is most important for inducing a mechano-transduction gene expression response in MFCs in type I collagen scaffolds. The apparent beneficial effects of extended DC cycling periods are largely due to the time delay in harvesting compared to short loading periods. More aggressive DC loading, achieved through larger strain offsets, increases the magnitude of the mechanotransduction response at the gene expression level. Mechano-hypoxia conditioning as applied here, i.e., 5 minutes of DC from 30-40% strain at 1 Hz applied 4x/day for 3 weeks, supported mechanical property development and suppression of the hypertrophic phenotype. Applied appropriately, mechano-hypoxia conditioning could be

a useful tool for promoting development of mechanically competent fibrocartilage in tissue engineered meniscus.

8.8 Acknowledgements

8.9 Funding sources

8.10   Author contributions

AS, DL, SA, LW, AA: design and ideation. AS, DL, MS, HM, MK, AMS: Data collection. DL, HM: RNA seq analysis. AS: Writing and statistical analysis. NJ: Procurement of meniscus specimens. SA, LW, NJ, AA: Supervision. LW, AA: acquisition of research funding support. All authors contributed to data or manuscript review.

8.11   Supporting information
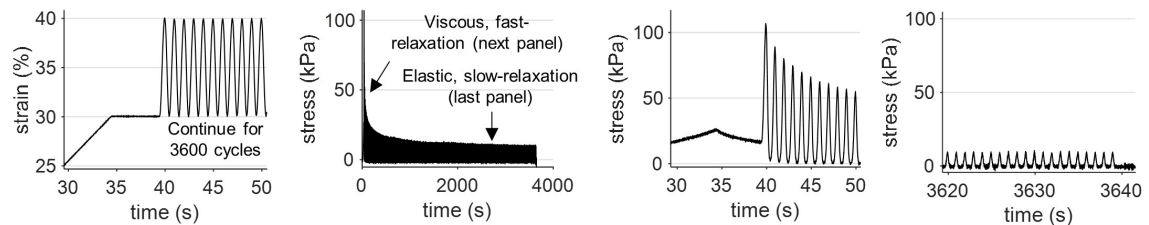
Figure S8.1: Typical loading curves from dynamic compression of type I collagen scaffold-based engineered meniscus tissues.

Table S8.1: Meniscus tissue donor details. Shape and colour refer to how donors are presented in quantitative data figures.

	Sex/age	**Population doublings**	**Shape**	**Colour**
Experiments I & II				
Donor 1	Male/21y	6.3	Circle	Blue
Donor 2	Male/22y	7.7	Diamond	Green
Donor 3	Female/45y	6.0	Triangle	Orange
Experiments III & IV				
Donor 1	Female/21y	7.2	Circle	Mustard
Donor 2	Female/25y	5.3	Diamond	Brown
Donor 3	Male/40y	6.5	Triangle	Red

Table S8.2: Gene-specific primer sequences used for quantitative real-time polymerase chain reaction.

Gene	Forward	Reverse	GenBank
ACAN	AGGGCGAGTG GAATGATGTT	GGTGGCTGTG CCCTTTTTAC	NM_001135.3
ADAMTS1	GCTCATCTGC CAAGCCAAAG	ATCTACAACC TTGGGCTGCA A	NM_006988.5
β-actin	AAGCCACCCC ACTTCTCTCT AA	AATGCTATCA CCTCCCCTGT GT	NM_001101.4
B2M	TGCTGTCTCC ATGTTTGATG TATCT	TCTCTGCTCC CCACCTCTAA GT	NM_004048.3
c-FOS	CGTCTCCAGT GCCAACTTCA	GGTCCGGACT GGTCGAGAT	NM_005252.4
CCN1	AAATCCCCCG AACCAGTCA	GGGCCGGTAT TTCTTCACAC T	NM_001554.5
COL1A1	CAGCCGCTTC ACCTACAGC	TTTTGTATTC AATCACTGTC TTGCC	NM_000088.4
COL1A2	GCTACCCAAC TTGCCTTCAT G	GCAGTGGTAG GTGATGTTCT GAGA	NM_000089.3
COL10A1	GAAGTTATAA TTTACACTGA GGGTTTCAAA	GAGGCACAGC TTAAAAGTTT TAAACA	NM_000493.3
COL2A1	CTGCAAAATA AAATCTCGGT GTTCT	GGGCATTTGA CTCACACCAG T	NM_001844.5
MMP1	ATGAGTCTTT GCCGGAGGAA	GTGACACCAG TGACTGCACA TG	NM_002421.4

Continued on next page

Gene	Forward	Reverse	GenBank
MMP13	CATCCAAAAA CGCCAGACAA	CGGAGACTGG TAATGGCATC A	NM_002427.4
MMP3	AGGCATCCAC ACCCTAGGTT T	ATCAGAAATG GCTGCATCGA T	NM_002422
NR4A1	AGCATTATGG TGTCCGCACA T	TGCACTGTGC GCTTGAAGA	NM_- 001202234.2
PTGS2	GAATCATTCA CCAGGCAAAT TG	TGCGGGTGGA ACATTCCTA	NM_000963.4
SOX9	CTTTGGTTTG TGTTCGTGTT TTG	AGAGAAAGAA AAAGGGAAAG GTAAGTTT	NM_000346.3
VEGF	GCACGGTCCC TCTTGGAA	CGGTGATTTA GCAGCAAGAA AA	NM_- 001025366.3
YWHAZ	TCTGTCTTGT CACCAACCAT TCTT	TCATGCGGCC TTTTTCCA	NM_003406.3
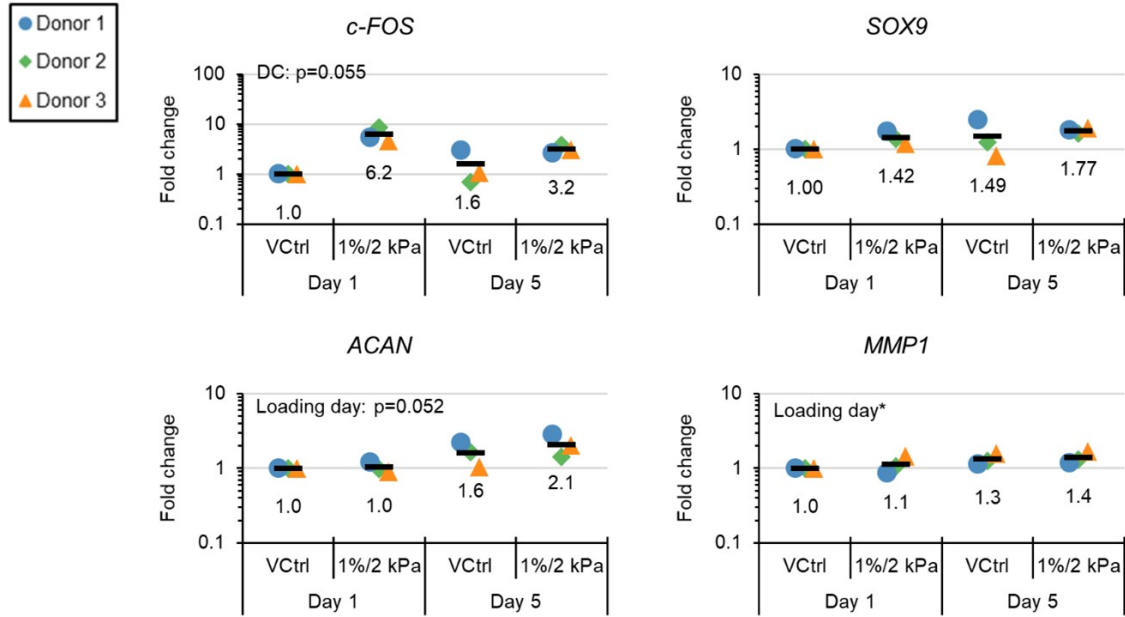
Figure S8.2: mRNA expression levels measured by qRT-PCR compared to Day 1 VCtrl in each group. Tissues were loaded either 1 or 5 days in NRX for 1h with the 1%/2 kPa regime.
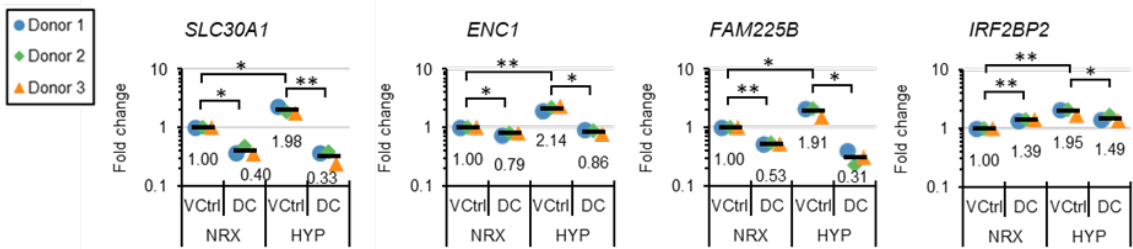
Figure S8.3: Genes having significant (q<0.05) interactions and total count≥250. Groups were compared by ANOVA with mechanical loading and oxygen tension as fixed factors and donor as a random factor. *: p<0.05, **: p<0.01, ***: p<0.001.
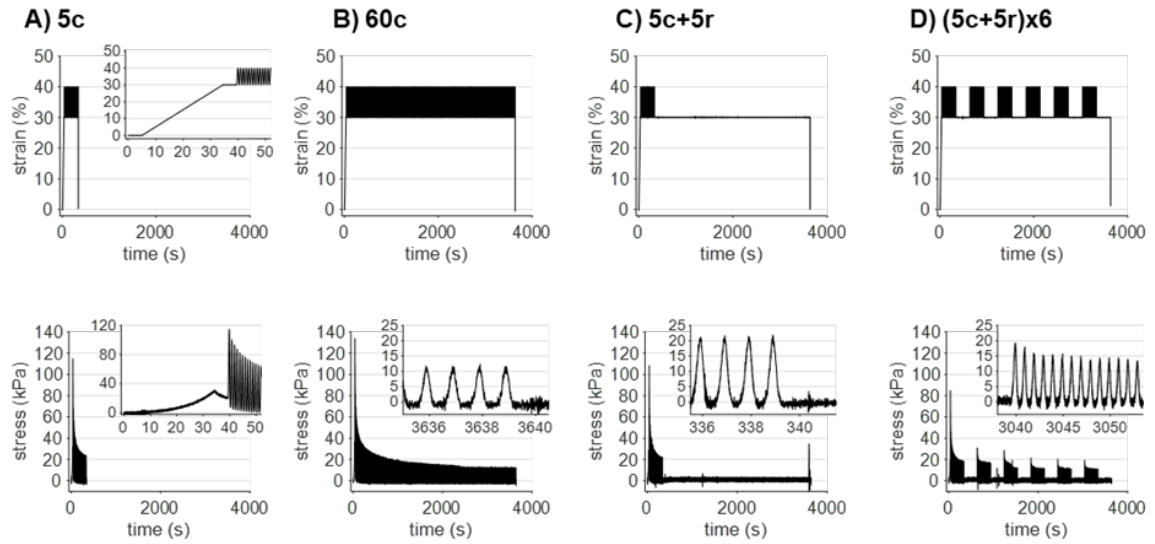
Figure S8.4: Experiment II: A-D) Representative strain and stress vs. time for the four loading groups. The magnified sub-panels show regions of interest for each curve.
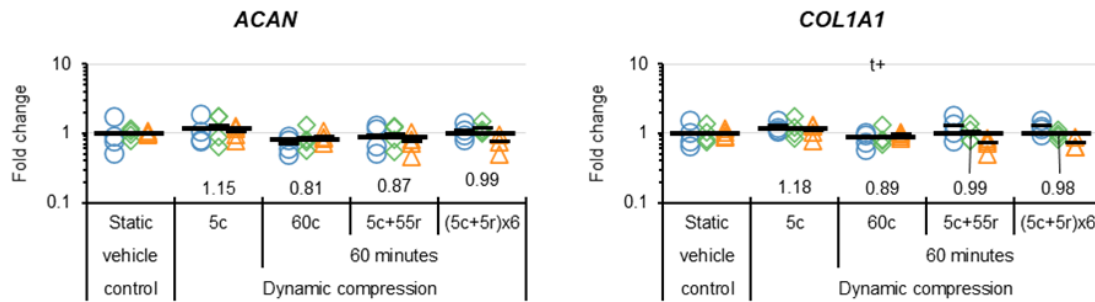
Figure S8.5: Experiment II: *ACAN* and *COL1A1* gene expression. "t" indicates that a DC group is significantly different than 5c. +: p<0.10.

Chapter 9

Summary and Future Directions

Contributing authors:

Alexander R. A. Szojka

This Chapter has not been published nor peer-reviewed.

9.1   Summary

This thesis began with an introduction to the adult human knee menisci, highlighting differences between their inner and outer regions in terms of i) cell and ECM morphology, ii) blood supply, oxygen, and healing capacity, and iii) mechanical loading. It was proposed that the fibrocartilaginous phenotype of the inner meniscus was the product of combined hypoxia and mechanical loading experienced in the inner regions.

Chapter 2 demonstrated that this hypothesis was generally consistent with evidence from developmental biology and comparative anatomy. The fibrocartilage phenotype in the inner human meniscus develops gradually over time, as weight-bearing increases in the first decades of life. Further, the fibrocartilage phenotype develops as a response to compressive mechanical loading in otherwise tensile-loaded tissues such

as ligament and tendon, suggesting a similar phenomenon occurs in the menisci. A possible mechanism for this process is forced closure of blood vessels by pressurization resulting in a hypoxic environment, as proposed in [54]. Evidence from tissue engineering studies in meniscus and hyaline cartilage demonstrated that meniscus cells modulate their matrix-forming phenotypes in response to hypoxia and a wide range of mechanical signals in an additive manner.

Chapter 3 had a different focus in meniscus tissue engineering: development and production of 3D printed polymeric meniscus scaffolds that are biomimetic in their fibre architecture, shape, and suture attachment sites. The main weakness of this study was that there was little no focus on how the scaffold could be used to form functional meniscus tissues. The polycaprolactone material could be chemically modified or substituted with a cell-laden bio-ink based on type I collagen. Successful meniscus tissue engineering with these scaffolds will likely require multiple iterations of sophisticated cell-based experiments with revisions of the 3D models.

The remaining experiments in this thesis returned to the central hypoxia and mechanical loading theme. Each study investigated formation of meniscus tissue using human meniscus fibrochondrocytes (MFCs) from young donors undergoing partial meniscectomy for non-healing injuries.

Chapter 4 demonstrated that fibrocartilaginous tissue formation by MFCs in a small-scale pellet model is synergistically enhanced by hypoxia and TGF-β3 supplementation. Chapter 4 also showed that hypoxia alone without growth factor supplementation was insufficient to induce fibrochondrogenesis in pellets.

Chapter 5 demonstrated that hypoxia alone and hypoxia combined with low strain dynamic compression are insufficient to induce or promote fibrochondrogenesis of MFCs in a larger scale type I collagen scaffold, regardless of TGF-β3 supplementation. Since hypoxia did not promote fibrochondrogenesis, the effects of hypoxia thus vary between the pellet (Chapter 4) and scaffold models, and TGF-β3 supplementation or some other stimulation is necessary for induction of matrix synthesis. The mechanical

and mRNA results suggested that higher strain levels than 0-10% are necessary for inducing detectable effects and that the tissues had poor properties at the early time points investigated (2 weeks pre-culture) even with TGF-β3 supplementation.

The purpose of Chapter 6 was to identify more appropriate pre-culture conditions for applying dynamic compression in the type I collagen scaffold given the outcome of Chapter 5. It was demonstrated that MFCs expanded to passage 1 vs. passage 2 (3 vs. 6 population doublings) have similar matrix forming capacities. Extended culture with TGF-β3 (up to 9 weeks investigated) led to continual increases in mechanical properties, accumulation of hyaline cartilage-type matrix constituents, and, in normoxia, an increasingly hypertrophic phenotype. Apart from suppression of the hypertrophic phenotype, hypoxia did not have clear fibrocartilaginous matrix-promoting outcomes as in Chapter 4, which was consistent with the outcome of Chapter 5.

In a similar time frame to Chapter 6, a functional comparison of human MFCs and human bone marrow mesenchymal stem cells (BMSCs) was performed on the same collagen scaffold as described in Appendix A. It was evident that BMSCs were less contractile and had a much larger capacity than MFCs to produce the matrix constituents of hyaline and hypertrophic cartilage.

Based on the outcomes of Chapter 6, in Chapter 7 the pre-culture condition was 6 weeks in normoxia followed by short-term treatments with hypoxia (24h) and higher-strain dynamic compression (30-40% for 5 minutes). This time, it was shown that hypoxia could have pro-fibrocartilage effects at the gene expression level (especially with regards to hyaline cartilage-type matrix) in the type I collagen scaffold, which was likely due to the MFCs already having a well-established matrix. This is in contrast to the immediate hypoxia exposure on the scaffolds after seeding as in Chapters 5 and 6, in which case the cells are spread out and exposed in the large pores of the scaffold and, under scanning electron microscopy, somewhat resemble isolated aphids in a pile of fallen leaves. The dynamic compression treatment induced desirable fibrocartilage genes such as *SOX9* and *COL1A1*, but the effects were small with generally

few genes regulated compared to hypoxia. There was no evidence of synergy in gene regulation between hypoxia and dynamic compression, but the treatments were extremely short, which was addressed in Chapter 8.

Chapter 8 was a large study comprising four experiments. In these studies, the pre-culture time was shortened to 3 weeks now that a positive outcome had been identified with the higher strain loading regime in Chapter 7.

- The first used a 5-day treatment of hypoxia with either 30-40% dynamic compression, 1% compression/cycle and offload to 2 kPa dynamic compression, or cyclic hydrostatic pressure from 0-0.5 MPa, with all loading treatments lasting for 1h. There was no evidence of synergistic regulation of select genes by hypoxia and dynamic compression. The 30-40% dynamic compression treatment had the largest and most consistent effects of the loading treatments and thus progressed to RNA sequencing. RNA sequencing identified thousands of genes regulated by both hypoxia and dynamic compression. There was a small cluster of nucleus-related genes that had synergistic regulation by the treatments, but it was evident that the treatments overwhelmingly acted in an additive manner, which included co-regulation of many of the same genes. In comparing the hypoxia and dynamic compression group to double control group, the treatment induced a pro-fibrocartilage gene profile with large increases in *COL2A1* and *SOX9* and suppression of *MMPs*. It was clear that hypoxia was driving most of the pro-fibrocartilage effects, although dynamic compression did have some beneficial effects on its own as well. This experiment had several weaknesses. The hydrostatic pressure part was limited by the maximum capability of the device and higher pressures such as 5 or 10 MPa as used by the Athanasiou research group would have been likely much more interesting. The rest of the study was limited in that the long-term outcomes of combined hypoxia and dynamic compression were not evaluated.

- The second experiment demonstrated that the effects of dynamic compression quickly approach saturation, and that only a few minutes are sufficient to induce most of the gene expression response.

- The third experiment aimed to identify how dynamic compression loading regime aggression, manipulated by the use of different pre-culture times and strain levels, affected gene expression. This study would fill in some gaps between Chapters 5, 7, and the first experiments of Chapter 8, because different strain levels and pre-culture times were used in each. While higher strains not surprisingly induced larger gene regulation, the outcomes were not clear for pre-culture time.

- The last experiment aimed to bring all the work so far together in long-term conditioning of the meniscus tissues under combined hypoxia and dynamic compression ("mechano-hypoxia conditioning"). The outcomes were generally promising, with a multi-fold increase in mechanical properties compared to the baseline. However, the outcomes were not always consistent. For example, there was increased *SOX9* but reduced expression of all measured matrix genes in the mechano-hypoxia group compared to static normoxia and hypoxia alone. Interestingly, *COL10A1* was suppressed a remarkable 9-fold in the mechano-hypoxia group. The technical implementation of this project was not ideal due to the need to circulate medium into a separate hypoxia chamber and a lack of medium changes for a three week period, as it was not economical to change medium regularly given the excessive volume of the chambers for the number of constructs being cultured. The resulting build-up of waste products in the medium and depletion of growth factors could have negatively affected results, resulting in the plateau in matrix property development for some donors. Ongoing iterations of this experiment use improvements such as 3D-printed space fillers that reduce the required volume of medium to fill the chambers and regular medium changes.

Taken altogether, as well as with the literature reviewed in Chapter 2, a summary table can be constructed of the likely outcomes of hypoxia and different types of mechanical loading on engineered meniscus (Table 9.1). The outcomes are consistent with the notion that the fibrocartilage phenotype of the adult inner human meniscus reflects an adaptation to a mechanically-loaded and hypoxic environment. They also provide early evidence that combined hypoxia and mechanical loading can be a useful strategy for fibrocartilage histogenesis by MFCs *in vitro*.

Table 9.1: Thesis outcomes and external references for MFCs by oxygen tension and loading environment. All outcomes listed are qualified by "under the appropriate conditions" because, as has been observed countless times within this thesis, the effects of hypoxia and mechanical loading are quite sensitive to variations in experimental parameters. No fibrocartilage formation was ever observed here in the absence of growth factor stimulation (specifically TGF-β3). FC: fibrocartilage, GFs: growth factors, P: pressure.

Loading	Normoxia (NRX)	Hypoxia (HYP)
Static (free-swelling)	FC induced by GFs. More hypertrophy & Saf-O/type II col with time (≥6 weeks) with GFs (TGF-β)	Enhances FC (pro-*SOX9* /*COL2A1* /*ACAN*, suppresses col X, MMPs, contraction), needs GF stim.
Static compression (SC)	Short-term (5 min): intermediate effect to DC, induce early genes. See [159, 162] (not human)	Short-term: the effects of loading in HYP should be similar to those in NRX because there were limited interactions; however, culture will benefit from the additional pro-FC effects of HYP
Dynamic compression (DC)	Short-term (30-40%, 5 min): pro-FC and inflammation genes; medium term (30-40%, 1 h/day/5 days): pro-FC & inflammation genes, thousands of regulated genes. See [73, 160, 162, 233, 234] (non human)	Low strain (10%): no effect ±TGF-β3. Short/med-term (30-40%, 5 min/1 day or 1h/day/5 days): like NRX but with large pro-FC gene effect of HYP. Few interactions. Long-term (30-40%, 5 min/4x/day/3 weeks): more *SOX9*, suppressed matrix proteins and genes incl. *MMPs* and *COL10A1*. This may protect the matrix from DC-induced inflammation. See [82, 83] (not meniscus)
Hydrostatic pressure (HP)	Med-term low P (0-0.5 MPa, 1 h/day/5 days): induce early genes but no FC effect, less than 30-40% DC. See [65, 66]	Like NRX except with added pro-FC effects of HYP. See [79, 80] (not meniscus)
Dynamic tension	See [67–69]	Unknown. Perhaps promotes hyaline cartilage based on [68]

Table 9.1: *Continued from previous page*

Loading	Normoxia (NRX)	Hypoxia (HYP)
Compression and shear	See [235, 236] (not meniscus)	See [81] (not meniscus)
Microgravity	See [237]	Unknown. Likely pro-hyaline cartilage and anti-hypertrophic.
Boundary conditions (clamped ends)	See [73, 231] (not human)	Unknown. HYP may be useful to enhance FC after boundary-condition & dynamic tension-induced organization

9.2　Future directions

This thesis demonstrated that each of hypoxia and mechanical loading could have promising pro-fibrocartilage effects at the gene expression level. More iterations of the long-term study (experiment IV) in Chapter 8 are necessary to determine if the pro-fibrocartilage gene expression outcomes from the shorter term treatments (1 and 5 days) can clearly and reliably lead to superior fibrocartilage histogenesis at the matrix level.

The immediate next steps for this work would be to address the limitations outlined for experiment IV in Chapter 8. For example, the culture system should be modified with the objectives of attaining continuous increases in mechanical properties over time without a plateau and attaining consistency between the different levels of analysis (gene expression, biochemistry, histology, and mechanical properties). It would also be useful to compare mechanical properties between loaded and unloaded controls. Further, it would be convincing to establish a dose-effect with mechanical loading, e.g., with superior outcomes for more frequent loading incidents. A project carried out between chapters 7 and 8 attempted to do this with loading 0, 1, 2, and 5 times a week, but the groups were not consistently different. This data is not included in this thesis but it may be eventually published elsewhere after peer-review.

Although dynamic compression regulated thousands of genes in experiment I of Chapter 8, the collective functions of these genes were much less clear than for the complementary set of genes regulated by hypoxia, which clearly promoted the hyaline cartilage-like aspect of fibrocartilage. This is one reason why it will be important to iterate upon the long-term mechano-hypoxia experiment from Chapter 8 in future work. Longer treatments will favour divergence of experimental groups and larger effect sizes of hypoxia and mechanical loading treatments as the gene regulation leads to differential protein synthesis. A time course experiment similar to Chapter 6 but with mechano-hypoxia conditioning could be useful in this regard.

The boundary condition strategy demonstrated by Puetzer in [73, 231] in animal MFCs, wherein MFCs in a high density collagen hydrogel contract and form fibres aligned between two clamped ends, appears very promising for promoting biomimetic fibre bundling. The contractile tendencies of T1F2-expanded MFCs drew ire throughout this entire research project as the resulting geometric changes led to confounding diffusion differences between groups and made mechanical testing less consistent. However, the Puetzer boundary condition strategy could potentially harness the contractile property of these cells. T1F2-expanded human MFCs could be suspended in similar collagen gels and fixed between two points for aligned fibre formation to occur. Contraction could be promoted by expansion to P2 rather than P1, culture in normoxia (both as demonstrated in Chapter 6), and potentially increased concentration of TGF-β1 during expansion. Upon generation of appropriate fibres, the tissues could then be treated with mechano-hypoxia conditioning (with dynamic compression) to promote fibrocartilage formation. Towards full-scale meniscus tissue engineering, circumferential directional information could be impregnated into the scaffolds using the biomimetic meniscus-shaped models developed as in Chapter 3.

A reasonable criticism of this work is that the abundant staining for Safranin-O and type II collagen demonstrated in this thesis, especially when tissues were cultured beyond 3 weeks with TGF-β3, would be pathological were they found in human meniscus.

One response to this criticism would be that overshooting the degree of hyaline cartilage-type matrix abundance in an engineered tissue could be an appropriate strategy for translational purposes if it provides adequate compressive mechanical properties for an implanted graft to survive long enough for remodelling to a more appropriate phenotype to occur "à la Pauwels" in response to stresses experienced in the knee joint. A second response would be that the absolute levels of these matrix constituents (aggrecan and type II collagen) may not be far off from the native meniscus on a wet weight basis, and the problem is actually that the amount of type

I collagen accumulating in the constructs is too low. The lowest water content of the engineered meniscus tissues generated in this project was measured at 85% after 14 weeks of normoxic culture (not included in any experiment shown here) compared to 70-75% for native human meniscus[127]. This suggests the tissues still have a long way to go with regard to achieving native meniscus-levels of solid matrix, and the gap could be closed with type I collagen. No experiments in this project were designed to specifically promote type I collagen accumulation, but this could be the focus of future work before beginning a regime of mechano-hypoxia conditioning. Efforts to achieve more type I collagen in the matrix-poor core regions of engineered tissues, such as those in Figure 8.7, could be fruitful. While this criticism would weaken the external validity of results in the model system for the inner human meniscus used here, it may not be so critical if gene regulation by hypoxia and mechanical loading is not fundamentally changed by the concentration of hyaline cartilage matrix constituents. There was some consistency in transcriptome expression patterns in the short-term loading study despite wide differences between donors in hyaline cartilage-type matrix staining (Chapter 7), and there were similar responses to DC in the measured genes between the fibrous and more cartilaginous tissues in experiment III of Chapter 8, manipulated by use of different pre-culture periods. Finally, the research demonstrating the amount of type II collagen present in human meniscus is surprisingly severely limited; important references in this regard are [32, 39, 127, 238]. To the best of my knowledge, type II collagen has not been demonstrated in human menisci during development and childhood. Due to the technical difficulties in its specific detection and measurement, it is not clear to what extent this reflects an absence of evidence versus evidence of absence. Future work should quantify the major collagens in healthy adult human meniscus and clearly demonstrate their distribution to provide a target for tissue engineering, an idea that was partially covered in [239].

As a final note, if mechano-hypoxia conditioning can promote the hyaline cartilage-

type phenotype and suppression of hypertrophic markers in MFCs under the appropriate conditions, then it stands to reason that it is likely to be a useful tool for directly tissue engineering hyaline cartilage using other cell types such as bone marrow-derived mesenchymal stem cells. Towards this end, extending previous works such as [81, 82] with further optimization the loading regimes could be a fruitful endeavour.

Bibliography

[1] A. R. Szojka, K. Lalh, S. H. Andrews, N. M. Jomha, M. Osswald, and A. B. Adesida, "Biomimetic 3D printed scaffolds for meniscus tissue engineering," *Bioprinting*, vol. 8, pp. 1–7, 2017.

[2] A. R. Szojka, B. D. Lyons, C. N. Moore, Y. Liang, M. Kunze, E. Idrees, A. Mulet-Sierra, N. M. Jomha, and A. B. Adesida, "Hypoxia and TGF-β3 Synergistically Mediate Inner Meniscus-Like Matrix Formation by Fibrochondrocytes," *Tissue Engineering - Part A*, vol. 25, no. 5-6, pp. 446–456, 2019.

[3] A. R. Szojka, C. N. Moore, Y. Liang, S. H. Andrews, M. Kunze, A. Mulet-Sierra, N. M. Jomha, and A. B. Adesida, "Engineered human meniscus matrix-forming phenotype is unaffected by low strain dynamic compression under hypoxic conditions," *PLoS ONE*, vol. 16, no. 3 March, F. Zhao, Ed., e0248292, 2021.

[4] A. R. Szojka, Y. Liang, R. d. C. Marqueti, C. N. Moore, E. J. N. Erkut, M. Kunze, A. Mulet-Sierra, N. M. Jomha, and A. B. Adesida, "Time course of 3D fibrocartilage formation by expanded human meniscus fibrochondrocytes in hypoxia," *Journal of Orthopaedic Research*, jor.25046, 2021.

[5] A. R. Szojka, R. d. C. Marqueti, D. X. Li, C. W. Molter, Y. Liang, M. Kunze, A. Mulet-Sierra, N. M. Jomha, and A. B. Adesida, "Human engineered meniscus transcriptome after short-term combined hypoxia and dynamic compression," *Journal of Tissue Engineering*, vol. 12, 2021.

[6] A. R. A. Szojka, D. X. Li, M. E. J. Sopcak, Z. Ma, M. Kunze, A. Mulet-Sierra, S. M. Adeeb, L. Westover, N. M. Jomha, and A. B. Adesida, "Mechano-Hypoxia Conditioning of Engineered Human Meniscus," *Frontiers in Bioengineering and Biotechnology*, vol. 9, Article 739438, 2021.

[7] H. A. Elkhenany, A. R. Szojka, A. Mulet-Sierra, Y. Liang, M. Kunze, X. Lan, M. Sommerfeldt, N. M. Jomha, and A. B. Adesida, "Bone Marrow Mesenchymal Stem Cell-Derived Tissues are Mechanically Superior to Meniscus Cells," *Tissue Engineering Part A*, ten.TEA.2020.0183, 2020.

[8] Y. Liang, E. Idrees, S. H. Andrews, K. Labib, A. R. Szojka, M. Kunze, A. D. Burbank, A. Mulet-Sierra, N. M. Jomha, and A. B. Adesida, "Plasticity of Human Meniscus Fibrochondrocytes: A Study on Effects of Mitotic Divisions and Oxygen Tension," *Scientific Reports*, vol. 7, no. 1, Article 12148, 2017.

[9] Y. Liang, E. Idrees, A. R. Szojka, S. H. Andrews, M. Kunze, A. Mulet-Sierra, N. M. Jomha, and A. B. Adesida, "Chondrogenic differentiation of synovial fluid mesenchymal stem cells on human meniscus-derived decellularized matrix requires exogenous growth factors," *Acta Biomaterialia*, vol. 80, pp. 131–143, 2018.

[10] Y. Liang, A. R. Szojka, E. Idrees, M. Kunze, A. Mulet-Sierra, and A. B. Adesida, "Re-Differentiation of Human Meniscus Fibrochondrocytes Differs in Three-Dimensional Cell Aggregates and Decellularized Human Meniscus Matrix Scaffolds," *Annals of Biomedical Engineering*, vol. 48, no. 3, pp. 968–979, 2020.

[11] D. Zhalmuratova, T. G. La, K. T. T. Yu, A. R. Szojka, S. H. Andrews, A. B. Adesida, C. I. Kim, D. S. Nobes, D. H. Freed, and H. J. Chung, "Mimicking "j-Shaped" and Anisotropic Stress-Strain Behavior of Human and Porcine Aorta by Fabric-Reinforced Elastomer Composites," *ACS Applied Materials and Interfaces*, vol. 11, no. 36, pp. 33 323–33 335, 2019.

[12] F. R. Barin, I. V. de Sousa Neto, G. Vieira Ramos, A. Szojka, A. L. Ruivo, C. T. M. Anflor, J. D. H. Agualimpia, A. C. Domingues, O. L. Franco, A. B. Adesida, J. L. Q. Durigan, and R. d. C. Marqueti, "Calcaneal Tendon Plasticity Following Gastrocnemius Muscle Injury in Rat," *Frontiers in Physiology*, vol. 10, 2019.

[13] A. Rahman, S; Szojka, ARA; Liang, Y; Kunze, M; Goncalves, V; Mulet-Sierra, A; Jomha, NM; Adesida, "Inability of low oxygen tension to induce chondrogenesis in human infrapatellar fat pad-mesenchymal stem cells," *Frontiers in Cell and Developmental Biology*, vol. Accepted a, 2021.

[14] K. Messner and J. Gao, "The menisci of the knee joint. Anatomical and functional characteristics, and a rationale for clinical treatment," *Journal of Anatomy*, vol. 193, no. 2, pp. 161–178, 1998.

[15] E. A. Makris, P. Hadidi, and K. A. Athanasiou, "The knee meniscus: Structure-function, pathophysiology, current repair techniques, and prospects for regeneration," *Biomaterials*, vol. 32, no. 30, pp. 7411–7431, 2011.

[16] N. Caplan and D. F. Kader, "Knee joint changes after meniscectomy," en, *Classic Papers in Orthopaedics*, vol. 30-B, no. 4, pp. 173–175, 2014.

[17] L. S. Lohmander, P. M. Englund, L. L. Dahl, and E. M. Roos, "The long-term consequence of anterior cruciate ligament and meniscus injuries: Osteoarthritis," en, *American Journal of Sports Medicine*, vol. 35, no. 10, pp. 1756–1769, 2007.

[18] M. Englund, A. Guermazi, and L. S. Lohmander, "The Meniscus in Knee Osteoarthritis," *Rheumatic Disease Clinics of North America*, vol. 35, no. 3, pp. 579–590, 2009.

[19] R. Papalia, A. Del Buono, L. Osti, V. Denaro, and N. Maffulli, *Meniscectomy as a risk factor for knee osteoarthritis: A systematic review*, 2011.

[20] U. G. Longo, M. Ciuffreda, V. Candela, G. Rizzello, V. D'Andrea, N. Mannering, A. Berton, G. Salvatore, and V. Denaro, "Knee Osteoarthritis after Arthroscopic Partial Meniscectomy: Prevalence and Progression of Radiographic Changes after 5 to 12 Years Compared with Contralateral Knee," *Journal of Knee Surgery*, vol. 32, no. 5, pp. 407–413, 2019.

[21] Arthritis Alliance of Canada, "The impact of arthritis in Canada: today and over the next 30 years," *Arthritis Alliance of Canada*, vol. Fall, p. 52, 2011.

[22] J. Sanchez-Adams and K. A. Athanasiou, "The knee meniscus: A complex tissue of diverse cells," *Cellular and Molecular Bioengineering*, vol. 2, no. 3, pp. 332–340, 2009.

[23] W. Petersen and B. Tillmann, "Collagenous fibril texture of the human knee joint menisci," *Anatomy and Embryology*, vol. 197, no. 4, pp. 317–324, 1998.

[24] Aarti Sareen, *Meniscal blood supply*, 2013.

[25] M. L. Upton, F. Guilak, T. A. Laursen, and L. A. Setton, "Finite element modeling predictions of region-specific cell-matrix mechanics in the meniscus," *Biomechanics and Modeling in Mechanobiology*, vol. 5, no. 2-3, pp. 140–149, 2006.

[26] S. M. Adeeb, "Load-bearing across diarthrodial joints with special reference to peripheral structures and the menisci of the knee," Ph.D. dissertation, University of Calgary, 2005, p. 72.

[27] R. Pittman, "Oxygen transport.," in *Morgan and Claypool Life Sciences*, Morgan and Claypool Life Sciences, 2011.

[28] S. P. Arnoczky and R. F. Warren, "Microvasculature of the human meniscus," en, *The American Journal of Sports Medicine*, vol. 10, no. 2, pp. 90–95, 1982. arXiv: NIHMS150003.

[29] K. Lund-Olesen, "Oxygen tension in synovial fluids," *Arthritis and Rheumatism*, vol. 13, no. 6, pp. 769–776, 1970.

[30] S. H. Andrews, A. B. Adesida, Z. Abusara, and N. G. Shrive, "Current concepts on structure–function relationships in the menisci," *Connective Tissue Research*, vol. 58, no. 3-4, pp. 271–281, 2017.

[31] H. E. Kambic and C. A. McDevitt, "Spatial organization of types I and II collagen in the canine meniscus," en, *Journal of Orthopaedic Research*, vol. 23, no. 1, pp. 142–149, 2005.

[32] T. Pufe, W. J. Petersen, N. Miosge, M. B. Goldring, R. Mentlein, D. J. Varoga, and B. N. Tillmann, "Endostatin/collagen XVIII - An inhibitor of angiogenesis - Is expressed in cartilage and fibrocartilage," *Matrix Biology*, vol. 23, no. 5, pp. 267–276, 2004.

[33] C. Clark and J. Ogden, "Prenatal and Postnatal Development of Human Knee Joint Menisci," *The Iowa Orthopaedic Journal*, vol. 1, no. 1, pp. 20–27, 1981.

[34] I. Fukazawa, T. Hatta, Y. Uchio, and H. Otani, "Development of the meniscus of the knee joint in human fetuses," en, *Congenital Anomalies*, vol. 49, no. 1, pp. 27–32, 2009.

[35] C. R. Clark and J. A. Ogden, "Development of the menisci of the human knee joint. Morphological changes and their potential role in childhood meniscal injury," *Journal of Bone and Joint Surgery - Series A*, Including Papers Presented Before the XXX Annual International Congress of the British Association of Paediatric Surgeons, vol. 65, no. 4, pp. 538–547, 1983.

[36] W. Petersen and B. Tillmann, "Age-related blood and lymph supply of the knee menisci:a cadaver study," *Acta Orthopaedica*, vol. 66, no. 4, pp. 308–312, 1995.

[37] T. P. McMurray, "The semilunar cartilages," *British Journal of Surgery*, vol. 29, no. 116, pp. 407–414, 1942.

[38] J. C. Birnholz, J. C. Stephens, and M. Faria, "Fetal movement patterns: A possible means of defining neurologic developmental milestones in utero," *American Journal of Roentgenology*, vol. 130, no. 3, pp. 537–540, 1978.

[39] W. Fedje-Johnston, F. Tóth, M. Albersheim, C. S. Carlson, K. G. Shea, A. Rendahl, and M. Tompkins, "Changes in Matrix Components in the Developing Human Meniscus," *American Journal of Sports Medicine*, vol. 49, no. 1, pp. 207–214, 2021.

[40] W. Petersen, T. Pufe, B. Kurz, R. Mentlein, and B. Tillmann, "Angiogenesis in fetal tendon development: Spatial and temporal expression of the angiogenic peptide vascular endothelial cell growth factor," *Anatomy and Embryology*, vol. 205, no. 4, pp. 263–270, 2002.

[41] Z. Lu, T. Furumatsu, M. Fujii, A. Maehara, and T. Ozaki, "The distribution of vascular endothelial growth factor in human meniscus and a meniscal injury model," *Journal of Orthopaedic Science*, vol. 22, no. 4, pp. 715–721, 2017.

[42] M. Fujii, T. Furumatsu, Y. Yokoyama, T. Kanazawa, Y. Kajiki, N. Abe, and T. Ozaki, "Chondromodulin-I derived from the inner meniscus prevents endothelial cell proliferation," *Journal of Orthopaedic Research*, vol. 31, no. 4, pp. 538–543, 2013.

[43] T. Pufe, B. Kurz, W. Petersen, D. Varoga, R. Mentlein, S. Kulow, A. Lemke, and B. Tillmann, "The influence of biomechanical parameters on the expression of VEGF and endostatin in the bone and joint system," *Annals of Anatomy*, vol. 187, no. 5-6, pp. 461–472, 2005.

[44] E. Folkesson, A. Turkiewicz, M. Rydén, H. V. Hughes, N. Ali, J. Tjörnstrand, P. Önnerfjord, and M. Englund, *Proteomic characterization of the normal human medial meniscus body using data-independent acquisition mass spectrometry*, 2020.

[45] M. Benjamin and J. R. Ralphs, "The cell and developmental biology of tendons and ligaments," *International Review of Cytology*, vol. 196, pp. 85–130, 2000.

[46] M. Benjamin and J. R. Ralphs, "Biology of Fibrocartilage Cells," *International Review of Cytology*, vol. 233, no. Iv, pp. 1–45, 2004.

[47] C. M. Waugh, A. J. Blazevich, F. Fath, and T. Korff, "Age-related changes in mechanical properties of the Achilles tendon," *Journal of Anatomy*, vol. 220, no. 2, pp. 144–155, 2012.

[48] M. Tissakht and A. M. Ahmed, "Tensile stress-strain characteristics of the human meniscal material," *Journal of Biomechanics*, vol. 28, no. 4, pp. 411–422, 1995.

[49] H. N. Chia and M. L. Hull, "Compressive moduli of the human medial meniscus in the axial and radial directions at equilibrium and at a physiological strain rate," eng, *Journal of Orthopaedic Research*, vol. 26, no. 7, pp. 951–956, 2008.

[50] V. C. Mow, S. C. Kuei, W. M. Lai, and C. G. Armstrong, "Biphasic creep and stress relaxation of articular cartilage in compression: Theory and experiments," *Journal of Biomechanical Engineering*, vol. 102, no. 1, pp. 73–84, 1980.

[51] A. C. AufderHeide and K. A. Athanasiou, "Mechanical stimulation toward tissue engineering of the knee meniscus," en, *Annals of Biomedical Engineering*, vol. 32, no. 8, pp. 1161–1174, 2004.

[52] M. Benjamin and J. R. Ralphs, "Fibrocartilage in tendons and ligaments - an adaptation to compressive load," *Journal of Anatomy*, vol. 193, no. 4, pp. 481–494, 1998.

[53] F. Pauwels, *Biomechanics of the Locomotor Apparatus*. Springer Berlin Heidelberg, 1980.

[54] S. Krompecher and L. Toth, "Die Konzeption von Kompression, Hypoxie und konsekutiver Mucopolysaccharidbildung in der Kausalen Analyse der Chondrogenese," *Zeitschrift fur Anatomie und Entwicklungsgeschichte*, vol. 124, no. 3, pp. 268–288, 1964.

[55] A. B. Adesida, L. M. Grady, W. S. Khan, and T. E. Hardingham, "The matrix-forming phenotype of cultured human meniscus cells is enhanced after culture with fibroblast growth factor 2 and is further stimulated by hypoxia," *Arthritis Research and Therapy*, vol. 8, no. 3, R61, 2006.

[56] A. B. Adesida, L. M. Grady, W. S. Khan, S. J. Millward-Sadler, D. M. Salter, and T. E. Hardingham, "Human meniscus cells express hypoxia inducible factor-1α and increased SOX9 in response to low oxygen tension in cell aggregate culture," *Arthritis Research and Therapy*, vol. 9, no. 4, R69, 2007.

[57] A. B. Adesida, A. Mulet-Sierra, L. Laouar, and N. M. Jomha, "Oxygen tension is a determinant of the matrix-forming Phenotype of cultured human meniscal Fibrochondrocytes," *PLoS ONE*, vol. 7, no. 6, e39339, 2012.

[58] R. Croutze, N. Jomha, H. Uludag, and A. Adesida, "Matrix forming characteristics of inner and outer human meniscus cells on 3D collagen scaffolds under normal and low oxygen tensions," *BMC Musculoskeletal Disorders*, vol. 14, no. 1, p. 353, 2013.

[59] G. K. Tan, D. L. M. Dinnes, P. T. Myers, and J. J. Cooper-White, "Effects of biomimetic surfaces and oxygen tension on redifferentiation of passaged human fibrochondrocytes in 2D and 3D cultures," *Biomaterials*, vol. 32, no. 24, pp. 5600–5614, 2011.

[60] A Adesida, S Millward-Sadler, and T Hardingham, "Human meniscus cells contain a progenitor cell population," in *The Centenary (190th) Meeting of the Pathological Society of Great Britain and Ireland*, The Journal of Pathology, 2006.

[61] C Lee, S Grad, M Wimmer, and M Alini, "The Influence of Mechanical Stimuli on Articular Cartilage Tissue Engineering," *Topics in Tissue Engineering*, vol. 2, no. 2, pp. 1–32, 2006.

[62] U. Cheema, C. B. Chuo, P. Sarathchandra, S. N. Nazhat, and R. A. Brown, "Engineering functional collagen scaffolds: Cyclical loading increases material strength and fibril aggregation," *Advanced Functional Materials*, vol. 17, no. 14, pp. 2426–2431, 2007.

[63] D. E. Anderson and B. Johnstone, "Dynamic mechanical compression of chondrocytes for tissue engineering: A critical review," *Frontiers in Bioengineering and Biotechnology*, vol. 5, no. DEC, Article 76, 2017.

[64] A. L. McNulty and F. Guilak, "Mechanobiology of the meniscus," *Journal of Biomechanics*, vol. 48, no. 8, pp. 1469–1478, 2015.

[65] T. Suzuki, T. Toyoda, H. Suzuki, N. Hisamori, H. Matsumoto, and Y. Toyama, "Hydrostatic pressure modulates mRNA expressions for matrix proteins in human meniscal cells," *Biorheology*, vol. 43, no. 5, pp. 611–622, 2006.

[66] J. Zellner, M. Mueller, Y. Xin, W. Krutsch, A. Brandl, R. Kujat, M. Nerlich, and P. Angele, "Dynamic hydrostatic pressure enhances differentially the chondrogenesis of meniscal cells from the inner and outer zone," *Journal of Biomechanics*, vol. 48, no. 8, pp. 1479–1484, 2015.

[67] B. Baker, R. Shah, and Silverstein, "Dynamic Tension Improves the Mechanical Properties of Nanofiber-Based Engineered Meniscus Constructs," in *56th Annual Meeting of the Orthopaedic Research Society*, 2010.

[68] T. Kanazawa, T. Furumatsu, M. Hachioji, T. Oohashi, Y. Ninomiya, and T. Ozaki, "Mechanical stretch enhances COL2A1 expression on chromatin by inducing SOX9 nuclear translocalization in inner meniscus cells.," *Journal of orthopaedic research : official publication of the Orthopaedic Research Society*, vol. 30, no. 3, pp. 468–474, 2012.

[69] T. Furumatsu, T. Kanazawa, Y. Miyake, S. Kubota, M. Takigawa, and T. Ozaki, "Mechanical stretch increases Smad3-dependent CCN2 expression in inner meniscus cells," *Journal of Orthopaedic Research*, vol. 30, no. 11, pp. 1738–1745, 2012.

[70] D. J. Huey and K. A. Athanasiou, "Tension-compression loading with chemical stimulation results in additive increases to functional properties of anatomic meniscal constructs," *PLoS ONE*, vol. 6, no. 11, 2011.

[71] J. J. Ballyns and L. J. Bonassar, "Dynamic compressive loading of image-guided tissue engineered meniscal constructs," en, *Journal of Biomechanics*, vol. 44, no. 3, pp. 509–516, 2011. arXiv: www.cancer.org.

[72] J. L. Puetzer, J. J. Ballyns, and L. J. Bonassar, "The effect of the duration of mechanical stimulation and post-stimulation culture on the structure and properties of dynamically compressed tissue-engineered menisci," ENG, *Tissue Engineering - Part A*, vol. 18, no. 13-14, pp. 1365–1375, 2012.

[73] J. L. Puetzer and L. J. Bonassar, "Physiologically Distributed Loading Patterns Drive the Formation of Zonally Organized Collagen Structures in Tissue-Engineered Meniscus," *Tissue Engineering - Part A*, vol. 22, no. 13-14, pp. 907–916, 2016.

[74] E. Y. Salinas, J. C. Hu, and K. Athanasiou, "A Guide for Using Mechanical Stimulation to Enhance Tissue-Engineered Articular Cartilage Properties," *Tissue Engineering - Part B: Reviews*, vol. 24, no. 5, pp. 345–358, 2018.

[75] B. K. Hall, "Hypoxia and differentiation of cartilage and bone from common germinal cells in vitro," *Life Sciences*, vol. 8, no. 10 PART 2, pp. 553–558, 1969.

[76] J. A. Steen, "Allograft Derived Bioscaffolds for Tissue Engineering of the Meniscus: An in vivo Ovine Study and the Effect of Hypoxic Culture on Seeded Meniscus Constructs," *ProQuest Dissertations and Theses*, 2012.

[77] R. J. Egli, E. Wernike, S. Grad, and R. Luginbühl, "Physiological cartilage tissue engineering. Effect of oxygen and biomechanics," in *International Review of Cell and Molecular Biology*, vol. 289, Elsevier Inc., 2011, pp. 37–87.

[78] C. Gaut and K. Sugaya, "Critical review on the physical and mechanical factors involved in tissue engineering of cartilage," ENG, *Regenerative Medicine*, vol. 10, no. 5, pp. 665–679, 2015.

[79] C. Domm, J. Fay, M. Schünke, and B. Kurz, "Influence of intermittent hydrostatic pressure and low oxygen partial-pressure on the redifferentiation of dedifferentiated articular chondrocytes in alginate culture," *Der Orthopäde*, vol. 29, no. 2, pp. 0091–0099, 2000.

[80] U. Hansen, M. Schünke, C. Domm, N. Ioannidis, J. Hassenpflug, T. Gehrke, and B. Kurz, "Combination of reduced oxygen tension and intermittent hydrostatic pressure: A useful tool in articular cartilage tissue engineering," *Journal of Biomechanics*, vol. 34, no. 7, pp. 941–949, 2001.

[81] E. Wernike, Z. Li, M. Alini, and S. Grad, "Effect of reduced oxygen tension and long-term mechanical stimulation on chondrocyte-polymer constructs," en, *Cell and Tissue Research*, vol. 331, no. 2, pp. 473–483, 2008.

[82] E. G. Meyer, C. T. Buckley, S. D. Thorpe, and D. J. Kelly, "Low oxygen tension is a more potent promoter of chondrogenic differentiation than dynamic compression," *Journal of Biomechanics*, vol. 43, no. 13, pp. 2516–2523, 2010.

[83] E. Parker, S. Vessillier, B. Pingguan-Murphy, W. A. Abas, D. L. Bader, and T. T. Chowdhury, "Low oxygen tension increased fibronectin fragment induced catabolic activities - response prevented with biomechanical signals," *Arthritis Research and Therapy*, vol. 15, no. 5, R163, 2013.

[84] B. Hinz, "The extracellular matrix and transforming growth factor-β1: Tale of a strained relationship," *Matrix Biology*, vol. 47, pp. 54–65, 2015.

[85] H. Kurosawa, T. Fukubayashi, and H. Nakajima, "Load-bearing mode of the knee joint: Physical behavior of the knee joint with or without menisci," eng, *Clinical Orthopaedics and Related Research*, vol. NO 149, no. 149, pp. 283–290, 1980.

[86] M. Englund and L. S. Lohmander, "Risk factors for symptomatic knee osteoarthritis fifteen to twenty-two years after meniscectomy," eng, *Arthritis and Rheumatism*, vol. 50, no. 9, pp. 2811–2819, 2004.

[87] S. W. Kang, S. M. Son, J. S. Lee, E. S. Lee, K. Y. Lee, S. G. Park, J. H. Park, and B. S. Kim, "Regeneration of whole meniscus using meniscal cells and polymer scaffolds in a rabbit total meniscectomy model," en, *Journal of Biomedical Materials Research - Part A*, vol. 77, no. 4, pp. 659–671, 2006.

[88] B. B. Seedhom, "Transmission of the load in the knee joint with special reference to the role of the menisci. Part I. Anatomy, analysis and apparatus," *Engineering in Medicine*, vol. 8, no. 4, pp. 207–219, 1979.

[89] S. H. Andrews, J. B. Rattner, H. A. Jamniczky, N. G. Shrive, and A. B. Adesida, "The structural and compositional transition of the meniscal roots into the fibrocartilage of the menisci," en, *Journal of Anatomy*, vol. 226, no. 2, pp. 169–174, 2015.

[90] D. L. Skaggs, W. H. Warden, and V. C. Mow, "Radial tie fibers influence the tensile properties of the bovine medial meniscus," en, *Journal of Orthopaedic Research*, vol. 12, no. 2, pp. 176–185, 1994.

[91] N. Dorman, "Citations," English. *BioTechniques*, vol. 53, no. 3, p. 127, 2012.

[92] R. Allaire, M. Muriuki, L. Gilbertson, and C. D. Harner, "Biomechanical consequences of a tear of the posterior root of the medial meniscus: Similar to total meniscectomy," *Journal of Bone and Joint Surgery - Series A*, vol. 90, no. 9, pp. 1922–1931, 2008.

[93] P. Beaufils and R. Verdonk, *The meniscus*, en. Berlin, Heidelberg: Springer Berlin Heidelberg, 2010, pp. 1–407.

[94] D. H. Lee, B. S. Lee, J. M. Kim, K. S. Yang, E. J. Cha, J. H. Park, and S. I. Bin, "Predictors of degenerative medial meniscus extrusion: Radial component and knee osteoarthritis," en, *Knee Surgery, Sports Traumatology, Arthroscopy*, vol. 19, no. 2, pp. 222–229, 2011.

[95] J. Baek, X. Chen, S. Sovani, S. Jin, S. P. Grogan, and D. D. D'Lima, "Meniscus tissue engineering using a novel combination of electrospun scaffolds and human meniscus cells embedded within an extracellular matrix hydrogel," en, *Journal of Orthopaedic Research*, vol. 33, no. 4, pp. 572–583, 2015.

[96] J. Baek, S. Sovani, N. E. Glembotski, J. Du, S. Jin, S. P. Grogan, and D. D. D'Lima, "Repair of Avascular Meniscus Tears with Electrospun Collagen Scaffolds Seeded with Human Cells," en, *Tissue Engineering - Part A*, vol. 22, no. 5-6, pp. 436–448, 2016.

[97] I. F. Cengiz, M. Pitikakis, L. Cesario, P. Parascandolo, L. Vosilla, G. Viano, J. M. Oliveira, and R. L. Reis, "Building the basis for patient-specific meniscal scaffolds: From human knee MRI to fabrication of 3D printed scaffolds," *Bioprinting*, vol. 1-2, pp. 1–10, 2016.

[98] C. H. Lee, S. A. Rodeo, L. A. Fortier, C. Lu, C. Erisken, and J. J. Mao, "Protein-releasing polymeric scaffolds induce fibrochondrocytic differentiation of endogenous cells for knee meniscus regeneration in sheep," en, *Science Translational Medicine*, vol. 6, no. 266, 266ra171–266ra171, 2014.

[99] B. B. Mandal, S. H. Park, E. S. Gil, and D. L. Kaplan, "Multilayered silk scaffolds for meniscus tissue engineering," *Biomaterials*, vol. 32, no. 2, pp. 639–651, 2011. arXiv: NIHMS150003.

[100] B. B. Rothrauff, P. on Numpaisal, B. B. Lauro, P. G. Alexander, R. E. Debski, V. Musahl, and R. S. Tuan, "Augmented repair of radial meniscus tear with biomimetic electrospun scaffold: an in vitro mechanical analysis," En, *Journal of Experimental Orthopaedics*, vol. 3, no. 1, p. 23, 2016.

[101] Z. Z. Zhang, D. Jiang, J. X. Ding, S. J. Wang, L. Zhang, J. Y. Zhang, Y. S. Qi, X. S. Chen, and J. K. Yu, "Role of scaffold mean pore size in meniscus regeneration," *Acta Biomaterialia*, vol. 43, pp. 314–326, 2016.

[102] Z. Z. Zhang, S. J. Wang, J. Y. Zhang, W. B. Jiang, A. B. Huang, Y. S. Qi, J. X. Ding, X. S. Chen, D. Jiang, and J. K. Yu, "3D-Printed Poly(epsilon-caprolactone) Scaffold Augmented with Mesenchymal Stem Cells for Total Meniscal Substitution: A 12- and 24-Week Animal Study in a Rabbit Model," en, *American Journal of Sports Medicine*, vol. 45, no. 7, pp. 1497–1511, 2017.

[103] T. Zantop, A. K. Eggers, V. Musahl, A. Weimann, and W. Petersen, "Cyclic testing of flexible all-inside meniscus suture anchors: Biomechanical analysis," en, *American Journal of Sports Medicine*, vol. 33, no. 3, pp. 388–394, 2005.

[104] P. B. Warren, P. Huebner, J. T. Spang, R. A. Shirwaiker, and M. B. Fisher, "Engineering 3D-Bioplotted scaffolds to induce aligned extracellular matrix deposition for musculoskeletal soft tissue replacement," *Connective Tissue Research*, vol. 58, no. 3-4, pp. 342–354, 2017.

[105] J. R. Yoon, H. I. Jeong, M. J. Seo, K. M. Jang, S. R. Oh, S. Song, and J. H. Yang, "The use of contralateral knee magnetic resonance imaging to predict meniscal size during meniscal allograft transplantation," *Arthroscopy - Journal of Arthroscopic and Related Surgery*, vol. 30, no. 10, pp. 1287–1293, 2014.

[106] M. A. Woodruff and D. W. Hutmacher, "The return of a forgotten polymer - Polycaprolactone in the 21st century," *Progress in Polymer Science (Oxford)*, vol. 35, no. 10, pp. 1217–1256, 2010.

[107] H. Sun, L. Mei, C. Song, X. Cui, and P. Wang, "The in vivo degradation, absorption and excretion of PCL-based implant," *Biomaterials*, vol. 27, no. 9, pp. 1735–1740, 2006.

[108] H. Zhang and S. Hollister, "Comparison of bone marrow stromal cell behaviors on poly(caprolactone) with or without surface modification: Studies on cell adhesion, survival and proliferation," en, *Journal of Biomaterials Science, Polymer Edition*, vol. 20, no. 14, pp. 1975–1993, 2009.

[109] A. B. Adesida, A. Mulet-Sierra, and N. M. Jomha, "Hypoxia mediated isolation and expansion enhances the chondrogenic capacity of bone marrow mesenchymal stromal cells," eng, *Stem Cell Research & Therapy*, vol. 3, no. 2, p. 9, 2012.

[110] N. F. Matthies, A. Mulet-Sierra, N. M. Jomha, and A. B. Adesida, "Matrix formation is enhanced in co-cultures of human meniscus cells with bone marrow stromal cells," en, *Journal of Tissue Engineering and Regenerative Medicine*, vol. 7, no. 12, pp. 965–973, 2013. arXiv: NIHMS150003.

[111] D. J. Saliken, A. Mulet-Sierra, N. M. Jomha, and A. B. Adesida, "Decreased hypertrophic differentiation accompanies enhanced matrix formation in co-cultures of outer meniscus cells with bone marrow mesenchymal stromal cells," eng, *Arthritis Research and Therapy*, vol. 14, no. 3, R153, 2012.

[112] A. D. Olubamiji, Z. Izadifar, J. L. Si, D. M. Cooper, B. F. Eames, and D. X. Chen, "Modulating mechanical behaviour of 3D-printed cartilage-mimetic PCL scaffolds: Influence of molecular weight and pore geometry," en, *Biofabrication*, vol. 8, no. 2, p. 25 020, 2016.

[113] P. Bursac, S. Arnoczky, and A. York, "Dynamic compressive behavior of human meniscus correlates with its extra-cellular matrix composition," *Biorheology*, vol. 46, no. 3, pp. 227–237, 2009.

[114] R. Spencer Jones, G. C. Keene, D. J. Learmonth, D. Bickerstaff, N. S. Nawana, J. J. Costi, and M. J. Pearcy, "Direct measurement of hoop strains in the intact and torn human medial meniscus," *Clinical Biomechanics*, vol. 11, no. 5, pp. 295–300, 1996.

[115] S. H. Andrews, J. B. Rattner, N. G. Shrive, and J. L. Ronsky, "Swelling significantly affects the material properties of the menisci in compression," English, *Journal of Biomechanics*, vol. 48, no. 8, pp. 1485–1489, 2015.

[116] K. N. Hauch, D. F. Villegas, and T. L. Haut Donahue, "Geometry, time-dependent and failure properties of human meniscal attachments," *Journal of Biomechanics*, vol. 43, no. 3, pp. 463–468, 2010.

[117] A. Marsano, C. M. Medeiros da Cunha, S. Ghanaati, S. Gueven, M. Centola, R. Tsaryk, M. Barbeck, C. Stuedle, A. Barbero, U. Helmrich, S. Schaeren, J. C. Kirkpatrick, A. Banfi, and I. Martin, "Spontaneous In Vivo Chondrogenesis of Bone Marrow-Derived Mesenchymal Progenitor Cells by Blocking Vascular Endothelial Growth Factor Signaling," *STEM CELLS Translational Medicine*, vol. 5, no. 12, pp. 1730–1738, 2016.

[118] N. G. Shrive, J. J. O'Connor, and J. W. Goodfellow, "Load-bearing in the knee joint," English. *Clinical Orthopaedics and Related Research*, vol. NO.131, pp. 279–287, 1978.

[119] T. Fukubayashi and H. Kurosawa, "the contact area and pressure distribution pattern of the knee: A study of normal and osteoarthrotic knee joints," en, *Acta Orthopaedica*, vol. 51, no. 1-6, pp. 871–879, 1980.

[120] S. C. Mordecai, N. Al-Hadithy, H. E. Ware, and C. M. Gupte, "Treatment of meniscal tears: An evidence based approach," *World Journal of Orthopedics*, vol. 5, no. 3, pp. 233–241, 2014.

[121] H. Roos, T. Adalberth, L. Dahlberg, and L. S. Lohmander, "Osteoarthritis of the knee after injury to the anterior cruciate ligament or meniscus: the influence of time and age," eng, *Osteoarthritis and Cartilage*, vol. 3, no. 4, pp. 261–267, 1995.

[122] J. B. McGinity, L. F. Geuss, and R. A. Marvin, *Partial or total meniscectomy. A comparative analysis*, 1977.

[123] L. E. Bolano and W. A. Grana, "Isolated arthroscopic partial meniscectomy: Functional radiographic evaluation at five years," eng, *The American Journal of Sports Medicine*, vol. 21, no. 3, pp. 432–437, 1993.

[124] T. Stein, A. P. Mehling, F. Welsch, R. Von Eisenhart-Rothe, and A. Jäger, "Long-term outcome after arthroscopic meniscal repair versus arthroscopic partial meniscectomy for traumatic meniscal tears," eng, *American Journal of Sports Medicine*, vol. 38, no. 8, pp. 1542–1548, 2010.

[125] C. J. Moran, A. Busilacchi, C. A. Lee, K. A. Athanasiou, and P. C. Verdonk, "Biological augmentation and tissue engineering approaches in meniscus surgery," *Arthroscopy - Journal of Arthroscopic and Related Surgery*, vol. 31, no. 5, pp. 944–955, 2015.

[126] P. Buma, N. N. Ramrattan, T. G. Van Tienen, and R. P. Veth, "Tissue engineering of the meniscus," eng, *Biomaterials*, vol. 25, no. 9, pp. 1523–1532, 2004.

[127] J. Herwig, E. Egner, and E. Buddecke, "Chemical changes of human knee joint menisci in various stages of degeneration," *Annals of the Rheumatic Diseases*, vol. 43, no. 4, pp. 635–640, 1984.

[128] A. Chevrier, M. Nelea, M. B. Hurtig, C. D. Hoemann, and M. D. Buschmann, "Meniscus structure in human, sheep, and rabbit for animal models of meniscus repair," en, *Journal of Orthopaedic Research*, vol. 27, no. 9, pp. 1197–1203, 2009. arXiv: NIHMS150003.

[129] K. Nakata, K. Shino, M. Hamada, T. Mae, T. Miyama, H. Shinjo, S. Horibe, K. Tada, T. Ochi, and H. Yoshikawa, "Human meniscus cell: Characterization of the primary culture and use for tissue engineering," in *Clinical Orthopaedics and Related Research*, Lippincott Williams and Wilkins, 2001.

[130] B. M. Baker, A. S. Nathan, G. R. Huffman, and R. L. Mauck, "Tissue engineering with meniscus cells derived from surgical debris," *Osteoarthritis and Cartilage*, vol. 17, no. 3, pp. 336–345, 2009.

[131] A. J. Fox, A. Bedi, and S. A. Rodeo, "The Basic Science of Human Knee Menisci: Structure, Composition, and Function," *Sports Health*, vol. 4, no. 4, pp. 340–351, 2012.

[132] S. Sart, A. C. Tsai, Y. Li, and T. Ma, *Three-dimensional aggregates of mesenchymal stem cells: Cellular mechanisms, biological properties, and applications*, 2014.

[133] A. M. Mackay, S. C. Beck, J. M. Murphy, F. P. Barry, C. O. Chichester, and M. F. Pittenger, "Chondrogenic differentiation of cultured human mesenchymal stem cells from marrow," eng, *Tissue Engineering*, vol. 4, no. 4, pp. 415–428, 1998.

[134] C. L. Murphy and J. M. Polak, "Control of Human Articular Chondrocyte Differentiation by Reduced Oxygen Tension," en, *Journal of Cellular Physiology*, vol. 199, no. 3, pp. 451–459, 2004.

[135] B. D. Markway, G. K. Tan, G. Brooke, J. E. Hudson, J. J. Cooper-White, and M. R. Doran, "Enhanced chondrogenic differentiation of human bone marrow-derived mesenchymal stem cells in low oxygen environment micropellet cultures," *Cell Transplantation*, vol. 19, no. 1, pp. 29–42, 2010.

[136] T. Sánchez-Elsner, L. M. Botella, B. Velasco, A. Corbí, L. Attisano, and C. Bernabéu, "Synergistic Cooperation between Hypoxia and Transforming Growth Factor-β Pathways on Human Vascular Endothelial Growth Factor Gene Expression," *Journal of Biological Chemistry*, vol. 276, no. 42, pp. 38 527–38 535, 2001.

[137] E. Duval, C. Baugé, R. Andriamanalijaona, H. Bénateau, S. Leclercq, S. Dutoit, L. Poulain, P. Galéra, and K. Boumédiene, "Molecular mechanism of hypoxia-induced chondrogenesis and its application in in vivo cartilage tissue engineering," *Biomaterials*, vol. 33, no. 26, pp. 6042–6051, 2012.

[138] Y. Takahashi, S. Takahashi, Y. Shiga, T. Yoshimi, and T. Miura, "Hypoxic induction of prolyl 4-hydroxylase α(I) in cultured cells," *Journal of Biological Chemistry*, vol. 275, no. 19, pp. 14 139–14 146, 2000.

[139] R. D. Chavez, G. Coricor, J. Perez, H. S. Seo, and R. Serra, "SOX9 protein is stabilized by TGF-β and regulates PAPSS2 mRNA expression in chondrocytes," *Osteoarthritis and Cartilage*, vol. 25, no. 2, pp. 332–340, 2017.

[140] G. Coricor and R. Serra, "TGF-β regulates phosphorylation and stabilization of Sox9 protein in chondrocytes through p38 and Smad dependent mechanisms," *Scientific Reports*, vol. 6, no. 1, p. 38 616, 2016.

[141] B. Berse, J. A. Hunt, R. J. Diegel, P. Morganelli, K. T. Yeo, F. Brown, and R. A. Fava, "Hypoxia augments cytokine (transforming growth factor-beta (TGF-β) and IL-1)-induced vascular endothelial growth factor secretion by human synovial fibroblasts," *Clinical and Experimental Immunology*, vol. 115, no. 1, pp. 176–182, 1999.

[142] I. Martin, G. Vunjak-Novakovic, J. Yang, R. Langer, and L. E. Freed, "Mammalian chondrocytes expanded in the presence of fibroblast growth factor 2 maintain the ability to differentiate and regenerate three- dimensional cartilaginous tissue," *Experimental Cell Research*, vol. 253, no. 2, pp. 681–688, 1999.

[143] S. E. Maxwell and H. D. Delaney, "Designing Experiments and Analysing Data: A Model Comparison Perspective.," *Biometrics*, vol. 47, no. 2, p. 784, 1991.

[144] B. K. Slinker, "The statistics of synergism," *Journal of Molecular and Cellular Cardiology*, vol. 30, no. 4, pp. 723–731, 1998.

[145] K. Pelttari, A. Winter, E. Steck, K. Goetzke, T. Hennig, B. G. Ochs, T. Aigner, and W. Richter, "Premature induction of hypertrophy during in vitro chondrogenesis of human mesenchymal stem cells correlates with calcification and vascular invasion after ectopic transplantation in SCID mice," *Arthritis and Rheumatism*, vol. 54, no. 10, pp. 3254–3266, 2006.

[146] G. L. Semenza, "Hypoxia-inducible factor 1: Master regulator of O2 homeostasis," *Current Opinion in Genetics and Development*, vol. 8, no. 5, pp. 588–594, 1998.

[147] E. A. Makris, R. F. MacBarb, N. K. Paschos, J. C. Hu, and K. A. Athanasiou, "Combined use of chondroitinase-ABC, TGF-β1, and collagen crosslinking agent lysyl oxidase to engineer functional neotissues for fibrocartilage repair," *Biomaterials*, vol. 35, no. 25, pp. 6787–6796, 2014.

[148] N. J. Gunja and K. A. Athanasiou, "Additive and synergistic effects of bFGF and hypoxia on leporine meniscus cell-seeded PLLA scaffolds," en, *Journal of Tissue Engineering and Regenerative Medicine*, vol. 4, no. 2, pp. 115–122, 2010.

[149] B. A. Byers, R. L. Mauck, I. E. Chiang, and R. S. Tuan, "Transient exposure to transforming growth factor beta 3 under serum-free conditions enhances the biomechanical and biochemical maturation of tissue-engineered cartilage," *Tissue Engineering - Part A.*, vol. 14, no. 11, pp. 1821–1834, 2008.

[150] A. H. Huang, A. Stein, R. S. Tuan, and R. L. Mauck, "Transient exposure to transforming growth factor beta 3 improves the mechanical properties of mesenchymal stem cell-laden cartilage constructs in a density-dependent manner," *Tissue Engineering - Part A*, vol. 15, no. 11, pp. 3461–3472, 2009.

[151] B. D. Markway, H. Cho, and B. Johnstone, "Hypoxia promotes redifferentiation and suppresses markers of hypertrophy and degeneration in both healthy and osteoarthritic chondrocytes," *Arthritis Research and Therapy*, vol. 15, no. 4, R92, 2013.

[152] C. P. Bracken, M. L. Whitelaw, and D. J. Peet, *The hypoxia-inducible factors: Key transcriptional regulators of hypoxic responses*, 2003.

[153] P. C. Verdonk, R. G. Forsyth, J. Wang, K. F. Almqvist, R. Verdonk, E. M. Veys, and G. Verbruggen, "Characterisation of human knee meniscus cell phenotype," *Osteoarthritis and Cartilage*, vol. 13, no. 7, pp. 548–560, 2005.

[154] P. T. Paradowski, L. S. Lohmander, and M. Englund, "Osteoarthritis of the knee after meniscal resection: Long term radiographic evaluation of disease progression," *Osteoarthritis and Cartilage*, vol. 24, no. 5, pp. 794–800, 2016.

[155] K. A. Athanasiou and J. Sanchez-Adams, "Engineering the Knee Meniscus," en, *Synthesis Lectures on Tissue Engineering*, vol. 1, no. 1, pp. 1–97, 2009.

[156] I. B. Coimbra, S. A. Jimenez, D. F. Hawkins, S. Piera-Velazquez, and D. G. Stokes, "Hypoxia inducible factor-1 alpha expression in human normal and osteoarthritic chondrocytes," *Osteoarthritis and Cartilage*, vol. 12, no. 4, pp. 336–345, 2004.

[157] F. Pauwels and Y. C. Fung, *Biomechanics of the Locomotor Apparatus, Contributions on the Functional Anatomy of the Locomotor Apparatus*, 4. 1982, vol. 104, pp. 346–347.

[158] N. J. Gunja, R. K. Uthamanthil, and K. A. Athanasiou, "Effects of TGF-β1 and hydrostatic pressure on meniscus cell-seeded scaffolds," *Biomaterials*, vol. 30, no. 4, pp. 565–573, 2009.

[159] S. M. Imler, A. N. Doshi, and M. E. Levenston, "Combined effects of growth factors and static mechanical compression on meniscus explant biosynthesis," *Osteoarthritis and Cartilage*, vol. 12, no. 9, pp. 736–744, 2004.

[160] B. Zielinska, M. Killian, M. Kadmiel, M. Nelsen, and T. L. Haut Donahue, "Meniscal tissue explants response depends on level of dynamic compressive strain," *Osteoarthritis and Cartilage*, vol. 17, no. 6, pp. 754–760, 2009.

[161] T. Natsu-Ume, T. Majima, C. Reno, N. G. Shrive, C. B. Frank, and D. A. Hart, "Menisci of the rabbit knee require mechanical loading to maintain homeostasis: Cyclic hydrostatic compression in vitro prevents derepression of catabolic genes," in *Journal of Orthopaedic Science*, vol. 10, Springer Japan, 2005, pp. 396–405.

[162] M. L. Upton, J. Chen, F. Guilak, and L. A. Setton, "Differential effects of static and dynamic compression on meniscal cell gene expression," en, *Journal of Orthopaedic Research*, vol. 21, no. 6, pp. 963–969, 2003.

[163] A. C. Aufderheide and K. A. Athanasiou, "A direct compression stimulator for articular cartilage and meniscal explants," en, *Annals of Biomedical Engineering*, vol. 34, no. 9, pp. 1463–1474, 2006.

[164] S. jin Shin, B. Fermor, J. B. Weinberg, D. S. Pisetsky, and F. Guilak, "Regulation of matrix turnover in meniscal explants: Role of mechanical stress, interleukin-1, and nitric oxide," *Journal of Applied Physiology*, vol. 95, no. 1, pp. 308–313, 2003.

[165] C.-Y. C. Huang, K. L. Hagar, L. E. Frost, Y. Sun, and H. S. Cheung, "Effects of Cyclic Compressive Loading on Chondrogenesis of Rabbit Bone-Marrow Derived Mesenchymal Stem Cells," en, *Stem Cells*, vol. 22, no. 3, pp. 313–323, 2004.

[166] K. D. Allen and K. A. Athanasiou, "Viscoelastic characterization of the porcine temporomandibular joint disc under unconfined compression," *Journal of Biomechanics*, vol. 39, no. 2, pp. 312–322, 2006.

[167] K. J. Livak and T. D. Schmittgen, "Analysis of relative gene expression data using real-time quantitative PCR and the 2-ΔΔCT method," *Methods*, vol. 25, no. 4, pp. 402–408, 2001. arXiv: 1003.3921v1.

[168] A. Namiki, E. Brogi, M. Kearney, E. A. Kim, T. Wu, T. Couffinhal, L. Varticovski, and J. M. Isner, "Hypoxia induces vascular endothelial growth factor in cultured human endothelial cells," *Journal of Biological Chemistry*, vol. 270, no. 52, pp. 31 189–31 195, 1995.

[169] E. A. Makris, J. C. Hu, and K. A. Athanasiou, "Hypoxia-induced collagen crosslinking as a mechanism for enhancing mechanical properties of engineered articular cartilage," en, *Osteoarthritis and Cartilage*, vol. 21, no. 4, pp. 634–641, 2013. arXiv: NIHMS150003.

[170] J. B. Fitzgerald, M. Jin, D. Dean, D. J. Wood, M. H. Zheng, and A. J. Grodzinsky, "Mechanical Compression of Cartilage Explants Induces Multiple Time-dependent Gene Expression Patterns and Involves Intracellular Calcium and Cyclic AMP," *Journal of Biological Chemistry*, vol. 279, no. 19, pp. 19 502–19 511, 2004.

[171] S. Scholtes, E. Krämer, M. Weisser, W. Roth, R. Luginbühl, T. Grossner, and W. Richter, "Global chondrocyte gene expression after a single anabolic loading period: Time evolution and re-inducibility of mechano-responses," *Journal of Cellular Physiology*, vol. 233, no. 1, pp. 699–711, 2018.

[172] A. C. Aufderheide and K. A. Athanasiou, "Assessment of a bovine co-culture, scaffold-free method for growing meniscus-shaped constructs," *Tissue Engineering*, vol. 13, no. 9, pp. 2195–2205, 2007.

[173] D. Wendt, A. Marsano, M. Jakob, M. Heberer, and I. Martin, "Oscillating perfusion of cell suspensions through three-dimensional scaffolds enhances cell seeding efficiency and uniformity," *Biotechnology and Bioengineering*, vol. 84, no. 2, pp. 205–214, 2003.

[174] R. L. Mauck, C. C. Wang, E. S. Oswald, G. A. Ateshian, and C. T. Hung, "The role of cell seeding density and nutrient supply for articular cartilage tissue engineering with deformational loading," *Osteoarthritis and Cartilage*, vol. 11, no. 12, pp. 879–890, 2003.

[175] C. R. Lee, A. J. Grodzinsky, and M. Spector, "Biosynthetic response of passaged chondrocytes in a type II collagen scaffold to mechanical compression," *Journal of Biomedical Materials Research - Part A*, vol. 64, no. 3, pp. 560–569, 2003.

[176] O. Schätti, S. Grad, J. Goldhahn, G. Salzmann, Z. Li, M. Alini, and M. J. Stoddart, "A combination of shear and dynamic compression leads to mechanically induced chondrogenesis of human mesenchymal stem cells.," *European cells and materials*, vol. 22, no. 214-225, pp. 214–225, 2011.

[177] S. H. Andrews, J. B. Rattner, Z. Abusara, A. Adesida, N. G. Shrive, and J. L. Ronsky, "Tie-fibre structure and organization in the knee menisci," eng, *Journal of Anatomy*, vol. 224, no. 5, pp. 531–537, 2014.

[178] A. Bertolo, L. Ettinger, N. Aebli, D. Haschtmann, M. Baur, U. Berlemann, S. J. Ferguson, and J. V. Stoyanov, "The in vitro effects of dexamethasone, insulin and triiodothyronine on degenerative human intervertebral disc cells under normoxic and hypoxic conditions," *European Cells and Materials*, vol. 21, pp. 221–229, 2011.

[179] R. L. Mauck, C. T. Hung, and G. A. Ateshian, "Modeling of Neutral Solute Transport in a Dynamically Loaded Porous Permeable Gel: Implications for Articular Cartilage Biosynthesis and Tissue Engineering," *Journal of Biomechanical Engineering*, vol. 125, no. 5, pp. 602–614, 2003.

[180] N. J. Gunja and K. A. Athanasiou, "Passage and reversal effects on gene expression of bovine meniscal fibrochondrocytes," *Arthritis Research and Therapy*, vol. 9, no. 5, pp. 1–12, 2007.

[181] J. M. Patel, B. C. Wise, E. D. Bonnevie, and R. L. Mauck, *A Systematic Review and Guide to Mechanical Testing for Articular Cartilage Tissue Engineering*, 2019.

[182] S. M. Vickers, L. S. Squitieri, and M. Spector, "Effects of cross-linking type II collagen-GAG scaffolds on chondrogenesis in vitro: Dynamic pore reduction promotes cartilage formation," *Tissue Engineering*, vol. 12, no. 5, pp. 1345–1355, 2006.

[183] B. Kinner and M. Spector, "Smooth muscle actin expression by human articular chondrocytes and their contraction of a collagen-glycosaminoglycan matrix in vitro," *Journal of Orthopaedic Research*, vol. 19, no. 2, pp. 233–241, 2001.

[184] T. Takroni, L. Laouar, A. Adesida, J. A. Elliott, and N. M. Jomha, "Anatomical study: comparing the human, sheep and pig knee meniscus," *Journal of Experimental Orthopaedics*, vol. 3, no. 1, 2016.

[185] E. G. Lima, L. Bian, K. W. Ng, R. L. Mauck, B. A. Byers, R. S. Tuan, G. A. Ateshian, and C. T. Hung, "The beneficial effect of delayed compressive loading on tissue-engineered cartilage constructs cultured with TGF-β3," *Osteoarthritis and Cartilage*, vol. 15, no. 9, pp. 1025–1033, 2007.

[186] C. Pauli, S. P. Grogan, S. Patil, S. Otsuki, A. Hasegawa, J. Koziol, M. K. Lotz, and D. D. D'Lima, "MAcroscopic And Histopathologic Analysis Of Human Knee Menisci In Aging And Osteoarthritis," *Osteoarthritis and Cartilage*, vol. 19, no. 9, pp. 1132–1141, 2011.

[187] L. Wachsmuth, S. Söder, Z. Fan, F. Finger, and T. Aigner, "Immunolocalization of matrix proteins in different human cartilage subtypes," *Histology and Histopathology*, vol. 21, no. 4-6, pp. 477–485, 2006.

[188] Y. Sun, "Histological Examination of Collagen and Proteoglycan Changes in Osteoarthritic Menisci," *The Open Rheumatology Journal*, vol. 6, no. 1, pp. 24–32, 2012.

[189] I. E. Erickson, S. R. Kestle, K. H. Zellars, M. J. Farrell, M. Kim, J. A. Burdick, and R. L. Mauck, "High mesenchymal stem cell seeding densities in hyaluronic acid hydrogels produce engineered cartilage with native tissue properties," *Acta Biomaterialia*, vol. 8, no. 8, pp. 3027–3034, 2012.

[190] R. Santoro, A. L. Olivares, G. Brans, D. Wirz, C. Longinotti, D. Lacroix, I. Martin, and D. Wendt, "Bioreactor based engineering of large-scale human cartilage grafts for joint resurfacing," *Biomaterials*, vol. 31, no. 34, pp. 8946–8952, 2010.

[191] K. Shahin and P. M. Doran, "Tissue engineering of cartilage using a mechanobioreactor exerting simultaneous mechanical shear and compression to simulate the rolling action of articular joints," *Biotechnology and Bioengineering*, vol. 109, no. 4, pp. 1060–1073, 2012.

[192] B. L. Schumacher, T. A. Schmidt, M. S. Voegtline, A. C. Chen, and R. L. Sah, "Proteoglycan 4 (PRG4) synthesis and immunolocalization in bovine meniscus," *Journal of Orthopaedic Research*, vol. 23, no. 3, pp. 562–568, 2005.

[193] C. Rangger, T. Klestil, W. Gloetzer, G. Kemmler, and K. P. Benedetto, "Osteoarthritis After Arthroscopic Partial Meniscectomy," *The American Journal of Sports Medicine*, vol. 23, no. 2, pp. 240–244, 1995.

[194] N. J. Gunja, D. J. Huey, R. A. James, and K. A. Athanasiou, "Effects of agarose mould compliance and surface roughness on self-assembled meniscus-shaped constructs," en, *Journal of Tissue Engineering and Regenerative Medicine*, vol. 3, no. 7, pp. 521–530, 2009.

[195] R. L. Mauck, M. A. Soltz, C. C. Wang, D. D. Wong, P. H. G. Chao, W. B. Valhmu, C. T. Hung, and G. A. Ateshian, "Functional tissue engineering of articular cartilage through dynamic loading of chondrocyte-seeded agarose gels," *Journal of Biomechanical Engineering*, vol. 122, no. 3, pp. 252–260, 2000.

[196] L. W. Gamer, R. R. Shi, A. Gendelman, D. Mathewson, J. Gamer, and V. Rosen, "Identification and characterization of adult mouse meniscus stem/progenitor cells," *Connective Tissue Research*, vol. 58, no. 3-4, pp. 238–245, 2017.

[197] H. Sun, X. Wen, H. Li, P. Wu, M. Gu, X. Zhao, Z. Zhang, S. Hu, G. Mao, R. Ma, W. Liao, and Z. Zhang, "Single-cell RNA-seq analysis identifies meniscus progenitors and reveals the progression of meniscus degeneration," *Annals of the Rheumatic Diseases*, vol. 79, no. 3, pp. 408–417, 2019.

[198] W. Shen, J. Chen, T. Zhu, L. Chen, W. Zhang, Z. Fang, B. C. Heng, Z. Yin, X. Chen, J. Ji, W. Chen, and H.-W. Ouyang, "Intra-Articular Injection of Human Meniscus Stem/Progenitor Cells Promotes Meniscus Regeneration and Ameliorates Osteoarthritis Through Stromal Cell-Derived Factor-1/CXCR4-Mediated Homing," *STEM CELLS Translational Medicine*, vol. 3, no. 3, pp. 387–394, 2014.

[199] H. Muhammad, B. Schminke, C. Bode, M. Roth, J. Albert, S. Von Der Heyde, V. Rosen, and N. Miosge, "Human migratory meniscus progenitor cells are controlled via the TGF-β pathway," *Stem Cell Reports*, vol. 3, no. 5, pp. 789–803, 2014.

[200] H. Muhammad, "Human and mouse meniscus progenitor cells and their role in meniscus tissue regeneration," Ph.D. dissertation, Georg-August University Thesis, 2014.

[201] Y. Matsukura, T. Muneta, K. Tsuji, H. Koga, and I. Sekiya, "Mesenchymal stem cells in synovial fluid increase after meniscus injury," *Clinical Orthopaedics and Related Research*, vol. 472, no. 5, pp. 1357–1364, 2014.

[202] S. Tarafder, J. Gulko, K. H. Sim, J. Yang, J. L. Cook, and C. H. Lee, "Engineered Healing of Avascular Meniscus Tears by Stem Cell Recruitment," *Scientific Reports*, vol. 8, no. 1, p. 8150, 2018.

[203] S. P. Grogan, S. F. Duffy, C. Pauli, M. K. Lotz, and D. D. D'Lima, "Gene expression profiles of the meniscus avascular phenotype: A guide for meniscus tissue engineering," *Journal of Orthopaedic Research*, vol. 36, no. 7, pp. 1947–1958, 2018.

[204] K. Okada, D. Mori, Y. Makii, H. Nakamoto, Y. Murahashi, F. Yano, S. H. Chang, Y. Taniguchi, H. Kobayashi, H. Semba, N. Takeda, W. Piao, K. Hanaoka, T. Nagano, S. Tanaka, and T. Saito, "Hypoxia-inducible factor-1 alpha maintains mouse articular cartilage through suppression of NF-κB signaling," *Scientific Reports*, vol. 10, no. 1, pp. 1–11, 2020.

[205] J. L. Puetzer, B. N. Brown, J. J. Ballyns, and L. J. Bonassar, "The effect of IGF-I on anatomically shaped tissue-engineered menisci," *Tissue Engineering - Part A*, vol. 19, no. 11-12, pp. 1443–1450, 2013.

[206] T. M. Griffin and F. Guilak, "The role of mechanical loading in the onset and progression of osteoarthritis," *Exercise and Sport Sciences Reviews*, vol. 33, no. 4, pp. 195–200, 2005. arXiv: NIHMS150003.

[207] T. Furumatsu, T. Kanazawa, Y. Yokoyama, N. Abe, and T. Ozaki, "Inner meniscus cells maintain higher chondrogenic phenotype compared with outer meniscus cells," *Connective Tissue Research*, vol. 52, no. 6, pp. 459–465, 2011.

[208] B. L. Thoms, K. A. Dudek, J. E. Lafont, and C. L. Murphy, "Hypoxia Promotes the Production and Inhibits the Destruction of Human Articular Cartilage," *Arthritis and Rheumatism*, vol. 65, no. 5, pp. 1302–1312, 2013.

[209] A. V. Stone, R. F. Loeser, M. F. Callahan, M. A. McNulty, D. L. Long, R. R. Yammani, S. Bean, K. Vanderman, S. Chubinskaya, and C. M. Ferguson, "Role of the Hypoxia-Inducible Factor Pathway in Normal and Osteoarthritic Meniscus and in Mice after Destabilization of the Medial Meniscus," *Cartilage*, 2020.

[210] N. N. Taleb, *Antifragile: Things that gain from disorder*, 2012.

[211] H. M. Frost, *Bone's Mechanostat: A 2003 Update*, 2003.

[212] W. Roux, *Die Entwickelungsmechanik; ein neuer Zweig der biologischen Wissenschaft Vols I and II*. 1905.

[213] F. Guilak, D. L. Butler, S. A. Goldstein, and F. P. Baaijens, *Biomechanics and mechanobiology in functional tissue engineering*, 2014.

[214] D. Vader, A. Kabla, D. Weitz, and L. Mahadevan, "Strain-induced alignment in collagen gels," *PLoS ONE*, vol. 4, no. 6, J. Langowski, Ed., e5902, 2009.

[215] S. Thomopoulos, R. Das, V. Birman, L. Smith, K. Ku, E. L. Elson, K. M. Pryse, J. P. Marquez, and G. M. Genin, "Fibrocartilage tissue engineering: The role of the stress environment on cell morphology and matrix expression," *Tissue Engineering - Part A*, vol. 17, no. 7-8, pp. 1039–1053, 2011.

[216] A. J. Grodzinsky, M. E. Levenston, M. Jin, and E. H. Frank, "Cartilage tissue remodeling in response to mechanical forces," *Annual Review of Biomedical Engineering*, vol. 2, no. 2000, pp. 691–713, 2000.

[217] S. C. Tran, A. J. Cooley, and S. H. Elder, "Effect of a mechanical stimulation bioreactor on tissue engineered, scaffold-free cartilage," *Biotechnology and Bioengineering*, vol. 108, no. 6, pp. 1421–1429, 2011.

[218] H. Park, D. H. Rosenzweig, and S. N. Nazhat, "Tenogenic differentiation of mesenchymal stem cells in aligned dense collagen hydrogels by mechanical stimulation," in *Proceedings of the 36th Annual Meeting of the Canadian Biomaterials Society*, 2021.

[219] N. J. Gunja and K. A. Athanasiou, "Effects of hydrostatic pressure on leporine meniscus cell-seeded PLLA scaffolds," *Journal of Biomedical Materials Research - Part A*, vol. 92, no. 3, pp. 896–905, 2010.

[220] G. D. Nicodemus and S. J. Bryant, "Mechanical loading regimes affect the anabolic and catabolic activities by chondrocytes encapsulated in PEG hydrogels," *Osteoarthritis and Cartilage*, vol. 18, no. 1, pp. 126–137, 2010.

[221] L. F. Lau, *CCN1/CYR61: The very model of a modern matricellular protein*, 2011.

[222] B. Chaqour and M. Goppelt-Struebe, "Mechanical regulation of the Cyr61/CCN1 and CTGF/CCN2 proteins: Implications in mechanical stress-associated pathologies," *FEBS Journal*, vol. 273, no. 16, pp. 3639–3649, 2006.

[223] C. H. Turner, "Three rules for bone adaptation to mechanical stimuli," *Bone*, vol. 23, no. 5, pp. 399–407, 1998.

[224] D. M. Knapik, P. Perera, J. Nam, A. D. Blazek, B. Rath, B. Leblebicioglu, H. Das, L. C. Wu, T. E. Hewett, S. K. Agarwal, A. G. Robling, D. C. Flanigan, B. S. Lee, and S. Agarwal, *Mechanosignaling in bone health, trauma and inflammation*, 2014.

[225] J. Yu, F. Liang, H. Huang, P. Pirttiniemi, and D. Yu, "Effects of loading on chondrocyte hypoxia, HIF-1α and VEGF in the mandibular condylar cartilage of young rats," *Orthodontics and Craniofacial Research*, vol. 21, no. 1, pp. 41–47, 2018.

[226] T. Nagel and D. J. Kelly, "Mechanically induced structural changes during dynamic compression of engineered cartilaginous constructs can potentially explain increases in bulk mechanical properties," *Journal of the Royal Society Interface*, vol. 9, no. 69, pp. 777–789, 2012.

[227] J. E. Jeon, K. Schrobback, D. W. Hutmacher, and T. J. Klein, "Dynamic compression improves biosynthesis of human zonal chondrocytes from osteoarthritis patients," *Osteoarthritis and Cartilage*, vol. 20, no. 8, pp. 906–915, 2012.

[228] L. G. Alexopoulos, L. A. Setton, and F. Guilak, "The biomechanical role of the chondrocyte pericellular matrix in articular cartilage," *Acta Biomaterialia*, vol. 1, no. 3, pp. 317–325, 2005.

[229] N. E. Timmins, A. Scherberich, J. A. Früh, M. Heberer, I. Martin, and M. Jakob, "Three-dimensional cell culture and tissue engineering in a T-CUP (Tissue Culture under Perfusion)," *Tissue Engineering*, vol. 13, no. 8, pp. 2021–2028, 2007.

[230] R. M. Schulz, N. Wüstneck, C. C. Van Donkelaar, J. C. Shelton, and A. Bader, "Development and validation of a novel bioreactor system for load- and perfusion-controlled tissue engineering of chondrocyte-constructs," *Biotechnology and Bioengineering*, vol. 101, no. 4, pp. 714–728, 2008.

[231] J. L. Puetzer, T. Ma, I. Sallent, A. Gelmi, and M. M. Stevens, "Driving Hierarchical Collagen Fiber Formation for Functional Tendon, Ligament, and Meniscus Replacement," *Biomaterials*, vol. 269, p. 120 527, 2021.

[232] Z. Z. Zhang, Y. R. Chen, S. J. Wang, F. Zhao, X. G. Wang, F. Yang, J. J. Shi, Z. G. Ge, W. Y. Ding, Y. C. Yang, T. Q. Zou, J. Y. Zhang, J. K. Yu, and D. Jiang, "Orchestrated biomechanical, structural, and biochemical stimuli for engineering anisotropic meniscus," *Science Translational Medicine*, vol. 11, no. 487, p. 750, 2019.

[233] J. A. McHenry, B. Zielinska, and T. L. Haut Donahue, "Proteoglycan breakdown of meniscal explants following dynamic compression using a novel bioreactor," *Annals of Biomedical Engineering*, vol. 34, no. 11, pp. 1758–1766, 2006.

[234] A. L. McNulty, B. T. Estes, R. E. Wilusz, J. B. Weinberg, and F. Guilak, "Dynamic loading enhances integrative meniscal repair in the presence of interleukin-1," *Osteoarthritis and Cartilage*, vol. 18, no. 6, pp. 830–838, 2010.

[235] M. J. Stoddart, L. Ettinger, and H. J. Häuselmann, "Enhanced matrix synthesis in de novo, scaffold free cartilage-like tissue subjected to compression and shear," *Biotechnology and Bioengineering*, vol. 95, no. 6, pp. 1043–1051, 2006.

[236] Z. Li, S. J. Yao, M. Alini, and M. J. Stoddart, "Chondrogenesis of human bone marrow mesenchymal stem cells in fibrin-polyurethane composites is modulated by frequency and amplitude of dynamic compression and shear stress," in *Tissue Engineering - Part A*, vol. 16, Mary Ann Liebert Inc., 2010, pp. 575–584.

[237] W. M. Weiss, A. Mulet-Sierra, M. Kunze, N. M. Jomha, and A. B. Adesida, "Coculture of meniscus cells and mesenchymal stem cells in simulated microgravity," *npj Microgravity*, vol. 3, no. 1, pp. 1–13, 2017.

[238] D. R. Eyre and H. Muir, "Quantitative analysis of types I and II collagens in human intervertebral discs at various ages," *BBA - Protein Structure*, vol. 492, no. 1, pp. 29–42, 1977.

[239] A. A.J. and A. K.A., "Design characteristics for the tissue engineering of cartilaginous tissues.," *Annals of biomedical engineering*, vol. 32, no. 1, pp. 2–17, 2004.

[240] M. A. Sweigart and K. A. Athanasiou, "Toward tissue engineering of the knee meniscus," in *Tissue Engineering*, vol. 7, Tissue Eng, 2001, pp. 111–129.

[241] A. R. Markes, J. D. Hodax, and C. B. Ma, *Meniscus Form and Function*, 2020.

[242] I. D. McDermott and A. A. Amis, *The consequences of meniscectomy*, 2006.

[243] M. M. Pillai, J. Gopinathan, R. Selvakumar, and A. Bhattacharyya, *Human Knee Meniscus Regeneration Strategies: a Review on Recent Advances*, 2018.

[244] A. Marsano, S. J. Millward-Sadler, D. M. Salter, A. Adesida, T. Hardingham, E. Tognana, E. Kon, C. Chiari-Grisar, S. Nehrer, M. Jakob, and I. Martin, "Differential cartilaginous tissue formation by human synovial membrane, fat pad, meniscus cells and articular chondrocytes," en, *Osteoarthritis and Cartilage*, vol. 15, no. 1, pp. 48–58, 2007.

[245] C. Chiari, U. Koller, B. Kapeller, R. Dorotka, U. Bindreiter, and S. Nehrer, "Different behavior of meniscal cells in collagen II/I,III and Hyaff-11 scaffolds in vitro," *Tissue Engineering - Part A.*, vol. 14, no. 8, pp. 1295–1304, 2008.

[246] C. A. Pangborn and K. A. Athanasiou, "Growth factors and fibrochondrocytes in scaffolds," *Journal of Orthopaedic Research*, vol. 23, no. 5, pp. 1184–1190, 2005.

[247] C. A. Pangborn and K. A. Athanasiou, "Effects of growth factors on meniscal fibrochondrocytes," *Tissue Engineering*, vol. 11, no. 7-8, pp. 1141–1148, 2005.

[248] P. Angele, B. Johnstone, R. Kujat, J. Zellner, M. Nerlich, V. Goldberg, and J. Yoo, "Stem cell based tissue engineering for meniscus repair," *Journal of Biomedical Materials Research - Part A*, vol. 85, no. 2, pp. 445–455, 2008.

[249] C. Chiari, U. Koller, R. Dorotka, C. Eder, R. Plasenzotti, S. Lang, L. Ambrosio, E. Tognana, E. Kon, D. Salter, and S. Nehrer, "A tissue engineering approach to meniscus regeneration in a sheep model," *Osteoarthritis and Cartilage*, vol. 14, no. 10, pp. 1056–1065, 2006.

[250] E. Kon, G. Filardo, M. Tschon, M. Fini, G. Giavaresi, L. M. Reggiani, C. Chiari, S. Nehrer, I. Martin, D. M. Salter, L. Ambrosio, and M. Marcacci, *Tissue engineering for total meniscal substitution: Animal study in sheep model-results at 12 months*, 2012.

[251] H. Yu, A. B. Adesida, and N. M. Jomha, "Meniscus repair using mesenchymal stem cells - A comprehensive review," *Stem Cell Research and Therapy*, vol. 6, no. 1, pp. 1–10, 2015.

[252] Y. Moriguchi, K. Tateishi, W. Ando, K. Shimomura, Y. Yonetani, Y. Tanaka, K. Kita, D. A. Hart, A. Gobbi, K. Shino, H. Yoshikawa, and N. Nakamura, "Repair of meniscal lesions using a scaffold-free tissue-engineered construct derived from allogenic synovial MSCs in a miniature swine model," *Biomaterials*, vol. 34, no. 9, pp. 2185–2193, 2013.

[253] M. Anderson-Baron, M. Kunze, A. Mulet-Sierra, and A. B. Adesida, "Effect of cell seeding density on matrix-forming capacity of meniscus fibrochondrocytes and nasal chondrocytes in meniscus tissue engineering," *FASEB Journal*, vol. 34, no. 4, pp. 5538–5551, 2020.

[254] H. Kwon, W. E. Brown, C. A. Lee, D. Wang, N. Paschos, J. C. Hu, and K. A. Athanasiou, *Surgical and tissue engineering strategies for articular cartilage and meniscus repair*, 2019.

[255] J. Zellner, M. Mueller, A. Berner, T. Dienstknecht, R. Kujat, M. Nerlich, B. Hennemann, M. Koller, L. Prantl, M. Angele, and P. Angele, "Role of mesenchymal stem cells in tissue engineering of meniscus," *Journal of Biomedical Materials Research Part A*, vol. 9999A, no. 4, NA–NA, 2010.

[256] J. M. Murphy, D. J. Fink, E. B. Hunziker, and F. P. Barry, "Stem Cell Therapy in a Caprine Model of Osteoarthritis," *Arthritis and Rheumatism*, vol. 48, no. 12, pp. 3464–3474, 2003.

[257] Y. C. Chen, R. N. Chen, H. J. Jhan, D. Z. Liu, H. O. Ho, Y. Mao, J. Kohn, and M. T. Sheu, "Development and Characterization of Acellular Extracellular Matrix Scaffolds from Porcine Menisci for Use in Cartilage Tissue Engineering," *Tissue Engineering - Part C: Methods*, vol. 21, no. 9, pp. 971–986, 2015.

[258] Z. Ding and H. Huang, "Mesenchymal stem cells in rabbit meniscus and bone marrow exhibit a similar feature but a heterogeneous multi-differentiation potential: Superiority of meniscus as a cell source for meniscus repair Evolutionary developmental biology and morphology," *BMC Musculoskeletal Disorders*, vol. 16, no. 1, p. 65, 2015.

[259] T. D. Bornes, N. M. Jomha, A. Mulet-Sierra, and A. B. Adesida, "Hypoxic culture of bone marrow-derived mesenchymal stromal stem cells differentially enhances in vitro chondrogenesis within cell-seeded collagen and hyaluronic acid porous scaffolds," *Stem Cell Research and Therapy*, vol. 6, no. 1, pp. 1–18, 2015.

[260] T. D. Bornes, N. M. Jomha, A. Mulet-Sierra, and A. B. Adesida, "Optimal seeding densities for in vitro chondrogenesis of two- and three-dimensional-isolated and -expanded bone marrow-derived mesenchymal stromal stem cells within a porous collagen scaffold," *Tissue Engineering - Part C: Methods*, vol. 22, no. 3, pp. 208–220, 2016.

[261] R. W. Farndale, D. J. Buttle, and A. J. Barrett, "Improved quantitation and discrimination of sulphated glycosaminoglycans by use of dimethylmethylene blue," *BBA - General Subjects*, vol. 883, no. 2, pp. 173–177, 1986.

[262] T. Nakano, J. R. Thompson, and F. X. Aherne, "Distribution of glycosaminoglycans and the nonreducible collagen crosslink, pyridinoline in porcine menisci," *Canadian Journal of Veterinary Research*, vol. 50, no. 4, pp. 532–536, 1986.

[263] A. Banfi, A. Muraglia, B. Dozin, M. Mastrogiacomo, R. Cancedda, and R. Quarto, "Proliferation kinetics and differentiation potential of ex vivo expanded human bone marrow stromal cells: Implications for their use in cell therapy," *Experimental Hematology*, vol. 28, no. 6, pp. 707–715, 2000.

[264] S. R. Tew, Y. Li, P. Pothancharoen, L. M. Tweats, R. E. Hawkins, and T. E. Hardingham, "Retroviral transduction with SOX9 enhances re-expression of the chondrocyte phenotype in passaged osteoarthritic human articular chondrocytes," *Osteoarthritis and Cartilage*, vol. 13, no. 1, pp. 80–89, 2005.

[265] O. J. Marshall and V. R. Harley, "Molecular mechanisms of SOX9 action," *Molecular Genetics and Metabolism*, vol. 71, no. 3, pp. 455–462, 2000.

[266] W. Bi, J. M. Deng, Z. Zhang, R. R. Behringer, and B. De Crombrugghe, "Sox9 is required for cartilage formation," *Nature Genetics*, vol. 22, no. 1, pp. 85–89, 1999.

[267] M. C. McCorry and L. J. Bonassar, "Fiber development and matrix production in tissue-engineered menisci using bovine mesenchymal stem cells and fibrochondrocytes," *Connective Tissue Research*, vol. 58, no. 3-4, pp. 329–341, 2017.

[268] W. Kafienah, S. Mistry, S. C. Dickinson, T. J. Sims, I. Learmonth, and A. P. Hollander, "Three-dimensional cartilage tissue engineering using adult stem cells from osteoarthritis patients," *Arthritis and Rheumatism*, vol. 56, no. 1, pp. 177–187, 2007.

[269] J. Fischer, A. Dickhut, M. Rickert, and W. Richter, "Human articular chondrocytes secrete parathyroid hormone-related protein and inhibit hypertrophy of mesenchymal stem cells in coculture during chondrogenesis," *Arthritis and Rheumatism*, vol. 62, no. 9, pp. 2696–2706, 2010.

[270] D. F. Villegas and T. L. Donahue, "Collagen morphology in human meniscal attachments: A SEM study," *Connective Tissue Research*, vol. 51, no. 5, pp. 327–336, 2010.

[271] J. L. Puetzer and L. J. Bonassar, "High density type i collagen gels for tissue engineering of whole menisci," *Acta Biomaterialia*, vol. 9, no. 8, pp. 7787–7795, 2013.

[272] J. L. Puetzer, E. Koo, and L. J. Bonassar, "Induction of fiber alignment and mechanical anisotropy in tissue engineered menisci with mechanical anchoring," *Journal of Biomechanics*, vol. 48, no. 8, pp. 1436–1443, 2015.

[273] J. B. Thorlund, K. B. Hare, and L. S. Lohmander, "Large increase in arthroscopic meniscus surgery in the middle-aged and older population in Denmark from 2000 to 2011," *Acta Orthopaedica*, vol. 85, no. 3, pp. 287–292, 2014.

[274] C. A. McDevitt and R. J. Webber, "The ultrastructure and biochemistry of meniscal cartilage," *Clinical Orthopaedics and Related Research*, no. 252, pp. 8–18, 1990.

[275] T. Tanaka, K. Fujii, and Y. Kumagae, "Comparison of biochemical characteristics of cultured fibrochondrocytes isolated from the inner and outer regions of human meniscus," *Knee Surgery, Sports Traumatology, Arthroscopy*, vol. 7, no. 2, pp. 75–80, 1999.

[276] P. M. Mamatha, J. Gopinathan, V. Elakkiya, M. Sathishkumar, S. R. Sundarrajan, K. S. Sahanand, A. Bhattacharyya, and R. Selvakumar, *Knee Meniscus Injury: Insights on Tissue engineering Strategies Through Retrospective Analysis and In Silico Modeling*, 2019.

[277] R. J. Williams, J. C. Dreese, and C. T. Chen, "Chondrocyte Survival and Material Properties of Hypothermically Stored Cartilage: An Evaluation of Tissue Used for Osteochondral Allograft Transplantation," *American Journal of Sports Medicine*, vol. 32, no. 1, pp. 132–139, 2004.

[278] S. K. Williams, D. Amiel, S. T. Ball, R. T. Allen, V. W. Wong, A. C. Chen, R. L. Sah, and W. D. Bugbee, "Prolonged Storage Effects on the Articular Cartilage of Fresh Human Osteochondral Allografts," *Journal of Bone and Joint Surgery - Series A*, vol. 85, no. 11, pp. 2111–2120, 2003.

[279] S. T. Ball, D. Amiel, S. K. Williams, W. Tontz, A. C. Chen, R. L. Sah, and W. D. Bugbee, "The Effects of Storage on Fresh Human Osteochondral Allografts," *Clinical Orthopaedics and Related Research*, no. 418, pp. 246–252, 2004.

[280] J. T. Garrity, A. M. Stoker, H. J. Sims, and J. L. Cook, "Improved osteochondral allograft preservation using serum-free media at body temperature," *American Journal of Sports Medicine*, vol. 40, no. 11, pp. 2542–2548, 2012.

[281] E. A. Makris, D. J. Responte, N. K. Paschos, J. C. Hu, and K. A. Athanasiou, "Developing functional musculoskeletal tissues through hypoxia and lysyl oxidase-induced collagen cross-linking," *Proceedings of the National Academy of Sciences of the United States of America*, vol. 111, no. 45, E4832–E4841, 2014.

[282] N. J. Gunja and K. A. Athanasiou, "Passage and reversal effects on gene expression of bovine meniscal fibrochondrocytes," *Arthritis Research and Therapy*, vol. 9, no. 5, pp. 1–12, 2007.

[283] M. F. Rai, L. J. Sandell, J. M. Cheverud, and R. H. Brophy, "Relationship of age and body mass index to the expression of obesity and osteoarthritis-related genes in human meniscus," *International Journal of Obesity*, vol. 37, no. 9, pp. 1238–1246, 2013.

[284] M. Mesiha, D. Zurakowski, J. Soriano, J. H. Nielson, B. Zarins, and M. M. Murray, "Pathologic characteristics of the torn human meniscus," *American Journal of Sports Medicine*, vol. 35, no. 1, pp. 103–112, 2007.

[285] R. L. Mauck, G. J. Martinez-Diaz, X. Yuan, and R. S. Tuan, "Regional multilineage differentiation potential of meniscal fibrochondrocytes: Implications for meniscus repair," *Anatomical Record*, vol. 290, no. 1, pp. 48–58, 2007.

[286] J. Sanchez-Adams and K. A. Athanasiou, "Regional effects of enzymatic digestion on knee meniscus cell yield and phenotype for tissue engineering," *Tissue Engineering - Part C: Methods*, vol. 18, no. 3, pp. 235–243, 2012.

[287] K. R. Stone, D. W. Stoller, S. G. Irving, C. Elmquist, and G. Gildengorin, "3D MRI volume sizing of knee meniscus cartilage," *Arthroscopy*, vol. 10, no. 6, pp. 641–644, 1994.

[288] M. Sommerfeldt, T. Goodine, A. Raheem, J. Whittaker, and D. Otto, "Relationship Between Time to ACL Reconstruction and Presence of Adverse Changes in the Knee at the Time of Reconstruction," *Orthopaedic Journal of Sports Medicine*, vol. 6, no. 12, 2018.

[289] L. Brambilla, L. Pulici, G. Carimati, A. Quaglia, E. Prospero, C. Bait, E. Morenghi, N. Portinaro, M. Denti, and P. Volpi, "Prevalence of associated lesions in anterior cruciate ligament reconstruction," *American Journal of Sports Medicine*, vol. 43, no. 12, pp. 2966–2973, 2015.

[290] M. Sommerfeldt, A. Raheem, J. Whittaker, C. Hui, and D. Otto, *Recurrent Instability Episodes and Meniscal or Cartilage Damage After Anterior Cruciate Ligament Injury: A Systematic Review*, 2018.

[291] M. A. Kluczynski, J. M. Marzo, and L. J. Bisson, "Factors associated with meniscal tears and chondral lesions in patients undergoing anterior cruciate ligament reconstruction: A prospective study," *American Journal of Sports Medicine*, vol. 41, no. 12, pp. 2759–2765, 2013.

Appendix A: Bone Marrow Mesenchymal Stem Cell-Derived Tissues are Mechanically Superior to Meniscus Cells'

Contributing authors:

Hoda A. Elkhenany*, Alexander R. A. Szojka*, Aillette Mulet-Sierra, Yan Liang, Melanie Kunze, Xiaoyi Lan, Mark F. Sommerfeldt, Nadr M. Jomha, Adetola B. Adesida

*: Equal contributing authors

A.1   Abstract

Bone marrow–derived mesenchymal stem cells (BMSCs) have the potential to form the mechanically functional extracellular matrix of joint tissues such as the menisci of the knee joint. The purpose of this study was to assess BMSCs' potential to engineer meniscus-like tissue relative to meniscus fibrochondrocytes (MFC).

MFC were isolated from castoffs of partial meniscectomy from non-osteoarthritic knees. BMSCs were developed from bone marrow aspirates of the iliac crest. All cells were of human origin. Cells were cultured in type I collagen scaffolds under normoxia (21% O_2) for two weeks followed by hypoxia (3% O_2) for three weeks. The structural and functional assessment of the generated meniscus constructs were based on glycosaminoglycan (GAG) content, histological appearance, gene expression, and mechanical properties.

The tissues formed by both cell types were histologically positive for Safranin-O stain and appeared more intense in the BMSC constructs. This observation was confirmed by a 2.7-fold higher GAG content. However, there was no significant difference in collagen I (*COL1A2*) expression in BMSC- and MFC-based constructs (p=0.17). The expression of collagen II (*COL2A1*) and aggrecan (*ACAN*) were significantly higher in BMSCs than MFCs (p≤0.05). Also, the gene expression of the hypertrophic marker collagen X (*COL10A1*) was 199-fold higher in BMSCs than MFCs (p<0.001). Moreover, the relaxation moduli were significantly higher in BMSC-based constructs at 10–20% strain step than MFC-based constructs.

In conclusion, BMSC-based constructs were mechanically-superior with more chondrogenic and also hypertrophic matrix phenotypes than MFC-based constructs.

A.2 Introduction

The menisci are a pair of fibrocartilaginous structures located between the femur and tibia in the knee joint[15, 240]. Their functional role is central to the biomechanics and health of the knee[15, 28, 241]. The menisci have a limited blood supply and are susceptible to non-healing tears that impede function and predispose the knee to early development of post-traumatic osteoarthritis[28, 242].

The biomechanical functionality of the menisci is from the composition and organizational architecture of their extracellular matrix (ECM)[113]. The ECM is primarily composed of fibrillar type I collagen with some other collagen variants (including types

II, III, IV, VI and XVIII), and proteoglycans such as aggrecan[15].

Meniscus fibrochondrocytes (MFC) are responsible for the synthesis and assembly of the functional ECM of the meniscus, and accordingly MFCs have been advocated as a cell type to generate functional replacements of irreversibly damaged meniscus through tissue engineering (TE) strategies[55, 66, 95, 96, 126, 129, 130, 243]. Early TE attempts towards the fabrication of meniscus substitutes via the usage of human MFC revealed that the functional matrix-forming capacity of MFCs declines as an outcome of cellular and molecular de-differentiation processes during monolayer cell expansion protocols before three-dimensional (3D) tissue formation[129, 244, 245].

Cell culture protocols with specific growth factors that concomitantly mitigate the de-differentiation and augment the re-differentiation capacity of MFCs have been reported with variable success[2, 8, 158, 244, 246, 247] However, the search for alternative cell sources for cell-based meniscus TE has been undeterred[244, 248–254].

The abundance, ease of accessibility, high-proliferative properties, and the capacity of adult-derived mesenchymal stem cells (MSCs) to produce the ECM molecules that are characteristic of the functional components of the meniscus under defined cell culture conditions have made MSCs attractive for meniscus TE research[248, 251, 255, 256]. Among the different sources of MSCs, bone marrow-derived MSCs (BMSCs) have perhaps received the most attention in meniscus TE[15, 251, 254, 256–258].

In this study, we investigated the ECM-forming capacities of human MFC and BMSCs in 3D porous type I collagen scaffolds via cell culture protocols and conditions recently known to augment their differentiation to meniscus-like tissue structures[2, 8, 259]. A type I collagen scaffold was chosen for the study as this collagen is the predominant ECM component of the meniscus. We hypothesized that the biomechanical characteristics of engineered meniscus-like tissue structures from in vitro cultured human MFCs would be superior relative to those from BMSCs.

A.3 Materials and methods

A.3.1 Tissue procurement, cell isolation, and monolayer expansion

Our human cell sources were bone marrow aspirates from the iliac crest (n=4) and surgical castoffs of menisci from partial meniscectomies of acute injuries (n=8). We collected all tissues according to the protocol approved by the University of Alberta's Health Research Ethics Board-Biomedical Panel (Study ID: Pro00018778). Bone marrow aspirates were processed for MSC isolation within 24 hours of acquisition and the surgical castoffs of the menisci were processed within 72 hours. Table A.1 provides a summary of donor details. All tissue specimens were from male donors because of a limited availability of specimens from female donors at the time of this study.

Table A.1: Human meniscus fibrochondrocyte and bone marrow aspirate donor characteristics and expansion details. LIC: left iliac crest, RIC: right iliac crest.

Cell type	ID	Age (years)	Biological sex (M/F)	Source	CPD	PD/day
MFCs	Donor 1	18	M	Lateral	5.11	0.43
	Donor 2	20	M	Medial	3.35	0.33
	Donor 3	22	M	Lateral	4.87	0.35
	Donor 4	24	M	Medial	3.69	0.37
	Donor 5	25	M	Medial	4.88	0.35
	Donor 6	29	M	Medial	3.27	0.25
	Donor 7	31	M	Medial	4.13	0.32
	Donor 8	33	M	Medial	3.35	0.28
BMSCs	Donor 1	23	M	LIC	12.76	0.61
	Donor 2	28	M	RIC	14.21	0.44
	Donor 3	34	M	RIC	10.44	0.39
	Donor 4	39	M	LIC	12.68	0.30

Human BMSCs were isolated from bone marrow aspirates of the iliac crest (n=4)

as described by Adesida *et al.*[109]. BMSCs were expanded in α-MEM supplemented with 10% v/v fetal bovine serum (FBS), 100 mM 4-(2-hydroxyethyl)-1-piperazineethanesulfonic acid (HEPES), 1 mM sodium pyruvate (Sigma-Aldrich Co., MO, USA), 100 U/mL penicillin, 100 μg/ mL streptomycin, 0.29 mg/mL glutamine (PSG; Life Technologies, ON, Canada), and FGF-2 (5 ng/mL) (Neuromics, MN, USA).

MFC were isolated from human meniscus specimens (n=8) as described earlier by Liang *et al.*[8]. The isolated MFC were expanded in complete media comprising high-glucose Dulbecco's modified Eagle's medium (4.5 mg glucose/mL) supplemented with 100 mM HEPES, PSG, 5% v/v FBS, TGF-β1 (1 ng/mL)(Prospec, NJ, USA), and FGF-2 (5 ng/mL). Cells from both sources were expanded in the standard "normoxic" incubators (37°C, humidified 95% air and 5% CO_2).

A.3.2 Scaffold seeding and chondrogenic (re-)differentiation

To form meniscus tissue-like constructs, we seeded type I collagen sponge scaffolds (Integra Lifesciences Co., NJ, USA) with BMSCs or MFCs at a fixed density of 5×10^6 cells/cm^3 as described previously[57, 259, 260]. Before seeding, the dry scaffolds were 3.5 mm in height and 6 or 10 mm in diameter. We harvested cell-seeded scaffolds on day 0 to later confirm that there were no differences between cell sources in cell numbers seeded onto the scaffolds using the DNA assay described below.

The meniscus constructs were cultured in a defined serum-free chondrogenic medium containing 10 ng/mL TGF-β3 (Prospec, NJ, USA) as described previously[8, 259]. The constructs of 6 and 10 mm initial scaffold diameter received 1 and 2.8 mL medium, respectively, which we replaced twice in a week. For the first two weeks of culture, the constructs experienced normoxic incubator conditions (the same used for cell expansion). For the latter three weeks of culture, the constructs experienced "hypoxic" incubator conditions (37°C, humidified 3% O_2 and 5% CO_2) within an X3 incubator (Biospherix, USA). We hypothesized that this two-stage culture protocol would support chondrogenic (re)-differentiation based on our previous work; however, this

process was not specifically tested in this study relative to other culture strategies.

A.3.3 Gross morphology and geometric analysis

After five weeks of chondrogenic culture, we noted the general shapes and colours of constructs. We took images of the top and bottom surfaces of the constructs. Using these images, we measured the surface areas by using ImageJ software, averaged them, and calculated the average circular diameter to compute the extent of diametrical contraction. We measured the heights of 10 mm scaffold-based constructs, which were designed for mechanical testing, by compressing them to a pre-load of 0.01 N and measuring the distance between our mechanical test instrument's platens with calipers.

A.3.4 Biochemical analysis (DNA and GAG quantification)

The constructs were frozen at -80°C until they were needed for biochemical assays, as previously described[259]. Briefly, we digested 6 and 10 mm scaffold-based constructs in 250 or 750 µL proteinase K solutions, respectively, overnight at 56°C. Using the digest solutions, we quantified DNA by using the CyQuant cell proliferation assay (Invitrogen, ON, Canada) and glycosaminoglycans (GAGs) by the 1,9-dimethylmethylene blue assay (Sigma-Aldrich)[261].

We computed the % DNA/Wet weight (WW), % GAG/WW, and GAG/DNA ratios by using the specific DNA and WW data from each construct. Unfortunately, we did not have enough cells for BMSC donor M/23y to set up any day 0 controls. A methodological limitation among the initial scaffold sizes is that we measured DNA and GAG contents of 10 mm scaffolds after they were subjected to mechanical testing. This process inevitably caused the loss of some of these biochemical components; therefore, we expect that these values are slightly underestimated in the 10 mm groups.

A.3.5 Histological, immunofluorescence (IF), and scanning electron microscopy (SEM)

After five weeks of chondrogenic culture, the cell scaffold constructs were fixed in 10% (v/v) formalin (Anachemia, Canada) overnight at 4°C. After the fixation, the constructs were washed in phosphate buffered saline (PBS; Sigma), processed, and embedded in paraffin wax. The embedded constructs were cut at 5 µm sections using a Leica RM2125 RTS rotary microtome (Leica Biosystems, Canada). The sections were assessed histologically by 0.1% (w/v) Safranin-O (Sigma) and counter-stained with 1% w/v Fast Green FCF (Sigma) staining for the detection of sulfated GAGs. Also, one representative donor from each group were chosen based on age, GAG content, and gene expression level for IF staining of the characteristic cartilage matrix proteins, collagens I/II, using rabbit anti-human collagen I (CL50111AP-1, Cedarlane Laboratories Ltd, Canada) and mouse anti-collagen II (II-II6B3, DSHB, USA), along with goat anti-rabbit (ab150080; Abcam, Canada) and goat anti-mouse (ab150117; Abcam) secondary antibodies. Moreover, histological sections from both types of tissue constructs were stained for aggrecan using primary AB rabbit anti-aggrecan (ab36861; Abcam) and goat anti-rabbit IgG (H&L Alexa Fluor 594; Abcam) secondary antibody. Sections were stained for hypertrophic differentiation marker, collagen X using primary antibody rabbit anti-collagen X (ab58632; Abcam) and goat anti-rabbit IgG (H&L Alexa Fluor 594) as a secondary antibody. All sections were stained by 4',6-diamidino-2-phenylindole (Sigma) to detect the cell nuclei. All staining techniques were performed as described earlier[9].

SEM was used to measure the fibre diameters and assess the micro-architecture of 6 mm scaffold-derived constructs from one donor of each cell type. SEM was performed as described earlier[9]. Briefly, we put tissues into pre-warmed 2% (v/v) glutaralde-hyde (Sigma) and 2.5% (v/v) paraformaldehyde (Sigma) and then left them overnight at 4°C. We coated constructs with three conductive layers by using alternating 2% w/v osmium tetroxide and 2% w/v tannic acid in Milli-Q water every 15 minutes.

This step was followed by dehydration by using the serial dilution of ethanol (% v/v) and hexamethyldisilane treatment. The scaffolds were then air dried at the room temperature overnight. Images from different spots were captured by using a scanning electron microscope (Model S-4800, Hitachi, JA). ImageJ was used to measure the fibre diameters. All the reagents used were obtained from Electron Microscope Science, PA, USA.

A.3.6 mRNA gene expression by quantitative real-time polymerase chain reaction (qRT-PCR)

Using only 6 mm scaffold-derived constructs, we performed RNA isolation, cDNA synthesis, and qRT-PCR as previously described[2]. Briefly, we placed samples in 1 mL TRIzol (Life Technologies) and froze at -80degC until they were needed. We grounded samples by using a pestle and extracted the RNA fraction. We synthesized cDNA by GoScript reverse transcriptase with 1 µg of oligo (dt) primers (Promega Co., WI, USA). We performed qRT-PCR in a CFX Connect (Bio-Rad, CA, USA) by using hot start Taq and SYBR Green detection (Eurogentec North America Inc, San Diego, CA, USA).

The specific primers used in this study are available with the online version of this manuscript. We calculated the average Ct values from three housekeeping genes (HKG): *B2M*, *RPL13*, and *YWHAZ*. For each gene of interest (GOI), we calculated $\Delta Ct = Ct_{HKG}\text{-}Ct_{GOI}$ within the same sample. Only ΔCt values were used in the statistical analysis because these values tend to meet the normality assumption and treat up- and down-regulation symmetrically for parametric tests. We computed means and standard deviations of ΔCt values and then transformed these values and the individual ΔCt values for each construct to an exponential scale ($2^{\Delta Ct}$) for presentation. We grouped our GOIs as follows: fibrocartilage markers, hypertrophic markers, and transcription factors. To account for higher average expression of HKG across donors in MFC as compared to BMSCs ($\Delta Ct = $ -0.55), we assumed expression

differences to be meaningful only if they met the combined criteria of fold difference >2 and p<0.10 (statistical analyses are described below).

A.3.7 Compressive mechanical analysis

In our experience, type I collagen scaffold-based meniscus constructs demonstrate stiffening of strain and strain rate–dependent behaviour in unconfined stress relaxation tests. Thus, we tested our samples in all the five successive strain steps at a constant strain rate based on each sample's original height[166, 181]. We set up only 10 mm scaffold-based constructs for mechanical testing because the cylindrical shapes of the original scaffolds were better retained when there are larger initial scaffolds and the forces generated during the compressive testing of 10 mm scaffold-based constructs better fit the operating range of our 22 N load cell.

After rinsing in phosphate-buffered saline, we weighed the constructs and imaged their top and bottom surfaces. We used these images to calculate the average initial cross-sectional areas of the constructs for the average stress calculation. Thereafter, we placed the constructs between two flat stainless steel platens and gently pre-loaded them (0.01 N) as described above in a Biodynamic 5210 system Test Instrument (TA Instruments, USA). We then applied the following compression test to all the constructs: a precondition with a 5% compression sine wave for 15 s at 1 Hz followed by five successive 10% strain steps at 50% strains with 20 minute relaxation periods in between. We analyzed the time, displacement, and load data by a custom MATLAB script (R2018A). To remove noise from the force data, the script first used the smooth function with a LOWESS curve fit piecewise with fine-tuning around the steep initial relaxation. This method was found to accurately and reliably fit the load data, including the peak force at the end of each ramp. The instantaneous modulus at each strain step was computed as the change in force across each strain step divided by the initial contact area and the change in strain (0.1). The relaxation modulus at each strain step was computed as the change in force after 20 minutes of relaxation relative

to the force immediately before the previous ramp, divided by the initial contact area and the change in strain (0.1). We could not include mechanical testing data for MFC donor M/22y due to an equipment failure unrelated to the donor's performance.

A.3.8   Data presentation and statistical analysis

Quantitative data plots were performed by using Excel 2016. We plotted all data measurements for independent constructs within each donor in the figures, organized from left-to-right within conditions by increasing the donor age within each cell type. This was done to provide a visual representation of variability arising within the donors. For statistical analysis, we computed the average measurement of these independent constructs within each donor and condition to obtain more stable measurements. We then used these average values within statistical computations so that each donor was represented only once in each condition.

All statistical computations were performed by using IBM SPSS Statistics 26. For determining wet weight (WW), Original diameter %, Day 0 DNA content, five weeks of DNA content, % DNA/WW, GAG content, % GAG/WW, and GAG/DNA, we carried out two-way mixed analyses of variance with the between subjects variable cell type and repeated factor scaffold size as described in Laerd Online Statistical Guides, 2019. If there was a significant interaction ($p<0.05$) between these factors, then we compared the individual groups. However, if there was no significant interaction, then we looked only at the pooled main effects of each factor. Log-transformations were used in any case of violating the normality assumption. The data for five weeks of DNA content failed Box's test of equality of covariance matrices. In this case, we proceeded with the analysis using untransformed data, ignoring the violation. We performed independent samples t-test for % original height and all PCR-related data. For the mechanical test data, the data within each strain level and cell type did not meet the normality assumption at all strain steps, even after a log-transformation. We thus applied the Mann–Whitney U test at each strain level with the Bonferroni cor-

rection (all p-values multiplied by 5). In all cases, we interpreted p values below 0.10 as weak evidence and 0.05 as significant evidence. All our statistical computations used two-tailed tests.

A.4 Results

A.4.1 Cell expansion and population doublings

Table A.1 summarizes the list of tissue donors and their cell expansion-related information. All donors were male, in the age ranges 18–33 (MFC) and 23–39 (BMSCs) years. Cumulative population doublings for BMSCs (12.53±1.56) were approximately triple to that of MFC (3.97±0.76). Despite differences in the isolation protocols, there were no differences between the cell types in terms of population doubling per day, indicating similar division rates.

A.4.2 BMSC-based constructs possess higher geometrical stability in fibrochondrogenic differentiation than MFC-based constructs

At the end of the five-week culture period, BMSC-based constructs had similar colour to the MFC-based constructs (yellow-white) but had more rough-looking surfaces (Figure A.1). It was also apparent that MFC-based constructs tended to undergo more contraction than their BMSC-based counterparts. MFC-based constructs were 1.6-fold (p=0.008) lighter in WW (Figure A.2A) and underwent 1.2-fold (p=0.009) more diametrical contraction than BMSC-based constructs (Figure A.2B). There were no cell-type differences in contraction in the height direction between the groups (Figure A.2C).

A.4.3 BMSC-based constructs exhibit superior GAG content than MFC-based constructs

There were no cell-type differences in the DNA content on freshly seeded scaffolds at day 0 (Figure A.3A). Thus, we concluded that in terms of average initial cell numbers,
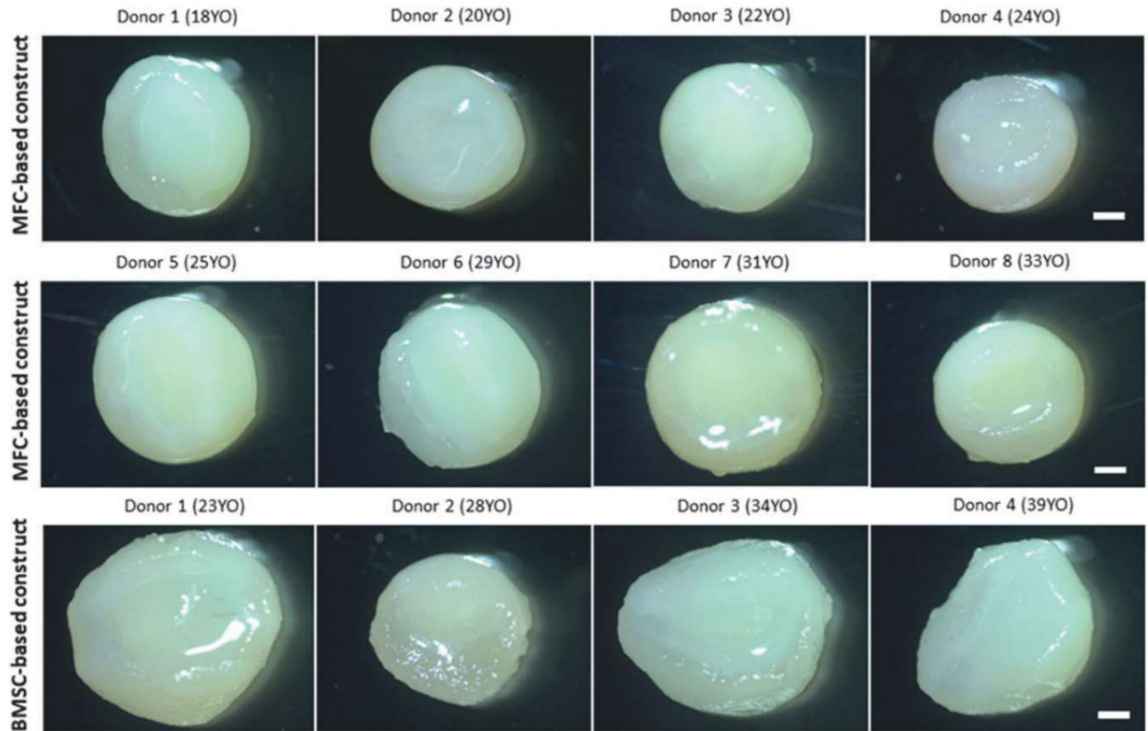
Figure A.1: Gross morphology of BMSC- and MFC-based constructs after 5 weeks of culture with TGF-β3 (10 mm diameter scaffolds) from all donors included in the study. Scale bar: 1 mm. BMSC, bone marrow-derived mesenchymal stem cell; MFC, meniscus fibrochondrocyte; TGF, transforming growth factor.
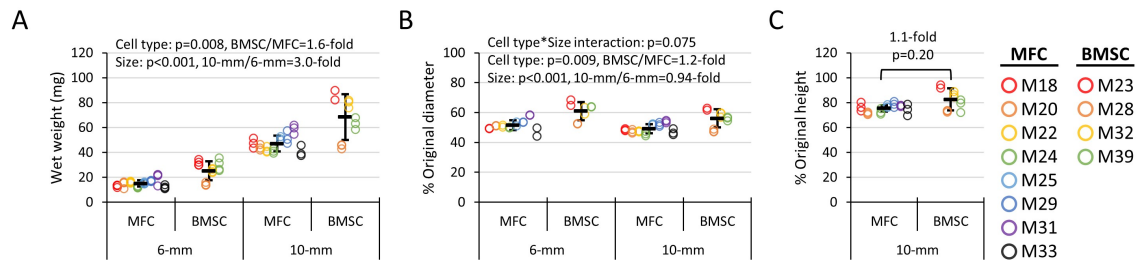

Figure A.2: Wet weight and contraction data of BMSC- and MFC-based constructs after 5 weeks of culture with TGF-β3. A) Wet weight. B) Radial contraction radio and C) longitudinal contraction ratio. Diameter of the constructs' scaffold dimensions are expressed as percentages of the dry collagen scaffold diameter values (6 and 10 mm diameter, 3.5 mm height) before cell seeding.

the cell type comparison in this study had a fair starting point. At the end of the five-week culture period, DNA contents tended to be higher in MFC- than BMSC-based constructs (6 mm: 1.2-fold, p=0.12 and 10 mm: 1.4-fold, p=0.11), but without statistically significant differences (Figure A.3A). Expressed as a percentage of WW,

257

MFC-based constructs had more than twice as much DNA (Figure A.3C). We took these results to indicate that MFC-based constructs likely had lesser matrix content.
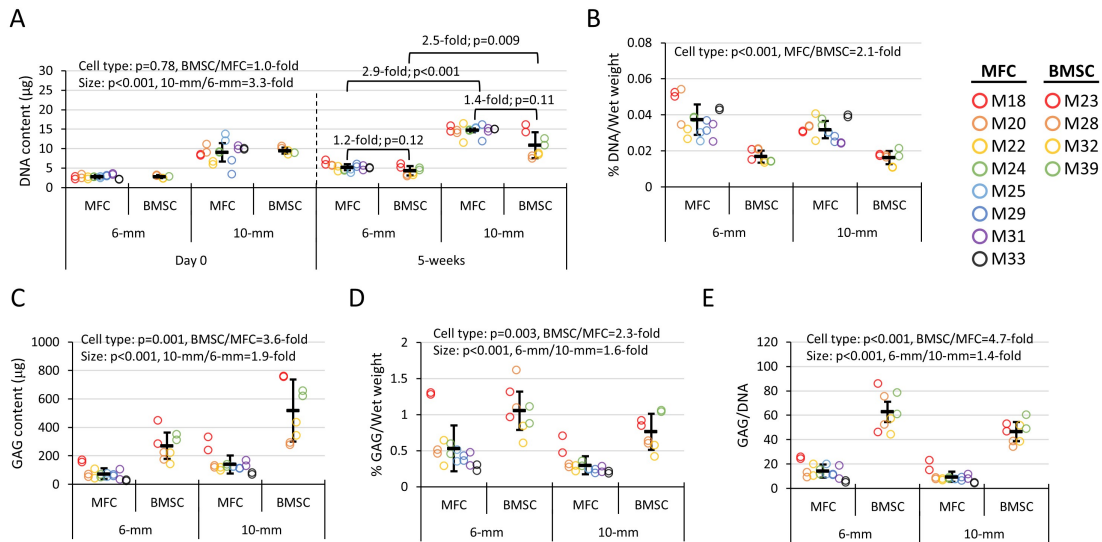
Figure A.3: DNA and GAG biochemical data of BMSC- and MFC-based constructs after 5 weeks of culture with TGF-β3. A) DNA content, B) GAG content, C) DNA normalized to wet weight, D) GAG normalized to DNA content, and E) GAG normalized to wet weight. Day 0 DNA controls indicate the quantity of DNA found on scaffolds harvested 15 minutes after cell seeding.

BMSC-based constructs contained 3.6-fold (p=0.001) and 2.3-fold (p=0.003) more GAG content (Figure A.3B) and percent WW of GAG, respectively. Constructs from 6 mm initial scaffold diameters had significantly larger parameter ratios of GAG/WW% (Figure A.3F; 1.6-fold, p<0.001) and GAG/DNA (1.4-fold, p<0.001) than 10 mm scaffold diameters (Figure A.3E).

Thus, we concluded that BMSC-based constructs contained larger amounts and concentrations of GAGs. The average BMSC compared to the average MFC produced and accumulated GAG within the newly formed ECM faster during chondrogenic culture. The cell performance in terms of biochemical accumulation declined with increasing initial scaffold size. After the confirmation of quantitative biochemical differences between the cell types, we assessed differences in the expression of specific proteins by qualitative histology and IF.

A.4.4 BMSC-based constructs displayed differential ECM content

The radial tissue cross-sections were used to visualize the ECM distribution within the constructs. Without exception, constructs from all BMSC and MFC donors stained positively for sulfated proteoglycans by Safranin-O staining. BMSCs tissue construct showed a more pronounced and abundant proteoglycan deposition than MFC tissue constructs in all the donors (Figure A.4). These results were consistent with the quantitative GAG contents (Figure A.3B).

To assess the engineered constructs microarchitecture, we performed SEM analysis of constructs from each cell type (Figure A.5). SEM images were taken from different spots (outside surface, inner surface, and centre of the construct) and analyzed to detect the differences between MFCs and BMSCs in terms of fibre diameter (Figure A.5). Fibre diameters of 6 mm BMSCs and MFC-based constructs at the end of the five-week culture at the outer surface were within a small range (0.039 ± 0.017 µm vs 0.09 ± 0.025 µm; $p > 0.05$; Fig.5C.1 vs 5B.1). However, MFCs resulted in more uniform fibres with a relatively larger range of diameter at the inner surface and centre of the constructs. Fibre diameters of BMSC-based constructs were relatively smaller in diameter than MFC-based constructs at the inner surface ($0.058 \pm 0.0.03$ µm vs 0.062 ± 0.008 µm; $p > 0.05$; Figure A.5C.2 vs B.2) and centre of the constructs (0.027 ± 0.014 µm vs 0.067 ± 0.012 µm; $p < 0.0001$, Fig. 5C.3 vs 5B.3).

Through IF, the BMSC-based constructs stained ubiquitously and intensely for types I, II, and X collagens. The MFC-based constructs had comparable type I collagen expression to their BMSC counterparts; however, staining for types II and X collagens was sparse and faint. Further, the BMSCs-based constructs stained much more abundantly for aggrecan than their MFC-based counterparts (Figure A.6 & Figure A.7).
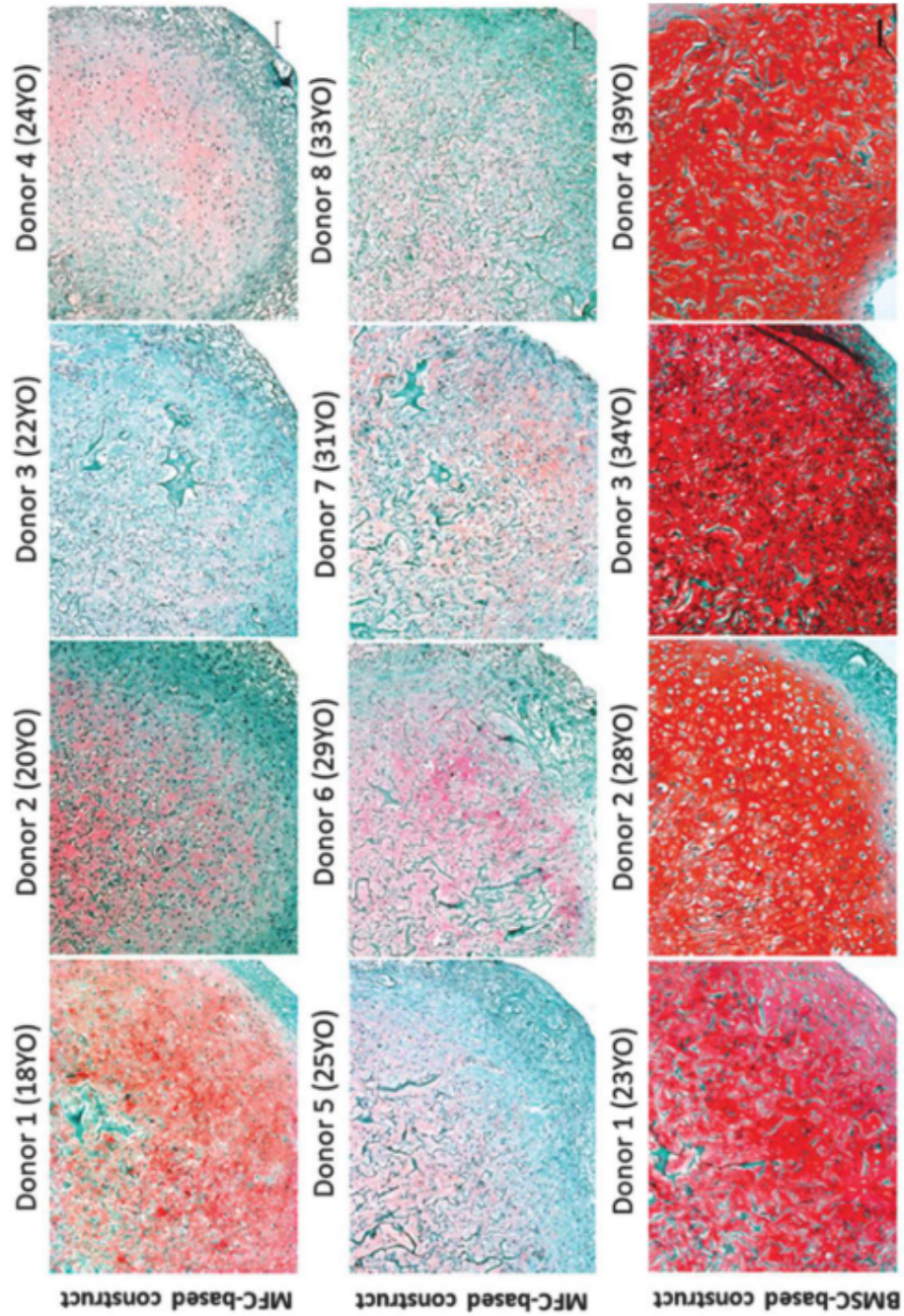
Figure A.4: Safranin-O staining of engineered tissue constructs with each cell type. Histological analysis of sulphated proteoglycans produced in BMSC- and MFC-based constructs after 5 weeks of culture with TGF-β3 (6 mm diameter scaffolds) from all donors included in the study. Scale bar: 100 μm. Colour images are available online.
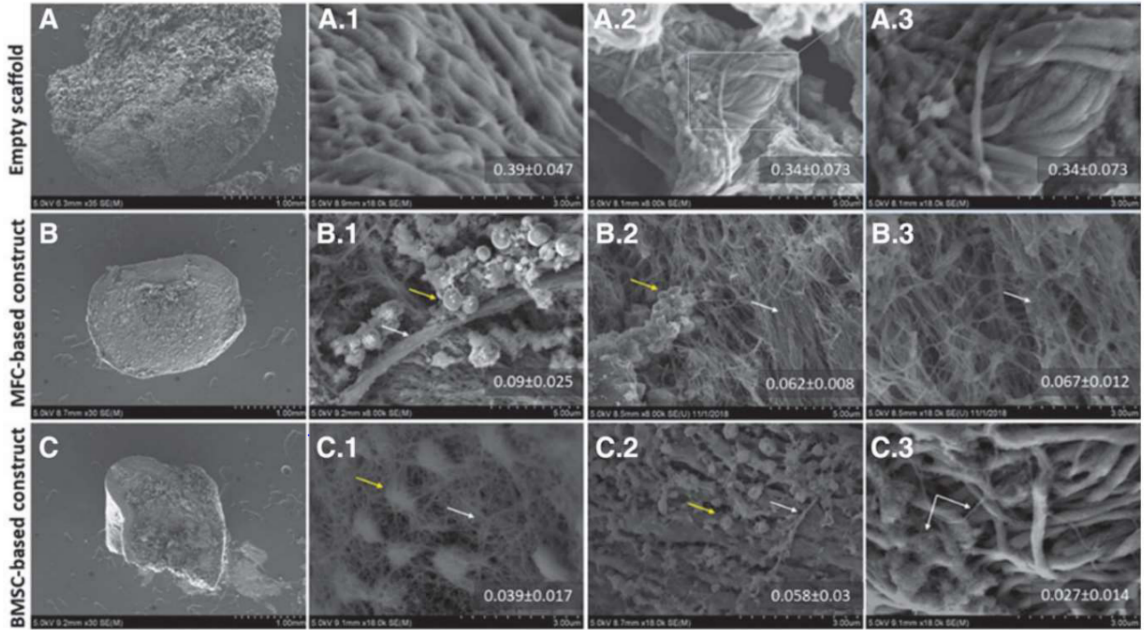
Figure A.5: Scanning electron microscopy of engineered tissue constructs. Scanning electron micrographs showing different fibre diameters of: A) empty scaffold, B) MFC-based constructs, and C) BMSC-based constructs after 5 weeks of culture with TGF-β3 (6 mm diameter). The images were taken from different spots: **A.1, B.1, C.1)** the outer surface of the scaffold/construct; **A.2, B.2, C.2)** inner surface zone just below the top surface; **A.3, B.3, C.3)** middle or the centre. White arrow indicates newly generated fibres, yellow arrow points to cells.

A.4.5 Gene expression supports the chondrogenic phenotype of BMSCs as well as the hypertrophic phenotype detected by histological analysis

Among the measured fibrocartilage markers in the 6 mm scaffold-derived constructs, BMSCs more highly expressed *ACAN* and *COL2A1*, whereas MFC more highly expressed *VCAN*, thereby encoding the outer meniscus-specific proteoglycan versican (Figure A.8A). Among measured hypertrophic markers, BMSCs expressed 199-fold more *COL10A1* but 4.6-fold less *MMP-13* (Figure A.8B). Among the measured transcription factors, MFC unexpectedly had an increased expression of the osteogenic regulator *RUNX2* and *HIF-1α* (Figure A.8C). There were no meaningful expressional differences between the cell types in any of the other genes measured *COL1A2*, *ALPL*, *SOX9*, and *HIF-2α* (Figure A.8A-C).

261
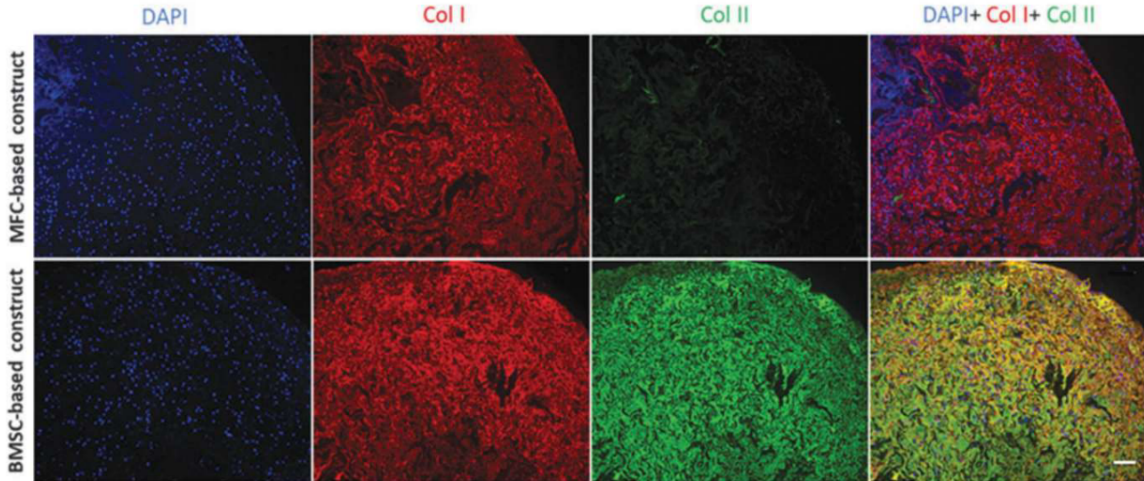
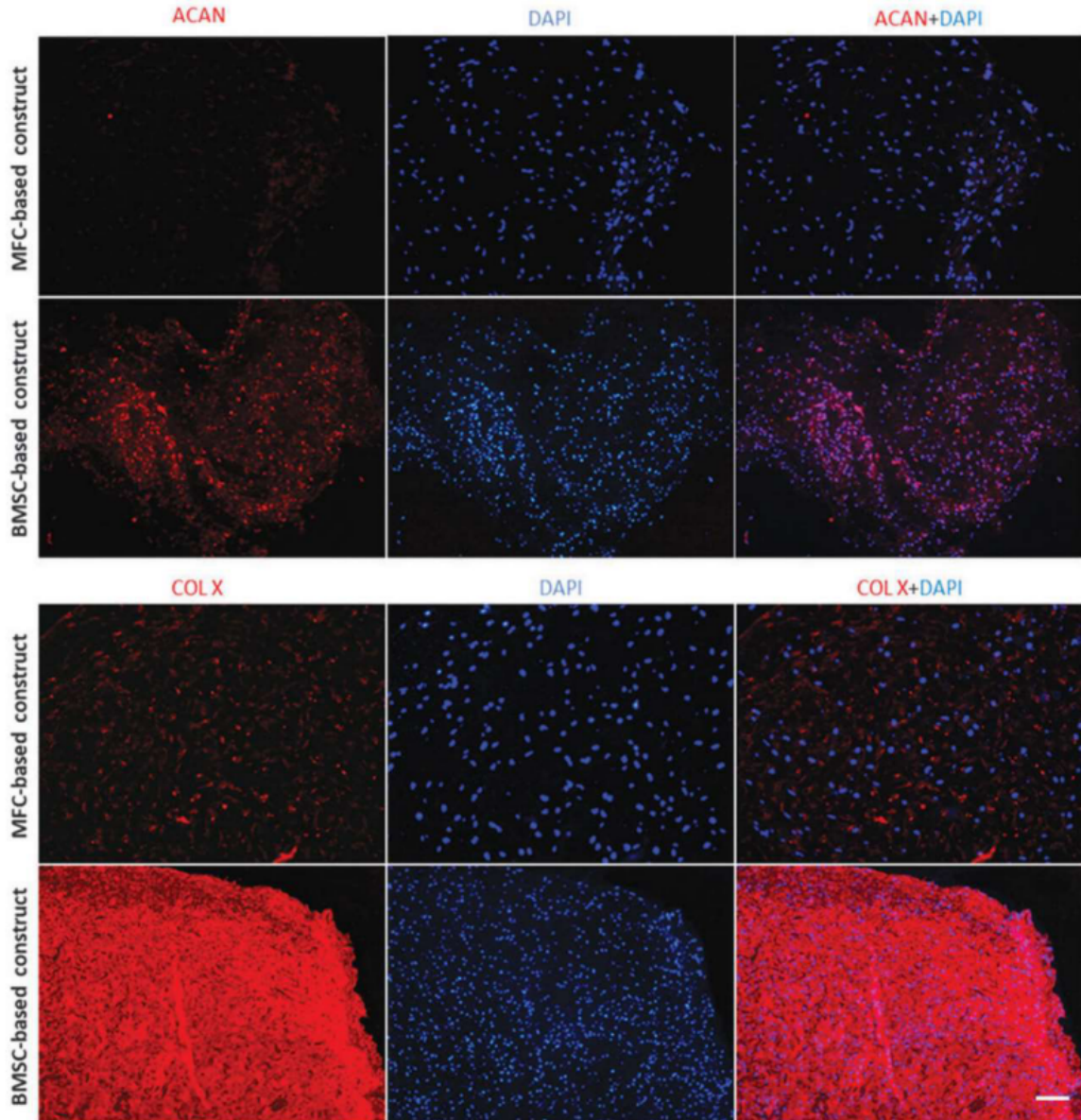Figure A.6: Immunofluorescence images of engineered tissue constructs. Immunofluorescence analysis of types I and II collagens in BMSC- and MFC-based constructs after 5 weeks of culture with TGF-β3 (6 mm diameter), one representative donor from each (MFCs, 29 years old, and BMSCs, 34 years old). Blue: nucleus (DAPI), red: collagen I, green: collagen II, yellow: coincidence of types I/II collagens.

The relative chondrogenic phenotype of each cell type was assessed by using gene expression ratios $ACAN/VCAN$, $COL2A1/COL1A2$, and $SOX9/RUNX2$ (Figure A.8D). The $ACAN/VCAN$ and $COL2A1/COL1A2$ ratios were both higher in BMSCs, thereby indicating that they expressed a phenotype more like the cartilage aspect of the inner meniscus. The $SOX9/RUNX2$ ratio was also significantly higher in BMSCs. However, because BMSCs exhibited a high expression of type X collagen protein—indicative of a more hypertrophic phenotype than MFC—we concluded that neither $RUNX2$ mRNA expression nor the $SOX9/RUNX2$ ratio were reliable predictors of a hypertrophic phenotype in this study (Figure A.8D). We also measured the expression of these same genes from the cells at the end of monolayer expansion culture (these data are provided as a supplement to this article (Figure SA.1).

A.4.6 BMSC-based construct displays a higher relaxation property than MFC-based construct

There was weak evidence of BMSC-based constructs outperforming their MFC counterparts in the instantaneous modulus at only the 10–20% (171.9±86.5 kPa for BMSCs

Figure A.7: Immunofluorescence images of engineered tissue constructs. Immunofluorescence analysis of aggrecan and type X collagen in BMSC- and MFC-based constructs after 5 weeks of culture with TGF-β3 (6 mm diameter), one representative donor from each (MFCs, 29 years old, and BMSCs, 34 years old). Blue: nucleus (DAPI).

vs. 116.6±55.5 kPa for MFC, p = 0.08) and 20–30% (369.6±152.7 kPa for BMSCs vs. 286.29±141 kPa for MFC, p=0.08) strain steps after applying the conservative Bonferroni correction (all P-values multiplied by five as presented in the Fig. 9A). However, BMSC-based constructs performed significantly higher in terms of relaxation modu-
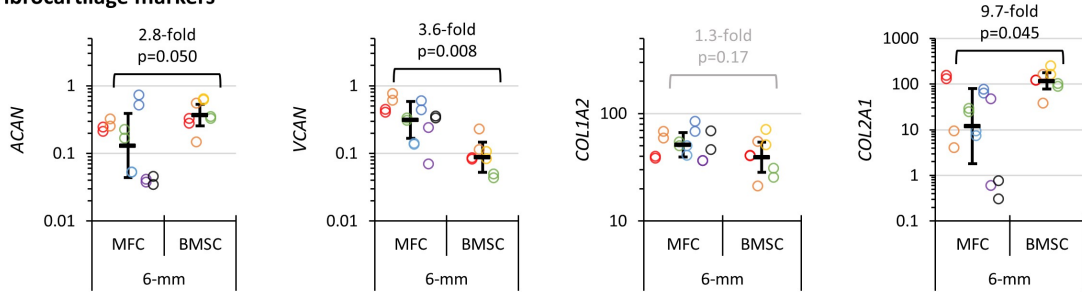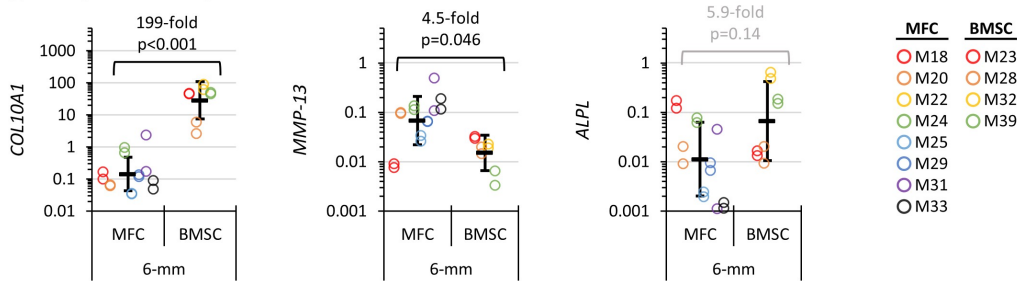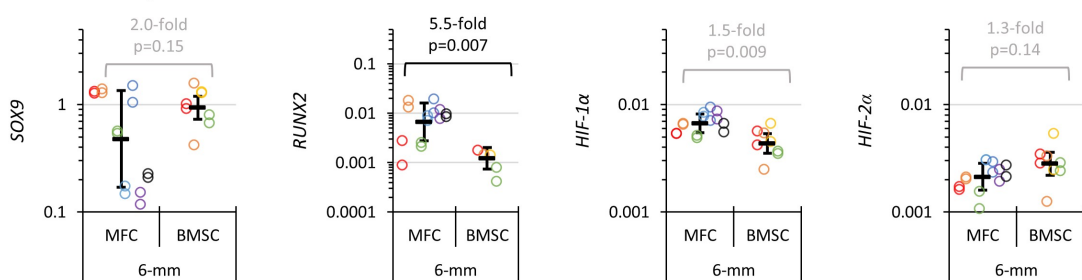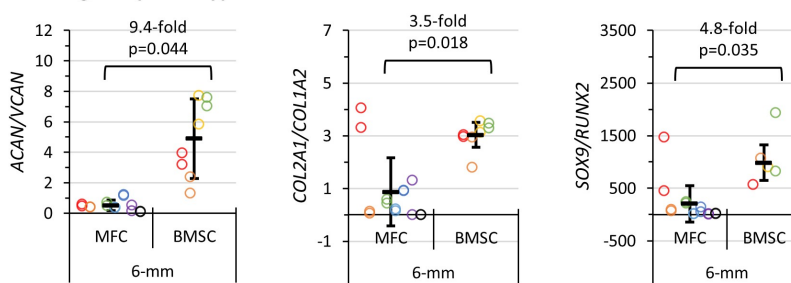
Figure A.8: Relative mRNA expression analysis by quantitative real-time polymerase chain reaction of BMSC- and MFC-based constructs on 6 mm diameter scaffolds after 5 weeks of culture with TGF-β3. A) Fibrochondrogenic markers aggrecan (*ACAN*), versican (*VCAN*), collagen I (*COL1A2*), and collagen II (*COL2A1*); B) Hypertrophic marker genes collagen X (*COL10A1*), matrix metalloproteinase-13 (*MMP-13*), and alkaline phosphatase (ALPL); C) Related transcription factors *SOX9*, *RUNX2*, hypoxia-inducible factors *HIF-1α* and *HIF-2α*; and D) chondrogenic phenotype ratios *ACAN/VCAN*, *COL2A1/COL1A2*, and *SOX9/RUNX2*.

lus at the 0-10% (6.34±3.25 kPa for BMSCs vs. 3.29±1.03 kPa for MFCs, p=0.03) and 10–20% (10.32±4.67kPa for BMSCs vs. 5.19±1.41 kPa for MFC, p=0.03) strain steps. Thus, the mechanical test revealed that BMSC-based constructs were superior only in terms of relaxation modulus at the first two strain steps (Figure A.9B).
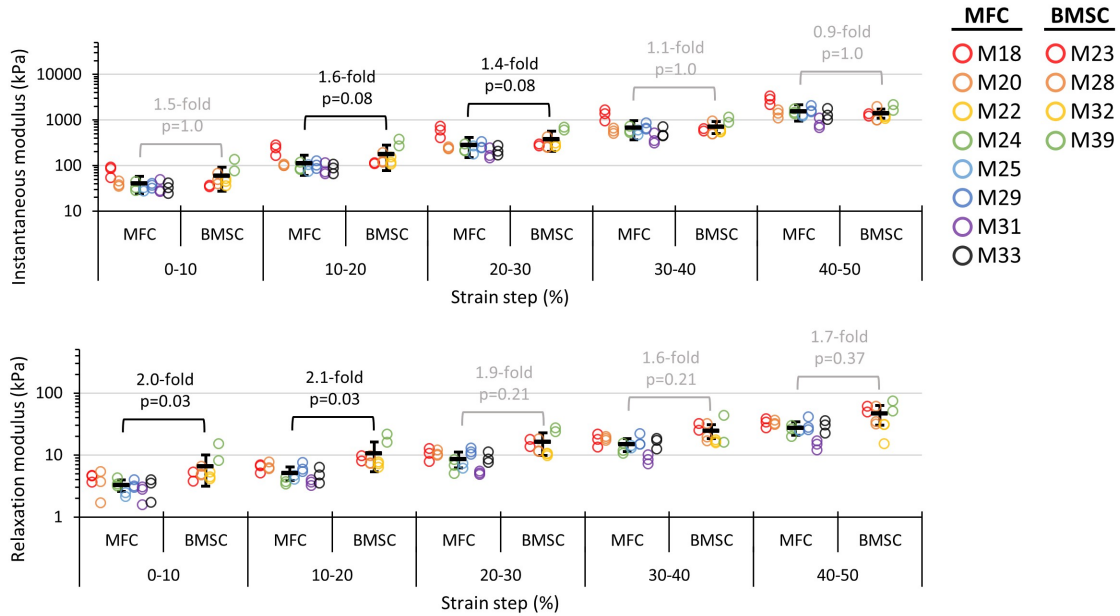

Figure A.9: Instantaneous and relaxation moduli of BMSC- and MFC-based constructs (10 mm diameter scaffolds) after 5 weeks of culture with TGF-β3 from unconfined compression stress relaxation tests with a strain rate of 50% strain/s. Top: Instantaneous modulus and bottom: relaxation modulus.

A.4.7 Correlations in donor age and biochemistry, gene expression

Because we had a reasonable number of independent MFC donors in this cell comparison study, we used this as an incidental opportunity to correlate the donor age to proliferative capacity in P1 (population doublings (PD) and PD per day, n=8 donors), cell performance after fibrochondrogenic culture (normalized biochemical parameters, n=8), and phenotype (gene expression, n=7). We used Spearman's rank test rather than Pearson's correlation due to the non-normal distribution of age and measured parameters. Neither PD nor PD/day in P1 correlated with donor age (p=0.87 and

p=0.53). We found a significant negative correlation between MFC donor age and %GAG/Wet weight in both 6 mm (p=0.001) and 10 mm (p=0.002) constructs, but not for GAG/DNA and %DNA/Wet weight nor for any of the chondrogenic phenotype ratios (*ACAN/VCAN*, *COL2A1/COL1A2*, and *SOX9/RUNX2*). We took these combined results to suggest a possible relationship among MFC donor age, cell proliferation rate, and the production of GAG-rich constructs.

A.5 Discussion

The biomechanical functionality of the knee meniscus is because of its ECM[15, 113]. As MFCs are responsible for the synthesis of the ECM, we had hypothesized that the ECM produced and deposited by MFC in the collagen scaffolds in this study will be mechanically superior relative to the ECM synthesized by BMSC after in vitro chondrogenesis.

The native meniscus fibrocartilage compression modulus has been shown to have a range between 0.1 and 1 MPa[49, 113]. However, in contrast, to our hypothesis, we found that the compression modulus of both MFC-based and BMSC-based constructs was roughly 0.1 MPa at 20% strain and 1 MPa at 50% strain, which is close to the native values. A previous report demonstrated a positive correlation between the compressive modulus and GAG content[262]. However, we reported a significantly higher GAG content in BMSC-based constructs relative to the MFC-based constructs. Yet, the instantaneous modulus of the BMSC-based construct was not significantly different from the MFC-based construct at all strain levels. But the relaxation modulus of the BMSC-based constructs was superior to the MFC-based constructs at 10-20% strain (Figure A.9).

Moreover, we report that the wet weight (Figure A.2), GAG/DNA (Figure A.3), and the chondrogenic phenotype (determined by *ACAN/VCAN*, *COL2A1/COL1A2*, and *SOX9/RUNX2*; Figure A.8), the intensities of Safranin-O staining (Figure A.4)), collagen II (Figure A.6) and aggrecan (Figure A.7) immunofluorescence of the BMSC-

based constructs were superior relative to MFC-based constructs. Collectively, these data demonstrate that the chondrogenic potential of the BMSCs was superior to that of the MFCs.

The chondrogenic potential of BMSCs and MFCs have been reported to decline with CPD[8, 263]. However, the overall data in this study showed that the chondrogenic potential of BMSCs is superior at a mean CPD of 13 relative to a mean CPD of 4 for MFCs (Table A.1). The mechanism underlying the superior chondrogenic potential may be associated with the mRNA expression of *SOX9*.

The transcriptional activity of *SOX9* is critical for chondrogenesis[264–266]. Our data showed that the mRNA expression of *SOX9* was 2.3-fold higher in the BMSC prior to chondrogenesis in the collagen scaffolds compared to the MFC (Figure SA.1). Moreover, the expression of *SOX9* in the BMSCs correlated positively with CPD (Pearson's R of 0.635, p value=0.008; supplemental data available with online version of manuscript). In contrast, the expression of *SOX9* and CPD in the MFC were inversely correlated albeit weakly and not significantly (Spearman's rank correlation coefficient of -232, p value=0.276).

The chondrogenic superiority of primary (unexpanded) bovine MFC relative to passaged four bovine BMSC in the absence of chondrogenic factors further attests to the potential influence of *SOX9* expression in the chondrogenic outcome of this study[267]. Primary human MFC express significantly higher *SOX9* mRNA than passaged MFC[55]. The upregulation of *SOX9* in passaged MFC via viral transduction may significantly improve the chondrogenic outcome of passaged MFC as previously demonstrated for passaged human articular chondrocytes with initial low expression of *SOX9*[264].

There is the possibility that the presence of 1 ng/mL of TGF-β1 during the expansion phase of the MFC in this study may have interfered or somewhat impact the chondrogenic potential of the MFC. Pangborn and Athanasiou had previously demonstrated that 10 ng/mL TGF-β1 stimulated GAG and collagen in monolayer

cultures of MFCs from New Zealand rabbits[247]. It is possible that the use of the TGF-β1 during the expansion phase may have rendered the MFCs less responsive to TGF-β3 in the chondrogenic medium even though the concentration of TGF-β1 in the expansion phase is 10-fold less than reported by Pangborn and Athanasiou.

The significant expression of *COL10A1* (Figure A.8) and the intensity of type X collagen (Figure A.7) in the BMSC-based tissue constructs relative to the MFC-derived tissue constructs indicate that the BMSCs underwent hypertrophic chondrogenesis and have the risk of undergoing endochondral ossification if implanted *in vivo*[145]. The inclusion of parathyroid hormone related protein (PTHrP) during *in vitro* chondrogenesis may mitigate the risk of *in vivo* bone formation by suppression of the expression of *COL10A1*[268, 269].

The microstructure of the generated construct revealed that MFCs produced a *de novo* ECM, which is characterized by organized, uniform sized, and straight/silk fibre patterns similar to the native meniscus as reported by Villegas and Donahue[270]. However, BMSCs resulted in less uniform fibres with a small range of diameter. These results are in agreement with the research of McCorry and Bonassar[267], in which they reported that the fibre diameter of MFC-based constructs was significantly larger than for BMSC-based constructs. It is worth mentioning that the initial scaffold collagen fibres were apparent, and the newly generated fibres were coating it without disturbing its initial alignment. However, in MFC-based constructs, any of the original scaffold fibres were rarely observed.

From the clinical point of view, the contraction properties of the engineered tissue are very important because by the end of the fabrication process, we want to obtain an exact graft size. The contractile properties of the generated tissue constructs from BMSCs showed that they better maintain the initial scaffold dimensions compared to MFCs. Notably, construct contraction and GAG content showed a strong correlation in the BMSC group. Similarly, previous studies have correlated contraction to the collagen content and reported a positive correlation[267, 271, 272].

A.6 Conclusion

Human BMSC-based constructs were superior in biochemical synthesis and/or accumulation of inner meniscal cartilage-like ECM and displayed a higher relaxation modulus relative to the human MFC-based constructs but expressed a much more hypertrophic phenotype. Future investigations to mitigate the hypertrophic characteristics of the BMSC-based constructs is needed and strategies to enhance the chondrogenic potential of passaged human MFCs is needed.
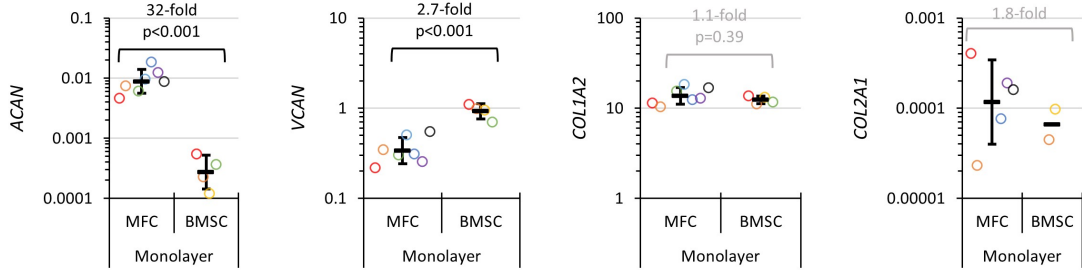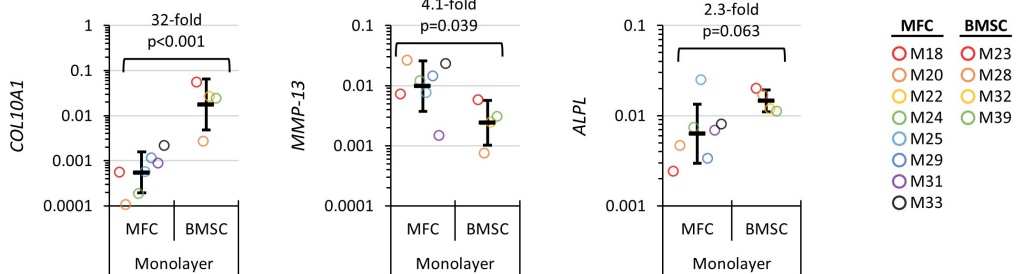
A.7 Funding Sources

A.8 Author Contributions

HE performed the experiments with assistance by AS, AMS, YL, MK and ML. HE performed data analysis and co-wrote the manuscript with AS and AA. ABA specifically wrote the Materials & Methods and Results sections. AS presented quantitative data and performed statistical analysis. MS and NJ performed human tissue procurement, manuscript review and writing. ABA conceived and supervised the study and was responsible for the final review of the manuscript. All authors read and approved the final manuscript.
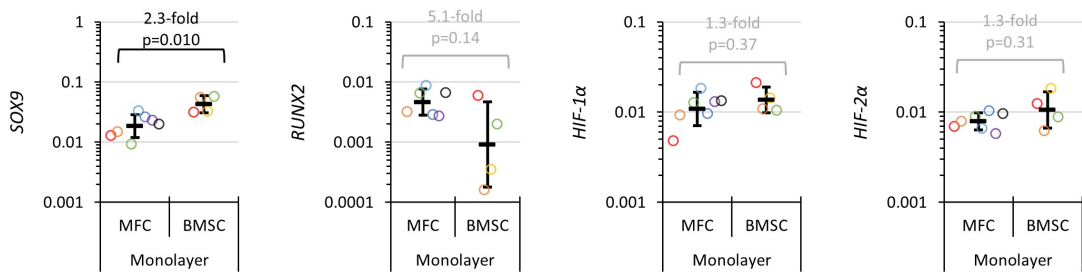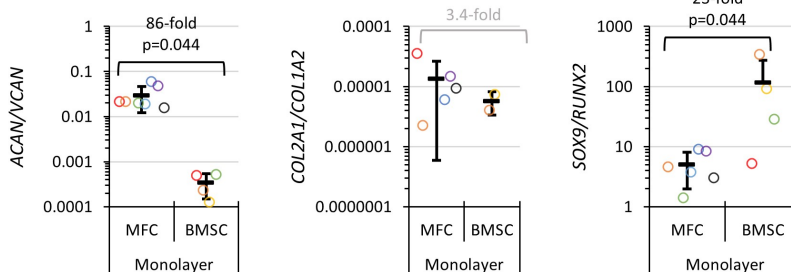
A.9 Supporting Figures

Figure SA.1: Relative mRNA expression by qRT-PCR of BMSCs and MFCs in monolayer prior to scaffold seeding.

Appendix B: Cell Yields from Human Inner Meniscus Tissues: Influence of Storage Time and Donor Characteristics

As of writing, this data has not been published in a peer-reviewed journal.

B.1 Abstract

Meniscus specimens are generated during arthroscopic partial meniscectomy and are typically discarded. They contain a heterogeneous population of cells known as meniscus fibrochondrocytes (MFCs) that are promising for applications in meniscus tissue engineering. The purpose of this retrospective study was to search for associations in MFC cell yield (normalized to tissue specimen size, i.e., yield/wet weight (WW)) with storage time after surgery, donor age, BMI, sex, and meniscus type. We performed analyses on our tissue database of partial meniscus specimens (n=311 in total) collected from two Edmonton (Alberta, Canada) hospitals from 2014-2019. Each tissue was initially stored in 37°C incubators in polypropylene containers in a standard nutritious medium. Meniscus fibrochondrocytes were then isolated by collagenase digestion and plastic adherence. The analysis showed that 63% of donated tissue were from male donors, 52% from right knees, and 80% from the medial meniscus. The mean donor age and yield/WW (for samples stored 7 days) or less were 29±9 years and $4.1 \pm 2.6 \times 10^6$ cells/g. Yield/WW decreased with increased storage time, espe-

cially beyond 7 days. In a dataset restricted to 7 days storage or less, yield/WW also decreased with each of age and BMI but the associations were weak. In conclusion, cell yields from meniscus specimens are maximized with short storage times. Most variability between donors remained unexplained and thus unexplored factors seem more important to cell yield.

B.2 Introduction

The medial and lateral menisci play important mechanical roles in the knee joint. These include transfer and distribution of body loads to protect the articular cartilage from excessive stress[30]. Injuries to the inner regions of the adult meniscus may disrupt knee function and do not heal effectively due to the tissue's avascular nature[28]. Frequently, irreparable non-healing injured meniscus tissue needs to be removed by arthroscopic partial meniscectomy to improve joint function[273]. Unfortunately, both meniscus injury and arthroscopic partial meniscectomy are tied to knee osteoarthritis development later in life[17, 193]. Research to develop cell-based meniscus tissue replacements is ongoing with the objectives to slow or prevent osteoarthritis development and restore knee function following non-healing meniscus injury[240].

A promising source of cells for meniscus tissue engineering are the meniscus specimens generated during arthroscopic partial meniscectomy that would otherwise be discarded during the procedure[130]. These specimens are generally resected from the non-healing inner meniscus regions. They contain a population of cells known as meniscus fibrochondrocytes (MFCs)[274]. MFCs show the capacity to synthesize the functional macromolecules of the meniscus extracellular matrix *in vitro*, suggesting that they could be used to generate partial or full meniscus replacements for implantation back into the donor with low risk for immune rejection[275].

Our research group and others regularly collect fresh partial meniscus specimens from local hospitals[276]. These tissues are immediately processed or stored in incuba-

tors for a short period prior to use in meniscus tissue engineering-related experiments. These experiments typically involve isolation of MFCs from the specimens, monolayer expansion, and subsequent re-differentiation using growth factors for generation of meniscus-like tissues. From 2014-2019, we collected over 300 meniscus specimens from arthroscopic partial meniscectomy along with non-identifying donor information: biological sex, age, height, weight, affected knee (left or right), and meniscus type (medial or lateral). The purpose of this study was to retrospectively test for associations between these factors and the cell yield normalized to meniscus tissue wet weight. A secondary purpose was to characterize the population of meniscus donors.

B.3 Materials and methods

B.3.1 Ethics and specimen collection

From 2014-2019, meniscus specimens from arthroscopic partial meniscectomies at the Grey Nuns Community Hospital and the University of Alberta Hospital in Edmonton were collected with patient consent waived in accordance with the University of Alberta human research ethics board. We recorded the following details from patients: biological sex, age, patient weight and height, knee (left or right), and meniscus type (medial or lateral). Specimens were the largest excised meniscus fragments from each procedure; thus, the wet weights described underestimate the actual amount of tissue removed during arthroscopic partial meniscectomy. This is an important consideration when attempting to identify associations between wet weight as recorded and any other factor in this study.

B.3.2 Meniscus specimen storage, digestion, and MFC isolation

Meniscus specimens were aseptically stored in polypropylene containers (Fisherbrand, catalog 16-320-730) with phosphate-buffered saline (PBS) at 4°C and were transported to our lab in ice on the same day as the procedure. Specimens were then

transferred to a high-glucose (4.5 g/mL) DMEM containing 10% fetal bovine serum (FBS), 100 U/mL penicillin, 100 μg/mL streptomycin, 2-mM L-glutamine, and 10 mM HEPES buffer and stored within a humidified 37°C incubator containing 5% CO2 and 95% air. Storage times for meniscus specimens prior to MFC isolation ranged from 0 to 30 days.

The MFC isolation procedure has been previously described in detail[8]. While there were minor methodological variations in the isolation procedure over time, the general procedure remained consistent. Digestions were performed by eleven researchers with varying experience.

Meniscus specimens were transferred to a Petri dish containing a small amount of phosphate-buffered saline to maintain hydration. Specimens were cut using a scalpel into pieces of about 1 to 3 mm^3 in size. The wet weight of the collective pieces was then recorded. They were then treated with high-glucose DMEM containing 5% PBS and 4500 U/mL of collagenase ("Type 2", Worthington, USA) for 22 h at 37°C and agitated at 250 revolutions per minute using an Innova 4000 incubator shaker (New Brunswick Scientific Company, USA). After the digestion period, 15 to 25 mL of the 10% FBS medium was added to the digest solution and any large undigested fragments were removed by a 100 μm filter. Typically, smaller pieces of cut meniscus resulted in fewer fragments after digestion. Visual inspection generally showed 90% or more solubilization of the meniscus. The filtrate was then centrifuged and the resulting cell pellet was suspended in PBS as a rinse to dilute and remove the collagenase. The cells were then re-centrifuged and the cells were suspended in the 10% FBS medium and plated into monolayer flasks at a typical ratio of about 75 cm^2 growth surface per 1 g original tissue. The MFCs were then allowed to attach to the flasks for 1 to 3 days, defined in our lab as "passage 0". There was no indication of cell proliferation during this time in comparing yields between donors given 1 vs. 3 days to attach.

At the end of passage 0, the culture medium was aspirated and the MFCs were rinsed once with PBS to remove non-adherent cells. The MFCs were then collected

and counted to obtain the total viable cell yield. These were then divided by the wet weight of the original tissue fragments to obtain the cell yield per wet weight (yield/WW).

B.3.3 Data presentation and statistical analysis

All figures were prepared using Excel 2016 (Microsoft, USA). Statistical computations were performed in SPSS 26 (IBM, USA). We first tested for relationships in yield/WW and the continuous variables of specimen storage time, donor age, and donor body mass index (BMI) using Pearson's correlation and adjusted R squared values. We then tested whether there were differences in age, BMI, and yield/WW between the categorical groups of biological sex (male vs. female), knee (left vs. right), and meniscus type (medial vs. lateral) using three-way analysis of variance (ANOVA). Finally, we analyzed the frequencies of meniscus donors in each combined category of biological sex, knee, and meniscus type using contingency tables with Fisher's exact test or Pearson's Chi-Square (all two-tailed). Data such as height and weight were often not available, and we assumed that any incomplete data was due to factors besides those under investigation. Donors with incomplete data were omitted from tables or figures that required that specific data; thus data points appearing on one plot often did not appear on others.

B.4 Results

B.4.1 Descriptive summaries

Of the 311 donated meniscus specimens, 196 were from male patients ($\hat{p}_{\text{male}}$=0.63), 161 were from right knees ($\hat{p}$right=0.52), and 249 were of the medial meniscus ($\hat{p}_{\text{medial}}$=0.80). When pooled, the average±standard deviation of yield/WW was 4.1±2.6×10^6 cells/g. The average tissue wet weight and total cell yield were respectively 1.9 g and 8.8×10^6 cells/g (Figure SB.1).

B.4.2   Correlation of viable cell yield with storage time, donor age, and BMI

The yield/WW of tissue had a weak negative correlation with the number of days the meniscus tissue was stored in medium in the incubator after surgery and prior to digestion (adjusted R^2=0.065, p=0.001) (Figure B.1). The overall trendline's slope indicated that each additional day of storage predicted 0.13×10^6 fewer cells/g tissue (Figure B.1). This implied that tissue storage in the incubator caused cell loss over time.

The linear best-fit line did not seem to satisfactorily capture the apparent relationship between variables. We then plotted a local weighted regression curve using SPSS 26. For storage times represented by a reasonable number of specimens, the local weighted regression curve was flat for low storage days but then became increasingly negatively-sloped as storage time increased. By inspection, the twenty donors with the highest cell yields were all stored seven days or less.

Donor age and BMI had a weak positive correlation (Figure B.1). Additionally, age and BMI each had weak negative linear correlations with yield/WW (Figure B.1). For yield/WW vs. BMI, the local weighted regression curve suggested that this relationship was most pronounced for BMIs greater than 25 (Figure B.1). Because age and BMI were weakly correlated and each of their simple correlations with yield/WW were similarly weak, it did not seem reasonable to investigate multiple regression of age and BMI with yield/WW for this study. The simple correlation coefficients indicated that: i) each 1-year increase in age predicted 0.09×10^6 fewer cells/g tissue (adjusted R^2=0.068, p=0.010) and ii) each 1-point increase in BMI predicted 0.18×10^6 fewer cells/g tissue (adjusted R^2=0.081, p=0.005). It should be recognized that most of the variability in yield/WW remained unexplained by storage time, age, and BMI.
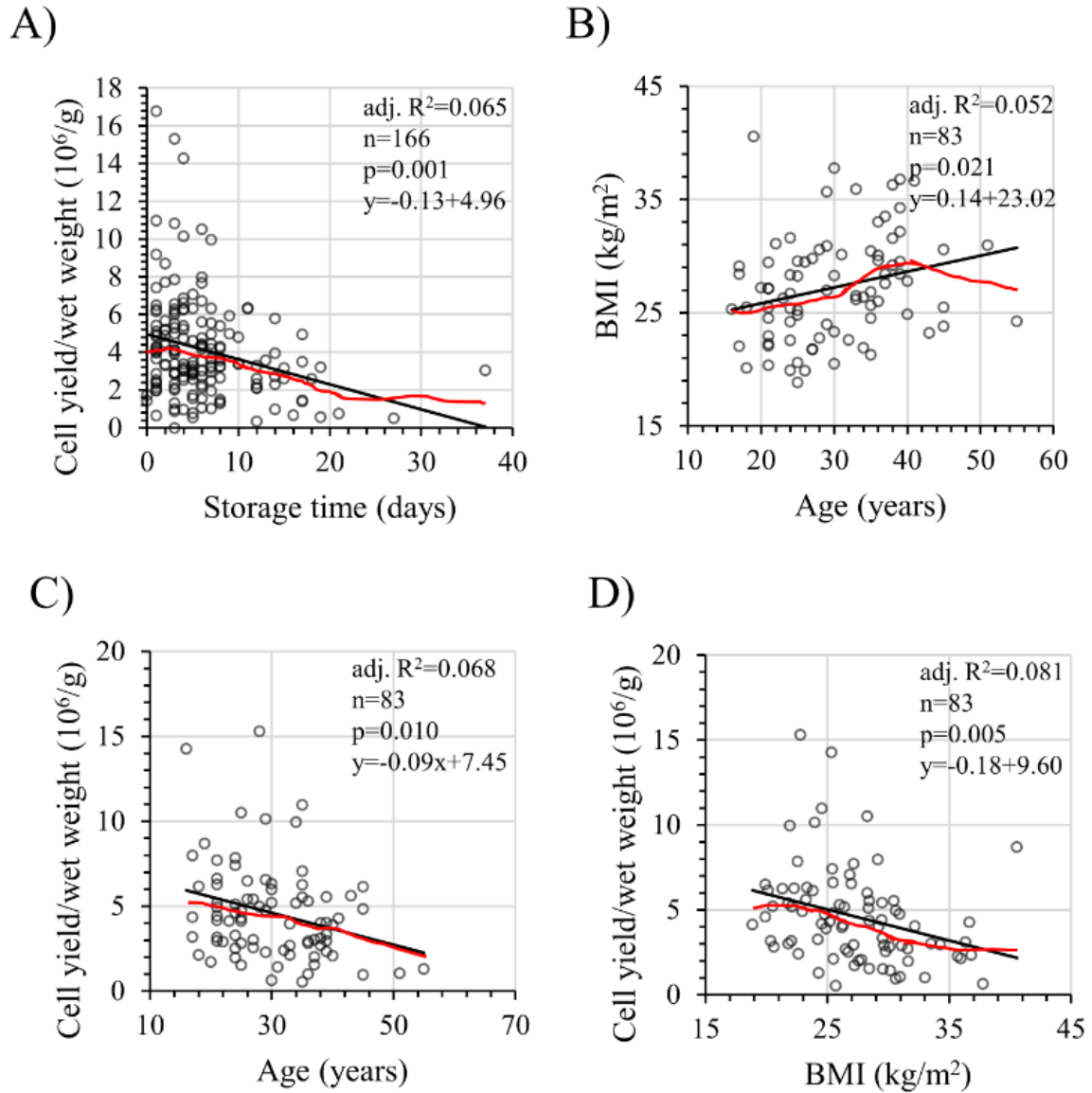
Figure B.1: Bivariate scatterplots of A) cell yield/wet weight (yield/WW) vs. storage time, B) donor age vs. donor body mass index (BMI), C) yield/WW vs. age, and D) yield/WW vs. BMI with local weighted regression (LOESS) curves in red. The text on each plot refers to Pearson's correlation.

B.4.3 Donor age, BMI, and tissue cell yield per wet weight by biological sex, knee, and meniscus type

Specimen sample sizes in this section varied between metrics because we lacked complete information for many donors. There were two reasons for this: i) one or more of a donor's age, weight, and height were not specified, and ii) the specimen was digested

for an experiment using a different protocol precluding comparison of yield/WW to those in this study and was therefore not included. To the best of our knowledge, these affected specimens at random and did not systematically affect results.

We did not find evidence for differences in donor age or BMI between groups stratified by biological sex, knee, and meniscus type (Figure B.2). It should be noted that some groups were poorly represented in our sample, especially the female-right-lateral group. Most groups had right-skew (mean>median) in both donor age and BMI, indicating that some older and higher-BMI donors were pulling up the means. When pooled, the mean donor age and BMI were respectively 29.3 years and 27.2 kg/m^2. We did not find evidence for differences in cell yield normalized to tissue wet weight (yield/WW) between biological sex (male vs. female), knee (left vs. right), and meniscus type (medial vs. lateral) (Figure B.2).
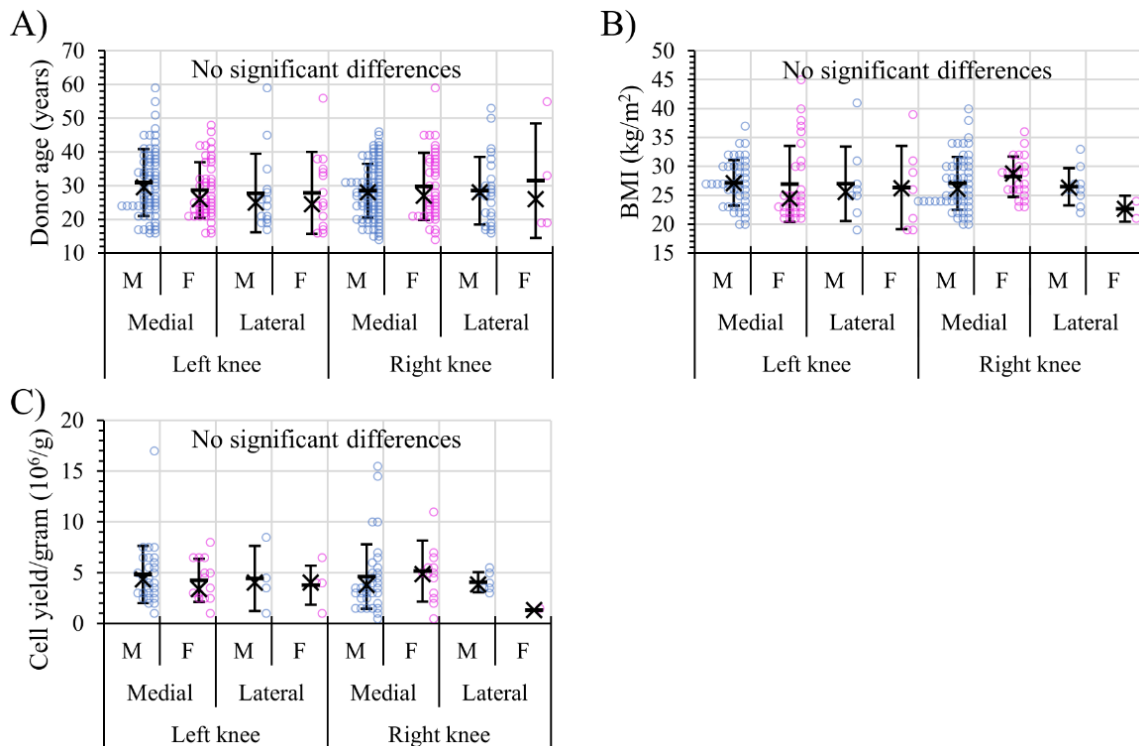

Figure B.2: The distributions of A) donor age, B) donor body mass index (BMI), and C) cell yield/wet weight (yield/WW) distributions by biological sex, knee, and meniscus type. Bars represent the mean ± standard deviations and x represents the median.

B.4.4 Specimen frequencies by biological sex, knee, and meniscus type

The observed frequencies of specimens in each of the 8 possible categories indicated a relationship between knee (right vs. left) and meniscus type (medial vs. lateral) in females (p=0.017) but not in males (p=0.37) by Fisher's exact two-sided test (Table B.1). Within females, right-lateral menisci were rarer than expected based on the proportions in the contingency table (4 observed specimens vs. 9 expected), whereas left-lateral menisci were more common than expected (18 vs. 13) (Table B.1). Because the female-right-lateral cell of the three-way contingency table had a small observed count (4), we pooled data across one variable at a time and looked for relationships between the remaining two variables by Pearson's Chi-square.

Table B.1: Three-way contingency table of biological sex, knee, and meniscus type. Numbers in brackets are the expected counts. P values are from Fisher's exact test (two-sided).

Sex	Knee	Type		Total	
		Medial	**Lateral**		
Male	**Right**	88 (91)	26 (23)	114	
	Left	68(65)	14 (17)	82	
	Total	156	40	196	p=0.37
Female	**Right**	43 (38)	4 (9)	47	
	Left	50 (55)	18 (13)	68	
	Total	93	22	115	p=0.017

In pooling right and left knee specimens together, there was no relationship between biological sex and meniscus type (p=0.79) ((*Table B*.2). In pooling men and women together, there likewise was no relationship between knee and meniscus type (p=0.55) ((*Table B*.2). Thus, the ratio of medial to lateral meniscus specimens did not vary with biological sex nor with knee type.

After pooling medial and lateral meniscus specimens together, there was a signif-

Table B.2: Two-way contingency table of biological sex and meniscus type. Numbers in brackets are the expected counts. P values are from Pearson's Chi-Square test (two-sided).

Sex	Type		Total	
	Medial	Lateral		
Male	156 (156.9)	40 (39.1)	196	
Female	93 (92.1)	22 (22.9)	115	
Total	249	62	311	p=0.79

Table B.3: Two-way contingency table of knee and meniscus type. Numbers in brackets are the expected counts. P values are from Pearson's Chi-Square test (two-sided).

Knee	Type		Total	
	Medial	Lateral		
Right	131 (128.9)	30 (32.1)	161	
Left	118 (120.1)	32 (29.9)	150	
Total	249	62	311	p=0.55

Table B.4: Two-way contingency table of biological sex and knee. Numbers in brackets are the expected counts. P values are from Pearson's Chi-Square test (two-sided).

Sex	Knee		Total	
	Right	Left		
Male	114 (101.5)	82 (94.5)	196	
Female	47 (59.5)	68 (55.5)	115	
Total	161	150	311	p=0.003

icant relationship between biological sex and knee (p=0.003) ((Table B.4). Notably, in male donors right-knee menisci were more common than left (114 vs. 82, $\hat{p}_{\text{right}}$ =0.58), whereas in female donors left-knee menisci were more common than right (47 vs. 68, $\hat{p}_{\text{right}}$=0.41).

B.5 Discussion

Herein we performed a retrospective study of human meniscus specimens generated in arthroscopic partial meniscectomies and collected by our research group from 2014-2019 (n=311 in total).

Our most important finding was that yield/WW declined with storage time, especially after one week. A secondary finding was that donor age and BMI were both negatively correlated with yield/WW. Finally, we observed that yield/WW did not seem to be related to biological sex, knee, and meniscus type.

Previously, chondrocyte viability in femoral and tibial sheep condyles stored at 4°C in a similar medium to ours showed a gradual decline in viability, falling to about 81% at day 29 and 52% at day 60[277]. As well, osteochondral plugs from human femoral condyles stored at 4°C in a serum-free minimum essential Eagle medium showed no decline in viability after 14 days (97.5±2.2% viable) but a decline to 70.7±11.4% by 28 days[278]. A comparison of lactated Ringer's solution (notably with no glucose) to culture medium showed that chondrocyte viability at 14 days declined only in the Ringer's solution[279]. Chondrocyte viability was much higher in canine osteochondral allografts stored at 37°C compared to 4°C at both 28 and 56-day storage intervals[280]. Generally, cartilage tissues degrade in matrix properties as well during storage[281]. Although none of these studies investigated the reasons for time-based declines in viability, it appears that a lack of nutrition and the non-physiological environment play an important role. Given the presence of migratory cells in the meniscus, outgrowth and emigration from the tissues could plausibly also play a role in our system[130, 199].

Given that storage time affects yield/WW, it could plausibly also affect cell performance in monolayer expansion and downstream tissue engineering applications such as chondrogenic re-differentiation. For example, immediate cell isolation could possibly help reduce the phenotypic de-differentiation experienced by meniscus fibrochondrocytes during monolayer expansion by minimizing the time spent outside their native environment[8, 282]. As well, prolonged storage times could inadvertently select for different cell populations based on: i) their motility, given that the menisci contain migratory cells that spontaneously outgrow through regions without an intact superficial zone[199], and ii) their tolerance of the static storage environment through attrition, which may be a function of their proximity to the surface and tolerance of nutrient deprivation and/or static culture. This could conceivably be desirable for engineering cartilaginous tissues since nutrient diffusion is often a limiting factor. Each of these examples could form the basis of interesting experiments.

Long storage times are not necessarily catastrophic to yield/WW. For example, our longest-stored tissue still contained $3.1{\times}10^6$ viable cells/g after 37 days in storage. "Good" yields/WW (e.g., $>2.0{\times}10^6$ cells/g) were obtained for 99/110 (90%) tissues stored 7 days or less and for 33/44 (75%) tissues stored more than 7 days.

Although it seemed that there was no decline in yield/WW for tissues harvested within a week of surgery, we did not measure any potential phenotypic changes in the cells. It is plausible that deleterious changes could occur during this week of storage if, for example, the cells are nutrient-deprived and starving. Thus, our conservative practical conclusion is that meniscus specimens should be processed as soon as possible after surgery to maximize yield/WW by collagenase digestion, although one-week of storage seems acceptable from a yield/WW perspective. Alternatively, improved storage methods could be developed towards better maintenance of yield/WW, perhaps by incorporating dynamic mixing of medium.

We next discovered that yield/WW was negatively correlated with each of donor age and BMI. We also found that age and BMI were positively correlated, suggest-

ing collinearity. Taken together with the weakness of all these correlations (adjusted $R^2<0.1$), it seemed that a multiple linear regression model adjusted for age or BMI would likely be unstable and unreliable. We thus presented the simple correlations and can only speculate whether decreased yield/WW is driven by age, BMI, or some other unknown factor. A study of gene expression in partial meniscectomy specimens also found a positive correlation between donor age and BMI[283]. They measured a panel of osteoarthritis and BMI-related genes and assessed for the effect of BMI after adjustment for age[283]. The researchers reported that it was age rather than BMI associated with the typically negative effects on gene expression that they observed[283]. Two histological studies found decreased meniscus cell densities in older donors, even in those from patients without histories of arthritis and knee trauma; however, they did not consider BMI[186, 284]. These findings make it plausible that age is an underlying causal factor in our observed decrease in yield/WW. However, we are left uncertain regarding the role of BMI in this regard.

Recently, researchers noted a fall in cell counts from digested menisci with increasing donor age (without adjustment for BMI). For example, their cell counts were 3.5×10^4 cells/mL in donors under 20 years old, 1.7×10^4 cells/mL in the 30-40 age group, and just 1.0×10^4 in the 40-50 age group[276]. This supports the decline in yield/WW that we observed with increasing age (Fig. 1D), although ours was less precipitous[276]. The patient population differences possibly underlying these contrasting results include the following. Their specimens were extracted in an orthopaedic centre in Southern India and compared to Western Canada[276]. In their study sample, 28-31% of patients were older than 40 compared to 13% in ours, and about 48% of patients were in BMI range 18.5-24.9 compared to 37% in ours[276]. Regarding meniscus type, their population had a lower percentage of medial vs. lateral meniscus tears (59% medial compared to 80% medial in our study) and was more dominated by males vs. females (86% male compared to 63% male in our study)[276].

As for the role of donor age in downstream tissue engineering applications, Baker

et al. found that it was not a robust predictor of meniscus-derived cells' biosynthetic capacity in their sample of ten meniscus donors of age range 18-84 years[130]. We previously observed similar results to theirs albeit in a smaller age range and sample size, finding that the extent of inner meniscus-like ECM formation by meniscus fibrochondrocytes from 41 and 46-year-old meniscus tissue donors was comparable to 19 and 26-year-old meniscus donors[2]. Thus, although it seems that younger donors of lower BMI may provide superior cell yields for meniscus tissue engineering, the capacity of these cells for chondrogenic re-differentiation may be comparable in young to middle-aged donors. It should be appreciated that in the present study most of the variability in yield/WW remained unexplained by age and BMI, and that "good" yields/WW (e.g., 2.0×10^6 cells/g) were still observed for 6 of 7 donors of BMI>35 and 4 of 7 donors of age>40 in our sample.

We found no significant differences in our sample in donor age, BMI, and yield/WW across the groups of biological sex, affected knee, and meniscus type. It is possible that true differences between groups exist and that we could not detect them due to inadequate statistical power. Yet, this absence of evidence provides some reassurance that donor biological sex, knee, and meniscus type may not be practically important considerations for obtaining an adequate yield/WW.

There could be differences across the groups of biological sex, affected knee, and meniscus type in the amount of inner vs. outer meniscus tissue typically removed in arthroscopic partial meniscectomy. Researchers have previously found that meniscus fibrochondrocytes from the inner vs. outer meniscus have greater capacities for chondrogenic re-differentiation[207]. However, our research group and another found no differences in meniscus fibrochondrocytes between the inner and outer meniscus in this regard[58, 285]. Yield/WW was reported to be about 4× higher in the inner vs. outer meniscus in one-week old bovines, although the actual trend in DNA contents between the inner and outer meniscus was reported to be the opposite[286].

As mentioned above, the pieces of meniscus collected by our lab are only usually

the largest fragments and do not represent the total amount of tissue removed during surgery. Duly noting this limitation, we found that the specimen wet weights were about 32% larger for male vs. female donors (p<0.001) and 28% larger for medial vs. lateral donors (p=0.003) (Figure SB.1). This first observation may simply reflect men being physically larger than women. The underlying reason for the second observation is less obvious, as the lateral meniscus has been reported to be no different in size or 11% larger than the medial[184, 287].

Our last findings were related to the frequency relationships of biological sex, affected knee, and meniscus type. It was interesting to find in females that specimens of the right lateral meniscus were rare while those of the left lateral meniscus were not. It was further interesting to find that left knee specimens were more common than right in women (68/115), whereas right knee specimens were more common than left in men (114/196). This suggests a possible role in left-right leg dominance in meniscus injury requiring surgery between the sexes, which warrants further investigation.

Most specimens in our study came from the medial meniscus. Early after ACL injury, it is likely that the rates of medial and lateral meniscus injury are similar; however, as wait-time for surgical treatment increases an association develops with a higher risk of medial meniscus injury[288–290]. It has been found that the presence of meniscus tears is correlated with the number of instability episodes after adjustment for the time between injury and surgical treatment[291]. It would be interesting to investigate if the time between meniscus injury and cell isolation led to differences in yield/WW and also downstream performance of the cells in meniscus tissue engineering-related applications. A histological study of human menisci from non-osteoarthritis joints found that aging was associated with declining cellularity, abnormal cell distributions, and greater Safranin-O staining intensity, which is suggestive of phenotypic changes in the cells[186].

Our study had several limitations, many of which were discussed in the preceding text. In addition to these, it should be understood that our yield/WW values

underestimate the true cell densities within the meniscus tissues. This is because cells could migrate out of the tissues or be otherwise lost during the storage and digestion stages. Further, any non-adherent cells at the end of our "passage 0" are lost in the phosphate-buffered saline rinse prior to trypsinization for cell counting. A final limitation to consider was that tissue storage and cell isolation protocols were performed by many different researchers, which likely contributed to the variability in yield/WW observed between donors. This should, however, improve the external validity of our results related to yield/WW.

B.6 Conclusion

To maximize human meniscus fibrochondrocyte yield normalized to meniscus specimen wet weight (yield/WW) by collagenase digestion, we suggest digestion of meniscus specimens as soon as possible after surgery or at least within a week. Yields/WW tended to be best for donors who are younger and/or of lower BMI; however, adequate yields/WW can nevertheless be obtained for donors over 40 years or with BMI beyond 35. Yield/WW does not seem to be affected by the donor's biological sex, knee, or meniscus type.
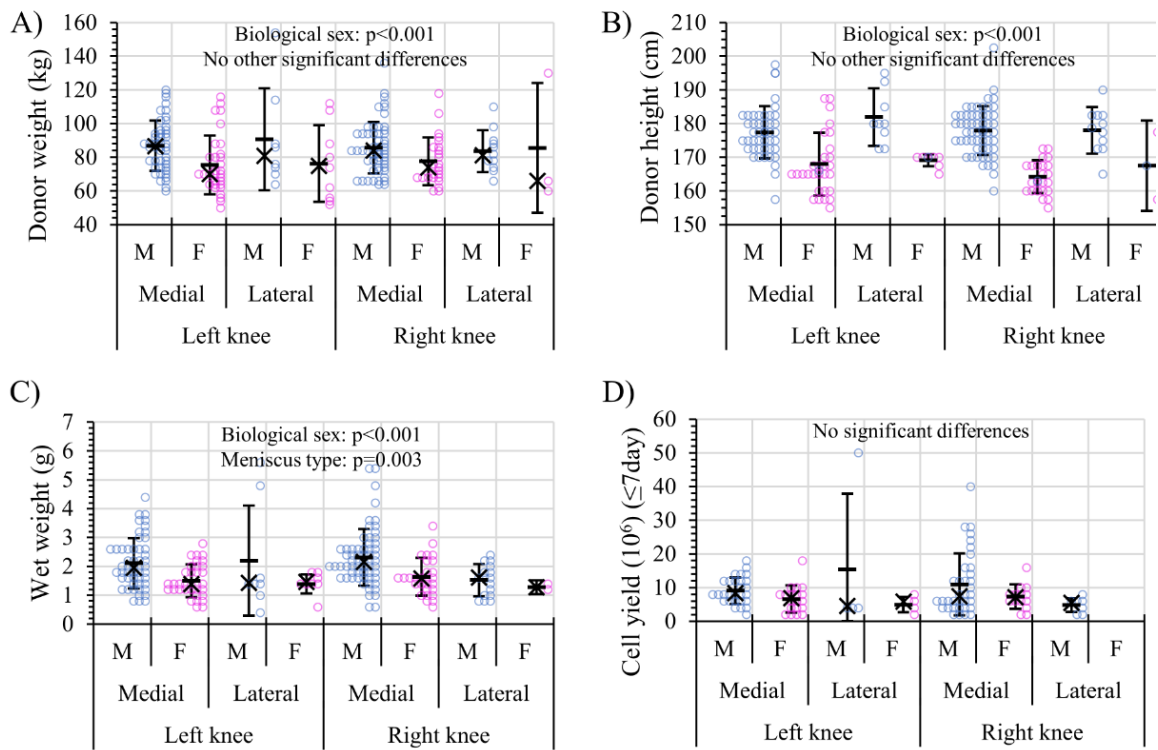
Figure SB.1: The distributions of A) donor weight, B) donor height, C) tissue wet weight, and D) total cell yield by biological sex, knee, and meniscus type. Bars represent the mean ± standard deviations and x represents the median. Mann Whitney U test was used with one factor at a time for panels A-C because homogeneity of variance assumption of ANOVA was not met.

Appendix C: Seeding Density Pilot Experiment (Chapter 8 Supplement)

This data has been published in Frontiers in Bioengineering and Biotechnology[6]. The methods associated with this data are described in Chapter 8. Most importantly, "SD" here refers to standard cell seeding density (5×10^6/cm^3, and "HD" is high-density (30×10^6/cm^3). The data herein is preliminary and its reproducibility has not been tested with multiple tissue donors.

C.1 Content
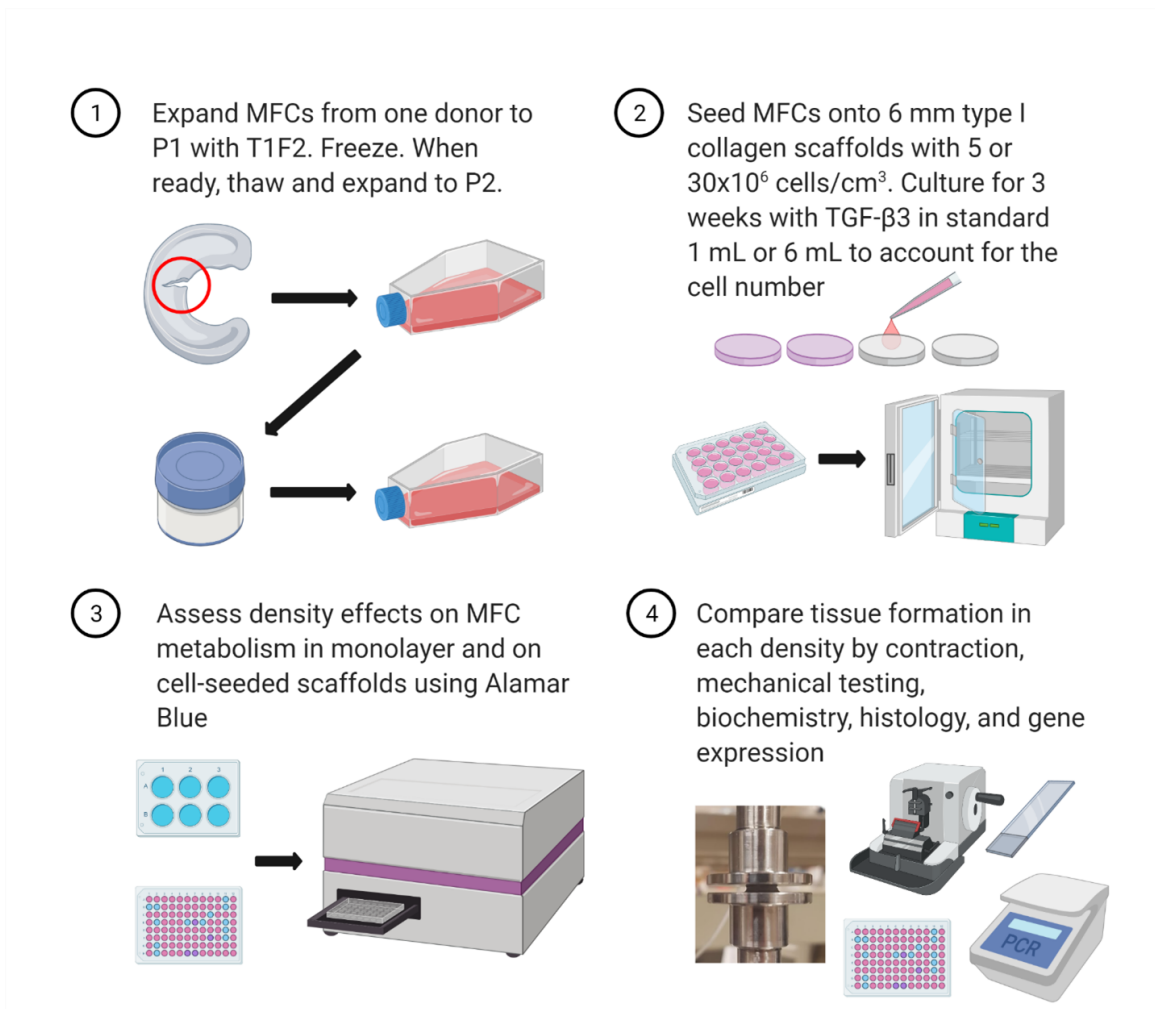
Figure C.1: The medium for expansion and tissue culture was the same as in the main experiments. MFCs: Meniscus fibrochondrocytes. T1F2: TGF-β1 and FGF-2. The donor was the same as Donor 3 used in experiments III & IV. Created using Biorender (2021).
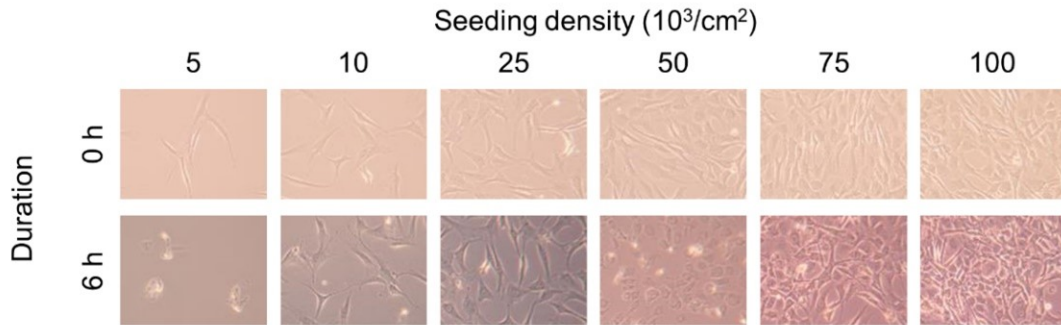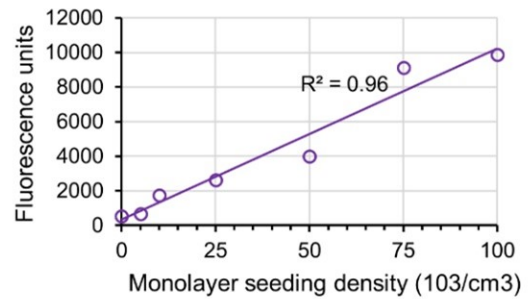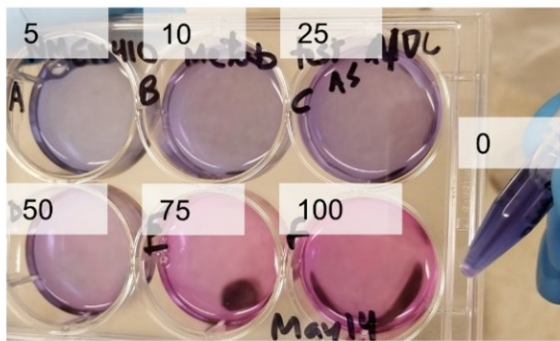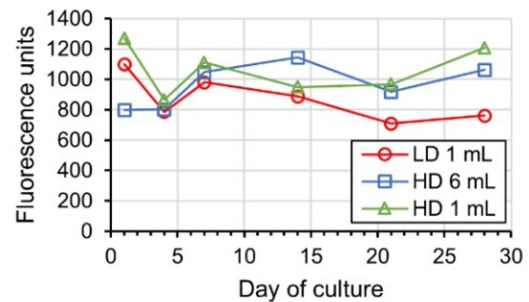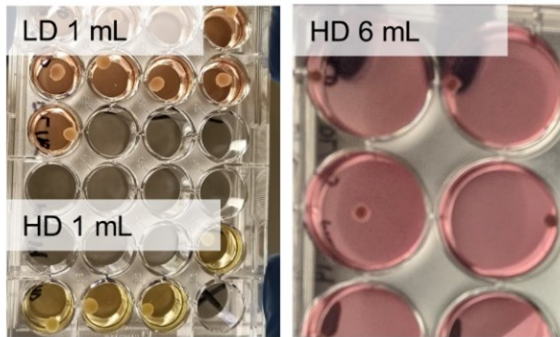
Figure C.2: A) 24h after seeding cells into 6 well plates at the indicated densities in expansion medium (but without T1F2), the cells were treated with 90% expansion medium (without T1F2) + 10% Alamar blue reagent for 6h (Thermofisher, USA). The Alamar blue treatment seemed to cause adverse changes in cell morphology in monolayer. B) Colour change after the 6h treatment and fluorescence measurement. C) Tissue culture medium turnover after 3 days. D) Alamar blue turnover after 30-minute treatments in 90% tissue culture medium repeated every few days on the same replicate construct. Alamar blue turnover did not show a clear relationship to the number of seeded cells in 3D. If anything it seemed to be a function of the surface area of the constructs. LD: low density ($5 \times 10^6/cm^3$), HD: high density ($30 \times 10^6/cm^3$).
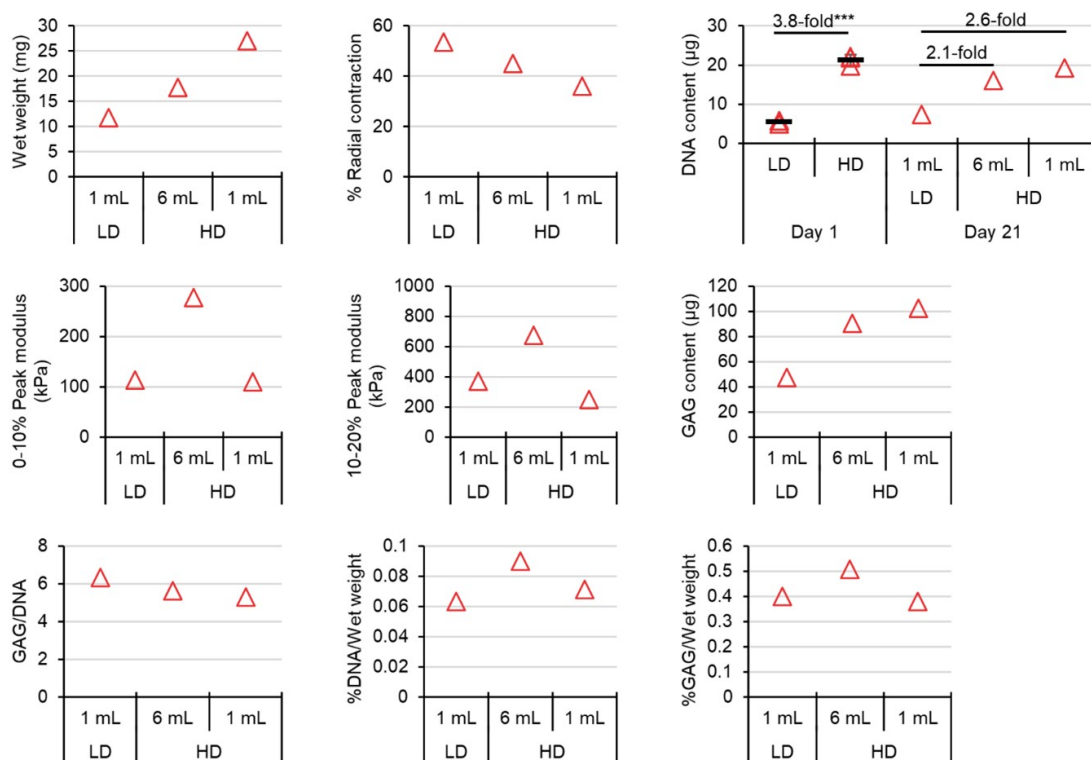
Figure C.3: Contraction, mechanical, and biochemical analysis after 3 weeks of tissue culture. Samples were tested in stress relaxation tests at a strain rate of 50% strain/s. DNA contents did not show a 6-fold difference on day 1 as had been expected. When seeding scaffolds, a cell pellet containing sufficient cells to seed all replicate scaffolds at the appropriate density is suspended in 25 µL of medium per scaffold. Each scaffold is then seeded with 25 µL of the suspension. The lower than expected DNA on day 1 in HD relative to LD reflects error in the assumption of negligible cell volumes during the cell seeding protocol, because the volume of cells is less trivial at higher densities relative to the volume of medium to seed each scaffold (25 µL).
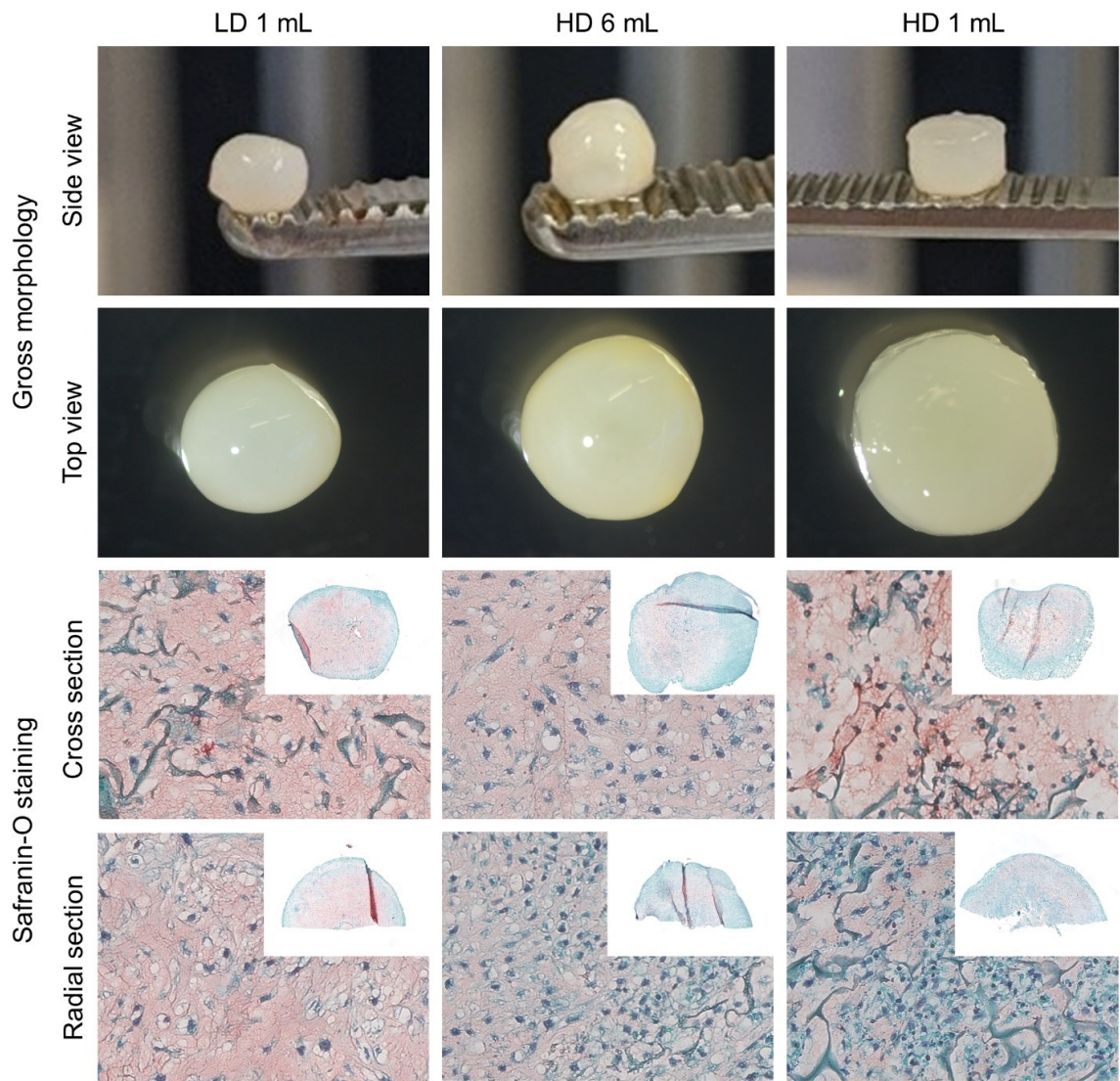
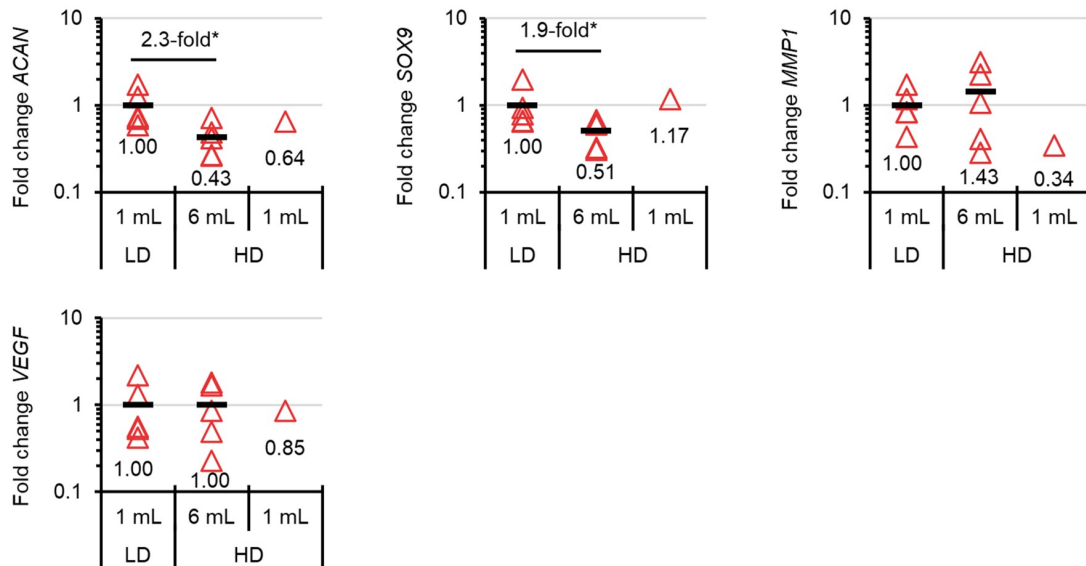Figure C.4: Morphology and Safranin-O/Fast Green FCF/Haematoxylin staining.

Figure C.5: mRNA expression levels measured by qRT-PCR compared to LD 1 mL in each group. Only one replicate was seeded in the HD 1 mL group for gene expression.

Appendix D: Orbital Shaking Pilot Experiment (Chapter 8 Supplement)

This data has been published in Frontiers in Bioengineering and Biotechnology[6]. The methods associated with this data are described in Chapter 8. The data herein is preliminary and its reproducibility has not been tested with multiple tissue donors.
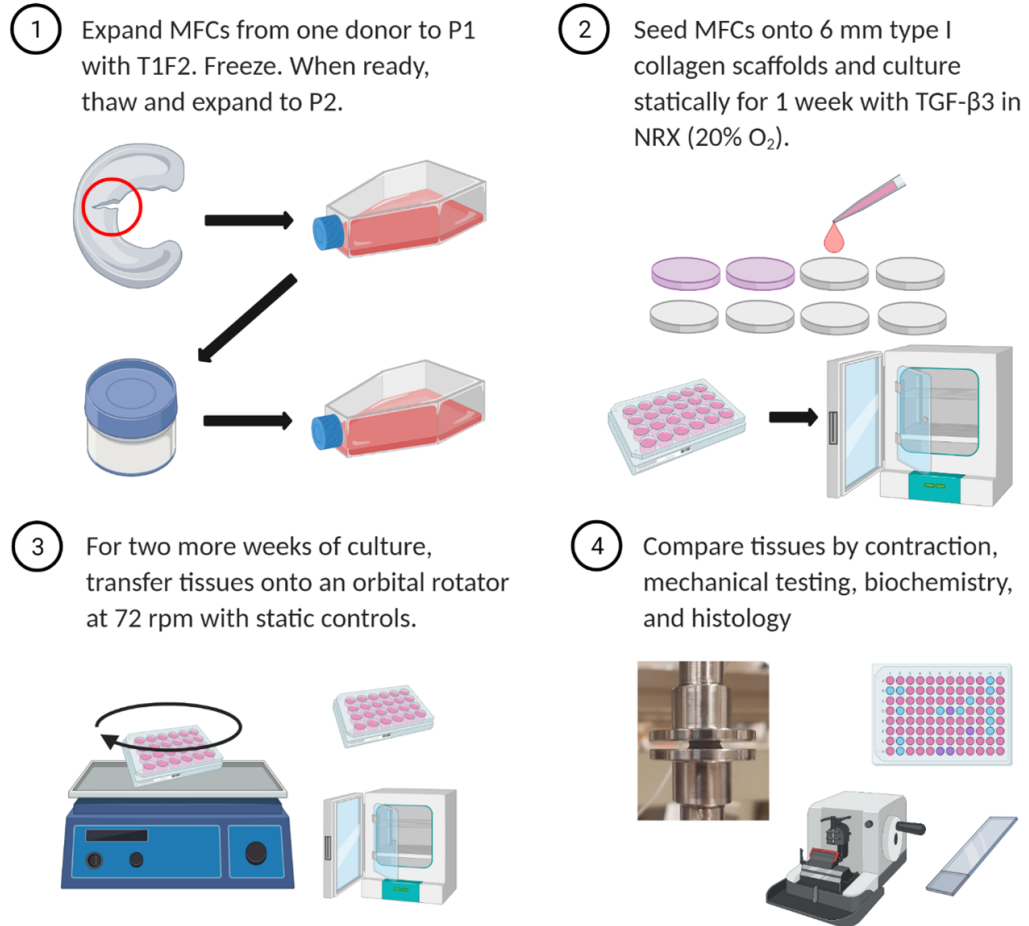
D.1 Content

Figure D.1: Orbital shaking pilot experiment. The donor was the same as Donor 1 used in experiments I & II. Created using Biorender (2021).
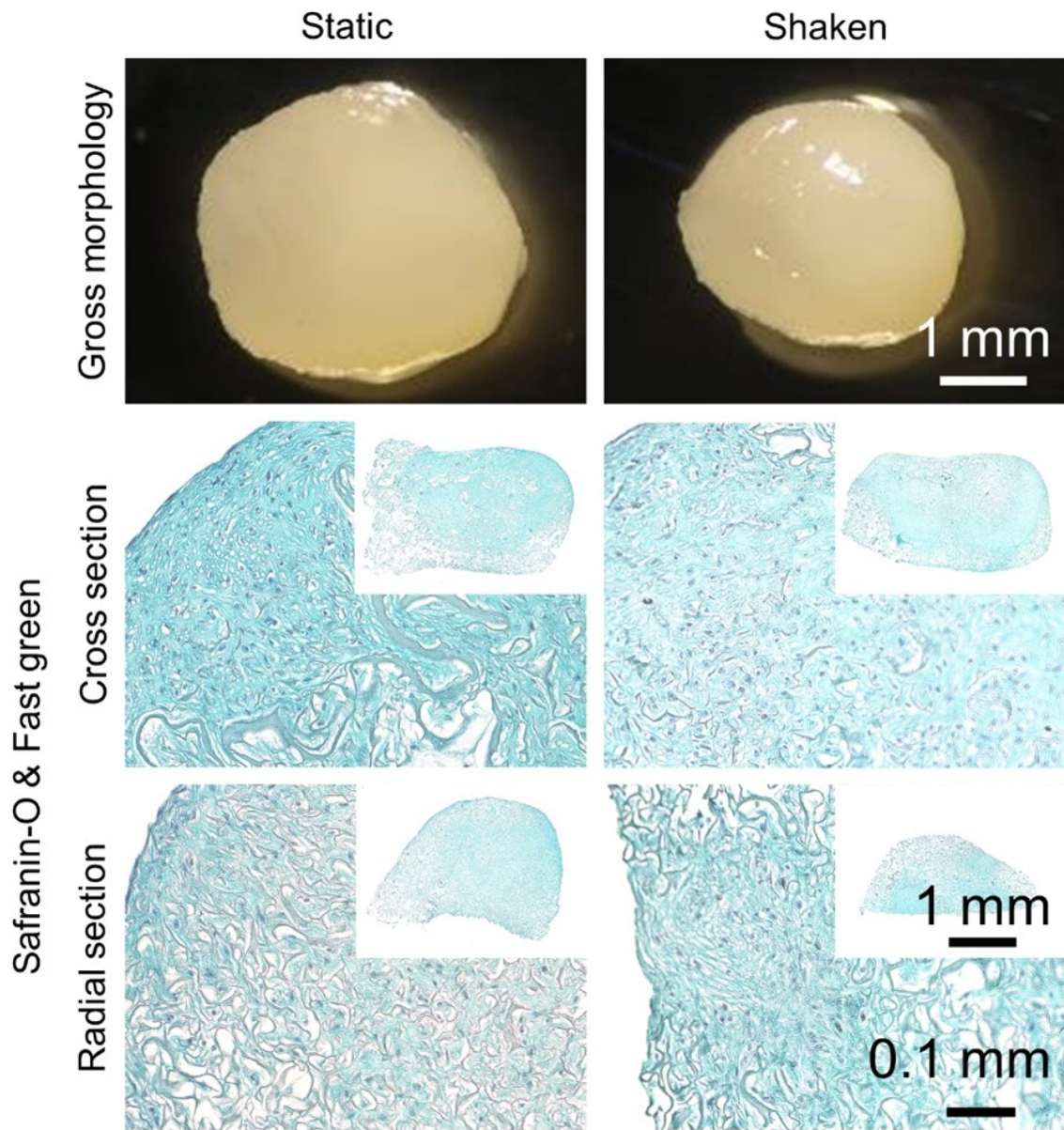
Figure D.2: Gross morphology and Safranin-O staining of static vs. shaken tissues.
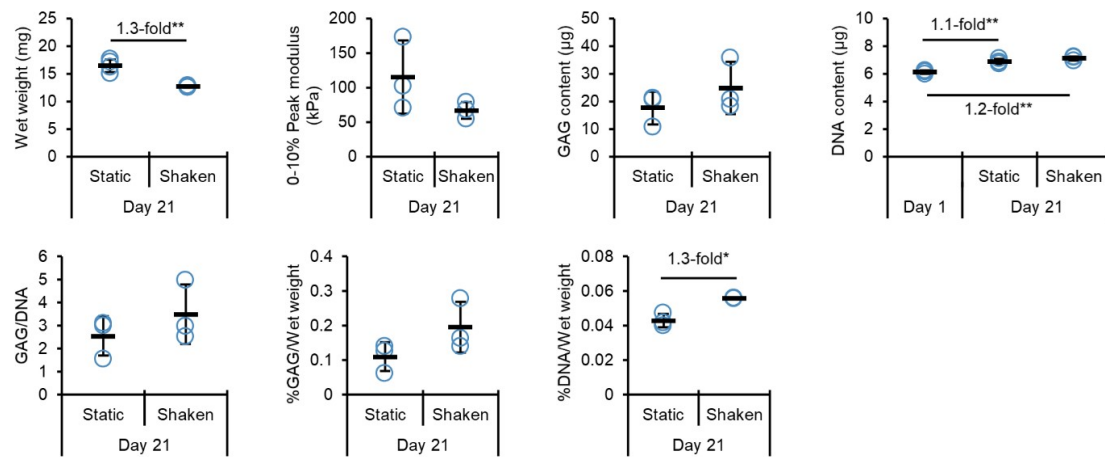
Figure D.3: Wet weight and mechanical and biochemical analysis of static vs. shaken tissues.